The Role of Prenylation in Vascular Calcification

A thesis submitted to the University of Manchester for the degree of

Doctor of Philosophy

in the Faculty of Medical and Human Sciences

2013

Arvind Ponnusamy

School of Medicine

TABLE OF CONTENTS

Word count: 48,894

Index of Figures

Index of Tables

Abstract

Arvind Ponnusamy
PhD in the Faculty of Medical and Human Sciences, 2013
Role of Prenylation in Vascular Calcification

Vascular calcification is an active, regulated process in which vascular smooth muscle cells (VSMCs) differentiate into osteoblast-like cells and deposit a mineralised matrix. It is well established that patients with chronic kidney disease and diabetes have poor cardiovascular outcomes which is thought to be due to increased vascular calcification and atherosclerosis. Previous work from the host laboratory has shown that nitrogen-containing bisphosphonates attenuate vascular calcification by inhibiting farnesyl pyrophosphate synthase, depleting cells of farnesyl pyrophosphate and geranylgeranyl pyrophosphate which are essential for the prenylation and activation of small GTPases such as Ras and Rho. Therefore, the initial aim of this study was to determine the effects of farnesyl transferase inhibitors (FTI-277 and manumycin A) on vascular calcification using a well validated *in vitro* model in which VSMCs are induced to deposit a mineralised matrix in the presence of β-glycerophosphate.

FTI-277 significantly inhibited β-glycerophosphate-induced calcification of VSMCs *in vitro* ($p<0.001$), and this inhibition occurred in a dose- and time-dependent manner. In contrast, manumycin A had no effect on this process. Active Ras pull-down assays and western blotting confirmed that both FTI-277 and manumycin A decreased Ras GTPase activation in VSMCs. Western blot analysis also showed that FTI-277, but not manumycin A, increased Akt phosphorylation in these cells. To determine whether FTI-277 inhibited mineralisation by promoting PI3K/Akt signalling, VSMCs were induced to mineralise in the presence of FTI-277 plus either wortmannin (a PI3K inhibitor), SH6 (an Akt inhibitor) or vehicle alone. These reagents decreased the inhibitory effect of FTI-277 on mineral deposition by VSMCs, demonstrating that the effects of FTI-277 can be negated, at least partially, by preventing downstream PI3K or Akt signalling. Incubation of VSMCs with wortmannin alone significantly promoted mineral deposition by VSMC ($p<0.001$). In addition, FTI-277 significantly inhibited phosphate-induced apoptosis of human VSMC ($p<0.05$), and prevented PDGF-induced VSMC migration. FTI-277 also inhibited β-glycerophosphate-induced Runx2, Msx 2 and alkaline phosphatase mRNA expression ($p<0.05$), promoted matrix Gla protein mRNA expression ($p<0.05$), and maintained α-smooth muscle actin expression. Using an *ex vivo* assay, it was also demonstrated that FTI-277 inhibits phosphate-induced mineralisation of aortic rings from rats with early and end stage renal disease and sham-operated controls.

To determine the effects of more specific Ras inhibition on VSMC mineralisation, Farnesyl Thiosalicylic Acid (FTS) was used. FTS (40 μM) inhibited mineralisation ($p<0.001$), decreased Ras GTPase activation and increased Akt phosphorylation but inhibited Erk phosphorylation *in vitro.* However lower doses of FTS increased mineralisation ($p<0.001$), but had no effect on Ras activation, or on Akt or Erk phosphorylation. FTS also appeared to delay PDGF-induced VSMC migration and induce apoptosis of human VSMCs in the absence of serum. *Ex vivo* studies demonstrated that FTS (40 μM) inhibited phosphate induced mineralisation of aortic rings from rats with end stage renal disease and sham-operated controls.

This study demonstrates that farnesylation, or Ras specifically, could be a potential novel therapeutic target for the inhibition of vascular calcification.

Declaration

No portion of the work referred to in the thesis has been submitted in support of an application for another degree or qualification of this or any other university or other institute of learning.

Copyright Statement

Acknowledgements

Firstly, I would like to extend my greatest debt of gratitude to my supervisors, Professor Ann Canfield and Professor Philip Kalra for providing me with the opportunity to carry out this research and for being incredibly supportive. I am grateful for their extreme patience in guiding me towards the completion of this research. I would also like to extend a special thank you to Dr. Smeeta Sinha, whose initial work formed the basis for this research project. I would also like to thank my advisor Dr Andrew Gilmore for his help, support and training in generation of lentivirus. I thank Dr. Nick Ashton for all his help and support.

I thank the current and previous members of Canfield lab (Gareth Hyde, Colette Inkson, Rebecca Taylor, Sarah Farrar, Samantha Borland, Tom Morris and Alice Baddeley). Each of you has made a unique contribution in shaping this work and helping me to complete this Phd. I thank the NIHR Manchester Biomedical Research Center and Renal Research Fund, Salford Royal NHS Trust for funding this project.

I'd like to thank both of my parents and brother (Ranjit) for their love and encouragement which they have given me throughout this time. I thank Deepa for encouraging me to take this research project. Not forgetting my friends especially Gani & Anu, Souvik & Saji, Shanthini, Ramadas, Shiv Bhutani and Karen for their loyal and warm friendship. For all the times you have listened and consoled, I am grateful.

Finally, I dedicate this thesis to my son, Adhithya Arvind and my parents

Publication

*Ponnusamy A, *Sinha S, Hyde G, Taylor RF, Pond E, Eyre H, Inkson C, Gilmore A, Ashton N, Kalra PA & Canfield AE. FTI-277 inhibits vascular calcification by up-regulating phosphatidylinositol 3-kinase/Akt signalling and MGP expression and inhibiting apoptosis (submitted to Circulation Research)

Oral Presentation

Ponnusamy A, Sinha S, Hyde G, Kalra. PA, Canfield AE. FTI-277 inhibits calcification by promoting Akt signalling and regulating osteogenic differentiation of VSMC. Journal of American Society Nephrology, SA-OR059, 2012

Ponnusamy A, Sinha S, Hyde G, Kalra PA, Canfield AE, Comparison of the effects of manumycin A and FTI−277 on vascular calcification. Journal of American Society Nephrology, SA−FC350, 2010

Poster Presentation

Ponnusamy A, Sinha S, Hyde G, Kalra PA, Canfield AE. FTI-277 inhibits vascular calcification by activating downstream PI3K/AKT signalling and preventing apoptosis of vascular smooth muscle cells. Renal Association (UK) Birmingham, 2011

Abbreviations

Apo	Apoprotein
ALP	Alkaline phosphates
ASMA	Apha smooth muscle actin
ßGP	ß-glycerophosphate
BCA	Bicinchoninic acid
BMP	Bone morphogenic protein
BSA	Bovine serum albumin
Cbfa-1	Core binding factor -1
CENP	Centromere associated proteins
CKD	Chronic kidney disease
CVCs	Calcifying vascular cells
CVD	Cardiovascular disease
DMEM	Dulbecco's modified Eagle's medium
DMSO	Dimethyl sulphoxide
DNA	Deoxyribonucleic acid
DN	Dominant negative
Erk	Extracellular signal regulated kinase
FCS	Fetal calf serum
FFP	Farnesyl pyrophosphate
FTI	Farnesyl transferase inhibitors
FTS	Farnesyl Thiosalicylic Acid
GAPs	GTPase activating proteins
Gas6	Growth arrest-specific gene 6
GEFs	Guanine nucleotide exchange factors
Gla	γ-Carboxyglutamic
Grb2	Growth factor receptor-bound protein 2
GTP	G-proteins
GST	Glutathione-S-transferase
HBSS	Hank's buffered salt solution
HCVSMC	Human coronary artery VSMC
HRP	Horseradish peroxidase
LDLR	Low density lipoprotein receptor
MAPK	Mitogen activated protein kinase
MSC	Mesenchymal stem cells
MGP	Matrix Gla protein
MMP-9	Matrix metalloproteinase-9
Msx2	Muscle segmentation homeobox 2
mTOR	Mammalian target of rapamycin
NF-kB	Nuclear factor- kB
OPN	Osteopontin
OPG	Osteoprotogerin
PBS	Phosphate buffered saline
PBST	PBS 0.05% (v/v) tween 20
PCR	Polymerase chain reaction
PI3K	Phosphatidyl inositol-3-kinase
PPMTase	Prenylated protein methyltransferase
PPi	Pyrophosphate
RBD	Ras Binding Domain

RCE1	Ras converting enzyme 1
RNA	Ribonucleic acid
ROCK	Rho kinase
ROS	Reactive oxygen species
SDS	Sodium dodecyl sulphate
SDS-PAGE	SDS-Polyacrylamide gel electrophoresis
SF	Serum-free
SOS	Son of sevenless
Sox9	SRY-related homobox protein 9
TBS	Tris buffered saline
TNF-	Tumour necrosis factor-
VSMCs	Vascular smooth muscle cell

Chapter 1

Introduction

1.1 General introduction to vascular calcification

Cardiovascular disease (CVD) is the leading cause of premature death in the United Kingdom. There are many risk factors for the development of CVD, including age, smoking, hypertension and chronic kidney disease (CKD). Diabetes mellitus, another established risk factor for CVD, confers a two to threefold increased risk. Patients on dialysis exhibit a thirty-fold increase in mortality from CVD when compared to the general population, even when adjusted for age, gender, race and the presence of hypertension and diabetes (Foley et al., 1998). In other words, a 30 year-old person on dialysis has the same mortality rate from CVD as a 70 year-old in the general population There is also evidence that people with less severe kidney disease have an increased risk of CVD, although this risk is markedly lower (Weiner DE et al., 2006).

Mortality and morbidity in diabetes and CKD patients are largely due to vascular diseases, for example, coronary heart disease and peripheral vascular disease. Vascular calcification, which involves mineral deposition, cartilage and bone formation within the atherosclerotic plaque, vessel medial layer and cardiac valve, is strongly associated with both diabetes and CKD, and has recently been established as an independent risk factor for the development of CVD (Johnson et al., 2006). Medial arterial calcification (see Figure 1.1 A), also known as Mönkeberg's sclerosis, is most often associated with CKD, diabetes mellitus and aging. For example, the presence of medial calcification in patients with type 2 diabetes can lead to increased morbidity due to a higher incidence of lower limb amputations (Everhart et al., 1988). Calcification within the intimal layer of vessels is usually associated with atherosclerosis. The degree of calcification in coronary arteries is correlated with an increased risk of cardiovascular events and death (Keelan et al., 2001).

Atherosclerosis is a complex process which involves the uptake of lipid from the blood into the arterial wall, resulting in inflammation, proliferation of vascular smooth muscle cells (VSMCs), increased oxidative stress, apoptosis and necrosis. Ultimately this leads to the formation of a plaque within the intima and narrowing of the blood vessel. A nidus of calcification can occur within a plaque (see Figure 1.1 B) and this may contribute to plaque instability (Rao et al., 2005; Shanahan et al., 1999). Bone related proteins are detected early in the pathogenesis of atherosclerosis and, as the lesion progresses, osteogenesis becomes more pronounced, to the extent that, in some cases, marrow is detected in the vessel wall (Hunt et al., 2002). Calcification seen in atherosclerosis is

thought to be secondary to the osteo/chrondogenic differentiation of VSMCs. The classical clinical manifestation of atherosclerosis is angina due to reduced blood supply to the myocardium. In more severe cases, this can result in myocardial infarction.

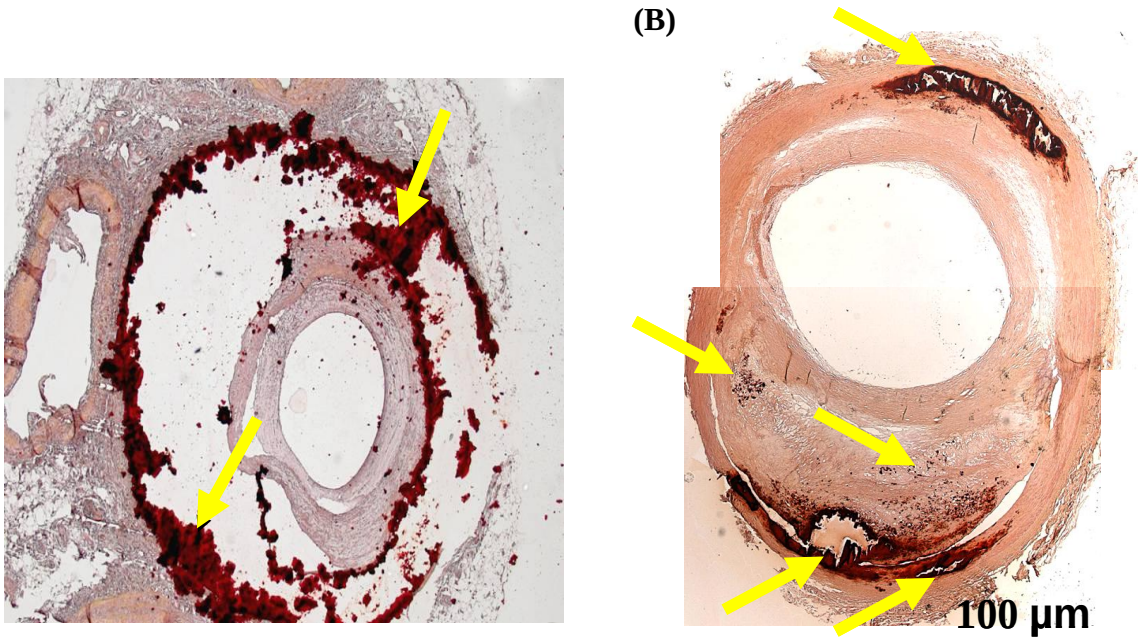

Figure 1.1: Histological sections of calcified human arteries stained with alizarin red. Calcification (dark red stain; arrows) is detected in the medial layer (Mönckeberg's sclerosis) (A, B) and at the base and edges of an atherosclerotic plaque (B). Note that in (A), the calcification is so extensive that the majority of the medial layer has been lost during sample processing. Images were kindly provided by Prof MY Alexander (Manchester Metropolitan University).

In contrast, medial calcification occurs in a more generalised pattern throughout the vessel wall (see Figure 1.1 A). The blood vessels become stiff without any obvious narrowing of the lumen, leading to a series of downstream effects including hypertension, increased pulse wave velocity, left ventricular hypertrophy, reduced coronary perfusion and ultimately congestive cardiac failure (Covic et al. 2010) These sequelae are independent predictors of mortality. Calciphylaxis (also known as calcific uraemic arteriopathy) is a further clinical manifestation of medial calcification. This condition usually presents with skin necrosis and carries a high mortality (Hayashi, 2013).

Effective bone turnover appears to be important for protection against vascular calcification. Osteoporosis is a known risk factor for the development of medial calcification (Rubin and Silverberg, 2004). Bone acts as an important acid-base buffer and

is also thought to be involved in the maintenance of serum calcium and phosphate levels (Pendigo et al., 2012). This suggestion is supported by the association of adynamic bone disease (low bone turnover) with ectopic calcification (Tomiyama et al., 2010).

Vascular calcification is a highly complex process although the molecular mechanisms regulating this process are still not fully understood (see Section 1.2). It is also becoming apparent that there are differences between intimal calcification and medial calcification, not only in aetiology but also in clinical sequelae. These differences are summarised in Table 1.1. Therefore, it is important to determine how vascular calcification is regulated, as this may lead to the development of novel treatments which could in turn reduce cardiovascular morbidity and mortality.

	Atherosclerosis/ intimal calcification	**Medial calcification/ Mőnckeberg's sclerosis/ arteriosclerosis**
Calcification	• Focal	• Generalised
Aetiology	• Hyperlipidemia	• Chronic kidney disease, hypertension, diabetes, aging, osteoporosis
Mechanisms	• Lipid formation • Inflammation • Oxidative stress • Differentiation of VSMC to osteoblastic and chrondocytic cells • Matrix vesicle and apoptosis	• Differentiation of VSMC to osteoblastic and chrondocytic cells • Matrix vesicles, apoptosis • Loss of inhibitors of calcification • Dysregulated calcium and phosphate metabolism
Clinical Features	• Ischaemia, infarction	• Arterial stiffness, increase pulse wave velocity, isolated systolic hypertension

Table 1.1: Comparison of intimal and medial calcification.

1.2 Overview of the molecular and cellular regulation of vascular calcification

A number of different mechanisms are thought to be involved in regulating the initiation and/or progression of vascular calcification (see Figure 1.2). Several reviews have been recently published discussing various mechanisms that are involved in regulating vascular calcification (Giachelli, 2009; Sage et al., 2010; Shanahan et al., 2012; Fang et al., 2013).

Vascular calcification and bone mineralisation display many similarities. Osteogenic and chondrogenic differentiation of VSMCs involves the up-regulation of transcription factors for bone and cartilage, such as Cbfa-1/Runx2, osterix, Msx2 and Sox9 (Shanahan et al., 1999; Moe et al., 2003). Bone related proteins, for example bone sialoprotein, osteocalcin, type 1 collagen and alkaline phosphatase and cartilage related proteins such as type 2 collagen and aggrecan, are also detected in mineralised blood vessels (Tyson et al., 2003). Osteo/chondrogenic differentiation of VSMCs occurs early in the pathogenesis of vascular calcification as shown in a study by Shroff *et al.* (Shroff et al., 2008). The occurrence of vascular calcification increases with continued exposure to mineral dysregulation in patients with CKD (Fang et al., 2013). In addition, smooth muscle cell markers such as SM22α and α-smooth muscle actin are down-regulated in mineralised vessels (Demer and Tintut, 2008). This was confirmed in a study that showed an increase in DNA methyltransferase activity and methylation in the promoter region of the SM22α gene of human VSMCs and rat aortic rings cultured in the presence of high phosphate (Montes de Oca et al., 2010). Methylation resulted in the loss of SM22α expression, which was in turn reversed by inhibition of promoter methylation. VSMCs have been shown to differentiate into osteoblast-like cells *in vitro* when cultured in the presence of high phosphate and calcium (Yang et al., 2004; Ciceri et al., 2012). Further *in vivo* work confirmed that VSMCs give rise to osteo/chondrogenic precursors and chondrocytes in calcifying arteries of $MGP^{-/-}$ mice (Speer et al., 2009). In this study, the authors also showed increased phosphorylation of Erk 1/2 prior to the loss of VSMC markers in mouse aortic medial VSMCs treated with high phosphate.

Pericytes, calcifying vascular cells (CVCs) and adventitial fibroblasts can also undergo osteo/chrondogenic differentiation (reviewed by Johnson et al., 2006; Giachelli, 2009). CVCs are a subpopulation of VSMCs that share similar features to pericytes (Bostrom et al., 1993). Both CVCs and pericytes express 3G5 and form calcified nodules

in the presence of elevated phosphate (as reviewed by Collett and Canfield, 2005). These nodular cells also have increased levels of apoptosis (Proudfoot et al., 2000). It is clear from these studies that a variety of cell types present in the vessel wall are capable of undergoing osteo/chrondogenic differentiation.

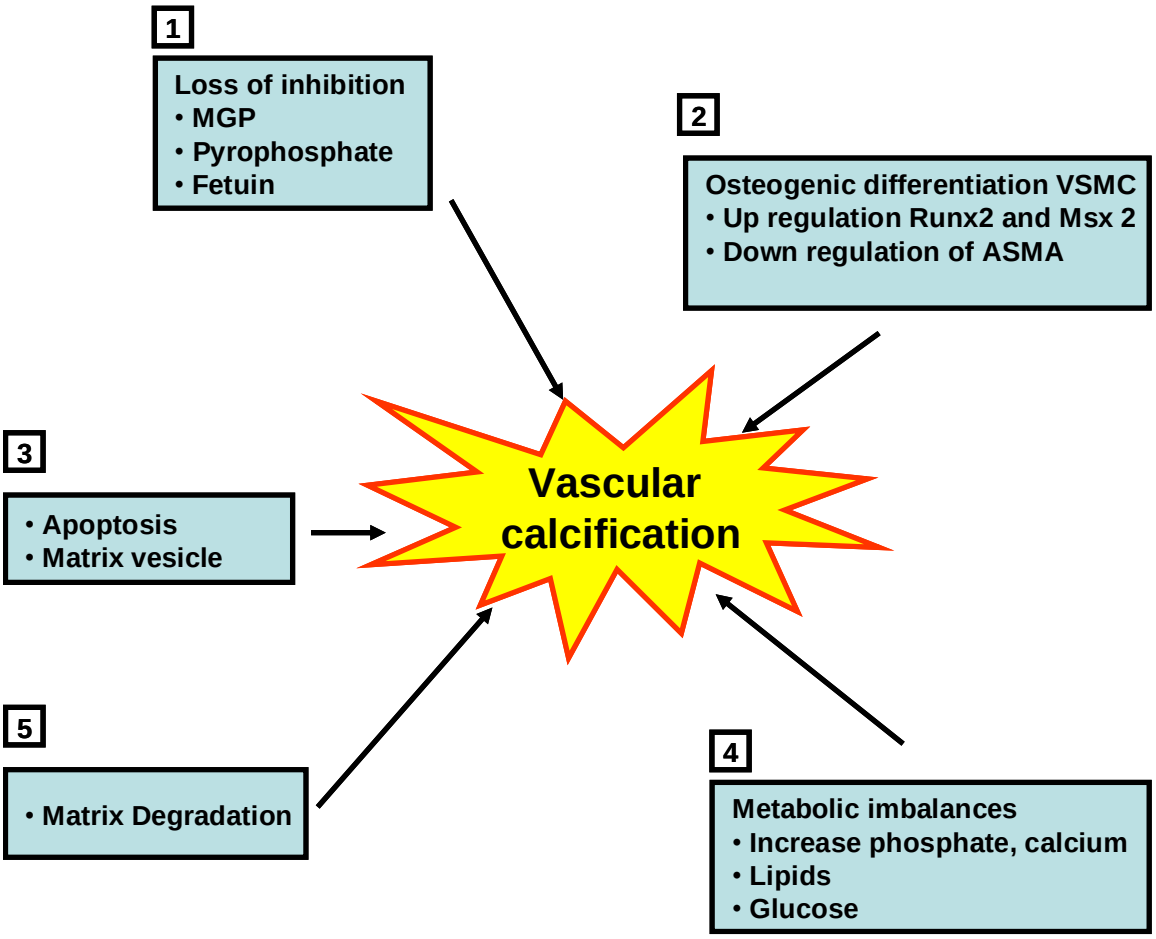

Figure 1.2: A number of factors are involved in modulating vascular calcification (1) loss of inhibition, (2) osteo/chondrogenic differentiation of vascular cells, (3) apoptosis, (4) dysregulation of calcium and phosphate homeostasis, lipid, glucose, and (6) matrix degradation. These factors are all involved in the initiation and/or progression of vascular calcification. Modified and adapted from Giachelli, 2009

Apoptotic bodies and matrix vesicles are produced by VSMCs in response to insults such as uraemic toxins, elevated calcium and phosphate, hypertension and oxidative stress (as reviewed in Kapustin and Shanahan, 2009). Matrix vesicles and apoptosis are

observed as part of the normal bone mineralisation process (Nahar et al., 2008). Matrix vesicles bud off from the plasma membrane of VSMCs and are smaller than apoptotic bodies (Proudfoot et al., 2000). Matrix vesicles and apoptotic bodies can both act as a nidus for hydroxyapatite deposition. Under normal circumstances, these vesicles are removed by phagocytosis. However, when the insults are severe, phagocytosis is limited, thus initiating the calcification process (Shanahan, 2006). Bennett's group also showed that induction of VSMC apoptosis in $ApoE^{-/-}$ mice using Diptheria toxin was associated with an increase in the size and calcification of atherosclerotic plaques (Clarke et al., 2008). A recent study of iliac arteries taken from dialysis patients showed that these microcalcifications contained hydroxyapatite and whitlockite. A further review suggested that these microcalcifications arise from nanocrystals and their core-shell structure contains apoptotic bodies and matrix vesicles that form the nidus for calcification (Schlieper et al., 2010).

Elastin degradation is thought to be one of the initial steps in the development of calcification both in the intimal and medial layers (Janzen and Vuong, 2001; Hosaka et al., 2009). The breakdown of elastin, which is a major component of the vessel wall, is mediated by matrix metalloproteinase-9 (MMP-9) (Basalyga et al., 2004). Elastin degradation products stimulate TGF-ß release (Shantsila and Lip, 2009), which then up-regulates osteogenic transcription factors, such as Runx2/Cbfa1 (Franceschi and Xiao, 2003). Clinically, elastin degradation products are detected in patients with Marfan's syndrome who can develop aortic calcification (Mizobuchi et al., 2009).

Mineral metabolism in CKD patients plays an important role in the pathogenesis of vascular calcification. As CKD progresses, hyperphosphatemia worsens and vitamin D levels are reduced (Fang et al., 2013). Increased phosphate levels have been shown to be associated with atherosclerotic calcification in uraemic, high fat-fed $LDLR^{-/-}$ mice (Davies et al., 2003). Hyperphosphatemia may induce vascular calcification in CKD patients in a number of ways. First, high extracellular phosphate levels up-regulate the expression of the type III sodium-phosphate co-transporter, Pit 1, thereby increasing intracellular phosphate (Giachelli, 2009), which results in increased expression of Runx2/Cbfa1. Second, hyperphosphatemia causes the down-regulation Gas6-Axl signalling, which results in VSMCs apoptosis (Collett et al., 2007; Son et al., 2006), which in turn can promote vascular calcification (Proudfoot et al., 2000). Furthermore, it has been shown that a high phosphate diet induces calcification in DBA/2 mice (El-Abbadi et al., 2009). Studies have

also shown that calcium increases mineral deposition by VSMCs in the presence of normal phosphate levels (Yang et al., 2004). In the presence of high phosphate levels the process of calcification is further increased by calcium. Low levels of vitamin D are also seen in patients with CKD, and vitamin D deficiency has been shown to be associated with increased vascular calcification (Barreto et al., 2009). On the other hand, a supra-physiological dose of vitamin D has been shown to induce vascular calcification in a rat model of secondary hyperparathyroidism (Henley et al., 2005). Fibroblast growth factor-23 (FGF-23) with its cofactor klotho has been shown to decrease phosphate absorption in kidneys and inhibit active vitamin D production. It has been shown that klotho deficiency is associated with calcification in chronic kidney disease patients (Hu et al., 2011).

Physiologically, calcium and phosphate are both present within the extracellular fluid, but interestingly there is no spontaneous ectopic precipitation, which suggests the presence of circulating endogenous inhibitors of calcification (see Table 1.2). A range of calcification promoters which drive VSMC osteogenic differentiation can also be present in the blood (see Table 1.2). It has been suggested that vascular calcification may result from an imbalance between inhibitors and promoters of the condition. Inhibitors of calcification have also been identified using knock-out mouse models, including Matrix Gla Protein (MGP), Fetuin A, bone morphogenetic protein-7 (BMP-7), osteoprotegerin (OPG) and pyrophosphate (reviewed by Kapustin and Shanahan, 2009), several of which have been linked with gene mutations in humans (see Table 1.3).

Inhibitors	**Promoters**
MGP	Alkaline phosphatase
Fetuin A	BMP-2 & 4
Pyrophosphate	Smad 4
Osteoprotegerin	High phosphate levels
BMP-7	Warfarin

Table 1.2: Some of the factors which inhibit or promote vascular calcification.

Gene	Mouse Mutant Phenotype	Human Genetic Mutation
Matrix Gla Protein	Arterial and valve calcification (Luo et al., 1997)	Keutel Syndrome/cartilage and soft tissue calcifications (Hur et al., 2005)
Fetuin A	Soft tissue calcifications (Schafer et al., 2003)	Not known
Osteoprotegerin	Vascular calcification and osteoporosis (Bucay et al., 1998)	Not known
Ank (pyrophosphate transporter)	Soft tissue calcifications (Harmey et al., 2004)	Calcium Pyrophosphate Deposition Disease (Zaka et al., 2006)
Smad 6	Endocardial cushion defects, valvular calcification (Galvin et al., 2000)	Not known
Lamin A (LMNA)	Cardiac and skeletal myopathy; progressive loss of vascular SMC and calcification (Varga et al., 2006)	Hutchinson-Gilford Progeria/calcification associated with atherosclerosis (Eriksson et al., 2003)
Osteopontin (OPN)	Increased calcification in OPN -/-, MGP-/-mice (Speer et al., 2002)	Not known

Table 1.3: Genetic mutations associated with vascular calcification in mouse models and in humans (modified from Giachelli, 2009; Persy and D'Haese, 2009.)

Inflammatory cytokines play important roles in the pathogenesis of atherosclerosis. Monocytes and macrophages internalise calcium and phosphate crystals, which in turn stimulates the release of TNF-α, and Interleukin-6 and 8 (Nadra et al., 2005). TNF-α stimulates the Wnt/β-catenin pathway which then up-regulates Msx2 resulting in osteogenic differentiation of VSMCs (Al-Aly et al., 2007). TNF-α also has been shown to

inhibit the activation of Gas 6 thus promoting apoptosis, which induces vascular calcification (Son et al., 2008)

In conclusion, vascular calcification is the development of mineralised tissue in blood vessels. It is an active, cell-mediated and highly regulated process which involves multiple factors. Over the past decade, there has been a greater understanding of the mechanisms that contribute to and modulate the progression of vascular calcification. However, it is still unclear how (or whether) this process can be regressed or prevented. Therefore, there are many unresolved issues and challenges to overcome before a novel targeted therapy can be developed.

This project has developed from work in the host lab that has examined the mechanisms by which bisphosphonates may regulate vascular calcification. These studies are discussed below.

1.3 Regulation of vascular calcification by bisphosphonates

Bisphosphonates have been used for many years to treat osteoporosis and other conditions, in particular osteitis deformans (Paget's disease of the bone), hypercalcaemia, and multiple myeloma. There are two groups of bisphosphonates with distinct modes of action; these are nitrogen-based bisphosphonates and non-nitrogen based bisphosphonates. Bisphosphonates are non-hydrolysable pyrophosphate (PPi) analogues and PPi is a well known inhibitor of calcification. Studies have shown that bisphosphonates inhibit calcification in uraemic rats and in humans (Lomashvili et al., 2009; Russell et al., 1972).

Nitrogen-based bisphosphonates act via the mevalonate pathway (Figure 1.3), which is involved in multiple processes including the synthesis of both cholesterol and non sterol isoprenoids (Buhaescu and Izzedine, 2007). Non sterol isoprenoids are vital for the post translational modification of small GTPases through a process called ‘prenylation’ (Coxon et al., 2004). GTPases are important for cell growth, migration and differentiation. In studies using cancer cells, it has been shown that nitrogen-based bisphosphonates inhibit farnesyl pyrophosphate synthase, an essential enzyme in the mevalonate pathway (Swanson and Hohl, 2006), with an ensuing decrease in isoprenoid lipids. Small GTPases and prenylation are discussed further in section 1.4.

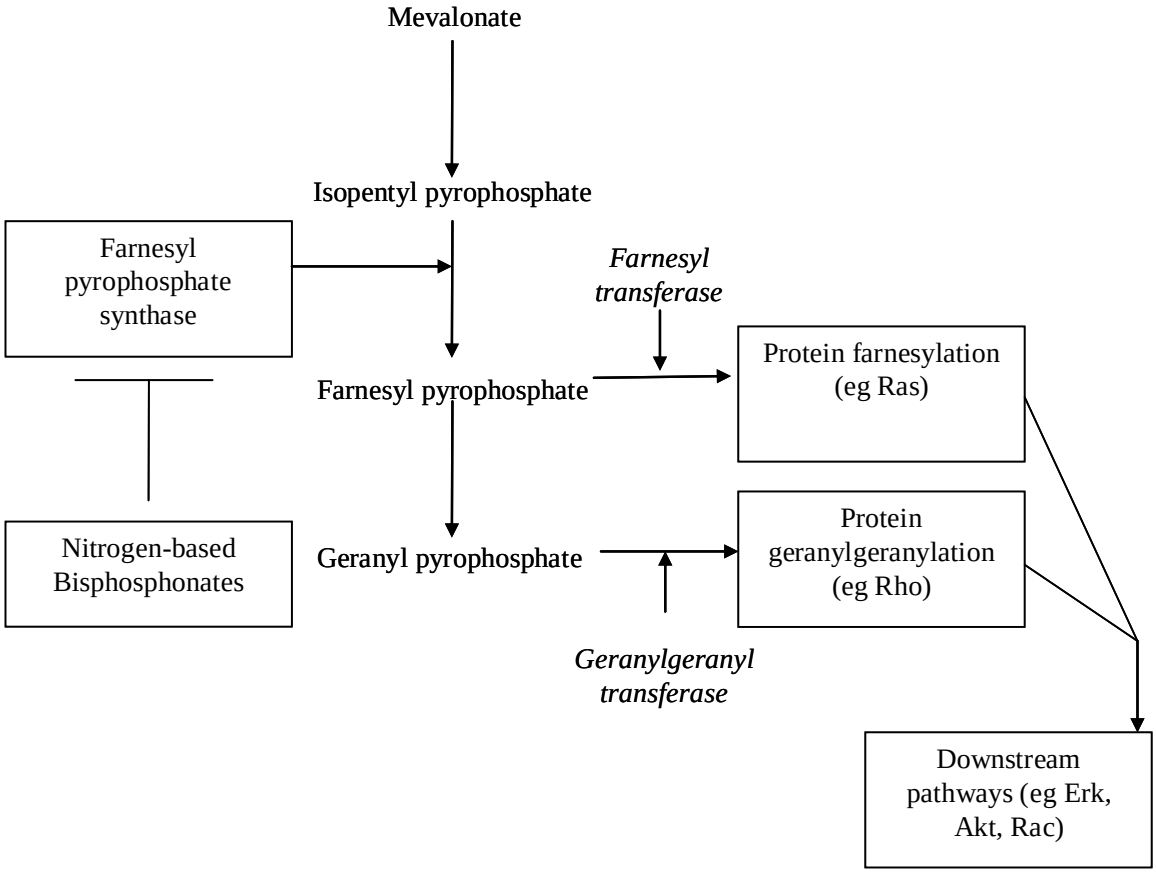

Figure 1.3: The Mevalonate pathway. Nitrogen based bisphosphonates inhibit the enzyme farnesyl pyrophosphate synthase resulting in reduced farnesyl and geranylgeranyl pyrophosphate, which are essential for the prenylation of small GTPases (e.g. Ras, Rho) which, in turn, are important for intracellular signalling, cell growth and proliferation.

Unpublished data from the host laboratory has shown that nitrogen-based bisphosphonates inhibit mineralisation by their effects on the mevalonate pathway (Sinha, 2010). VSMCs were treated with a mineralisation-inducing medium containing either a nitrogen-based bisphosphonate (zoledronate) or control. These studies demonstrated that zoledronate inhibited mineral deposition by VSMCs. Farnesyl pyrophosphate was then given to the zoledronate group, which resulted in the restoration of mineralisation, suggesting that nitrogen-based bisphosphonates inhibit calcification by inhibiting farnesyl pyrophosphate synthase and the production of farnesyl pyrophosphate. Work from the host laboratory further demonstrated that non-nitrogenous based bisphosphonates do not inhibit vascular calcification by this mechanism.

The effect of nitrogen-based bisphosphonates on the small GTPase Ras was then determined. Accordingly, pull-down assays, cell fractionation and western blotting demonstrated that zoledronate decreased Ras GTPase activation and membrane localisation. These studies suggest that prenylation of GTPases may be involved in the regulation of mineral deposition by VSMCs, thereby raising the exciting possibility that prenylation could be a potential target for therapeutic intervention of vascular calcification. This possibility will be investigated further in this study.

1.4 Prenylation and GTPases

GTPases are small proteins with a molecular weight of between 20 and 40 KDa. Over one hundred GTPases have been identified, including Ras, Rho, Rab, Sarl/ADP and Ran (Takai et al., 1990). A number of intracellular signals are dependent on these GTP-binding proteins. For example, activated Ras proteins regulate many downstream protein kinases which then regulate cellular proliferation, differentiation, growth and apoptosis, as well as the actin cytoskeleton (Lowy and Willumsen, 1993).

Four different Ras proteins (H-Ras, K-Ras 4B, K-Ras 4A and N-Ras) are expressed from three Ras genes (Saxena et al., 2008). The size of the Ras protein is 21 KDa. Ras mutations have been detected in approximately 30% of all cancers. For example, 90% of patients with pancreatic cancer, colorectal (50%) and lung cancers (30%) have mutated Ras (Malumbres and Barbacid, 2003). Ras requires post-translational modification in order to be activated. The post-translational modification involves prenylation, proteolysis,

carboxymethylation and palmitoylation (Glomset and Farnsworth, 1994) (see below and Figure 1.4). This modification results in the conversion of the GTPase into a more lipophilic state, allowing its transfer from the cytosol to the inner surface of the plasma membrane (Clarke, 1992).

Protein prenylation is the covalent attachment of either a farnesyl (15-carbon) or a geranylgeranyl (20-carbon) moiety to the cysteine residue located in a tetrapeptide CAAX (C = cysteine, A = any aliphalitic amino acid, X is either methionine or serine) sequence of G-proteins and is mediated by the enzymes farnesyl tranferase and geranylgeranyl transferase, respectively (Zhang and Casey, 1996)**.** This process is termed either farnesylation or geranylgeranylation. N-Ras and K-Ras can be either farnesylated or geranylgeranylated. H-Ras is more likely to be farnesylated, however cross prenylation can also occur (Casey et al., 1991).

The prenylated protein then moves to the endoplasmic reticulum where Ras converting enzyme 1 (RCE1) removes AAX by proteolysis. Subsequently the prenylated protein methyltransferase (PPMTase) mediates the methylation of the carboxy terminus. N-Ras, H-Ras and K-Ras4A then undergo palmitoylation and are transferred to the plasma membrane (Saxena et al., 2008). However, K-Ras4B does not undergo the palmitoylation process and instead is transported directly to the plasma membrane (Hancock et al., 1989.)

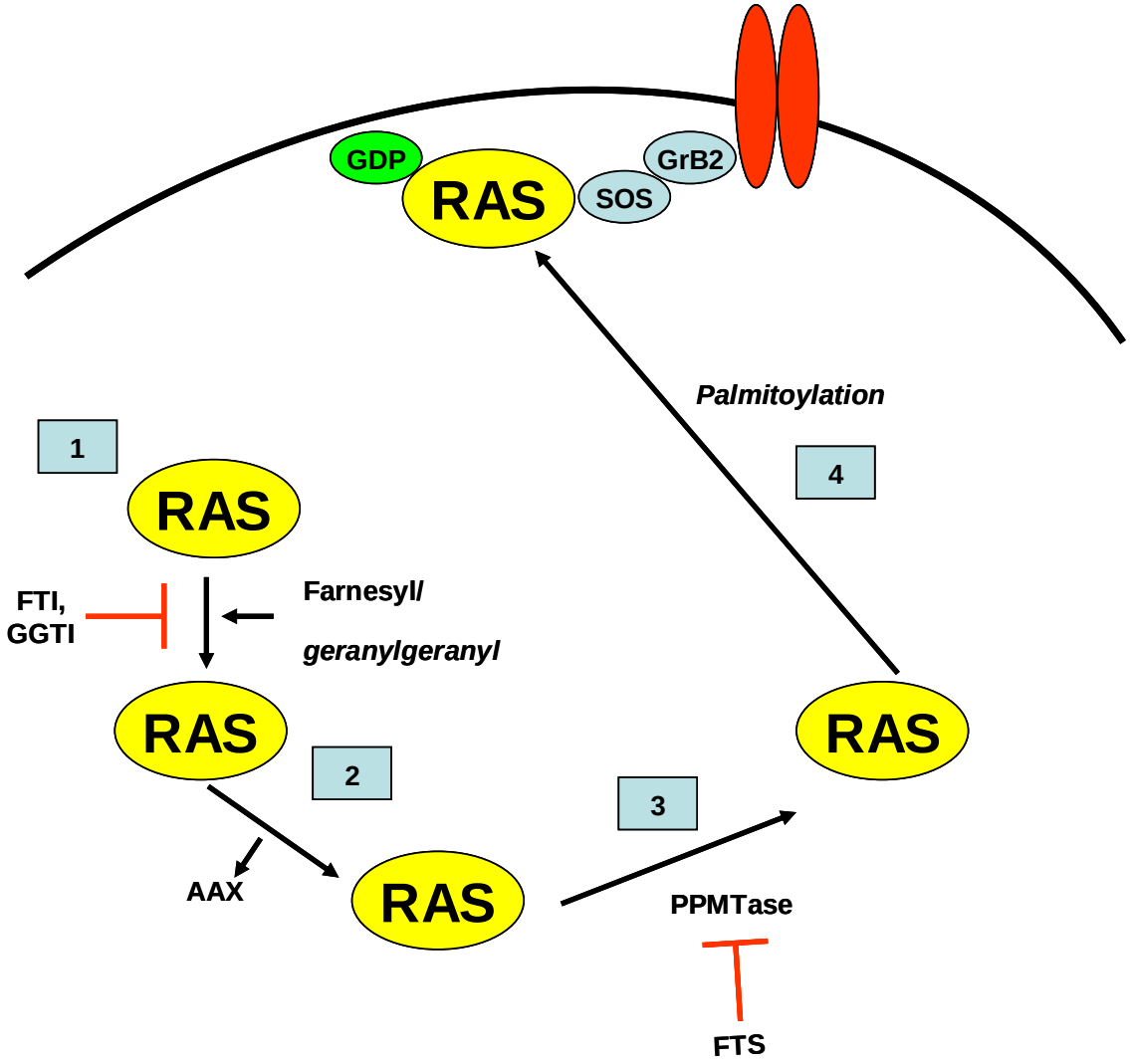

Figure 1.4: A schematic showing the process of post-translational modification of GTPase Ras. This process involves four stages resulting in the localisation of Ras in the plasma membrane. **1. Prenylation** – This process involves farnesylation (mediated by farnesyl transferase) or geranylgeranylation (mediated by geranylgeranyl transferase), which can be inhibited by farnesyl transferase inhibtiors (FTI) or geranylgeranyl transferase inhibitors (GGTI). **2**. **Proteolysis** – Removal of the AAX moiety, forming carboxyl-terminal S-farnesylcysteine. **3**. **Methylation** - carboxyl-terminal S-farnesylcysteine is carboxylmethylated by prenylated protein methyltransferase (PPMTase). This process can be inhibited by Farnesyl Thiosalicylic Acid (FTS). **4. Palmitoylation** – A reversible process which is important for the attachment to the cell membrane.

Ras is activated by the binding of GTP which is mediated by guanine nucleotide exchange factors (GEFs). GTPase activating proteins (GAPs) convert activated Ras to an inactive form bound to GDP (Takai et al., 2001), thereby preventing activation of its downstream pathways. Extracellular signals such as growth factors and cytokines bind to tyrosine kinase receptors resulting in the activation of Ras by GEF (see below; Figure 1.5). In cancer cells, GAPs are dysregulated, which allows uninhibited stimulation by the mutated Ras. Activation of Ras can lead to the stimulation of a series of downstream effector pathways including Raf/ERK/MAPK, PI3K/AKT, PLC/PKC/cyclin D1 and Rac/Rho (see below and Figure 1.6).

Finally, Ras activity is tightly controlled by the interaction between GEF and GAP. This step also involves the guanine-nucleotide exchange factor, Son of Sevenless (SOS). SOS moves to the surface from the cytoplasm through the help of adapter proteins such as Grb2 (Boriack-Sjodin et al., 1998). SOS forms a complex with Grb2 by binding with the carboxy-terminus of SOS (Schlessinger, 1993). The presence of Ras at the surface increases the amount of SOS which allows for GEFs to bind to Ras.

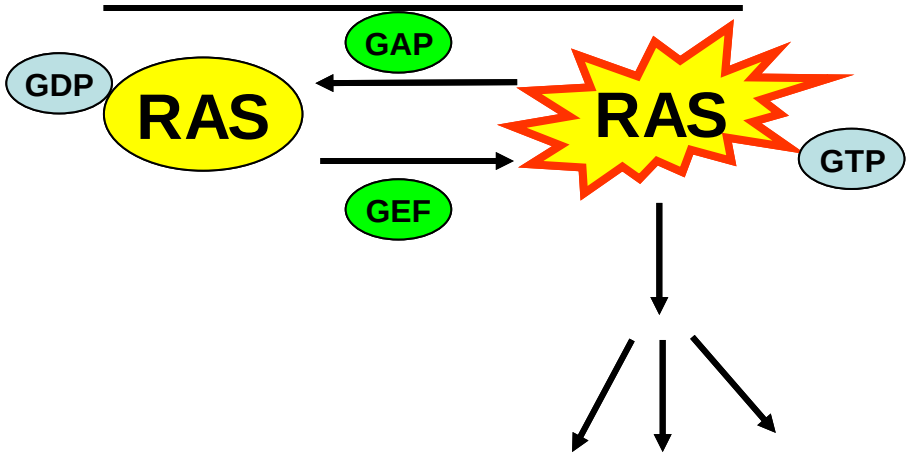

Figure 1.5: Regulation of small G-Protein activity is controlled by guanine exchange factors (GEF) and GTPase activating proteins (GAP)

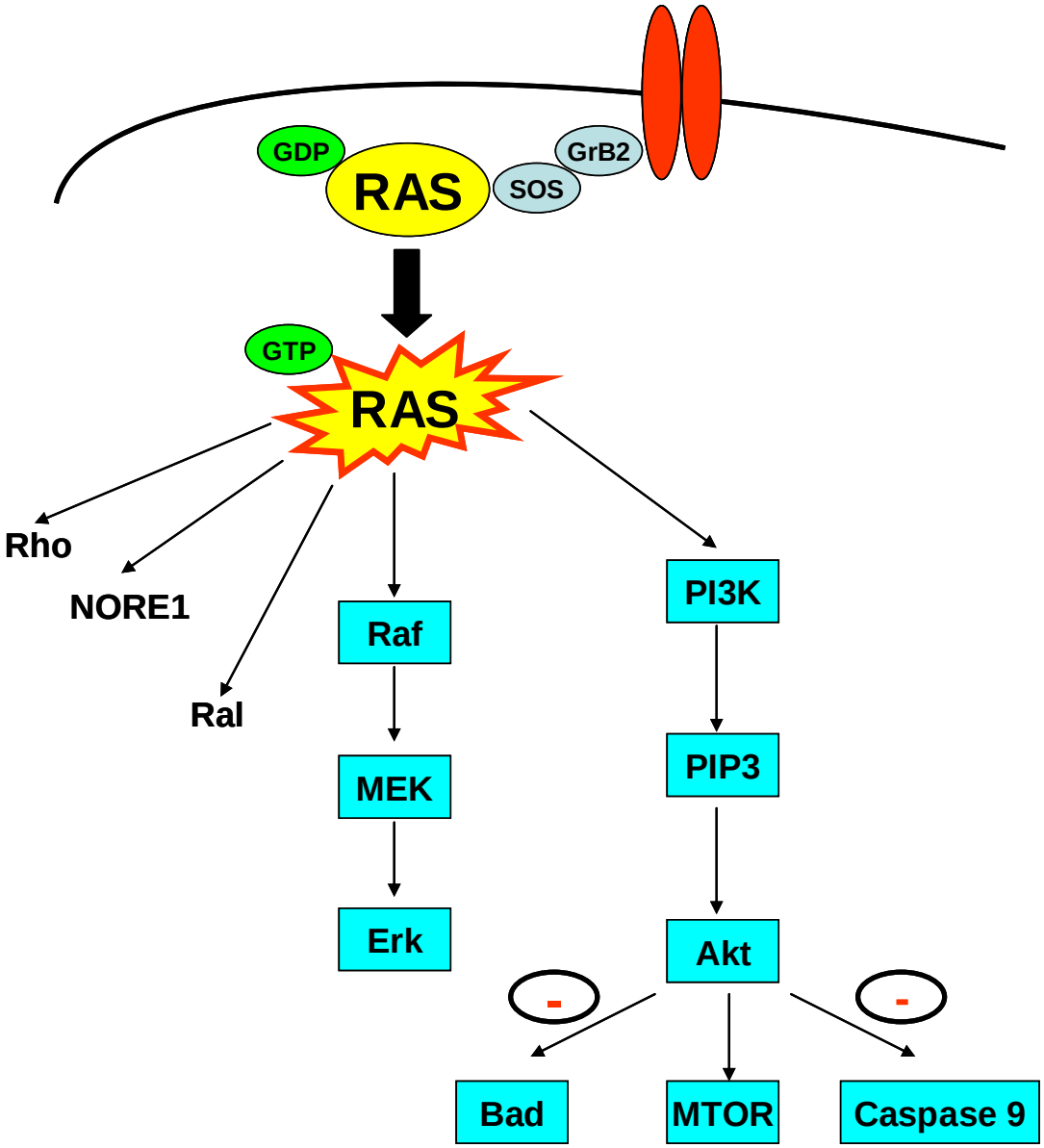

Figure 1.6: Ras effector pathways. Growth factors stimulate guanine nucleotide factor SOS which is attached to the receptor by forming a complex with Grb2 complex. This results in activation of Ras by attachment of GTP. Ras can then activate a number of downstream signalling pathways.

1.5 Signalling pathways: downstream effectors of Ras

A number of downstream signalling pathways are activated by Ras (see below; Figure 1.6). These pathways have a number of effects downstream that include cell proliferation, differentiation, inhibition of apoptosis and cell cycle progression. These pathways will be discussed further below.

1.5.1 Ras/Raf

Raf, a serine threonine kinase, is a direct downstream effector of activated Ras. There are three types of Raf (A-Raf, B-Raf, C-Raf). Phosphorylation is important for the activation of Raf. Ras binds to the amino terminal portion of Raf and this interaction results in phosphorylation of Raf (Pumiglia et al., 1995). Raf–Ras then stimulates MEK1/2. MEKs further activate Erk1/2 or MAPKs. Phosphorylated Erk1/2 activates transcription factors, for example Elk1, c-jun, c-myc and c-Fos, which are important for cell proliferation (Lewis et al., 1998). The Ras/Raf pathway is important for the progression of cells from G1 into the S phase.

1.5.2 Ras/PI3K/Akt signalling

The Ras/PI3K/Akt pathway is particularly important for cell survival. PI3K is a lipid kinase and can be activated by either Ras or receptor tyrosine kinase (RTK). There are 3 subtypes of PI3K, Class 1, 2, 3 (Fry, 1994). PI3K class 1 contains a catalytic subunit of 110 kDa, which contains a Ras binding domain and a regulatory subunit of 85 kDa (Fruman et al., 1998). Ras binds to the catalytic subunit of PI3K, which results in the formation of PIP3 (phophatidylinositol tri-phosphate) (Fry, 2001). PIP3 act as a second messenger activating the serine/threonine kinase Akt (Protein Kinase B, PKB). In the presence of growth factor signalling, the level of PIP3 increases, resulting in phosphorylation of Akt. Akt can be divided into 3 different isoforms (Akt1, Akt2, Akt3). All 3 types of Akt are activated by PI3K. Phosphorylation of both Threonine-308 and Serine-473 of Akt is required for its activation (Jiang et al., 2000).

Akt is anti-apoptotic and essential for cell survival (Datta et al., 1999). There are several downstream pathways by which Akt is involved in cell survival. This includes phosphorylation of glycogen synthase kinase 3 (GSK-3) by Akt, resulting in the accumulation of β-catenin and activation of c-myc and cyclin D1 (Cross et al., 1995; Diehl et al., 1998). In addition, Akt inactivates caspase-9, a negative regulator of Bad, and

Foxhead transcription factor (FKH) (Brunet et al., 1999), which are both pro- apoptotic proteins. Akt also stimulates mammalian target of rapamycin (mTOR), which is essential for cell cycle progression, and is also known to stimulate NF-kB (Ozes et al., 1999),

1.5.3 Ras/Ral

Ras also activates Ral-A and Ral-B which are known to be important in cell proliferation and survival (Wolthuis and Bos, 1999). It is thought that Ras GTPase also stimulates phopholipase D1 and Cdc42 working alongside the Akt pathway (Saxena et al., 2008). The activity of Ras GTPase occurs not only by binding to the effectors but also by recruitment of other GTPases such as those in the Rap and Rho subfamily.

1.5.4 Ras/Rho/Rac

Rho proteins belong to the Ras superfamily of small GTPases and are important for the regulation of the actin cytoskeleton, focal adhesion and cell proliferation. Examples of Rho proteins include Rho, Rac, and Cdc42 (Crul et al., 2001). Cdc42 activates Rac which stimulates Rho. Rho is important for the regulation of cell adhesion, filopodia formation, membrane ruffling and the actin cytoskeleton (Saxena et al., 2008). Rho kinase (ROCK) is a downstream effector of this pathway. Unregulated ROCK activity is associated with endothelial dysfunction, cerebral ischaemia, coronary vasospasms and the metabolic syndrome (Zhou and Liao, 2009). Recent studies have shown that inhibition of RhoA/ROCK signalling increases vascular calcification *in vitro* by increasing alkaline phosphatase activity in VSMCs (Varga et al., 2006). The authors in the study concluded that RhoA/ROCK signalling is an important inhibitor of vascular calcification. Rho also inhibits p21, resulting in cells moving into the S phase of the cell cycle (Olson et al., 1998).

1.5.5 Other effectors of Ras signalling pathway

There are other effectors of Ras signalling which include AF-6, protein kinase C-zeta and Nore1. The interaction between AF-6 and Ras is considered to be mediated by Bcr Kinase (Radziwill et al., 2003), whilst the interaction between Ras and Nore1 may possibly regulate of apoptosis, and this is discussed further below.

1.5.6 Ras and apoptosis

Depending on the cellular context, Ras may stimulate either anti- or pro-apoptotic signalling by activating various downstream effectors of Ras, as shown in Figure 1.7. The

binding of Ras to PI3K activates Akt, which results in anti-apoptotic signalling via the various mechanisms described above. Ras can also activate Rac GTPase via the Rac-specific GEF, Tiam1 (Cox and Der, 2003). Rac activation results in the formation NF-κB, which simulates anti-apoptotic signalling (Romashkova and Makarov, 1999). However, activation of the Ras/Raf/MEK/Erk pathway can result in either anti- or pro-apoptotic signalling depending on the situation. For example, when fibroblasts are induced to undergo apoptosis, Ras has been shown to stimulate a pro-apoptotic pathway mediated by Raf/Erk (Kauffmann-Zeh et al., 1997) and apoptosis was prevented by PI3K activation. In a related study, activated MEK1 has been shown to have 2 different effects in 3Y1 rat fibroblasts (Tsuneoka and Mekada, 2000).

The other downstream effectors of Ras such as Nore1 and RASSF1 have been shown to promote apoptosis (Cox and Der, 2003; Feig and Buchsbaum, 2002). The interaction between Ras-GTP and RASSF1 induces apoptosis in 293T cells (Vos et al., 2000). Nore1 is closely related to RASSF1 and both are found in complexes with Mst1 protein, a proapoptotic protein kinase (Ortiz-Vega et al., 2002) that is capable of stimulating caspase 3 activation. Growth factor activation results in active Ras binding to RASSF1/Nore1/Mst1 to promote apoptosis (Khokhlatchev et al., 2002).

In conclusion, Ras involvement in cancer cell biology is well known, but its involvement in vascular calcification has not been investigated. Ras may be anti-apoptotic or pro-apoptotic depending on the cellular context. Therefore, one of the objectives of this project is to establish whether Ras plays a role in the regulation of vascular calcification

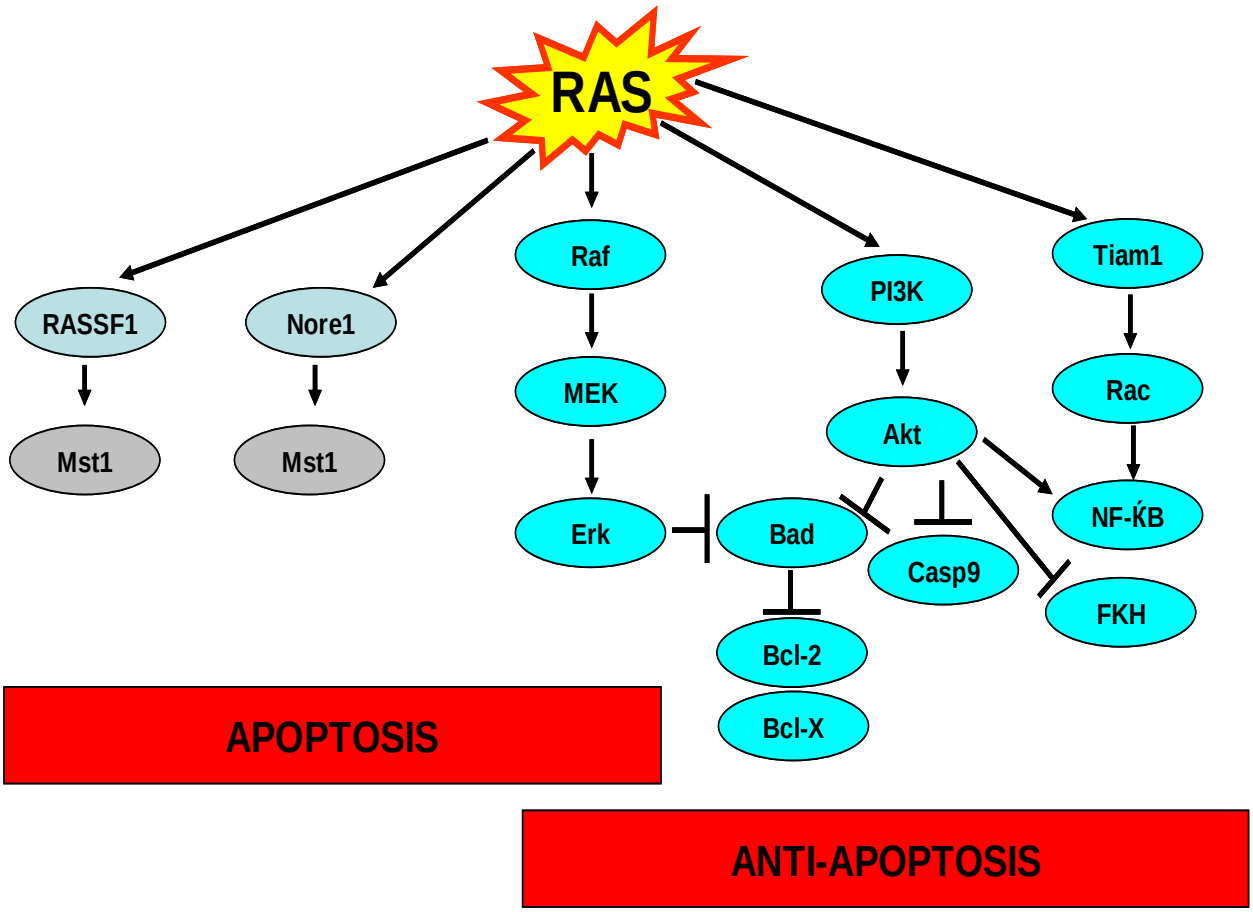

Figure 1.7: Ras GTPase can be anti or pro-apoptotic depending on the cellular context. Pro-apoptotic pathways are the RASSF1 and Nore. Both RASSF and Nore form complexes with Mst1 which is potent stimulator of caspase 3. The Raf/Erk pathway could pro- or anti-apoptotic depending in the situation. Anti-apoptotic pathways are the PI3K/Akt and Tiam1. Akt phosphorylation promotes survival factors such as Bcl-2 and Bcl-X by phosphorylating Bad. Akt also inhibits caspase 9 and forkhead transcription factors (FKH). Tiam1 (Ral-GEF) stimulated the production of NF-ḰB which is an anti-apoptotic. Modified and adapted from (Cox and Der, 2003)

1.6 Farnesylation as a novel therapeutic target for vascular calcification

The work produced by the host lab suggests that prenylation of GTPases may be involved in the modulation of vascular calcification (see section 1.3), thus making the inhibition of farnesylation a potential novel therapeuti**c** target for this devastating pathology. Ras is activated by farnesylation, which makes it a likely candidate to be involved in regulating vascular calcification, although, it is noteworthy that several other proteins can also undergo farnesylation (Basso et al., 2006) (see Table 1.4). Farnesylation can be inhibited by farnesyl transferase inhibitors (FTIs) which have been developed for use in cancer cells. These drugs and their role in cancer cells and vascular cells will be discussed below.

H- Ras	Rho B
K- Ras	(Protein Tyrosine phosphatase) PRL 1
N- Ras	(Protein Tyrosine phosphatase) PRL 2
Centromere associated proteins (CENP-E)	(ProteinTyrosine phosphatase)PRL 2
Centromere associated proteins (CENP-F)	Rheb
Prelamin A	Rheb2

Table 1.4: Farnesylated proteins. These farnesylated proteins undergo farnesylation which is mediated by farnesyl transferase.

1.7 Farnesyl transferase inhibitors (FTIs)

Following the discovery of the oncogenic action of mutated Ras, farnesyl transferase inhibitors (FTIs) were developed in order to try to prevent its downstream effects. FTIs can be divided by virtue of their mechanism of action into:

(i) Peptidomimetics; which mimic the CAAX attachment site and thereby compete with Ras for the binding of farnesyl (eg L-739,749; L744,832; FTI -276; FTI -277)

(ii) Farnesyl pyrophosphate (FPP) analogues; which compete with FPP at the FTase binding sites (eg L-704,272; manumycin A)

(iii) Bisubstrate analogues; which have both features (FPP analogue and peptidomimetic) (eg: BMS-186511)

The actions of these inhibitors on cancer cells and in cardiovascular cells are discussed below.

1.7.1 Effect of FTIs on cancer cell lines

The growth of a number of tumour cell lines is inhibited by FTIs, both *in vitro* and when cultured as xenografts *in vivo* (Liu et al., 1998). Inhibition of farnesylation results in G1 cell cycle arrest and subsequent apoptosis of cancer cells. Interestingly, the sensitivity of FTIs does not equate to the presence of oncogenic Ras mutations. For instance, breast cancer cells which are deficient in mutated Ras protein but have activated protein kinases still respond to these drugs (End et al., 2001), suggesting they may exert pleiotropic effects.

The inhibition of the PI3K/Akt pathway by FTIs may contribute to their pro-apoptotic effects on cancer cells. Work on ovarian and pancreatic cells has shown that FTIs can reduce Akt activity (Jiang et al., 2000), although other studies contradict this (Sun et al., 2004). It is clear from these studies that Ras can have different effects that are dependent on which signalling pathway is being activated. R-115777 (tipifarnib), SCH 66336 (lonafarnib) and BMS-214662 are drugs that have been extensively studied in haematological malignancies, especially acute myeloid leukaemia. Phase III trials of tipifarnib were negative in pancreatic cancers (Basso et al., 2006). One possible reason for this is that K–Ras and N-Ras can undergo geranylgeranylation when farnesylation is blocked. These geranylgeranylated Ras proteins can exert biological activity.

Controversy still remains with regard to which farnesylated proteins are the key targets for FTIs (Cox and Der, 1997). For example, centromere associated proteins (CENP-E and CENP-F) are involved in mitotic processes and these are farnesylated proteins. The inhibition of these farnesylated proteins will result in growth arrest in cancer cell lines.

1.7.2 Effect of FTIs on atherosclerosis and cardiovascular disease

Previous studies have shown that inhibition of Ras either by FTIs or dominant-negative farnesyl transferase results in reduction of VSMC proliferation and migration, which are important processes in the development of atherosclerosis (Kouchi et al., 1999; Solomon and Goalstone, 2001). It was demonstrated that local delivery of FTI, in this case, FPT111 prevented neointima formation after balloon angioplasty (Work et al., 2001). 3 deazaadenosine, a Ras inhibitor, has been shown to inhibit VSMC proliferation and migration (Sedding et al., 2009).

Transfection of dominant-negative Ras into carotid vessels results in decreased intimal thickness following carotid injury *in vivo* (Indolfi et al., 1995; Ueno et al., 1997). S-trans, trans-Farnesyl Thiosalicylic Acid (FTS), a prenylated protein methyltransferase inhibitor, has also been shown to attenuate atherosclerosis in $ApoE^{-/-}$ mice by reducing Ras activity (George et al., 2002). Furthermore, manumycin A reduces the development of atherosclerosis in $ApoE^{-/-}$ mice (Sugita et al., 2007). In this latter study there was a reduction in activated Ras and phosphorylated Raf-1, raising the possibility that this downstream effector pathway is involved in the development of atherosclerosis.

Hutchinson-Gilford progeria syndrome is a progeroid condition in which there is increased farnesyl-prelamin A expression (Mehta et al., 2010). This disease manifests as premature aging and patients usually die of heart attack or stroke. Interestingly, recent studies have shown that an FTI (R-115777, Zanestra) can prevent the onset and progression of cardiovascular disease in a mouse model of progeria (Capell et al., 2008). Furthermore, the results of the recent clinical trial on children with Hutchinson-Gilford progeria syndrome demonstrated that the farnesyl transferase inhibitor, lonafarnib, decreased arterial pulse wave velocity in these patients suggesting that it improved vascular stiffness (Gordon et al., 2012), which is associated with vascular calcification. Prelamin A has also been shown to be associated with degeneration of VSMCs in the medial layer and increased atherosclerosis (Ragnauth et al., 2010). Experiments have shown that prelamin A is predominantly expressed in cells undergoing senescence through increased oxidative stress subsequently contributing to the pathogenesis of vascular calfication (Ragnauth et al., 2010; Liberman et al., 2011).

FTI-277 and manumycin A, together with the prenylated protein methyltransferase inhibitor, FTS, which will be used in this thesis, will be discussed in more detail below. FTI-277 was used because it is a potent and specific farnesyl transferase inhibitor, which has been used previously in various cancer cell lines and in phase II trials (see section 1.8). Manumycin A is a farnesyl pyrophosphate (FPP) analogue, and the treatment of ApoE-/- mice with this drug has been shown to reduce atherosclerotic lesion formation (Sugita et al., 2007). The different biological activities of FTI-277 and manumycin A are summarised in Table 1.5.

1.8 FTI-277

The structure of FTI-277 is shown in Figure 1.8. FTI-277 is a peptidomimetic which has been shown to reduce Ras activity and attenuate the production of superoxide in pulmonary smooth muscle cells (Boota et al., 2000). FTI-277 appears to inhibit all isoforms of Ras protein, however there is evidence to suggest that the concentration needed to inhibit K-Ras is 10 times higher than H-Ras (Crul et al., 2001). This was further suggested by the work in myeloma cells, where K-Ras was shown to be more resistant to the cytotoxic effects of FTI-277 than N–Ras (Bolick et al., 2003). This latter study also demonstrated that FTI-277 induced apoptosis in a dose-dependent manner. Jiang et al., (2000) reported that the ability of FTI-277 to induce apoptosis was reversed by adding a constitutively active form of Akt. This group has also shown that FTI-277 blocks growth factor- and adhesion-stimulated PI3K and Akt-2 activation and subsequent phosphorylation of the pro-apoptotic protein, Bad. These studies, therefore, suggest that in cancer cells, FTI-277 induces apoptosis by a mechanism that involves inhibition of the PI3-Kinase/Akt-2 pathway. Interestingly, recent work on INS832/13 and normal rat islet has shown that FTI-277 increases Akt phosphorylation (Kyathanahalli and Kowluru, 2011). FTI-277 has also been shown to decrease the levels of expression of osteogenic transcription factors such as Runx2 in mesenchymal stem cells (MSC) (Duque et al., 2011).

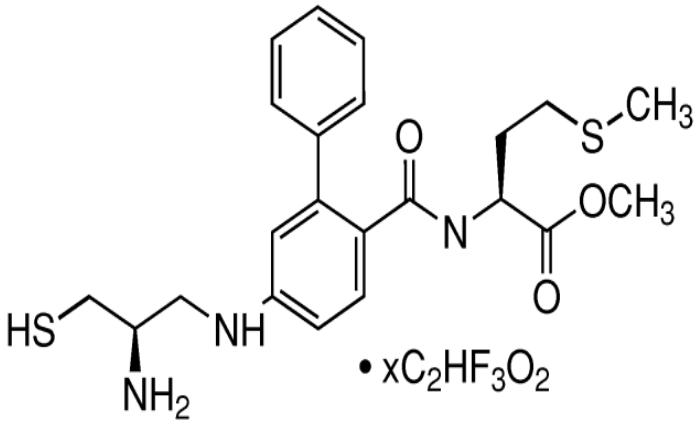

Figure 1.8: The structure of FTI–277. Reproduced from Sigma-Aldrich (www.sigmaaldrich.com).

1.9 Manumycin A

Manumycin A, a natural isolate from *Streptomyces parvulus*, is an FPP analogue and a potent FTI agent. The structure of manumycin A is shown in Figure 1.9. Manumycin A was initially thought to have anti-tumour properties due to its ability to disrupt Ras activity; however recent findings suggest that this agent also stimulates the production of reactive oxygen species (ROS) (Sears et al., 2008). In this latter study, ROS promoted MEK and Akt dephosphorylation and mediated the activation of caspase 9. Experiments on rat VSMCs have shown that manumycin A has anti–proliferative actions, inhibits the migration of these cells and promotes MAPK dephosphorylation (Kouchi et al., 1999). The treatment of ApoE-/- mice with manumycin A has also been shown to reduce fatty lesion formation in the aortic sinus (Sugita et al., 2007). Furthermore, this treatment was associated with a reduction in vascular smooth muscle-like cells in the aorta which may indicate an anti-proliferative action of manumycin A (Sugita et al., 2007). In addition, reduced levels of phosphorylated Raf were detected in these ApoE-/- mice. In separate study, manumycin A has also been shown to induce apoptosis in vascular smooth muscle cells in a dose dependent manner (Guijarro et al., 1998). The downstream effector of Raf is Erk which is essential for cell proliferation.

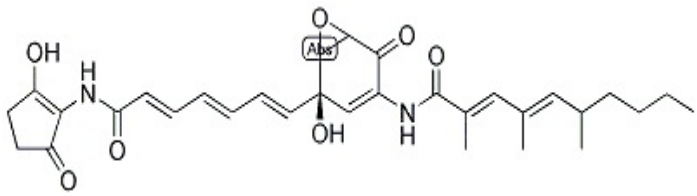

Figure 1.9: Structure of manumycin A. Reproduced from Sigma-aldrich (www.sigmaaldrich.com).

	FTI-277		Manumycin A	
	Cell types	Effects	Cell types	Effects
Ras Activity	VSMCs (Sinha et al., 2009)	Decrease	VSMCs	Decrease (Sugita et al., 2007)
	Cancer cells	Decrease (Bolick et al., 2003)	Cancer cells	Decrease (Zhou et al., 2003)
Cytoskeleton	VSMCs (Sinha et al., 2009)	Disrupted	VSMCs	Not known
	Cancer cells	Disrupted (Virtanen et al., 2010)	Cancer cells	Not known
Akt activation	VSMCs	Not known	VSMCs	No effect (Galaria et al., 2005)
	Ovarian cancer cells Lung Cancer Cells INS 832/13	Reduces (Jiang et al., 2000) No effect /Increases (Sun et al., 2004) Increases	Cancer cells	Reduces (Zhou et al., 2003)
Erk activation	VSMCs	Not known	VSMCs	Reduces (Sugita et al., 2007)
	Cancers cells	Reduces (Mazzocca et al., 2003)	Cancers cells	Reduces (Zhou et al., 2003)
Superoxide production/ROS	Pulmonary Smooth Muscle Cells	Reduces (Boota et al., 2000)	VSMCs	Not known
	Cancer cell	Not known	Cancer cells	Increases (Sears et al., 2008)
Apoptosis	VSMCs	Not known	VSMCs	Increases (Guijarro et al., 1998)
	Cancer cells	Increases (Mazzocca et al., 2003)	Cancer cells	Increases (She et al., 2005)
Proliferation	VSMCs	Not known	VSMCs	Reduces (Kouchi et al., 1999)
	Cancer cells	Reduces (Doisneau-Sixou et al., 2003)	Cancer cells	Reduces (Zhou et al., 2003)
Migration	VSMCs	Not known	VSMCs	Reduces (Kouchi et al., 1999)
	Cancer cells	Not known	Cancer cells	Not known

Table 1.5: Differences in the reported biological activities of FTI-277 and manumycin A.

1.10 Prenylated protein methyltransferase inhibitors (FTS)

Prenylated protein methyltransferase inhibitors are S-prenyl compounds that compete with Ras at its farnesyl dependent anchorage sites, preventing the mature Ras from binding at the membrane. Farnesyl Thiosalicylic Acid (FTS) is a product of thiosalicyclic acid and does not affect the maturation process of the Ras protein (Alvarado and Giles, 2007). The structure of FTS is shown in Figure 1.9. FTS has been shown to displace all isoforms of Ras from the membrane binding sites and studies have shown that it inhibits the growth of cancer cells *in vitro* (Marom et al., 1995). In cancer cells, FTS treatment results in suppression of PI3K activity thus affecting its downstream effector pathway, Akt (Yaari et al., 2005). Furthermore, work in human renal mesangial cells suggests that FTS inhibits glomerular cell proliferation in rat thy-1 nephritis (Clarke et al., 2003). This work suggests that the potential effect of FTS on cell proliferation occurs downstream of Ras via Erk phosphorylation. The interest in FTS with respect to the development of atherosclerosis grew with the work of George et al. (2002) (George et al., 2002). In this study, FTS was shown to reduce Ras activity and attenuate atherosclerosis in $ApoE^{-/-}$ mice, thereby confirming the role of Ras in modulating atherosclerosis (George et al., 2002). FTS has also been shown to inhibit VSMC migration (Reif et al., 1999), a feature that is important in the inhibition of atherosclerosis. The effect of FTS on vascular calcification is not currently known.

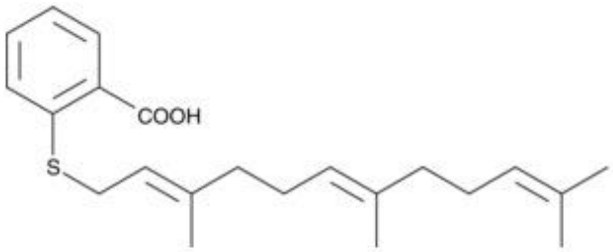

Figure 1.10: The structure of FTS. Reproduced from Santa Cruz Biotechnology (www.santacruz.com).

1.11 Summary

Vascular calcification is an active, regulated process in which VSMCs differentiate into osteoblast-like cells and deposit a mineralised matrix. It is well established that patients with vascular calcification have poor cardiovascular outcomes, due to the lack of therapeutics which target this process. Therefore, it is important to determine how vascular calcification is regulated, and in turn how these regulatory processes can be modulated, allowing for the development of novel treatments.

Previous work from the host laboratory has shown that nitrogen-based bisphosphonates attenuate vascular calcification by inhibiting farnesyl pyrophosphate synthase. Inhibited VSMCs become depleted of the isoprenoid lipids farnesyl pyrophosphate and geranylgeranyl pyrophosphate that are essential for the prenylation and activation of small GTPases such as Ras and Rho. Further preliminary work also suggested that farnesyl transferase inhibitors may inhibit vascular calcification, although the mechanism by which this inhibition occurs is not currently known.

Previous studies have raised the exciting possibility that inhibiting prenylation could be a potential target for therapeutic intervention of vascular calcification; however, it also raises several questions, including: (i) is mineralisation regulated by farnesylation? and (ii) how does inhibition of farnesylation regulate mineralisation? This knowledge is crucial in order to determine whether inhibitors of small GTPases can potentially be used to prevent vascular calcification in patients with CVD.

1.12 Aims of the project

This project will test the the hypothesis that vascular calcification is regulated by prenylation, and that inhibition of protein farnesylation attenuates vascular calcification by modulating downstream pathways. This study hopes to identify a novel pathway that regulates vascular calcification, therefore identifying potential targets for future therapeutic development. To achieve this aim the following investigation will be undertaken:

(i) Determine the effects of the prenylation inhibitors, FTI-277 and manumycin A, on vascular calcification *in vitro*.

(ii) Delineate the mechanism(s) by which prenylation- and Ras- inhibitors regulate vascular calcification.

(iii) Determine the effect of prenylation and Ras inhibitors on vascular calcification in a rat model of CKD *ex vivo*.

Chapter 2

Materials and Methods

2 Materials and Methods

2.1 Materials

The source of materials is provided below or in the Appendix (section 7.2). All buffers are listed in the Appendix (section 7.3). PKB-CAAX used in cloning was provided by Dr. Andrew Gilmore (University of Manchester) and was a gift from Dr. Boudewijn Burgering (van Weeren et al., 1998). Packaging vectors were also provided by Dr. Andrew Gilmore. Rats which had undergone a sub-total nephrectomy, or sham controls were used in collaboration with Dr. Nick Ashton (University of Manchester).

2.2 Cell culture

Cell culture was performed under aseptic conditions in a class II tissue culture hood. Cells were maintained in a humidified incubator at 37^{o}C in the presence of 5% CO_2, and the medium was changed every 2-3 days. Cell culture flasks and 6 well plates (Corning®) were purchased from Appleton Woods.

For experiments, cells were plated at 1 x 10^4 cells/cm^2 in either 75 cm^2 flasks (for Ras pull-down assays) or 6 well plates (for mineralisation and signalling assays), or at 2 x 10^4 cells/cm^2 in 75 cm^2 flasks (for apoptosis assays). Phase contrast images were captured using an Olympus DP70 digital camera attached to an Olympus IX51 inverted microscope and analysed using Analysis imaging software (Olympus Soft Imaging System, Munster, Germany). All experiments were repeated at least twice.

2.2.1 Bovine vascular smooth muscle cells

Bovine aortic vascular smooth muscle cells (VSMCs) (passage 8-11), which had been isolated and characterised by Dr. Smeeta Sinha in this laboratory, were used in these studies. Cells were cultured in Dulbecco's Modified Eagle's Medium (DMEM with 4500 mg glucose/L; Sigma) containing 10% (v/v) foetal calf serum (FCS), 1 mM sodium pyruvate, 2 mM L-glutamine, 1x non-essential amino acids, 100 U/ml penicillin and 170 μM streptomycin (this medium will be referred to hereafter as 10% FCS-DMEM). All reagents for culture of VSMCs were purchased from Sigma, Dorset, UK. The batch number of the FCS used in the mineralisation experiments was Lot 059K3397.

2.2.2 Human coronary vascular smooth muscle cells/29T3 cells

Human coronary artery VSMC (HCVSMC) (Invitrogen, Lot # 642644) were maintained in Medium 231 containing a smooth muscle growth supplement (Invitrogen). Cell culture was performed as described above, and cells were used between passage 6 and 8 in experiments. 293T cells were used to produce lentiviral particles and were cultured in 10% FCS DMEM-high glucose.

2.3 Induction of mineralisation

When VSMCs had reached 90% confluence (termed day 0), they were incubated in 10% FCS-DMEM containing 5 mM β-glycerophosphate (βGP). Controls were incubated in 10% FCS-DMEM. The medium was changed every 72 hours.

2.4 Farnesyltransferase inhibitors, farnesylthiosalicylic acid, wortmannin and SH6

Stock solutions of farnesyltransferase inhibitors (FTI-277, manumycin A – Sigma), a PI3K inhibitor (wortmannin – Sigma), an Akt inhibitor (SH6 - Calbiochem) and a Ras inhibitor (farnesylthiosalicylic acid, FTS – Cayman Chemicals) were prepared in dimethyl sulfoxide (DMSO) as described in the Appendix. FTI-277, manumycin A, wortmannin, SH6 or FTS were added to either serum-free DMEM, Medium 231 or 10% FCS-DMEM in the presence or absence of 5 mM βGP to give the final concentrations indicated in the figure legends. Control cells were incubated in the corresponding medium containing an equivalent volume of DMSO as detailed in the figure legends.

2.5 Assessment of mineralisation

2.5.1 Alizarin red staining

The medium was removed from VSMC cultures and cells were washed with phosphate buffered saline (PBS) three times. Cells were fixed with 2 ml 2% (v/v) formaldehyde, 1% (w/v) sucrose in dH_2O for 20 minutes and then washed with dH_2O. Subsequently, 1 ml of alizarin red (40 mM, pH 4.1 in dH_2O) was added to each well of the 6 well plates, which were then incubated on a rocking platform for 20 minutes. The cells were washed four times for 5 minutes with dH_2O (pH 7) and the plates were dried overnight. Areas of mineralisation appeared red. Phase contrast images were captured as described in Section 2.2.

2.5.2 Alizarin red dye elution

Eight hundred microlitres of 10% (v/v) acetic acid was added to each well and the plates were placed on a rocking platform for 30 minutes. Cells were then scraped into an eppendorf and heated for 10 minutes at 85°C. Subsequently, samples were cooled on ice and centrifuged (20,000 xg at 4°C for 15 minutes). The supernatant (500 µl) was transferred to a new eppendorf and 200 µl of 10% (v/v) ammonium hydroxide was added. The absorbance of the samples was read on a plate reader (MRX II absorbance reader, Dynex Technologies, West Sussex, UK) at a wavelength of 405 nm.

2.5.3 O-cresolphthalein complexone assay

O-cresolphthalein complexone assay was used to assess calcium accumulation. Aortic rings were washed with aortic wash buffer (see Appendix) for 48 hours; the wash buffer being changed at 24 hours. The samples were then incubated in the wash buffer at 37 ˚C in a shaker for a further 48 hours. Following this, the aortic rings were removed and blotted dry, and the wet weight of the tissue was measured. The rings were then placed into individual wells in a 24 well plate and incubated in 0.5 ml of 6 M HCl for 48 hours at room temperature. Following this, the HCl was removed from each well and placed into fresh tubes and vortexed. Ten microlitres of each sample or standard (5-25 mg/dl calcium) (from stock calcium standard 50 mg/dl) was added to a 96 well plate, following which, 100 µl of colour reagent and 2-amino-2-methyl-1-propanol (AMP) buffer (pH 10.7) were added. The mixture was then incubated at room temperature for 15 minutes. The absorbance of the samples was read on a plate reader (MRX II absorbance reader) at a wavelength of 570 nm.

2.6 Apoptosis assays

HCVSMCs were plated at 2 x 10^4 cells/cm^2 in 75 cm^2 flasks for protein isolation, or at 2 x 10^4 cells/cm^2 in chamber slides (Lab-tek II, Cole Parmer) for nuclear staining. The following day, the cells were washed three times with PBS and placed in serum-free DMEM with or without FTI-277 (10 µM) and / or SH6 (10 µM). Phosphate was then added to the medium to increase the concentration from 0.9 mM to 2.6 mM. Control cells were incubated in medium containing elevated phosphate and vehicle (DMSO, 1:1000). Two, 4 and 6 hours post-elevated phosphate addition, cells were washed twice with PBS and the protein collected (section 2.9.4) for analysis by western blotting.

Cells in chamber slides were stained 12 hours post-phosphate addition. These cells were washed in PBS and fixed in 4% (v/v) formaldehyde in PBS for 10 minutes at room temperature, before mounting in Vectorshield containing DAPI (Vector laboratories, Peterborough, UK). To quantify apoptosis, at least 300 cells were counted per treatment group per experiment, and the results were expressed as the percentage of total cells with apoptotic nuclei. Apoptotic cells were defined as cells with condensed or fragmented nuclei.

2.7 Migration Assays

2.7.1 Scratch wound migration assay

VSMCs were plated at 1 x 10^4 cells/cm^2 in 6 well plates and grown to confluence in 10% FCS-DMEM. Cells were then pre-incubated with FTI-277 (10 μM), or vehicle control, in serum-free DMEM overnight. The next day, cell-free zones were made by scratching the cell monolayer using a sterile 1 ml tip. Two areas within the length of each scratch were marked for monitoring migration. The cells were then washed with PBS to remove debris, and incubated with either serum-free DMEM containing 20 ng/ml PDGF ± 10 μM FTI-277, or serum free medium ± 10 μM FTI-277. The two marked areas were imaged after 24, 48 and 72 hours as detailed in Section 2.7.2.

For experiments using FTS, VSMCs were plated as described above, and then pre-incubated with 10 μM FTS in 0.5% FCS-DMEM overnight as described (Goldberg et al 2002), or in vehicle control. The next day, cell-free zones were generated as detailed above. The cells were then incubated with either 0.5% FCS-DMEM containing 20 ng/ml PDGF ± 10 μM FTS, or 0.5% FCS-DMEM ± 10 μM FTS. Two areas marked in each wound were imaged at 24 and 48 hours, as detailed in Section 2.7.2.

2.7.2 Analysis of scratch wound assay

Using Image J (National Institute of Health, USA), the width of each wound was measured at six equally-spaced points across the scratch at each time point (0, 24, 48, and 72 hours). The average wound width was determined at each time point and the width expressed as a percentage of the original wound size.

2.8 Rat aortic rings *ex vivo*

Male Sprague Dawley rats (8-12 weeks old) **(**Charles Rivers, Kent, UK) underwent either a 5/6 nephrectomy or a sham operation according to Home Office Licence Number 40/3438. Estimated glomerular filtration rate (eGFR) of the rats was monitored on a regular basis to determine the stage of kidney disease. Blood pressure and urinary albumin excretion was also monitored in these rats. All surgery and measurements were performed by Heather Eyre and Dr Nick Ashton (University of Manchester). Details of surgery are provided in the Appendix, section 7.1.

The rats were divided into two groups; (a) early stage renal disease- these rats were sacrificed at 7-8 weeks post 5/6 nephrectomy or sham surgery, and (b) end stage renal disease - these rats were sacrificed at least 6 months post 5/6 nephrectomy or sham surgery. Rats were sacrificed by general anaesthesia and cardiac puncture. A vertical incision was made in the abdomen and the bowels were displaced to visualise the descending aorta, which was then excised. The entire aortic arch, thoracic and abdominal aorta was placed in sterile PBS. Using a Stemi 2000-C dissection microscope (Zeiss, Hertfordshire, UK) the fat tissue and adventitia were removed from the vessel. The thoracic aorta was then dissected into 3-4 mm rings and washed with PBS. Each aortic ring was then placed sequentially into individual wells of a 48 well plate containing 1% FCS-DMEM and incubated at 37˚C overnight in a humidified incubator containing 5% CO_2. The next day, the media was removed and replaced with appropriate treatment media, as detailed below.

The treatment groups were: (i) serum-free DMEM + vehicle (DMSO), (ii) 3.3 mM phosphate (Pi) in serum-free DMEM containing alkaline phosphatase (3.75 U/ml)(New England BioLabs, Hitchin, UK) and vehicle control, (iii) 3.3 mM Pi in serum-free DMEM containing alkaline phosphatase (3.75 U/ml) and 10 μM FTI-277, and (iv) 3.3 mM Pi in serum-free DMEM containing alkaline phosphatase (3.75 U/ml) and 40 μM FTS. For some experiments in which FTS was used, 10% FCS-DMEM was used instead of serum-free DMEM. For the 3.3 mM Pi treatment groups, phosphate (sodium dihydrogen orthophosphate, NaH_2PO_4 was added to serum-free DMEM to increase phosphate from 0.9 mM to 3.3 mM.

Fresh medium was added every 48 hours. After 10 days, a calcium assay was performed on 3 or 4 rings from each treatment group using the O-cresolphthalein

complexone method, as described in Section 2.5.3.The remaining rings were fixed with 4% formaldehyde in PBS for 24 hours and then maintained in 70% industrial methylated spirit at 4˚C until processed for histology (see Section 2.8.1).

2.8.1 Histology

The aortic rings were placed in histology cassettes and processed using an automated tissue processor (Shandon Citadel 2000 Tissue Processor™, Thermo, UK). Subsequently, the rings were embedded in paraffin wax blocks (ThermoShandon Histocentre 2, Thermo, UK), sectioned into 7 μm sections using a microtome (Microm HM355S, Thermo), and placed onto superfrost plus microscope slides (Thermo).

2.8.2 Haematoxylin and Eosin staining

Tissue sections were stained with haematoxylin and eosin using an automatic Shandon Varistain 24-4 (Thermo). These slides were then mounted using Histo-clear (National Diagnostics, Hull, UK).

2.8.3 Alizarin red staining

Tissue sections were submerged in xylene for 5 minutes, and hydrated by placing in 100% (vol/vol) ethanol for 5 minutes, followed by 95% (vol/vol) ethanol for a further 5 minutes. The slides were then left to dry for one hour before being submerged in alizarin red stain 40 mM, pH 4.1 in dH_2O for 5 minutes, followed by rinsing in dH_2O. The slides were then rinsed in acetone, followed by 1:1 acetone:xylene and finally xylene. The slides were then mounted with Neo-Mount (MERCK, New Jersey, USA).

2.8.4 Von Kossa staining

Tissue sections were submerged in xylene for 10 minutes, and then rehydrated with graded concentrations of ethanol (100%, 95%, 70%, 50% ethanol - each for 5 minutes), followed by 5 minutes in dH_2O. The slides were then submerged in 1% (w/v) silver nitrate and placed in UV light for 30 minutes. Slides were then placed in 5% (w/v) sodium thiosulphate for 5 minutes and dehydrated with graded concentrations of ethanol (50%, 70%, 95%, 100% ethanol - each for 5 minutes) followed by xylene for 10 minutes. Slides were mounted with Neo-Mount.

2.8.5 Imaging

Images were captured using an Axiocamcolour CCD camera using Axiovision software attached to an Axioskop upright microscope (Zeiss). Stained rings were imaged using a Pannoramic 250 Flash slide scanner (3D HISTECH). Alizarin red staining was quantified using HistoQuant (3D HISTECH) and expressed as a percentage of section area. Nuclei were counted within a fixed 800 μm x 800 μm area with an average vessel length of ~1000 μm. One or two sections from 2-3 different animals were analysed per treatment group, blinded.

2.9 Protein extraction and analysis

Cells were rinsed with ice-cold Tris buffered saline (TBS –see Appendix) and incubated in cell lysis buffer (see Appendix; 1ml for 75 cm^2 flask and 200 μl for each well of a 6 well plate) for 2 minutes. The cell lysates were transferred into an eppendorf, vortexed and centrifuged (16,000 xg, 4^oC, 15 minutes). Supernatants were transferred to a new eppendorf and stored at -20°C before analysis. Protein assays of the cell lysates were performed using a Pierce BCA™ protein assay kit as per the manufacturer's instructions.

2.9.1 Preparation of samples for analysis of Ras effector pathways

VSMCs were plated at 1x 10^4 cells/cm^2 in 6 well plates and maintained in 10% FCS-DMEM to 80-90% confluence. Subsequently, VSMCs were incubated in 10% FCS-DMEM $\pm$ treatment (FTI-277, 10 μM; manumycin A, 10 μM; wortmannin 100 nM; control containing DMSO, 1:1000) for 77 hours. The medium was removed and cells were washed three times using Hanks balanced salt solution (HBSS). These cells were then incubated for 2 hours in serum-free DMEM containing either FTI-277 (10 μM), manumycinA (10 μM), wortmannin (100 nM) or DMSO (1:1000), as appropriate. This was followed by serum stimulation (10% FCS-DMEM) for either 5 minutes or 15 minutes. After this time, the VSMCs were placed onto ice, rinsed with TBS and then cell lysis buffer (see Appendix) (200 μl) was added. The cells were scraped into an eppendorf, vortexed and incubated on ice for 5 minutes. The cell lysates were centrifuged (16,000 xg, 4^oC, 15 minutes) and supernatants were transferred into new eppendorfs and stored at -20^oC before analysis. Protein assays were performed as described (see section 2.9) and the samples were analysed by western blotting (see section 2.9.4).

2.9.2 Active Ras Pull-Down assay

VSMCs were grown in 75 cm^2 flasks and maintained in 10% FCS-DMEM to 80-90% confluency. Subsequently, VSMCs were incubated in 10% FCS-DMEM ± treatments (FTI-277, 10 μM; Manumycin A, 10μM; FTS 10 μM or 40 μM; or DMSO control, 1:1000) for 77 hours. After this time, the medium was removed and cells were washed using HBSS. Cells were subsequently incubated with serum-free DMEM for 2 hours containing these treatments and then stimulated with 10% FCS-DMEM for 5 minutes. The following steps were all performed on ice. VMSCs were rinsed with ice-cold TBS and then 1000 μl of lysis buffer containing phosphatase and proteinase inhibitors (Active Ras Pull-Down and Detection kit, Thermo Fisher Scientific, Northumberland, UK) was added to the cells which were scraped off into an eppendorf, vortexed and incubated on ice for 5 minutes. The cell lysates were centrifuged (16,000 xg, 4°C, 15 minutes) and the supernatants transferred into new tubes. Spin cups were placed into collection tubes (Active Ras Pull-Down and Detection kit, Thermo Fisher Scientific). One hundred μl 50% (w/v) glutathione resin was added into the spin cups and the tubes were centrifuged (6,000 xg, 10-30 seconds). The flow-through was discarded and then 400 μl of lysis/binding/wash buffer (provided by the manufacturer) was added to each spin cup containing the resin. The collection tubes and spin cups containing lysis buffer and resins were inverted several times and then centrifuged (6,000 xg, 10-30 seconds). The flow-through was discarded and GST-Raf1-RBD (Ras Binding Domain, 80 μg) was added to the spin cups. Seven hundred μl of the cell lysates (containing at least 500 μg of total proteins) was immediately added to the spin cup and the sample was vortexed. The reaction mixture was then incubated at 4°C for 1 hour with gentle rocking. Following this incubation, the spin cups with collection tubes were centrifuged (6,000 xg, 10-30 seconds). Lysis buffer (400 μl) was added into the tubes; which were inverted three times and centrifuged (6,000 xg, 10-30 seconds). This step was repeated twice. Lamelli sample buffer (2X concentrated; 50 μl) containing 5% (v/v) β-mercaptoethanol was added to the spin cups. The samples were vortexed and incubated at room temperature for 2 minutes. The tubes were then centrifuged (6,000 xg, 2 minutes). The spin cups containing resin were removed and discarded. The eluted samples were heated (5 minutes at 95°C) and samples (25 μl) analysed by western blotting (see sections 2.9.3 and 2.9.4) using 12% resolving gels (see Appendix).

2.9.3 Sodium dodecyl sulphate polyacrylamide gel electrophoresis (SDS-PAGE)

Protogel (National Diagnostics, Leicestershire, UK) was used to prepare resolving gels (10% - for Akt and Erk; 12% - for Ras; 15% - for active caspase 3) and stacking gels. Lamelli sample buffer (5X) was added to protein samples (10 μg or 20 μg) and samples were heated (95°C, 5 minutes) prior to electrophoresis. Precision plus Protein™ standards (10 - 250 kDa) (BioRad) were separated by electrophoresis on the same gels. The gels were run using running buffer (see Appendix) in mini Trans blot apparatus (Bio Rad) at 90 – 120 V.

2.9.4 Western blotting

Proteins were transferred from SDS-PAGE gels to PVDF membranes (Amersham Hybond™) by semi-dry transfer using semi-dry transfer buffer (see Appendix) at 0.15 W (1 gel) or 0.30 W (2 gels) for 1 hour. Subsequently, the membranes were blocked using; 5% (w/v) Marvel® in PBS containing 0.05% (v/v) Tween (PBST) (for Akt and phosphorylated Akt blots), 1% (w/v) bovine serum albumin (BSA) in PBS containing 0.2% (v/v) Tween (for Erk and phosphorylated Erk blots), 3% (w/v) BSA in TBS containing 0.05% (v/v) Tween (TBST) (for Ras blots), or 2% (v/v) fish gelatin in TBST (for caspase 3 and active caspase 3 blots) for 1 hour. The membrane was then incubated with primary antibody at the appropriate dilution overnight at 4°C (see Table 2.1). Membranes were washed five times for 5 minutes each with either PBST or TBST and then incubated with the appropriate HRP-conjugated secondary antibody (see Table 2.2) for 1 hour at room temperature. Membranes were again washed five times for 5 minutes each in PBST or TBST. Finally, the membranes were incubated for 5 minutes with SuperSignal West Pico Chemiluminescent Substrate (Pierce) and exposed to Hyperfilm (GE Healthcare) in a dark room.

Primary antibody	**Antibody details**	**Supplier**	**Working Dilution**	**kDa**
Akt	Polyclonal rabbit anti-Akt (Cat No: 9272)	Cell Signalling Technologies	1:1000 in 5% Marvel in PBST	60
Phospho-Akt	Polyclonal rabbit anti-phosphoAkt (Ser4730) (Cat No: 9271)	Cell Signalling Technologies	1:1000 in 5% Marvel in PBST	60
Erk 1/2	Monoclonal rabbit anti-p44/42 (Cat No: 4685)	Cell Signalling Technologies	1:1000 in 1% BSA in PBS + 0.2% Tween	44/42
Phospho Erk1/2	Monoclonal rabbit anti-phospho–p44/42 (Thr202/Tyr204), (Cat No: 4370)	Cell Signalling Technologies	1:1000 in 1% BSA in PBS + 0.2% Tween	44/42
ß-Actin	Monoclonal mouse anti-β actin (Cat No: A1978)	Sigma	1:10000 in 5% Marvel in PBST	42
Ras	Monoclonal mouse Ig2aκ anti Ras (Cat No: 9855Y)	Pierce Thermo Scientific	1:200 in 3% BSA in TBST	21
Caspase 3	Polyclonal rabbit anti-Caspase3 (Cat No: 9662)	Cell Signalling Technologies	1:500 in 2% fish gelatin in TBST	35
Active Caspase 3	Polyclonal rabbit anti-Cleaved caspase3 (Cat No: 9661)	Cell Signalling Technologies	1:500 in 2% fish gelatin in TBST	17,19

Table 2.1: Details of the primary antibodies used in these studies.

Secondary Antibody	Supplier	Working Dilution	Primary antibody
HRP conjugated goat anti-rabbit immunoglobulins (Cat No: P0448)	Dako	1:1000 in 5% Marvel in PBST	Polyclonal rabbit anti-Akt, Polyclonal rabbit anti phosphoAkt, Monoclonal rabbit anti-p44/42, Monoclonal rabbit anti-phospho p44/42
Goat anti-mouse HRP (Cat No: 1858413)	Pierce Thermo Scientific	1:20000 in 5% Marvel in TBST	Mouse monoclonal Ig2aκ anti-Ras
Rabbit anti-mouse HRP (Cat No: 3118)	Pierce Thermo Scientific	1:1000 in5% Marvel in PBST	Monoclonal mouse anti-β-actin,

Table 2.2: Details of secondary antibodies used in these studies

2.10 RNA analysis

2.10.1 RNA extraction and purification

Cells were rinsed with PBS and collected in RNeasy Lysis Buffer (RLT) buffer (300 µl per well; QIAGEN, UK) following the manufacturer's protocol. The lysate was transferred into a QIAshredder spin column placed in a 2 ml collection tube and centrifuged (16,000 xg, 2 minutes), following which, 1 volume of 70% (v/v) ethanol (300 µl) was added into the homogenized lysate and mixed well by pipetting. The sample was transferred to an RNeasy spin column placed in a 2 ml collection tube and centrifuged (8000 xg, 15 seconds). The flow through was discarded, 700 µl buffer RW1 added to the RNeasy spin column, and the sample was centrifuged (8000 xg, 15 seconds). RPE buffer (500 µl) was added to the RNeasy spin column and the samples were re-centrifuged (> 8000 xg, 15 seconds). The flow-through was again discarded, and the above step was repeated, but this time the samples were centrifuged for 2 minutes. The RNeasy spin column was then placed into a new 1.5 ml collection tube, 30 µl RNeasy-free water was added directly into the spin column membrane, and the samples were centrifuged (8000 xg, 1 minute) to elute the RNA. Samples were stored at -80°C before analysis.

2.10.2 DNAse treatment and nucleic acid quantification

The RNA samples were treated using Ambion® DNA-free™ to remove any contaminating genomic DNA. DNAse buffer (10X, 3.5 µl) and DNAse (1.5 µl) were added to 1.5 µg RNA and the samples were incubated at 37°C for 30 minutes. The reactions were stopped by adding 3.5 µl of DNAse inactivation beads and incubated for 2 minutes following which samples were centrifuged (16,000 xg, 2 minutes). The supernatant was removed into a new 1.5 ml tube and RNA quantified using a Thermo Scientific, Nanodrop 1000 spectrophotometer with a 260/280 and 230/260 absorbance ratio with accepted ratio of >2 and >1.8.

2.10.3 cDNA synthesis

TaqMan® reverse transcription reagents (Applied Biosystems) were used for cDNA synthesis. Three micrograms of RNA was added to 1x RT buffer, 5 mM $MgCl_2$, 2 mM dNTPs, 1.5 µM random hexamers, 45 U RNAse inhibitor and 112.5 U reverse transcriptase. This was made up to a volume of 90 µl with DEPC-treated water (see Appendix). Reverse transcription of RNA was performed using a cycle of 25°C for 10 minutes, 48°C for 30 minutes and 95°C for 15 minutes. Samples were kept at -20°C before analysis.

2.10.4 Real-time quantitative polymerase chain reaction

An Applied Biosystems ABI Prism 7000 Real Time PCR machine was used for relative quantification of gene expression. The PCR reaction contained 6 µl 2x SYBRgreen (Applied Biosystems), 1.5 µl cDNA, 3 µM forward and reverse primers (see Table 2.3) and DEPC-treated water was added to make the total volume of 12 µl. Reactions were set up in 96-well optical reaction plates (Applied Biosystems). All samples were amplified in duplicate. The cycling conditions are detailed in Table 2.4.

The primers designed to amplify fragments from two housekeeping genes (RPL12, PP1A) were purchased from Primer Design (Southampton). They were optimized by Dr. Gareth Hyde in the laboratory. The relative expression of each gene of interest to housekeeping genes was calculated using the comparative C_t method ($2^{-\Delta Ct}$) as per the manufacturer's guidelines (Applied Biosystems).

Gene of Interest	Sequence	Supplier
Runx2	Forward sequence 5'CCCAAGTTGCCACCTATCAC 3' Reverse sequence 5'TGAGGCGATCAGAGAACCAAA 3'	Sigma
Msx 2	Forward sequence 5'AGGAGCTGGGACGTGGTAAA 3' Reverse sequence 5'CTGGTCAAACCCTTCGAGAC 3'	Eurogentec
αSMA	Forward sequence 5'ACCGCATGCAGAAGGGA 3' Reverse sequence 5' GAGCCACCAATCCAGACAGA 3'	Sigma
Matrix Gla Protein (MGP)	Forward sequence 5' AATAACGGTCGTAGGCAGCA 3' Reverse sequence 5' AGCCCAAGAGAGAATCCGAG 3'	Sigma
Alkaline phosphatase (ALP)	Forward sequence 5' CTTTACCTTTGGCGGCGGGTACA 3' Reverse sequence 5' TGAACGGCTTCTTGTCTGTG 3'	Eurogentec
BMP 2	Forward sequence 5' CACGGTGCGCAGCTTCCA 3' Reverse sequence 5' CCGGGTTGTTTTCCCACTCA 3'	Eurogentec

Table 2.3: Primers used in these studies

	Temperature	Time	Cycle
Stage 1	50 °C	2 minutes	1
Stage 2	95 °C	10 minutes	1
Stage 3	95 °C 60 °C 72 °C	0:15 seconds 1 minute 0:15 seconds	40
Stage 4	95 °C 60 °C 95 °C	0:15 seconds 0:20 seconds 0:15 seconds	1

Table 2.4: Real time qPCR cycling conditions

2.11 DNA analysis

2.11.1 DNA sequencing

DNA sequencing of the PKB-CAAX construct was performed using 2 µl 5x Big dye terminator® (Applied Biosystems), 1 µl of 5x sequencing buffer (Applied Biosystems), 1 µl DNA and 0.32 µl of either forward sequencing primer (either EF1 alpha or T7; see Table 2.5), or reverse primer (either WPRE, TURBO GFP or 2A; see Table 2.5). The volume was adjusted to 10 µl with deionised water. PCR reactions were carried out using an Eppendorf Mastercycle PCR machine, as detailed in Table 2.6.

Primer	Sequence
2A (Sigma)	Reverse sequence 5'AGGGCCGGGATTCTCCTCCAC 3'
Turbo GFP (Sigma)	Reverse sequence 5'CGATCTCCATGGCGGGCAGGCCGCTCTCG 3'
WPRE (Sigma)	Reverse sequence 5'CGTAAAAGGAGCAACATAGTTAAGAATACC 3'
T7 (Sigma)	Forward sequence 5'TAATACGACTCACTATAGGG 3'
EF1 alpha (Sigma)	Forward sequence 5'CTCCACGCTTTGCCTGACCCTGCTT 3'

Table 2.5: PCR primers used for DNA sequencing

	Temperature	Time	Cycles
PCR sequencing programme	96 °C	2 minutes	1
	96 °C 15 °C 60 °C	30 seconds 10 seconds 4 minutes	35
	60 °C	5 minutes	1

Table 2.6: PCR sequencing programme

Following PCR, 2 mM 0.1% (v/v) sodium acetate and 2.5% (v/v) 96% ethanol was added to the mixture. This reaction was incubated at room temperature for 30 minutes and then centrifuged (14,000 xg, 10 minutes). The DNA pellet was washed using 80% (v/v) ethanol, centrifuged (14,000 xg, 3 minutes), and then dried at 37°C for 30 minutes. The DNA precipitate was sent to a local DNA sequencing facility to be analysed using an AB1377 automated sequencer (Applied Biosystems). The DNA sequence was read using DNA baser software and confirmed using http://blast.ncbi.nlm.gov/blast.cgi.

2.11.2 Restriction enzyme digestion

To clone the PKB–CAAX into the pHIV zsgreen vector (Figure 2.1), Not1-HF (New England BioLabs, Hitchin, UK) and SpE1 (Roche, West Sussex, UK) restriction enzymes were used. The mixture was incubated at 37 °C for 1 hour. In the reaction which contained the vector, 1 unit of alkaline phosphatase (1 U/µl) was added and incubated for further 1 hour.

2.11.3 Agarose gel electrophoresis

DNA samples were separated by electrophoresis at 110 V for 20 minutes in 1% (w/v) agarose gels in 1x Tris-acetate EDTA (TAE) buffer containing 1x SyberSafe (Roche, West Sussex, UK). The DNA samples were visualized using UV light.

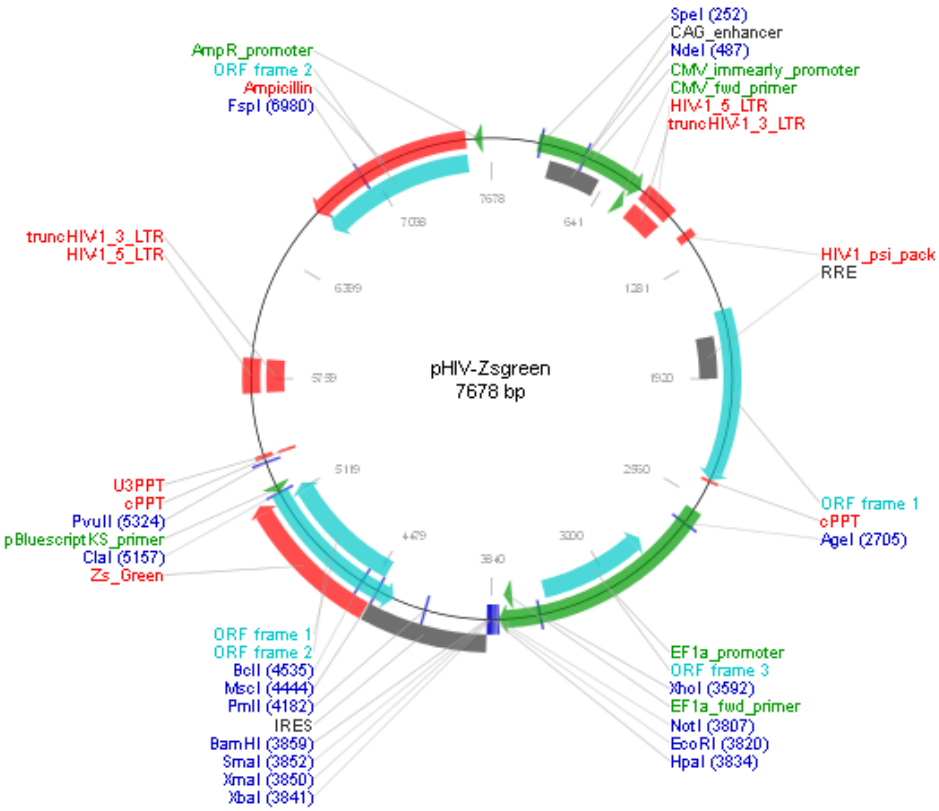

Figure 2.1: pHIVzsgreen: pHIV-Zsgreen was generated by removing the U6-TATAlox-CMVie-EGFP-TATAlox- WPRE content of pSICO, and adding the EF1-alpha promoter, a multiple cloning site (MCS), an internal ribosome entry site (IRES) and Zsgreen. The cDNA of interest can be cloned into the MCS (using NotI, EcoRI, HpaI, XbaI, SmaI or BamHI sites) to enable expression with Zsgreen (http://www.addgene.org/18121/)

2.11.4 DNA extraction

The DNA fragment of interest was excised from the gel and weighed. DNA extraction was then performed using a QIAquick gel extraction kit (QIAGEN, Cat No: 28704) according to the manufacturer's instructions. Briefly, three volumes of buffer QG, solubilisation buffer; were added to 1 volume of gel, and the samples were incubated at 50°C for 10 minutes until the gel dissolved at which time one volume of isopropanol was added. The sample was placed into a QIAquick column and centrifuged (17,900 xg, 1 minute). The flow-through was discarded and the QIAquick column was placed in a collection tube. Five hundred microliter of buffer QG was added into the QIAquick column and centrifuged (10,000 xg, 1 minute). This was followed by washing with 750 µl buffer PE and the samples were centrifuged (10,000 x g, 1 minute). The flow-through was

discarded and the QIAquick column centrifuged for a further minute. The QIAquick column was then placed in an eppendorf. To elute the DNA, 50 µl of buffer EB was added to the centre of the QIAquick column and centrifuged for 1 minute.

2.11.5 DNA purification

DNA was purified using a QIAGEN PCR purification kit according to the manufacturer's instructions. Five volumes of buffer PBI were added to 1 volume of the sample and the sample was then applied to the QIAquick column. The column was centrifuged (17,900 xg, 1 minute) and the flow-through discarded. Seven hundred and fifty µl of buffer PE was added to the QIAquick column and then centrifuged (10,000 xg, 1 minute). The flow-through was discarded and the column further centrifuged (10,000 xg, 1 minute). The QIAquick column was then place in a 1.5 ml eppendorf, 50 µl of buffer EB added to the centre of the QIAquick column and it was centrifuged for 1 minute to elute the DNA.

2.11.6 DNA ligation

DNA fragments were ligated using T4 DNA ligase (Roche) in a 10 µl reaction which contains: 1 µl of 10x ligation buffer, 2 µl vector, 6 µl insert DNA (1:3 vector:insert ratio), 1 µl T4 ligase). The reaction was incubated overnight at room temperature.

2.11.7 Bacterial culture

Escherichia coli bacteria (*E-coli*) were cultured in Luria-Bertani (LB) medium and LB agar plates (see Appendix) containing ampicillin (100 µg /ml).

2.11.8 Bacterial transformation

E-coli (competent cells, XL-1 Blue) (Agilent, Berkshire, UK) were provided by Dr. Andrew Gilmore. The ligation mixture (5 µl) was added to the *E-coli* and they were incubated on ice for 30 minutes. The bacteria containing the ligation mixture were then heat shocked at 45°C for 45 seconds and then incubated on ice for 2 minutes. Soc buffer (see Appendix) was added to the sample and incubated for 1 hour at 37^{o}C. The mixture was then spread on an LB agar plate containing ampicillin (100 µg /ml) and incubated overnight at 37°C.

2.11.9 Plasmid DNA purification

2.11.9.1 Miniprep

Bacterial colonies were picked from the agar plate, placed in 5 ml of LB containing ampicillin (100 µg/ml) and incubated overnight in a shaker at 37°C. The bacteria were collected by centrifugation (10,000 xg, 5 minutes, room temperature), and then resuspended in 250 µl buffer P1 (resuspension buffer) and P2 (lysis buffer) provided by manufacture (Qiaprep miniprep kit). The sample was thoroughly mixed by inverting the tube 6 times. Three hundred and fifty µl of N3 buffer (neutralisation buffer) was added and the mixture was inverted six times to avoid local precipitation. The samples were then centrifuged (17,900 xg, 10 minutes). The supernatant was applied to a QIAprep spin column, centrifuged (10,000 xg, 1 minute) and the flow-through discarded. The QIAprep spin column was washed using 500 µl buffer PB and centrifuged (10,000 xg, 1 minute). Further washing was performed using 750 µl buffer PE and centrifugation (10,000 xg, 1 minute). The flow-through was discarded and the QIAprep spin column was then centrifuged for another minute. The QIAprep spin column was then placed in an eppendorf and to elute the DNA, 50 µl buffer EB was added to the centre of the spin column and the sample was centrifuged for 1 minute.

2.11.9.2 Maxiprep

In order to attain a higher concentration of DNA, a single colony of bacteria was picked from the agar plate and placed in 100 ml of LB containing ampicillin (100 µg/ml) and then incubated overnight in a shaker at 37°C. DNA was then purified using Hispeed Plasmid maxi kits from QIAGEN according to their instructions. The bacteria were harvested by centrifugation (6000 xg, 15 minutes, 4°C), re-suspended in 10 ml of buffer P1(resuspension buffer) and lysed with buffer P2 (lysis buffer). The suspension was incubated at room temperature for 5 minutes, following which the chilled buffer P3 (neutralisation buffer) was added and mixed immediately by inverting the tube 4-6 times. The lysate was then poured into the barrel of the QIAfilter cartridge and incubated for 10 minutes. During this time, the Hispeed Maxi tip was equilibrated with 10 ml of buffer QBT. The lysate was then transferred to the previously equilibrated Hispeed Tip and the sample was allowed to enter the resin by gravity flow. The Hispeed Maxi tip was then washed using 60 ml of buffer QC and the DNA was eluted using 15 ml of buffer QF. The DNA was precipitated using 10.5 ml of isopropanol and kept at room temperature for 5

minutes. During this period, the QIAprecipitator Maxi module was attached to a 30 ml syringe and the eluted DNA containing isopropanol transferred into the syringe. The sample was filtered through the QIAprecipitator, washed using 2 ml 70% ethanol, and the DNA was eluted using 1 ml of buffer TE and kept at -20°C before analysis.

2.12 Lentivirus production

2.12.1 Lentivirus production using 293T cells

293T cells were used to produce lentiviral particles. These cells were grown to 70% confluency in a T75 flask prior to transfection. At the time of transfection (day 0), 4.5 μg of PsPAx2, 3 μg pMD2G (packaging vectors, Evrogen, Cambridge) and 6 μg of pHIV-PKB-CAAX or pHIV-Empty vector (control) were added to 250 μl of serum-free DMEM and incubated for 2 minutes. Twenty seven μl of 1x Polyethylenimine (PEI) in 150 mM NaCl was then added to the DMEM:DNA mix (transfection mix) and incubated for a further 30 minutes. Five hundred μl of the transfection mix was then added to each T75 flask containing 4.5 ml of 1% (v/v) serum containing DMEM, and incubated at 37˚C. After 6 hours, the transfection medium was changed for normal growth medium (10% FCS-DMEM).

The next day (day 1 after transfection) the media was removed and replaced with 1% FCS-DMEM containing 10 mM sodium butyrate. After 8 hours, the medium was then replaced with normal growth medium. After a further 24 hours (day 2), the virus-containing media was removed, sterile filtered and stored in tubes sealed with parafilm at 4˚C. On day 3, the collected medium was transferred into centrifuge tubes and weighed to within 0.02 g error. The virus containing medium was then centrifuged at 21,000 rpm at 4˚C for 4 hours. The supernatant was then removed and pellet resuspended in 200 μl of medium (DMEM) by gently pipetting over the bottom of the tube for 20 times. The centrifuge tube containing virus was then kept at 4˚C for 1 hour, following which, the re-suspension process was repeated by pipetting up and down 20 times. The virus was then aliquoted into cryovials and stored at -80˚C.

2.12.2.1 Transduction of VSMCs with lentiviral particles

VSMCs were plated in a 6 well plate and grown to 25% confluency. The cells were then treated with polybrene (10 mg/ml) (Milipore) in 10% FCS-DMEM. The virus (either pHIV Empty Vector (control), or pHIV PKB-CAAX) 100 μl was then added to the

medium and the 6 well plate was centrifuged (2500 xg, 30 minutes, room temperature). VSMCs were then incubated overnight and medium was changed the next day and grown to confluency. Western blot analysis was done to confirm overexpression of pHIV PKB-CAAX following serum starvation for 4 hours (see section 4.3.8).

2.13 Statistical analysis

Statistical analyses were performed using Microsoft Excel and Graph Pad Prism 4. Data are presented as mean +/- standard error of the mean (SEM) and were analysed using one way analysis of variance (ANOVA) or student's T test as appropriate. The significance of observed differences between groups was tested using Tukeys multiple test; Dunnett's test was used to compare against βGP alone. Differences were accepted as statistically significant at $p<0.05$.

Chapter 3

Comparison of the effects of FTI-277 and manumycin A on mineral deposition by VSMCs

3.1 Introduction

As discussed in Chapter 1, prenylation is a crucial step upstream of several intracellular signalling pathways that are important for regulating cell growth and differentiation. Therefore, it is perhaps not surprising that prenylation has been implicated in a number of pathological processes including cancer, atherosclerosis and Alzheimer's disease (McTaggart, 2006). Farnesylation is a specific type of prenylation, which involves the attachment of a farnesyl moiety (15-carbon) to the cysteine residue of CAAX. This results in the activation of a number of downstream proteins which are essential for cell differentiation and function (Zhang and Casey 2996). For example, lamin A is a farnesylated protein that is involved in regulating osteoblastogenesis (Duque et al., 2011).

To test the hypothesis that vascular calcification is regulated by farnesylation, the effects of two different farnesyl transferase inhibitors (FTI-277 and manumycin A) on vascular calcification were investigated using a well-validated *in vitro* model (Collett et al., 2007; Alam et al., 2009). FTI-277 is a peptidomimetic and is a specific farnesyl transferase inhibitor that inhibits all isoforms of Ras; although these effects are dose-dependent (see Section 1.8). FTI-277 has been shown to induce apoptosis of various cancer cell lines including myeloma (Bollick et al., 2003) and breast cancer (Ellis et al., 2003). FTI-277 has also been shown to decrease the levels of an osteogenic transcription factor (Runx2) in mesenchymal stem cells (MSC) at a dose of 10 μM (Duque et al., 2011), thereby preventing the osteogenic differentiation and mineral deposition by these cells. The introduction of alendronate to FTI-277 treated MSCs prevented the inhibitory effect of FTI-277 on differentiation and mineralisation, suggesting that farnesylation is crucial for these processes (Duque et al., 2011). Manumycin A is an FPP analogue. It is also a potent FTI, which has been used in many *in vitro* and *in vivo* studies (see section 1.9). Of particular relevance to these studies is that manumycin A has been shown to reduce fatty lesion formation and the number of aortic VSMC in ApoE-null mice fed a high fat diet (Sugita et al., 2007). In addition, manumycin A has been shown to inhibit VSMC proliferation and migration (Kouchi et al., 1999) and promote VSMC apoptosis (Guijarro et al., 1998) *in vitro*.)

The specific objectives of the studies performed in this chapter are to:

(i) Confirm that FTI-277 and manumycin A inhibit farnesylation in VSMC

(ii) Determine the effect of different doses of FTI-277 on βGP-induced VSMC mineralisation *in vitro*

(iii) Determine the effect of different doses of manumycin A on βGP-induced VSMC mineralisation *in vitro*

(iv) Determine the effect of FTI-277 on βGP-induced VSMC mineralisation when added at different time-points

(v) Identify the downstream signalling pathway(s) (e.g. Akt and Erk phosphorylation) by which FTI-277 and manumycin A exert their effects on VSMC

3.2 Results

3.2.1 FTI-277 and manumycin A inhibit Ras activation

Ras is activated by farnesylation. Therefore, to confirm that FTI-277 and manumycin A inhibit this process, Ras activation was assessed. VSMCs were pre-incubated with FTI-277 and manumycin A for 77 hours after which they were serum-starved for 2 hours and then stimulated with serum-containing medium for 5 minutes. Cell lysates were collected, Ras pull-down assays performed and the samples were analysed by western blotting. Total Ras expression in the cell lysates was also analysed.

As shown in Figure 3.1, both FTI-277 and manumycin A inhibited Ras GTPase activation when compared to the controls. This experiment was performed twice, with similar results obtained in both.

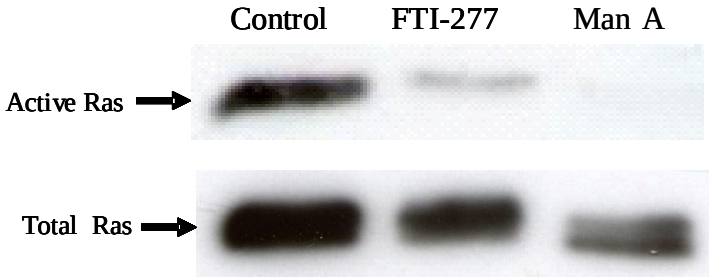

Figure 3.1: FTI-277 and manumycin A inhibit Ras GTPase activation. Confluent VSMCs were incubated with control medium (10% FCS-DMEM) or control medium + FTI-277 (10 µM) or manumycin A (Man A) (10 µM) for 77 hours. This was followed by serum starvation for 2 hours and stimulation with 10% FCS-DMEM for 5 minutes. Active Ras pull down assays were performed as detailed in section 2.9.2, and western blotting was conducted using an anti-Ras antibody for active Ras (top panel), and for total Ras (bottom panel) present in the cell lysates.

3.2.2 FTI-277 inhibits βGP-induced VSMC mineral deposition in a dose-dependent manner

To determine the effect of FTI-277 on mineralisation, VSMCs were cultured to approximately 90% confluency (termed day 0) and subsequently treated with ßGP-containing medium in the presence of FTI-277 (1, 10, 20 µM) or DMSO as the vehicle control (1:500, ßGP). The medium was changed every three days and cell cultures were stained with alizarin red on days 10 and 12 after the addition of these reagents (see Figure 3.2(i)).

The results showed that ßGP induced mineral deposition by VSMCs (Figure 3.2A and B). FTI-277 (10, 20 µM) inhibited ßGP-induced mineralisation of VSMCs at each time point examined (day 10 and day 12) (compare Figures 3.2A, B and E-H). Although some mineralisation was detected in the 1 µM FTI-277-treated cells (Figure 3.2C, D), it was considerably less than the levels detected with ßGP alone (Figure 3.2A, B). To quantify mineral deposition, alizarin red dye elution was performed and the results from two experiments were pooled. As shown in Figure 3.2 (ii), FTI-277 (10, 20 µM) significantly inhibited ßGP-induced mineralisation (* $p<0.05$, FTI-277 (10 µM) vs ßGP, *** $p<0.001$, FTI-277 (20 µM) vs ßGP).

3.2.3 Manumcyin A has no effect on ßGP-induced mineral deposition by VSMCs

The effects of a range of doses of manumycin A (1 – 50 µM) on ßGP-induced mineralisation were assessed as detailed above. During the time period prior to mineral deposition, it was noted that 50 µM manumycin A appeared to be toxic to the VSMC as many cells detached from the culture dish (Figure 3.3). This effect was not observed when manumycin A was used at lower doses (1, 10 or 20 µM). The results shown in Figure 3.4 (i) demonstrated that when used at doses between 1 and 20 µM manumycin A did not affect ßGP-induced mineralisation. No mineralisation was detected in cultures treated with 50 µM manumycin A, although it should also be noted that fewer cells were present (Figures 3.4(i) E). Confirmation that manumycin A (1, 10, 20 µM) had no effect on mineral deposition by VSMC was confirmed by elution of the alizarin red dye (Figure 3.4 (ii)).

(i)

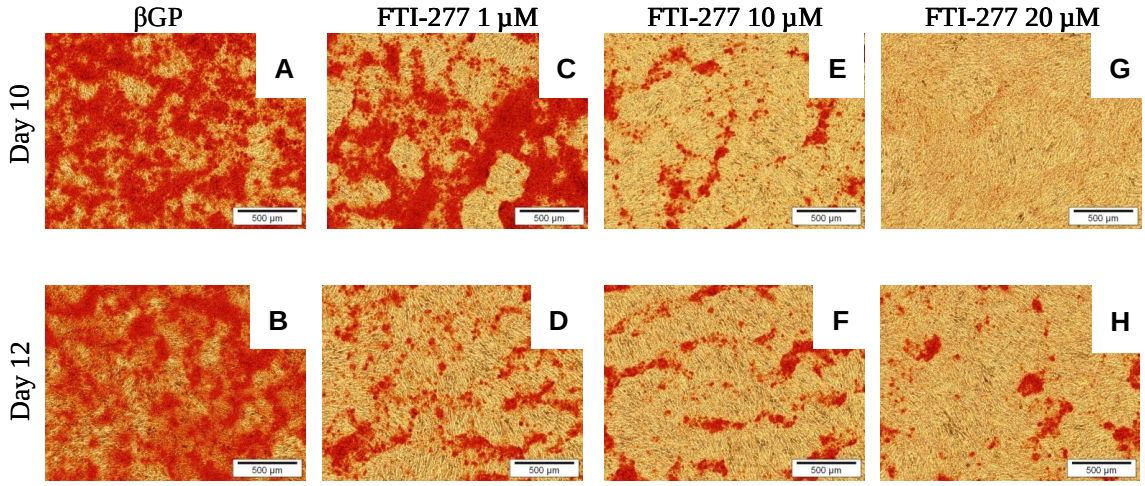

(ii)

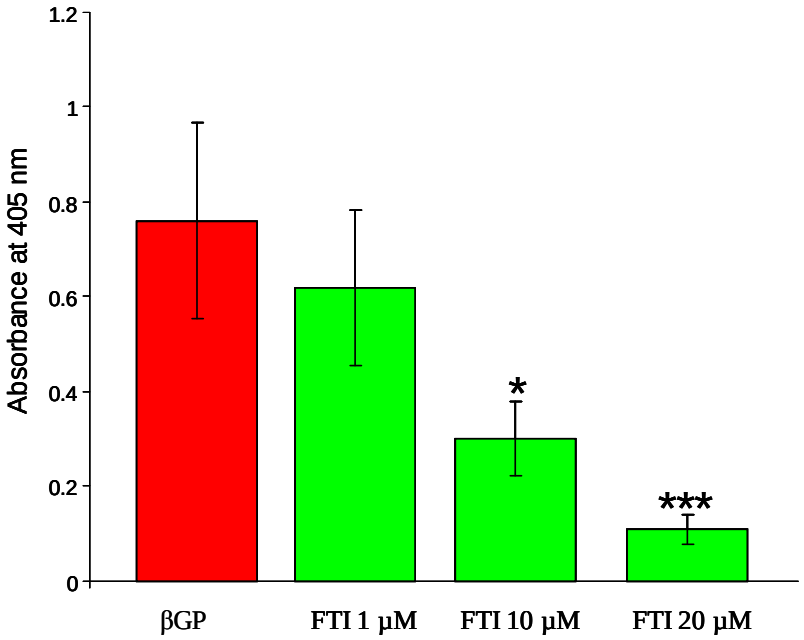

Figure 3.2: FTI-277 inhibits βGP-induced VSMC mineral deposition in a dose-dependent manner. (i) VSMCs were cultured in 6 well plates in 10% FCS-DMEM till 90% confluent, and then incubated in medium containing βGP (5 mM) and DMSO (1:500) (ßGP; A-B), or with medium containing βGP and FTI-277 (1 µM; C, D), (10 µM; E, F), (20 µM; G, H). Phase contrast images of cells stained with alizarin red on days 10 and 12 are shown. The red stain indicates areas of mineralisation. Scale bar = 500 µm. (ii) Alizarin red dye elution was performed to quantify mineralisation. The results presented are pooled from two experiments and are shown as mean ± SEM (n=12).*p<0.05, ***p<0.001, FTI-277 vs ßGP.

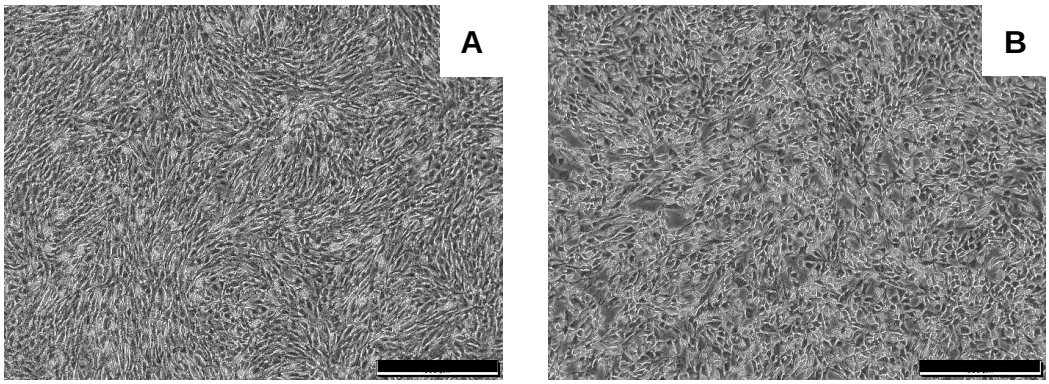

Figure 3.3: Manumycin A at 50 μM appears toxic to VSMCs. VSMCs were cultured in 6 well plates in 10% FCS-DMEM until 90% confluency, and then incubated in 10% FCS-DMEM containing ßGP and DMSO (1:250) (ßGP) (A), or 10% FCS-DMEM + ßGP + manumycin A (50 μM) (B). Phase contrast images of VSMCs on day 1 are shown. Scale bar = 500 μm.

(i)

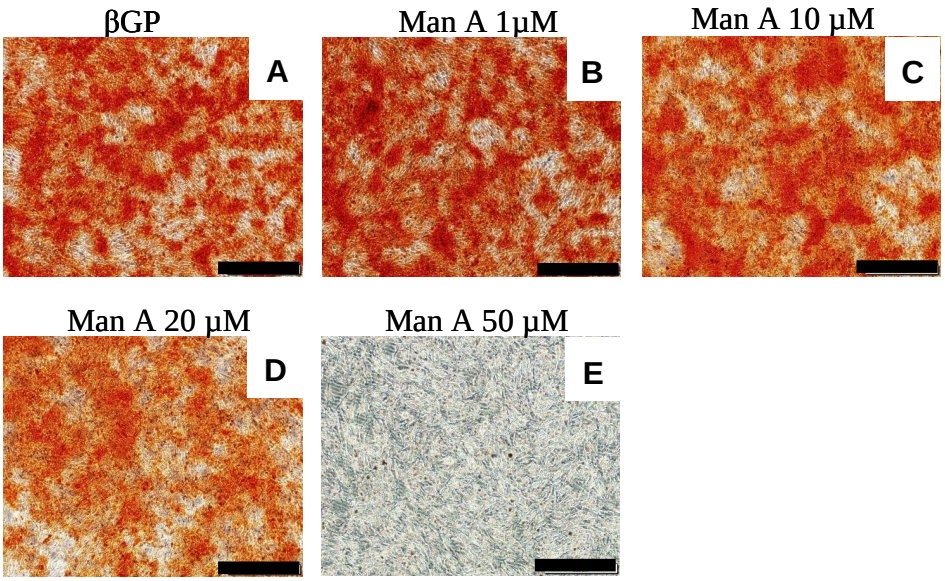

(ii)

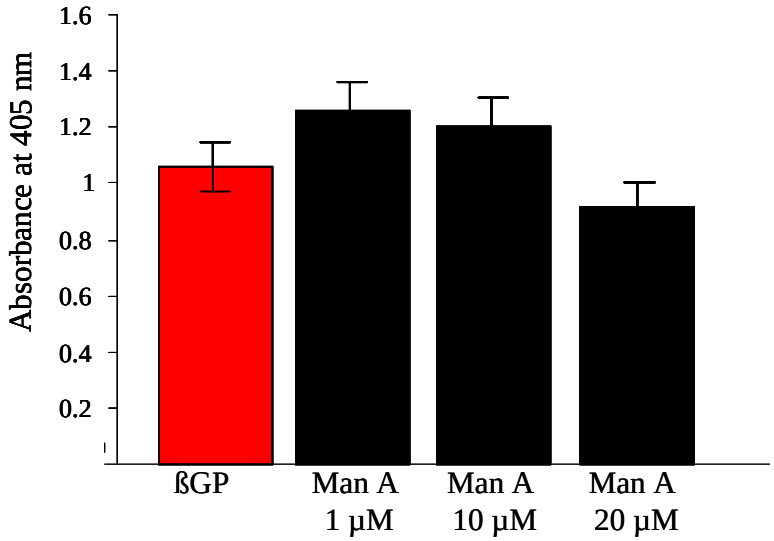

Figure 3.4: Manumcyin A has no effect on ßGP-induced mineral deposition by VSMCs. (i) VSMCs were cultured in 6 well plates in DMEM-10% FCS till 90% confluency, and were then incubated in 10% FCS-DMEM containing ßGP and DMSO (1:250) (ßGP, A), or with 10% FCS-DMEM + ßGP + manumycin A (Man A) (1 μM, B; 10 μM, C; 20 μM, D and 50 μM, E). Phase contrast images of alizarin red stained VSMCs on day 9 are shown. Scale bar = 500 μm. (ii) Alizarin red dye elution was performed to quantify mineral deposition. The results presented are pooled from two different experiments and are the mean ± SEM (n=8).

3.2.4 FTI-277 inhibits βGP-induced VSMC mineralisation in a time-dependent manner

In the next series of experiments, the ability of FTI-277 to inhibit mineralisation when added at different time points post-incubation of the cells in βGP-containing medium was investigated. In these experiments, FTI-277 (10 μM) was added to triplicate wells either from day 0, 2, 3, 4, 5, 6, or 7 after the addition of βGP containing medium. Mineralisation was assessed on day 8.

Figure 3.5 (i) shows phase contrast images of cells post alizarin red staining on day 8. Mineralisation was clearly detected in the βGP treated cells and cells in which FTI-277 treatment commenced on day 7 (Figure 3.5 A and H). However, FTI-277 added on days 0, 2, 3, 4, 5, or 6 markedly inhibited βGP-induced mineralisation of VSMCs (compare Figures 3.5A to B-G). These results were confirmed when mineralisation was quantified (Figure 3.5 (ii); ***$p<0.001$, FTI-277 vs βGP).

3.2.5 FTI-277 increases Akt phosphorylation in response to serum stimulation, but manumycin A has no effect

Next, the effects of FTI-277 and manumycin A on one of the downstream effectors of Ras, namely Akt, was examined. VSMCs were pre-incubated with FTI-277 (10 μM) or manumcyin A (10 μM) for 77 hours and then they were serum-starved for 2 hours. Cell lysates were collected prior to (T=0) and following serum stimulation for 5 or 15 minutes and analysed by western blotting for phosphorylated Akt (pAkt) and total Akt (see Section 2.9). Prior to serum stimulation (T=0) basal pAkt levels appeared similar in control, manumycin A, and FTI-277 treatment groups (Figure 3.6; compare lanes 1, 4, 7). However, after serum stimulation for 5 and 15 minutes, pAkt is markedly increased in VSMCs pre-incubated with FTI-277 compared to controls (Figure 3.6; compare lanes 8 & 9 to lanes 5 & 6). This increase was not detected in manumycin A-treated cells (Figure 3.6; compare lanes 2 & 3 to lanes 5 & 6). The reduction in Ras activity in the FTI-277 or manumycin A treated cells was also confirmed in these samples using active Ras pull-down assays as described in Section 3.2.1 (results not shown).

3.2.6 FTI-277 and manumycin A have inconsistent effects on Erk phosphorylation following serum stimulation

The effects of FTI-277 and manumycin A on Erk phosphorylation was also analysed. Samples were prepared as described above (see Section 3.2.5) and analysed by western blotting for phosphorylated Erk (pErk) and total Erk. These studies demonstrated that the effect of both FTI-277 and manumycin A on Erk phosphorylation was variable in different experiments. At T=0, the level of Erk phosphorylation appeared similar in all the samples (Figure 3.7, lanes 1, 4, 7). In two experiments, Erk phosphorylation was similar in VSMCs pre-incubated with FTI-277 following 5 and 15 minutes stimulation with serum compared to controls (data not shown). In one experiment, Erk phosphorylation was reduced by FTI-277 (Figure 3.7, compare lanes 8, 9 to 5, 6) after 5 and 15 minutes serum stimulation. In two experiments, manumcyin A had no effect on Erk phosphorylation compared to controls after 5 and 15 minutes serum stimulation (Figure 3.7, compare lanes 2, 3 to lane 5, 6). In another experiment, manumycin A appeared to reduce Erk phosphorylation after 5 minutes serum stimulation (results not shown).

(i)

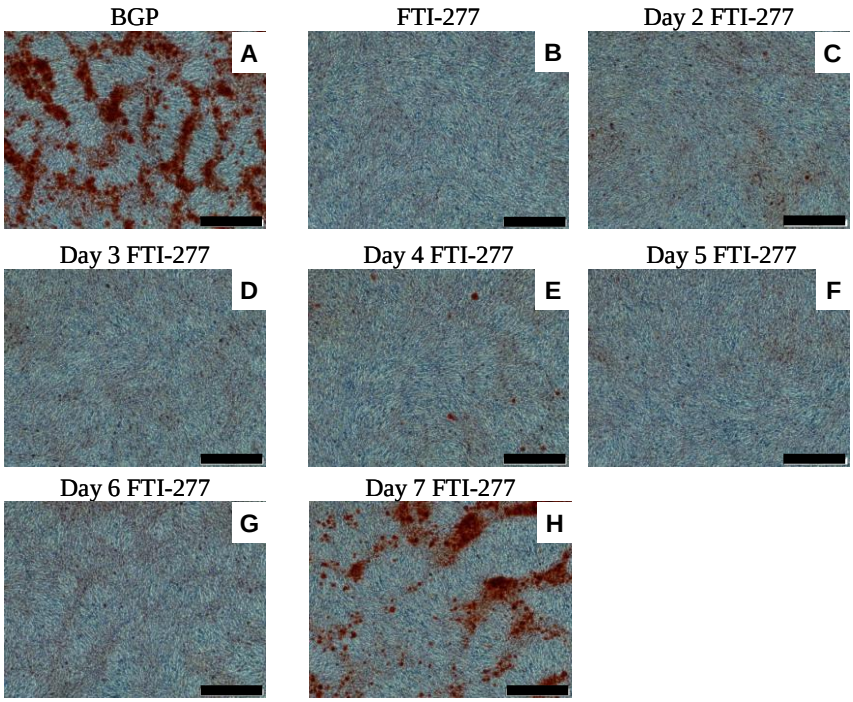

(ii)

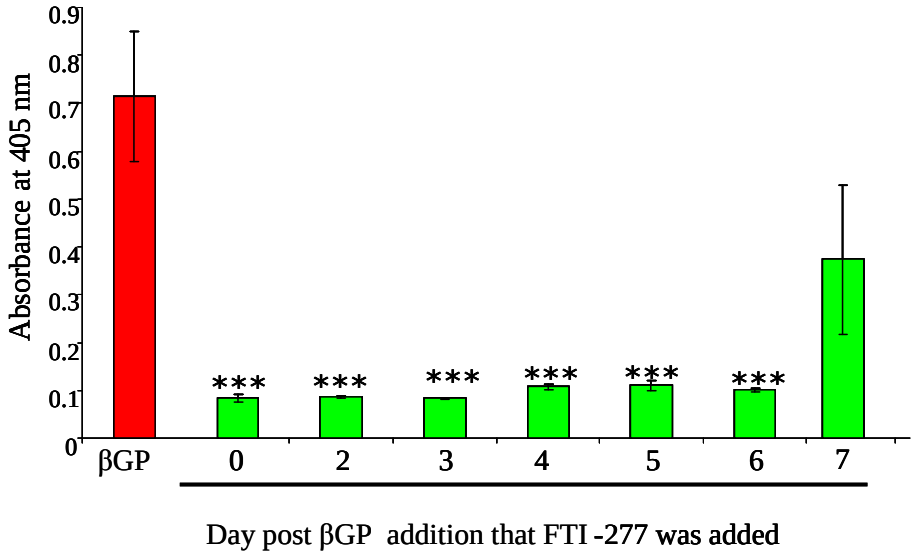

Figure 3.5: FTI-277 inhibits βGP-induced VSMC mineralisation in a time-dependent manner. (i) VSMCs were cultured in 6 well plates in 10% FCS-DMEM till 90% confluent, and were then incubated in medium containing βGP (5 mM) and DMSO (1:1000) (control; A), or with medium containing βGP and FTI-277 (10 μM; B). FTI-277 was then introduced to other wells on day 2 (C), day 3 (D), day 4 (E), day 5 (F), day 6 (G) and day 7 (H). Phase contrast images of cells stained with alizarin red on day 8 are shown. Scale bar = 500 μm (ii) Mineralisation was quantified by alizarin red dye elution (n=6, from two different experiments). ***p<0.001, FTI-277 vs βGP.

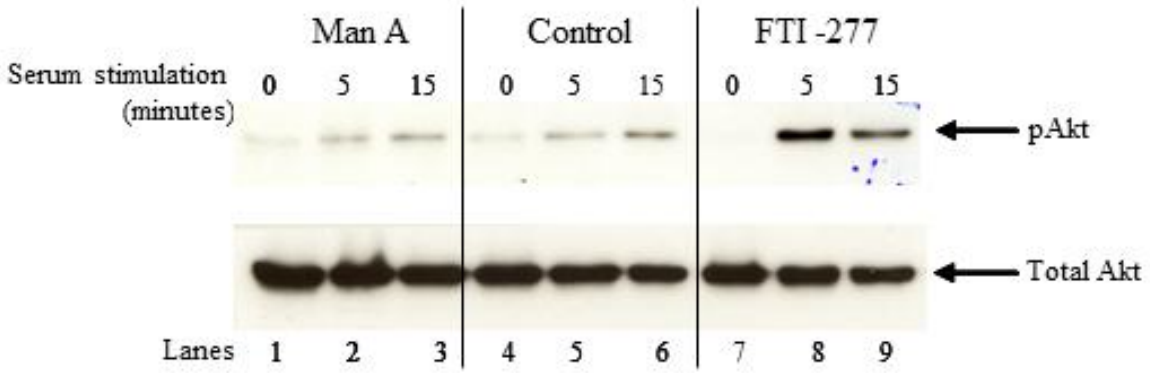

Figure 3.6: FTI-277 increases Akt phosphorylation in response to serum stimulation, but manumycin A has no effect. Confluent VSMCs were incubated with control medium (10% FCS-DMEM) or 10% FCS-DMEM + FTI-277 (10 µM) or Man A (10 µM) for 77 hours. Subsequently, VSMCs were incubated with serum-free medium for 2 hours with either FTI-277 or Man A, and then stimulated with 10% FCS-DMEM for 5 or 15 minutes. Cell lysates were collected and analysed for pAkt and total Akt expression using western blotting. Lanes 1, 4 and 7 contain samples collected prior to serum stimulation (T=0). Samples in lanes 2, 5 and 8 were collected after 5 minutes stimulation with serum-containing medium; samples in lanes 3, 6, 9 were collected after 15 minutes stimulation.

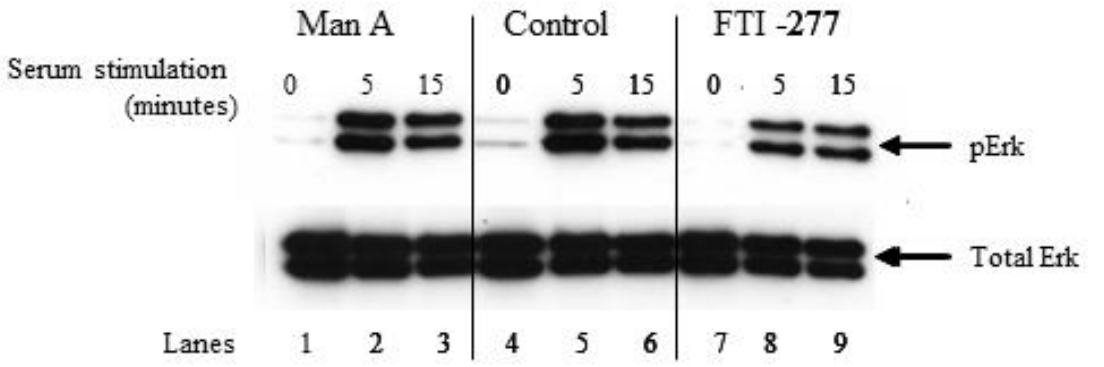

Figure 3.7: The effects of FTI-277 and manumycin A on serum-induced Erk phosphorylation. Confluent VSMCs were incubated as described in the legend to Figure 3.6, and cell lysates were collected and analysed for total Erk and pErk using western blotting. Lanes 1, 4 and 7 contain samples collected prior to serum stimulation (T=0). Samples in lanes 2, 5 and 8 were collected after 5 minutes stimulation with serum-containing medium; samples in lanes 3, 6, 9 were collected after 15 minutes stimulation.

3.2.7 FTI-277 increases Akt phosphorylation in long-term mineralisation assays

The results from section 3.2.5 showed that FTI-277 increases Akt phosphorylation in a short-term serum-stimulation assay. Therefore, the next aim was to determine the effect of FTI-277 on Akt phosphorylation in long-term mineralisation assays. In these experiments, protein was collected from VSMCs that were induced to calcify in the presence of βGP (Figure 3.8(i), B) or βGP + FTI-277 (Figure 3.8(i), C) on day 10 of the mineralisation experiment. Control cells were incubated in the absence of βGP (Figure 3.8(i), A). Cell lysates were analysed for Akt phosphorylation by western blotting. The results show that culturing VSMCs in the presence of βGP reduces Akt phosphorylation compared to controls, and that FTI-277 prevents this decrease (Figure 3.8(ii), compare lanes 1-3).

(i)

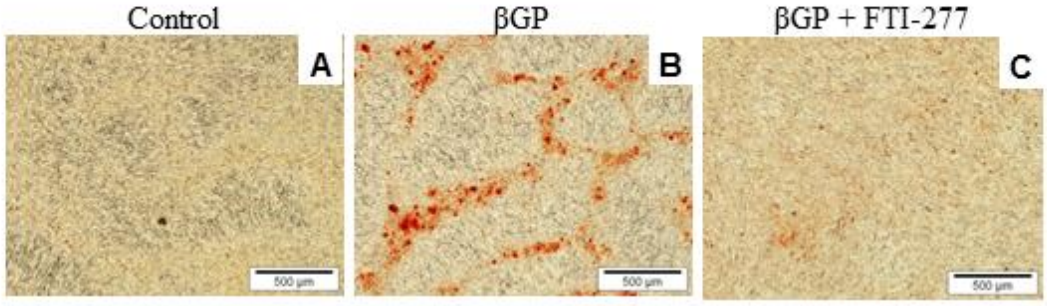

(ii)

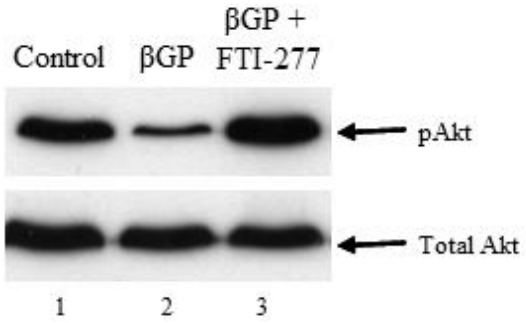

Figure 3.8: FTI-277 increases Akt phosphorylation in long-term mineralisation assays. VSMCs were cultured as detailed in the legend to Figure 3.2. (i) Phase contrast images of alizarin red stained cells on day 10. Scale bar = 500 μm. (ii) Cell lysates were collected from VSMCs on day 10 and analysed for phosphorylated Akt (pAkt) and total Akt using western blotting. Lane 1 (control), lane 2 (+ βGP), lane 3 (+ FTI-277 + βGP).

3.3 Discussion

This work demonstrated that the farnesyl transferase inhibitor, FTI-277, significantly inhibited the deposition of a mineralised matrix by VSMCs *in vitro* when added at the time of induction of mineralisation and at different time points during the mineralisation process. Second, using an active Ras pull-down assay and western blotting, it was demonstrated that FTI-277 significantly decreased Ras GTPase activation. Third, it was shown that FTI-277 increased Akt phosphorylation in short-term assays and in long-term mineralisation assays. However, FTI-277 either reduced or had no effect on serum-induced Erk phosphorylation. Interestingly, it was also shown that another farnesyl transferase inhibitor, manumycin A, had no effect on mineralisation of VSMCs *in vitro*. This inhibitor also reduced Ras activation after serum stimulation, but had no effect on serum-induced Akt phosphorylation and produced variable results on Erk phosphorylation. These results are discussed in more detail below.

3.3.1 FTI-277 and manumycin A inhibit Ras activation

FTI-277 is a potent Ras inhibitor with an IC_{50}=100 nM in NIH 3T3 cells (Lerner et al., 1995). Lerner et al showed that the potency of FTI-277 is due to the increased hydrophobicity of the central portion of the peptidomimetic. In contrast, manumycin A, has an IC_{50}=2.51 μM in human colon adenocarcinoma cells (Di Paolo et al., 2000). In addition, manumycin A can also inhibit other enzymes which use FPP, for example squalene synthetase and farnesyl diphosphate synthetase, the consequences of which are not known (Crul et al., 2001). In contrast, FTI-277 has been reported to be highly specific to its target enzyme (as reviewed in Khwaja et al., 2006.)

Therefore, it was important to determine whether both FTIs inhibited Ras activation at the concentrations used in these studies. Pre-incubation of VSMC with either FTI-277 or manumycin A markedly inhibited serum-stimulated Ras activation in these cells (Figure 3.1); although some active Ras was still detected in the FTI-277 treated cells (see Figure 3.1). In these studies, Ras activation was assessed using GST-Raf1-RBD (Raf1 is the main effector of Ras signalling), which detects all forms of active Ras. This assay was also used by Khawaja et al in their experiments (Khwaja et al., 2006). Interestingly, these authors suggested that prenylation may not be necessary for endogenous Ras activation, as both

prenylated and non-prenylated Ras are bound to GST-Raf1-RBD in normal mesangial cells (Khwaja et al., 2006). It is also known that certain isoforms of Ras are more resistant to FTIs than others. For example, K-Ras appears to be more resistant to FTIs than N-Ras. In the presence of FTIs, K-Ras undergoes cross-prenylation by geranylgeranyl transferase thus enabling it to exert functional activity (Bolick et al., 2003; Saxena et al., 2008; Prendergast and Oliff, 2000). In the experiments described in this report, it was not determined which isoforms of Ras are expressed in VSMCs (H-Ras, N-Ras or K-Ras). It is, therefore, possible that manumycin A and/or FTI-277 specifically block the farnesylation of certain isoforms of Ras, thereby allowing cross-prenylation. Furthermore, as many isoprenylated proteins can be affected by FTIs (Yeung et al., 2000), it is also possible that FTI-277 and manumycin A may exert their effects by modulating the activities of one or more of these proteins in VSMC.

3.3.2 FTI-277 inhibits βGP-induced VSMC mineralisation in a dose- and time-dependent manner, but manumycin A has no effect on this process

FTI-277 and manumycin A are farnesyl transferase inhibitors that inhibit farnesylation by different mechanisms. FTI-277 is a peptidomimetic which competes with Ras for the binding of farnesyl, whereas manumycin A is a FPP analogue which competes with FPP at the FTase binding site (see sections 1.8 and 1.9). In this study, it was shown that FTI-277 at a dose of 10 and 20 μM significantly inhibited mineral deposition by VSMC ($p<0.001$; see Figures 3.2 and 3.3). The cells appeared healthy during the time course of the experiments and FTI-277 had no effect on ridge formation in the cultures (which is where mineral is usually deposited). Furthermore, it was shown that the introduction of FTI-277 at different time points following the addition of βGP (day 2, 3, 4, 5, 6) also inhibited mineralisation (Figure 3.5). This result showed that FTI-277 is inhibitory even if it is given to the cells several days after the differentiation and mineralisation process has been initiated with βGP. However, it is noteworthy that the introduction of FTI-277 on day 7 of the experiment (just before the first spicules of mineralisation were detected) did not reduce mineralisation in the cultures. These results may be important if FTI-277 were to be developed for therapeutic use, particularly as the calcification process can start early on in patients with CKD.

The experiments performed in this chapter showed that 1-20 μM manumycin A had no effect on mineral deposition by VSMC (Figures 3.4). Interestingly, when used at higher concentrations (50 μM), many cells detached from the dish (see Figure 3.3), suggesting that manumycin A is cytotoxic at this concentration. This result is consistent with a previous study showing that 50 μM of manumycin A was cytotoxic to rat VSMC; no toxicity was detected at 25 μM (Guijarro et al., 1998). However, in another study, toxicity was detected at 0.9 μM in rat VSMC (Kouchi et al., 1999). The reason for these discrepancies is not known, but may reflect differences in the cell types used or the assay conditions.

3.3.3 FTI-277 increases Akt phosphorylation in VSMCs but manumycin A has no effect

The differences in the effects of FTI-277 and manumycin A on mineralisation could be due to their different modes of action. Therefore, experiments were conducted to analyse the effects of FTI-277 and manumycin A on the activation of signalling pathways downstream of Ras. In the first series of experiments, the effects of pre-incubating cells with FTI-277 and manumycin A on serum-induced activation of Akt were assessed. These studies were performed because previous studies had shown that (i) PI3K/Akt signalling is downstream of Ras (Datta et al., 1999); (ii) PI3K/Akt signalling inhibits apoptosis and apoptosis stimulates vascular calcification (Proudfoot et al., 2000), and (iii) inhibition of PI3K/Akt signalling promotes mineral deposition by VSMCs (Collett et al., 2007).

Interestingly, FTI-277 pre-treatment was shown to stimulate serum-induced Akt phosphorylation in VSMC after 5 and 15 minutes (see Figure 3.6). The level of Ras activation was also reduced in these samples (results not shown). As shown in Figure 3.2, FTI-277 inhibited βGP-induced VSMC mineralisation over a 10-12 day time-course. FTI-277 also increased Akt phosphorylation in these samples (Figure 3.8). These results confirm that FTI-277 increased Akt phosphorylation in both short-term (serum-induced) and long-term (mineralisation) assays.

Previous studies have shown that FTI-277 reduces Akt phosphorylation and promotes apoptosis in ovarian cancer cells (Jiang et al., 2000), but that it either has no effect or increases Akt phosphorylation in certain lung cancer cell lines (Sun et al., 2004).

More recently, studies using INS832/13 and normal rat islet cells have shown FTI-277 also increases Akt phosphorylation (Kyathanahalli and Kowluru, 2011). In this latter study, the cells were incubated with FTI-277 for 12 hours. Stimulation of these cells for 5 and 15 minutes with IGF -1 increased Akt phosphorylation even further (Kyathanahalli and Kowluru, 2011). These authors suggested that FTI-277 inhibited an unidentified farnesylated endogenous protein kinase B inhibitory protein (which they named probin) which then promoted Akt phosphorylation.

The reasons for the different effects of FTI-277 on Akt phosphorylation in different cells are not clear, but it may be related to the mutational status of Ras in the cancer cells, for example. It is also known that in the presence of FTI-277, K-Ras or N-Ras can become geranylgeranylated (see above) which can then induce downstream Akt signalling (Cox and Der, 2003). Indeed, the finding that some active Ras was still detected in FTI-277 treated VSMC (see Figure 3.1) may suggest that geranylgeranylation has occurred; although why Akt phosphorylation should be enhanced in FTI-277 treated VSMC compared to controls is unclear. It is also possible that growth factors present in serum may activate Akt in a Ras-independent manner in VSMCs; although if this is the case, then why there is more Akt phosphorylation in FTI-277 treated cells than in controls is also not clear. An alternative explanation is that FTI-277 may modulate Akt phosphorylation in VSMC by another mechanism unrelated to Ras.

In marked contrast, manumycin A was found to have no effect on serum-induced Akt phosphorylation in VSMC (see Figure 3.6). These results are consistent with a previous study which showed that manumcyin A does not affect Akt activation in murine smooth muscle cells (Galaria et al., 2005). However, work on cancer cells (lymphoid and myeloma cells) suggests that manumycin A reduces Akt phosphorylation in a ROS-dependent manner (Sears et al., 2008).

Together, these data show that FTI-277, but not manumycin A, promoted Akt phosphorylation, even though Ras activation was reduced following both treatments. The reason for this difference is not clear, but it is possible that Ras-independent effects of these FTIs may be involved. Previous studies have shown that FTI-277 reduces superoxide production in pulmonary smooth muscle cells (Boota et al., 2000), whereas manumycin A increases ROS (Sears et al., 2008). ROS can reduce Akt phosphorylation. It is therefore

possible that FTI-277 reduces superoxide production in VSMCs which, in turn, promotes Akt phosphorylation, cell survival and inhibits mineralisation.

Studies using another Ras inhibitor, FTS, have shown that this inhibitor reduced Akt phosphorylation and promoted apoptosis in prostate cancer cells (Erlich et al., 2006). Khawaja et al. have also demonstrated that FTS inhibited PDGF-induced Akt phosphorylation, but not serum-induced Akt phosphorylation in human mesangial cells (Khwaja et al., 2005). FTS also increased apoptosis in the presence of PDGF, but not serum. FTS inhibited PDGF-induced proliferation of mesangial cells, but had no effect on serum-induced proliferation (Khwaja et al., 2005), suggesting that serum-stimulation of Akt phosphorylation may work independently of Ras inhibition in mesangial cells. More recent work using 3-Deazaadenosine, which regulates cellular methyltransferase activity, showed that it inhibited serum-induced Ras activation and Akt phosphorylation in VSMC, but had no effect on apoptosis (Sedding et al., 2009). This compound also inhibited VSMC proliferation *in vitro* and neointima formation *in vivo* (Sedding et al., 2009). The effects of targeting Ras using FTS on mineral deposition by VSMC will be further investigated in chapter 5.

Taken together, the results detailed above suggest that FTI-277 may inhibit mineralisation of VSMCs by promoting Akt phosphorylation, which then inhibits apoptosis. Therefore, future work will investigate the link between FTI-277, Akt phosphorylation, apoptosis and mineralisation in VSMCs (see Chapter 4).

3.3.4 FTI-277 and manumycin A have inconsistent effects on Erk phosphorylation following serum stimulation

Erk is another downstream effector of Ras/Raf, and previous studies have shown that Erk signalling is important for smooth muscle differentiation under calcifying conditions (Speer et al., 2009). Further work has also suggested that the Erk pathway is important for regulating valvular interstitial cell calcification (Gu and Masters, 2009). Therefore, experiments were conducted to investigate the effects of pre-incubating cells with FTI-277 or manumycin A on Erk phosphorylation.

The studies described in this chapter demonstrated that Erk phosphorylation in VSMCs was variable. Previous studies have shown that manumycin A reduces Erk

phosphorylation in cancer cells (Sears et al., 2008) and rat smooth muscle cells (Sugita et al., 2007). FTI-277 also reduced Erk phosphorylation in multiple myeloma cells and this effect was brought about by the inhibition of Ras and IL-6 (Shi et al., 2003). The reason for the variability in results in this study is not clear. However, the demonstration that FTI-277 inhibited mineralisation, despite having variable effects on Erk phosphorylation, suggests that FTI-277 does not inhibit mineralisation via Erk.

Conclusions

In summary, these studies demonstrated that different doses of FTI-277 inhibited mineral deposition by VSMC, whereas manumycin A had no effect on this process. This study also suggested that this difference in mineralisation may be due to the increased Akt phosphorylation detected in the FTI-277 treated cells. Intriguingly, both farnesyl transferase inhibitors inhibited Ras GTPase activation, possibly suggesting that Akt activation may occur via a Ras-independent pathway. Furthermore, both FTI-277 and manumycin had variable effects on Erk phosphorlyation. Therefore, the rest of the work in this thesis will focus on determining the mechanism by which FTI-277 inhibits mineralisation.

Chapter 4

Delineating the mechanism by which FTI-277 inhibits mineralisation of VSMCs

4.1 Introduction

The purpose of the studies described in this chapter is to further delineate the mechanism(s) by which FTI-277 regulates mineral deposition by VSMC. The work described in Chapter 3 suggests that FTI-277 may inhibit mineralisation by promoting Akt phosphorylation. Phosphorylation of threonine-308 and serine-473 is required for activation of Akt and downstream signalling pathways (Jiang et al., 2000). The PI3K/Akt signalling pathway is known to play an important role in cell survival (Datta et al., 1999), and inhibiting apoptosis using zVAD.fmk inhibits mineral deposition by VSMCs (Proudfoot et al., 2000)**.**

The PI3K/Akt signaling pathway has previously been implicated in the regulation of vascular calcification. For example, previous work from this laboratory has shown that wortmannin (a PI3K inhibitor) prevents the inhibition of mineralisation induced by the over-expression of Axlin VSMCs, and that inhibition of apoptosis by zVAD.fmk negates the effect of kinase-dead Axl (Collett et al., 2007). In addition, omentin 1 has been shown to inhibit calcification by activating down-stream PI3K/Akt signalling (Duan et al., 2010).

It is not known whether stimulation of Akt phosphorylation is required for the inhibition of mineralisation by FTI-277. Furthermore, it is not known whether FTI-277 inhibits apoptosis of VSMC and, if so, whether this is the mechanism by which it inhibits mineral deposition by these cells. Vascular calcification is also associated with the osteogenic conversion of VSMCs as demonstrated by the up-regulation of osteogenic transcription factors such as Runx2, Msx2, and an increase in promoters of calcification such as ALP (Toussaint, 2011, Giachelli et al., 2011). A decrease in inhibitors of calcification such as MGP and loss of smooth muscle cell markers such as α-smooth muscle actin (ASMA) have also been described (Montes de Oca et al., 2010, Steitzet al., 2001). However, whether FTI-277 modulates the osteogenic differentiation of VSMCs is not known. Finally, it is not known whether FTI-277 stimulates Akt and inhibits mineralisation in a Ras-dependent or –independent manner. These questions will be addressed in the studies described in this chapter.

Therefore, the objectives of the studies described in this chapter are to:

(i) Determine whether inhibiting PI3K/Aktsignalling will prevent the inhibition of mineralisation by FTI-277.

(ii) Determine whether FTI-277 prevents apoptosis induced by serum-deprivation and high phosphate.

(iii) Determine the effects of FTI-277 on VSMCs migration

(iv) Determine whether FTI-277 modulates the mRNA expression of osteogenic markers (Runx2, Msx2), alkaline phosphatase (ALP) and MGP, and the smooth muscle cell marker, ASMA, during the mineralisation process.

(v) Determine the effects of FTI-277 on *ex vivo* mineralisation of aortic rings from rats with early and end stage renal disease

4.2 Results

4.2.1 FTI-277 inhibits mineralisation by promoting PI3K/Akt signalling

To determine whether FTI-277 inhibits mineralisation by promoting PI3K/Akt signalling, VSMCs were treated with ßGP-containing medium in the presence of FTI-277, wortmannin, or FTI-277 and wortmannin for up to 13 days. Mineralisation was clearly detected in cells incubated plus ßGP (Figure 4.1 A, E), wortmannin (C, G) and FTI-277/wortmannin (D, H). Interestingly, increased mineralisation was detected in cells treated with wortmannin compared to ßGP alone (compare Figure 4.1 C, G to A, E). As shown in Chapter 3, FTI-277 inhibited ßGP-induced mineralisation of VSMCs (Figure 4.1 B, F) compared to ßGP (Figure 4.1A, E). Although some mineralisation was detected in the FTI-277 treated cells on day 13 (Figure 4.1 F), it was considerably less than the levels detected in the other groups of cells at this time-point (compare Figure 4.1 F to E, G, and H). In the FTI-277/wortmannin-treated cells, some mineralisation was also detected, but it was not as intense as the wortmannin-alone treated group (compare Figure 4.1 D, H to C, G).

Quantification of mineralisation was performed by eluting the alizarin red dye and measuring the absorbance (Figure 4.2). These results confirm that wortmannin increased mineralisation compared to ßGP (***$p<0.001$), and that it partially negated the inhibitory effect of FTI-277 on mineralisation (***$p<0.001$, FTI-277 vs FTI-277/wortmannin).

The effects of FTI-277, wortmannin and FTI-277/wortmannin on Akt phosphorylation were also examined as described in Section 3.2.5. As shown in Chapter 3, Akt phosphorylation was increased in VSMCs pre-incubated with FTI-277 (Figure 4.3; lanes 4 - 6) compared to controls (Figure 4.3 lanes 1 - 3). Akt phosphorylation was reduced in the wortmannin-treated cells compared to the controls at time = 0 and after 5 mins serum-stimulation (Figure 4.3; compare lanes 7 and 8 with lanes 1 and 2). In comparison with wortmannin-alone treated cells, the FTI-277/wortmannin cells had higher levels of Akt phosphorylation (Figure 4.3; compare lanes 10 and 11 with lanes 7 and 8). These data suggest that FTI-277 prevents mineral deposition by increasing Akt phosphorylation in VSMC.

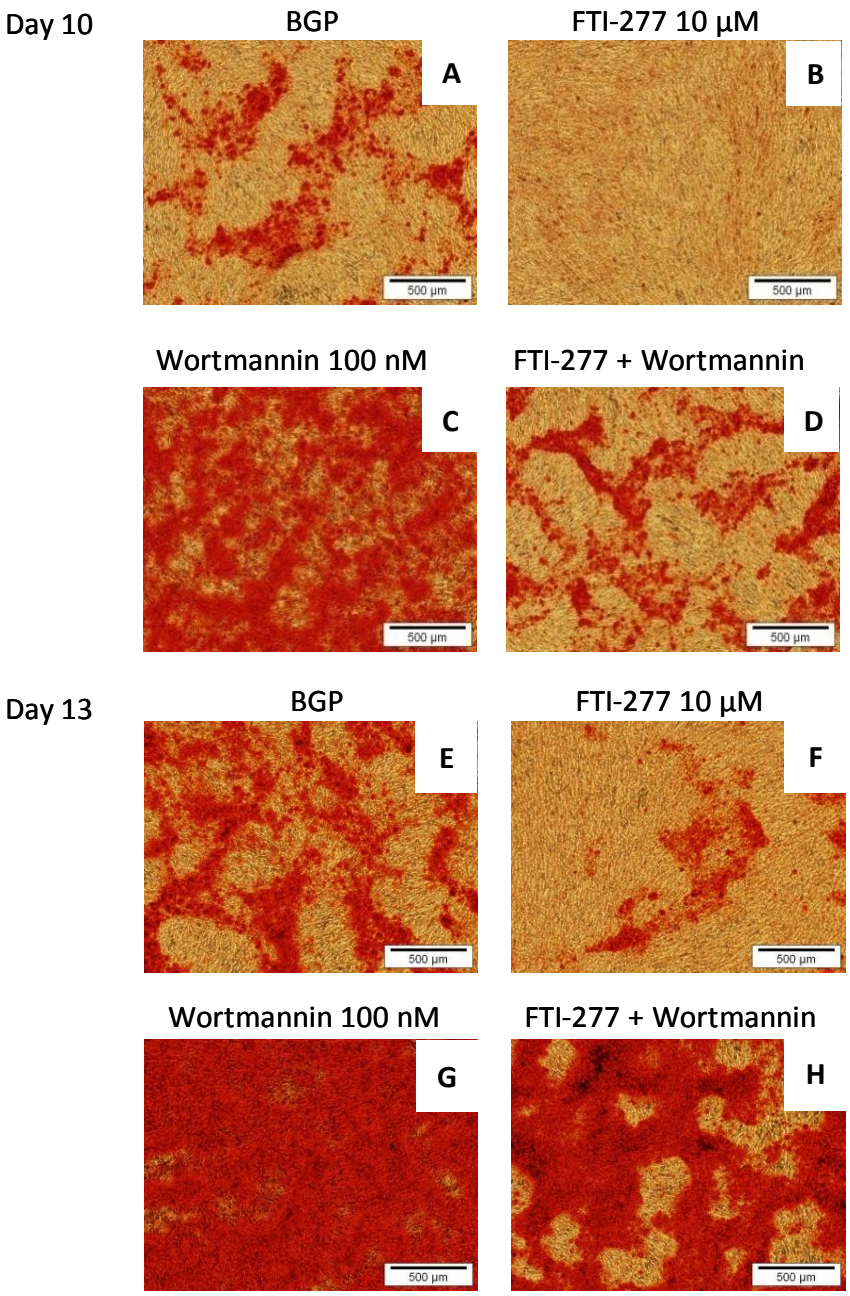

Figure 4.1: FTI-277 inhibits ßGP-induced mineralisation of VSMCs by promoting PI3K/Akt signalling.VSMCs were cultured in 6 well plates in DMEM-10% FCS till 90% confluency, and were then incubated in 10% FCS-DMEM containing ßGP and DMSO (1:1000; ßGP)(A,E), or with 10% FCS-DMEM + ßGP + FTI- 277 (10 µM) (B,F) or wortmannin (100 nM) (C,G) or FTI-277 + wortmannin (D,H). Phase contrast images of alizarin red stained VSMCs on day 10 and 13 are shown. Red indicates mineralisation. Scale bar = 500 µm**.**

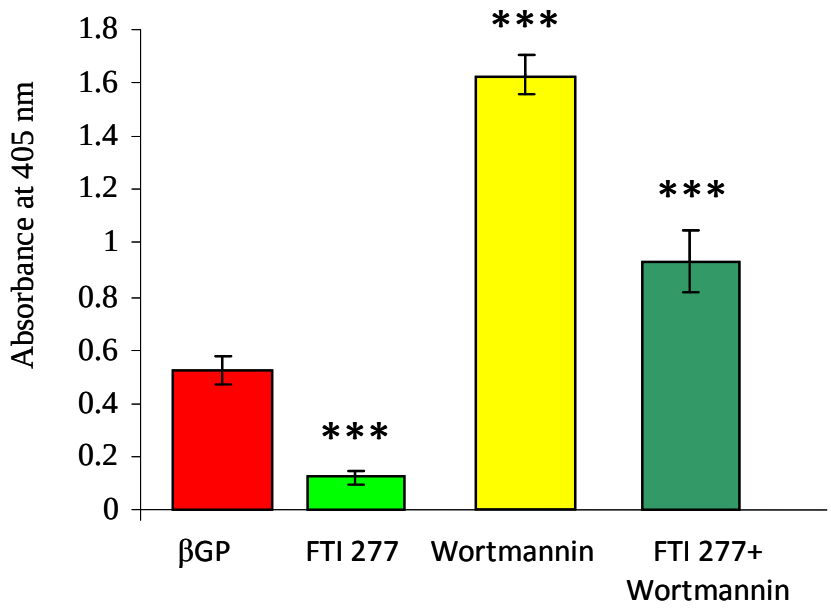

Figure 4.2: FTI-277 inhibits ßGP-induced mineralisation of VSMCs by promoting PI3K/Akt signalling. Samples were prepared as detailed in the legend to figure 4.1, and alizarin red dye elution was performed in order to quantify mineralisation in the cultures. The results presented are from two different experiments and data are shown as mean ± SEM (n=12). (***p<0.001 FTI-277 vs βGP, FTI-277 vs Wortmannin, FTI-277 vs Wortmannin/FTI-277, βGP vs Wortmannin).

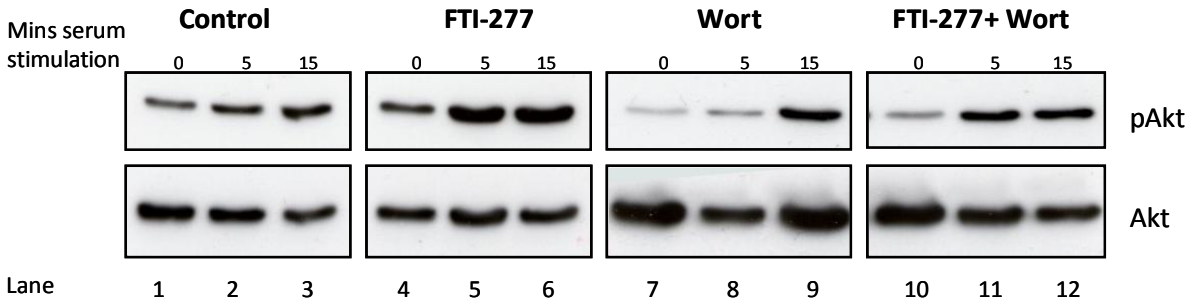

Figure 4.3: FTI-277 inhibits mineralisation by activating PI3K/Akt signalling. Confluent VSMCs were incubated 10% FCS-DMEM containing DMSO (1:1000; control), or with 10% FCS-DMEM + FTI- 277 (10 µM), wortmannin (100 nM) or FTI-277 + wortmannin for 77 hours. Subsequently, VSMCs were incubated with serum-free medium for 2 hours with reagents detailed above, followed by stimulation with 10% FCS-DMEM for 5 or 15 minutes. Cell lysates were collected prior to serum stimulation (T=0) and after 5 and 15 serum stimulation. They were analysed for phosphorylated Akt (pAkt) and total Akt expression using western blotting. Samples collected at T = 0 are in lanes 1, 4, 7 and 10. Lanes 2, 5, 8 and 11 contain samples collected after 5 minutes stimulation; samples in lanes 3, 6, 9 and 12 were collected after 15 minutes stimulation.

4.2.2 FTI-277 inhibits mineralisation by promoting Akt signalling

In order to confirm that Akt phosphorylation is required for the inhibition of mineralization by FTI-277, SH6, an AKT III inhibitor was used. The first experiment was performed to confirm that SH6 inhibits Akt phosphorylation in VSMCs. VSMCs were grown to confluence and serum-starved for 2 hours in the presence of SH6 (10 µM) or vehicle control (DMSO, 1:1000), after which they were stimulated with serum-containing medium (10% FCS-DMEM) for 5 minutes. Protein lysates were collected at baseline (T=0) and after 5 minutes serum stimulation. Figure 4.4 shows a reduction in Akt phosphorylation in VSMCs pre-incubated with SH6 (lanes 3 and 4) compared to controls (lanes 1 and 2).

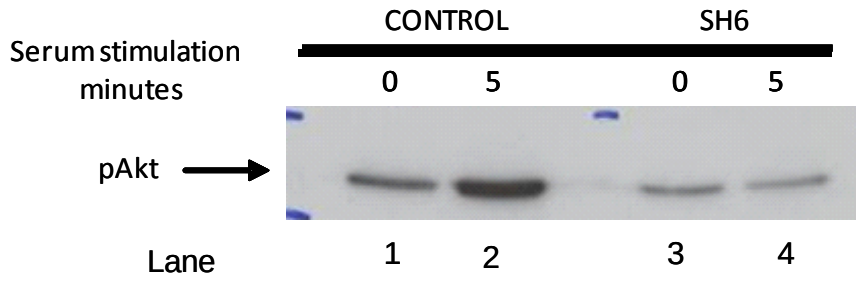

Figure 4.4: SH6 inhibits Akt phosphorylation in VSMCs. Confluent VSMCs were incubated in the presence DMSO (1:1000); control), or SH6 (10 µM) 2 hours. Subsequently, VSMCs were stimulation with 10% FCS-DMEM for 5 minutes. Cell lysates were collected prior to serum stimulation (T=0), after 5 serum stimulation. Protein samples were analysed for phospho-Akt expression using western blotting. Lanes 2, 4 contain samples collected after 5 minutes stimulation; T=0 samples are lane 1, 4.

To determine whether FTI-277 inhibits mineralisation by promoting Akt phosphorylation, VSMCs were treated with ßGP-containing medium with vehicle (DMSO 1:1000) (ßGP) in the presence of FTI-277(10 µM), SH6 (10 µM), or FTI-277 and SH6. Mineralisation was clearly detected in the ßGP (Figure 4.5 A), SH6 (B) and FTI-277/SH6 (D) groups of cells. FTI-277 inhibited ßGP-induced mineralisation of VSMCs on day 10 (Figure 4.5C).

Quantification of mineralisation was performed at each time point by eluting the alizarin red dye and measuring the absorbance. Figure 4.5 (ii) shows quantification from two different experiments (n=6). SH6 negated the inhibitory effect of FTI-277 on mineralisation FTI-277 vs FTI-277/SH6 (*$p<0.05$) (Figure 4.5 (ii)). This effect was also seen at the other time points (data not shown).

Protein was collected from the mineralisation experiments described above, and western blotting was performed in order to determine Akt phosphorylation following the various treatments. Figure 4.6 shows that Akt phosphorylation was increased in VSMCs pre-incubated with FTI-277 (lane 3) compared to + ßGP (lanes 1). Akt phosphorylation was reduced in the SH6-treated cells compared to + ßGP (compare lanes 2 and 1). SH6 was found to negate the stimulatory effect of FTI-277 on Akt phosphorylation (compare lanes 4 and 3).

(i)

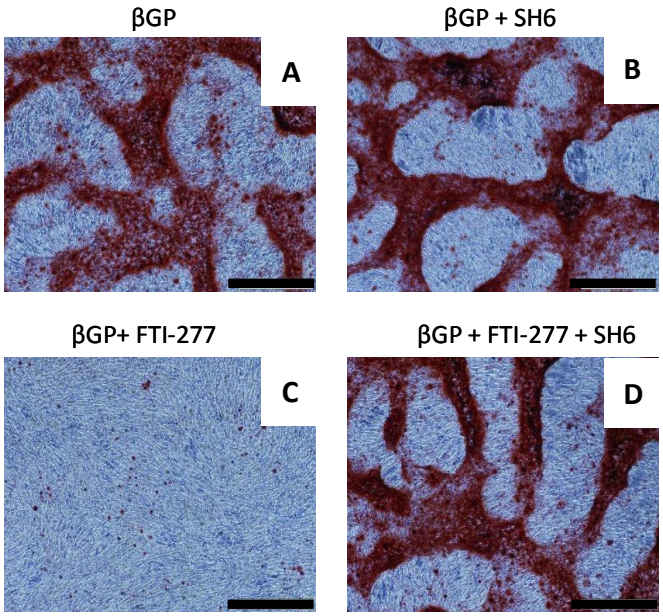

(ii)

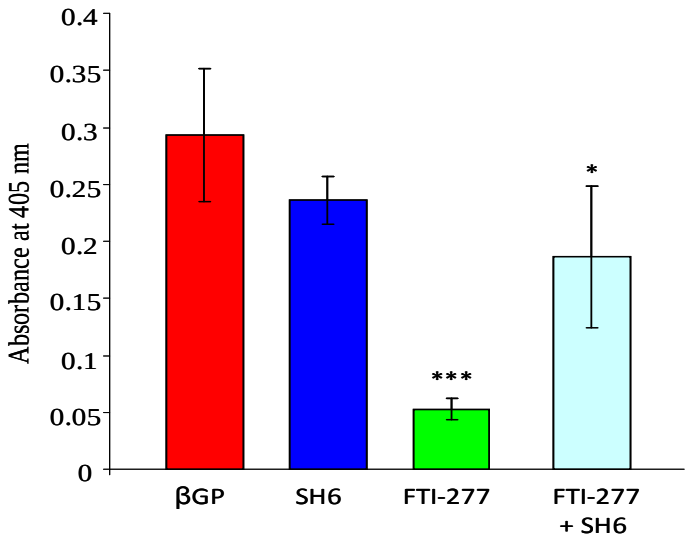

Figure 4.5: FTI-277 inhibits mineralisation by promoting Akt signalling. (i)VSMCs were cultured in 6 well plates in DMEM-10% FCS till 90% confluency, and were then incubated in 10% FCS-DMEM containing (A) ßGP and DMSO (1:1000; ßGP), or with 10% FCS-DMEM containing ßGP and either (B) SH6 (10 µM), (C)FTI-277 (10 µM) or (D) FTI-277 + SH6. Phase contrast images of alizarin red stained VSMCs on day 9 are shown. Scale bar = 500 µm. (ii) Alizarin red dye elution was performed in order to quantify mineralisation in the cultures. The results presented are pooled from two different experiments (n=6). *p<0.05, FTI-277 vs FTI-277/SH6, ***p<0.01 FTI-277 vs βGP

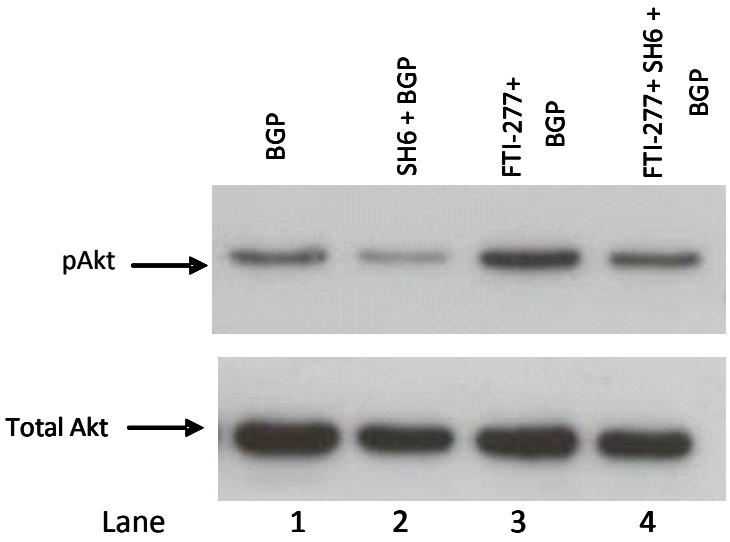

Figure 4.6: SH6 negates the effect of FTI-277 on Akt phosphorylation. Samples were prepared as detailed in the legend to Figure 4.5. Cell lysates were collected from these samples on day 10, and analysed for phosphorylated Akt (pAkt) and total Akt expression using western blotting. Lane 1 (βGP +DMSO, 1:1000), lane 2 (βGP +SH6), lane 3 (FTI-277 + βGP) and lane 4 (FTI-277 + SH6 + βGP).

4.2.3 Generation of lentivirus encoding dominant negative Akt

The studies detailed above demonstrated that targeting PI3K/Akt signalling using two different inhibitors (wortmannin and SH6) negated the effect of FTI-277 on mineralisation. The aim of this part of the project was to produce a lentivirus encoding a dominant negative form of Akt (mutant PKB) (pHIV-PKB-CAAX) (see Figure 4.7 i, ii) to confirm these effects.

4.2.3.1 Cloning PKB-CAAX into the lentiviral pHIV vector

PKB-CAAX (mutant PKB cDNA) was provided in a pcDNA3.1 vector for use in these studies. It was excised from this vector using restriction enzymes Not1-HF and SpE1 and separated by electrophoresis on a 1% agarose gel (see Figure 4.7 iii). The 1.5 kb band which corresponds to PKB-CAAX was excised from the gel and purified as described in section 2.9. The lentiviral vector, pHIVzsgreen, was purified (not shown), treated with alkaline phosphatase and re-purified. The PKB-CAAX cDNAand pHIVvector were ligated together (see section 2.9) and the ligation mixture transformed into competent cells. Six colonies were picked at random, purified (see section 2.9) and these samples were

sequenced (see section 2.9). One clone was chosen for future studies, pHIV-PKB-CAAX. In parallel studies, a control without the insert, termed pHIV-Empty vector, was obtained.

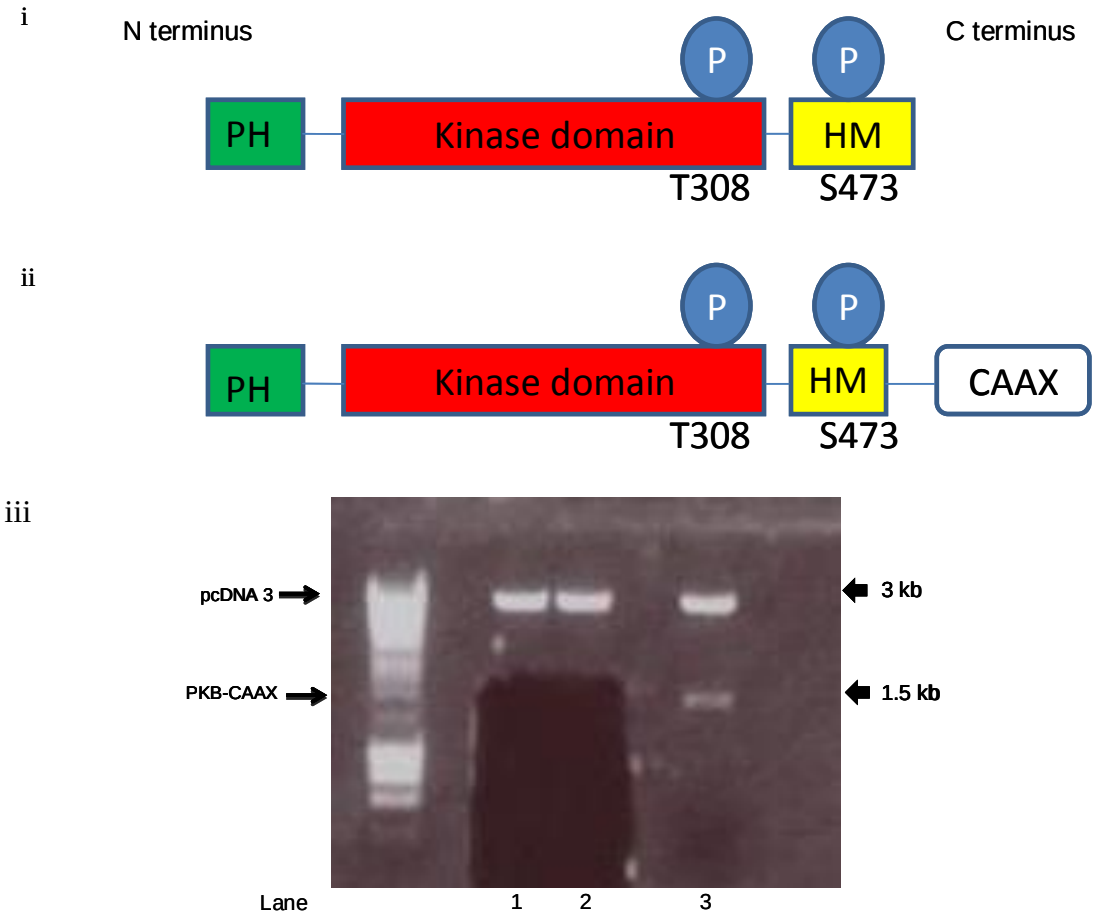

Figure 4.7: (i) PKB (ii) PKB-CAAX construct. Activation of Akt involves membrane binding at the N-terminal pleckstrin homology (PH) domain, and phosphorylation at Threonine 308 and Serine 473 in the hydrophobic motif (HM) (C-terminus). PKB-CAAX (dominant negative Akt) interferes with phosphorylation at Serine 473 and membrane binding at the PH domain. **(iii) Cloning PKB-CAAX into the lentiviral pHIV vector**. PKB-CAAX was excised from pcDNA3.1 using restriction enzymes Not1-HF and SpE1, and separated by electrophoresis on a 1% agarose gel.

4.2.3.2 Transduction of pHIV-PKB-CAAX into 293T cells

After reaching 70% confluence, 293T cells were incubated with either pHIV-Empty vector or pHIV-PKB-CAAX. Figure 4.8 (i) shows 293T cells with pHIV-Empty vector (A, B) or pHIV-PKB-CAAX (C,D) immediately after they were transduced, day 0 (A,C), and 1 (B,D). Cells incubated with pHIV-PKB-CAAX appeared unhealthy in comparison to cells incubated with the pHIV-Empty vector (D with B).

(i)

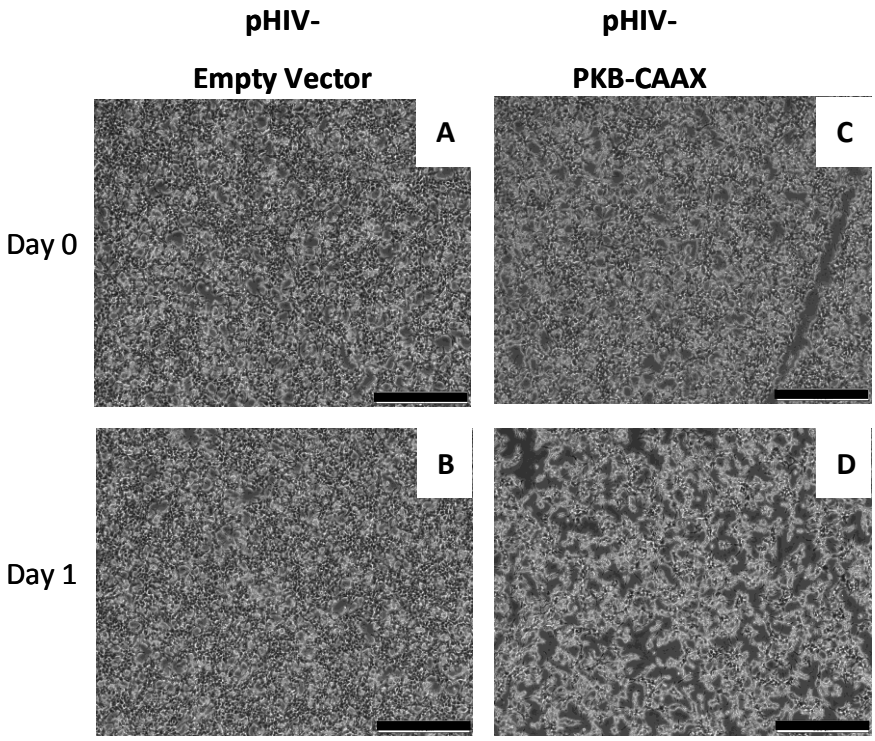

(ii)

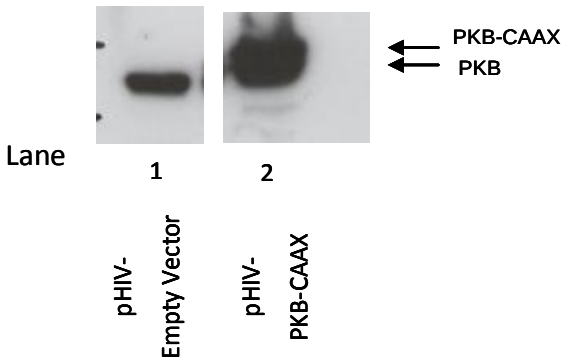

Figure 4.8: Transduction of 293T cells with pHIV-PKB-CAAX. (i) 293T cells were grown to 70% confluencyand then transduced with either pHIV-Empty vector (A, B) or pHIV-PKB-CAAX (C, D). Phase contrast images immediately after transduction (day 0) and one day after transduction are shown. Scale bar = 500 µm. (ii) Cell lysates were collected after 1 day and were analysed for total Akt by western blotting. Lane 1 = pHIV-Empty vector and lane 2 = pHIV-PKB-CAAX.

Protein samples were extracted and analysed for Akt (Figure 4.8 (ii)). Western blot analysis shows overexpression of Akt in pHIV-PKB-CAAX samples compared to pHIV-Empty vector samples.

4.2.3.3 Transduction of VSMCs with pHIV-PKB-CAAX or pHIV-Empty vector

VSMCs were grown to 70% confluency (Figure 4.9A) and viral particles containing either pHIV-PKB-CAAX or pHIV-Empty vector were then added to the medium (see section 2.12.2). On day one following transduction, VSMCs with pHIV-PKB-CAAX (Figure 4.9C) were less confluent that VSMCs with pHIV-Empty vector (Figure 4.9B). Immunofluorescence confirms the successful transduction of VSMCs with either pHIV-Empty vector (Figure 4.9D) or pHIV-PKB-CAAX (Figure 4.9E). The VSMCs that were transduced with pHIV-PKB-CAAX were termed dominant negative Akt (dn-Akt) and with pHIV-Empty vector were termed Empty vector.

4.2.3.4 Overexpression of dominant negative Akt in VSMCs

The next aim was to confirm that the dn-Akt VSMCs were overexpressing mutant Akt. Therefore, Dn-Akt and Empty vector VSMCs were grown to confluence and then serum starved for 4 hours. Dn-Akt VSMCs appeared unhealthy, sensitive to serum-free medium and there were gaps between the cells (Figure 4.10B, D). In contrast, Empty vector VSMCs appeared healthy, even after incubation in serum-free medium (Figure 4.10A, C). Following 4 hours of incubation in serum-free medium, VSMCs were stimulated with serum (10% FCS-DMEM) for 5 and 15 minutes. Protein lysates were collected at baseline (T=0), and after 5 and 15 minutes serum stimulation. Western blot analysis showed overexpression of total Akt in the dn-Akt VSMCs compared to Empty vector controls (Figure 4.10(ii), lower panel). Dn-Akt VSMCs have reduced Akt phosphorylation compared to Empty vector control following serum stimulation (Figure 4.10 (ii), upper panel). Interestingly, some Akt phosphorylation is detected in dn-Akt VSMCs prior to and after serum stimulation (Figure 4.10 (ii), upper panel), suggesting that not all of the cells were transduced with the virus.

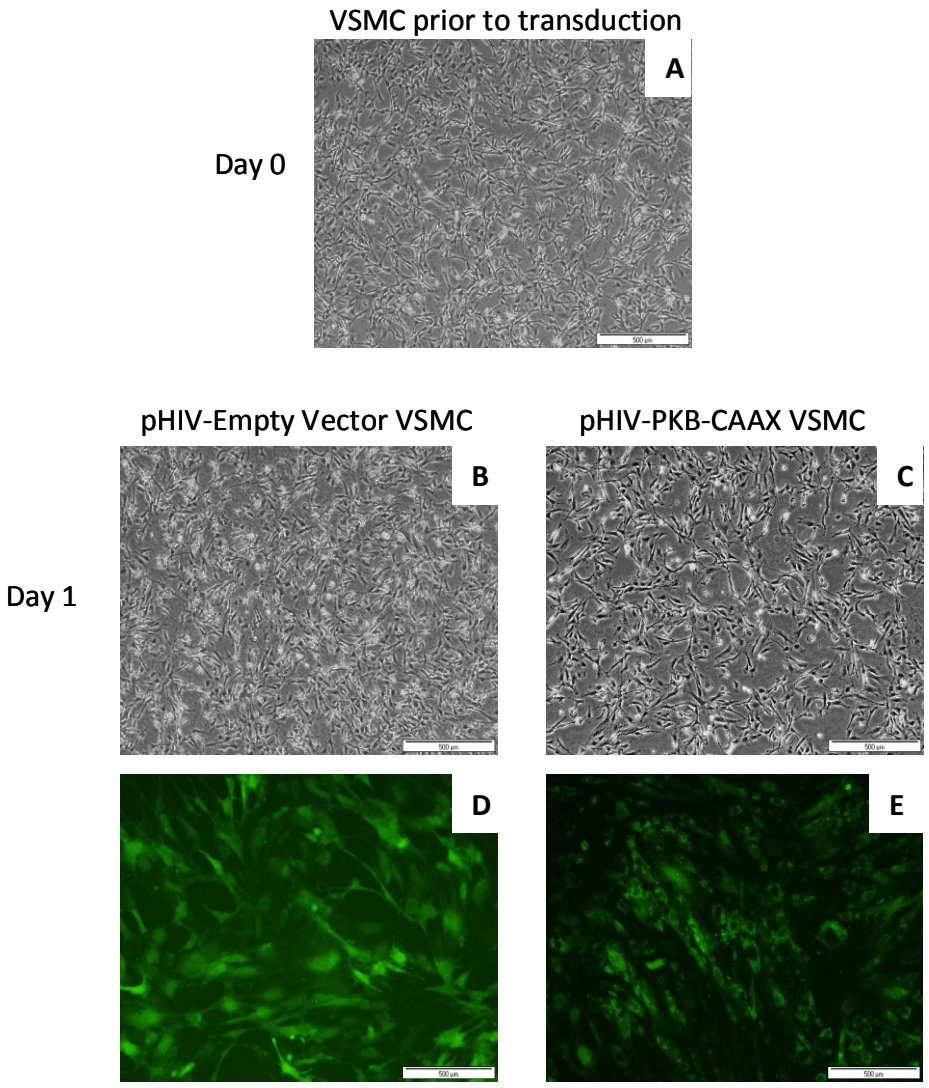

Figure 4.9: Transduction of VSMCs with pHIV-PKB-CAAX. VSMCs were grown to 70% confluency prior to transduction (A) (day 0). Phase contrast images of VSMCs one day after transduction with: (B) pHIV-Empty vector and (C) pHIV-PKB-CAAX. Immunofluorescence images on VSMCs one day after transduction with (D) pHIV-Empty Vector and (E) pHIV-PKB-CAAX. Scale bar = 500 µm.

(i)

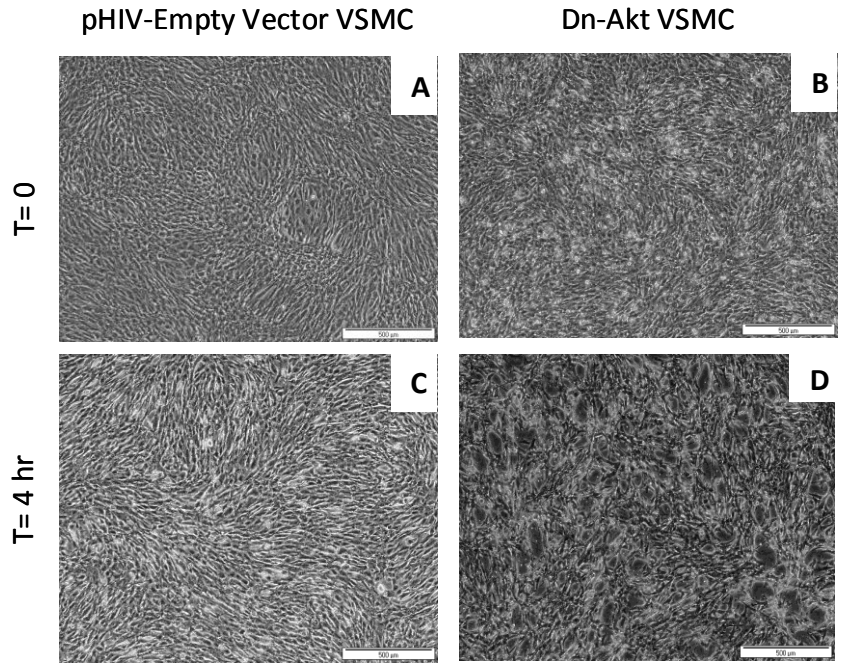

(ii)

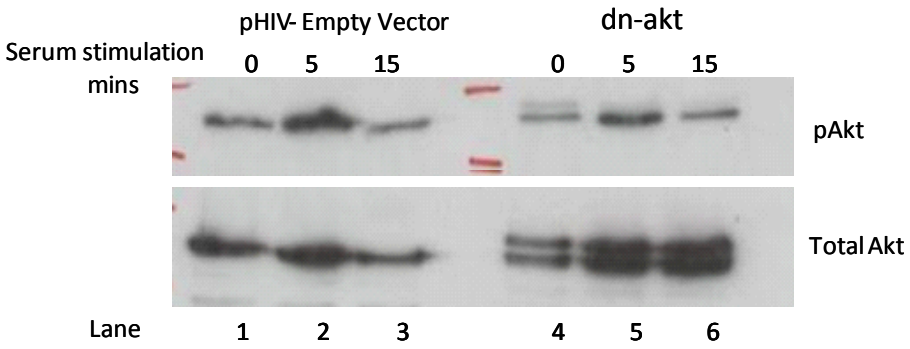

Figure 4.10: Overexpression of VSMCs with pHIV-PKB CAAX (dn-Akt). (i) Empty vector VSMCs (A) and dn-Akt VSMCs (B) were grown to confluency and serum-starved for 4 hours (C) (D). Scale bar = 500 µm. (ii) After 4 hours, VSMCs were stimulated with serum-containing medium for 5 and 15 minutes. Cell lysates were collected prior to serum stimulation (T=0), and after 5 and 15 minutes serum stimulation, and analysed for phosphorylated Akt (pAkt) and total Akt expression. Lanes 1 and 4 contain samples prior to serum stimulation. Lanes 2 and 5 contain samples collected after 5 minutes stimulation; lanes 3 and 6 contain samples collected after 15 minutes.

4.2.3.5 The effects of dn-Akt and FTI-277 on mineral deposition by VSMCs

Following confirmation of overexpression of dn-Akt, the effects of βGP and / or FTI-277 on mineral deposition by VSMCs transduced with either the Empty vector or dn-Akt were investigated. Phase contrast microscopy showed that when cultured under these conditions, Empty vector VSMCs appeared healthy, reached confluence after 5 days and formed multilayers at post-confluence (Figure 4.11), as previously shown for non-transduced VSMCs (see Chapter 3). Furthermore, alizarin red staining confirmed that Empty vector VSMCs incubated plus βGP deposited a mineralised matrix (Figure 4.12B); whereas cells incubated without βGP did not (Figure 4.12A), and FTI-277 prevented the induction of mineralisation by βGP (Figure 4.12C). These results confirm that transduction with lentivirus does not affect mineral deposition by these cells. In contrast, dn-Akt VSMCs took longer to reach confluency than Empty vector VSMCs (7 days compared to 5 days), and were unhealthy when maintained to post-confluency under all the conditions tested. Many cells died, multilayers were not formed, and eventually the cells detached (results not shown). These results suggest, perhaps not surprisingly, that functioning Akt is essential for the growth and maintenance of healthy VSMCs. Therefore, no further studies were pursued with this lentivirus.

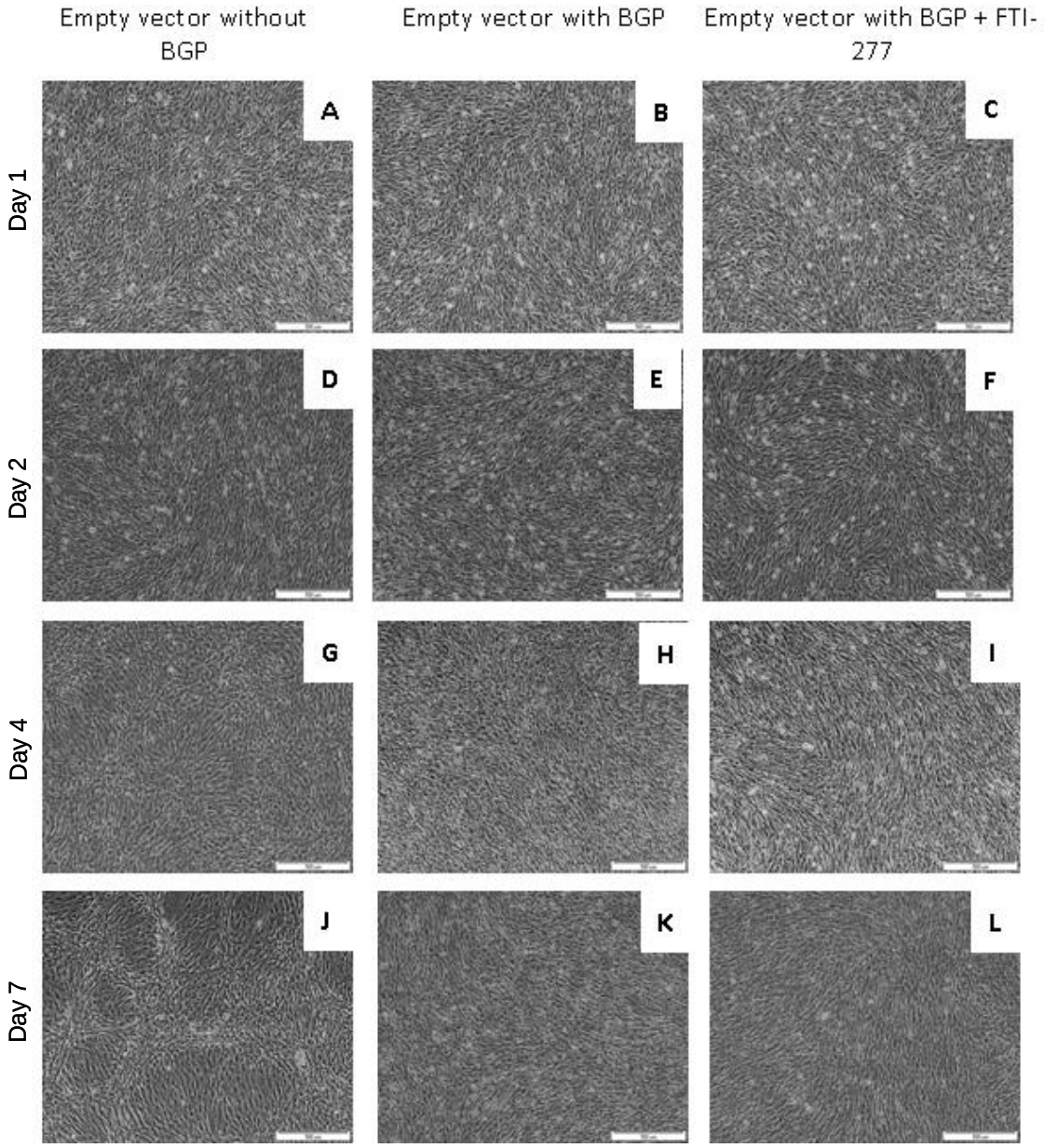

Figure 4.11: Phase contrast images of Empty vector VSMCs. Empty vector VSMCs were gown to confluency (day 0) and incubated +/- βGP and +/- FTI-277 as described previously. Phase contrast images of cells on day 1 (A, B, C), 2 (D, E, F), 4 (G, H, I), and 7 (J, K, L) are shown. Scale bar = 500 µm.

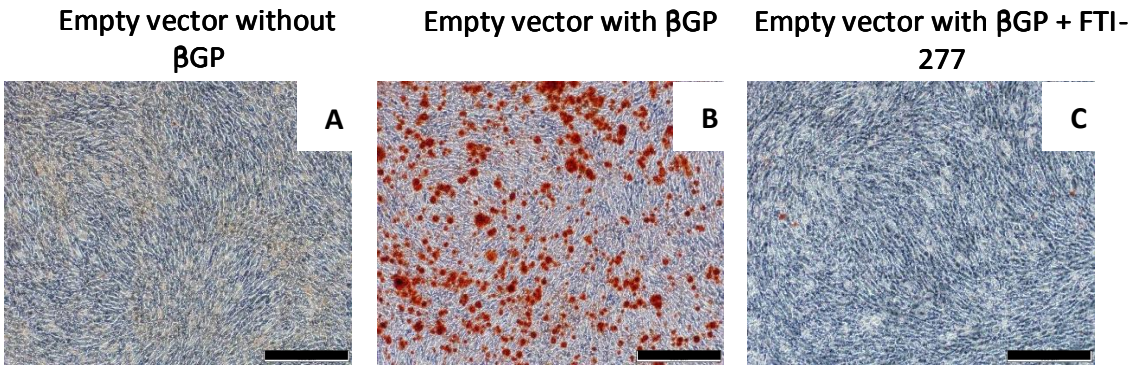

Figure 4.12: FTI-277 inhibits ßGP-induced mineralisation in Empty Vector VSMCs. Empty vector VSMCs were incubated +/-ßGPand FTI-277 as detailed in the legend to figure 4.11. Cells were stained with alizarin red on day 7. (A) Empty vector without ßGP; (B) with ßGP, (C) with ßGP +FTI-277. Red indicates mineralisation. Scale bar = 500 µm

4.2.4 FTI-277 inhibits phosphate-induced VSMC apoptosis

Human coronary VSMCs (HCVSMCs) were induced to undergo apoptosis by incubating in serum-free medium in the presence of elevated phosphate, as described in section 2.6. Prior to incubation with elevated phosphate (2.6 mM Pi), the cells appeared healthy and dense (Figure 4.13A). Following incubation of the cells in the presence of elevated phosphate, they became more sparsely distributed and appeared unhealthy (compare Figure 4.13; A to B-G). However, these features were more marked in the phosphate-treated cells when compared to FTI-277/phosphate-treated cells at every time point examined (Figure 4.13; compare B-D to E-G). After 6 hours, more dead cells were seen in the phosphate-alone treated cells compared to cells treated with FTI-277 plus phosphate (Figure 4.13 compare D to G).

Cell lysates were also collected for protein analysis at the different time points (0, 2 and 4 hours).Analysis of these samples revealed that the levels of phosphorylated Akt increased at 2 hours in FTI-277 and phosphate-treated cells compared to cells treated with increased phosphate alone (Figure 4.14; compare lanes 4 and 2) and also compared to levels at the start of the experiment (T=0) (Figure 4.14; lane 1). The blot was stripped and re-probed for total Akt which showed similar levels in the samples (Figure 4.14). Western blot analysis for active caspase 3 shows it was detected at 4 hours in the phosphate-treated cells (Figure 4.14, lane 3). In contrast, active caspase 3 was barely detected in the FTI-277/phosphate-treated cells (Figure 4.14, lanes 4, 5) or at T=0 (lane 1). The active caspase 3 blot was stripped and re-probed for total caspase3 (Figure 4.14).

As these results suggest that FTI-277 may be protective against phosphate-induced apoptosis of VSMC, the number of cells undergoing apoptosis was assessed using DAPI staining. HCVSMCs were incubated with elevated phosphate (2.6 mM Pi) +/- FTI-277 as detailed above (section 2.6) and stained with DAPI after 12 hours. More apoptotic nuclei (arrows) were identified in the cells incubated with elevated phosphate than in cells incubated + FTI-277 (Figure 4.15 (i)). The number of apoptotic cells were counted and expressed as a percentage of the total number of cells present. Figure 4.15 (ii) shows that FTI-277 significantly inhibited phosphate-induced apoptosis of VSMC ($p<0.05$).

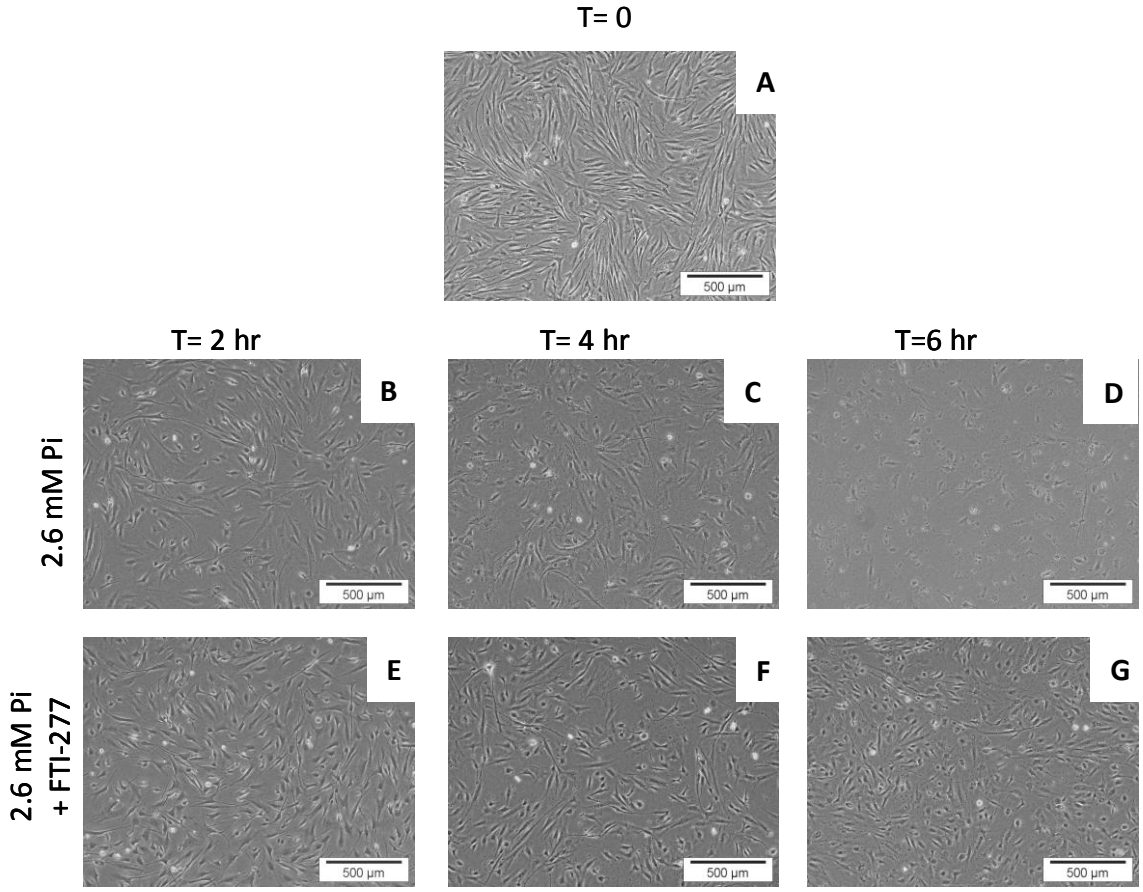

Figure 4.13: FTI-277 treated VSMCs appear to be more resistant to phosphate-induced cell loss. HCVSMCs were plated at 2 x 10^4 cells/cm^2 in 75 cm^2 flasks. The next day (T = 0), they were incubated in serum-free DMEM with (E - G) or without (B - D) FTI-277 (10 µM) for 15 minutes. After this time, phosphate (Pi) was added to elevate the concentration from 0.9 mM (present in the medium) to 2.6 mM in both treatment groups. Phase contrast images at the start of the experiment (T=0) and after 2 (B, E), 4 (C, F) and 6 (D, G) hours are shown. Scale bar = 500 µm.

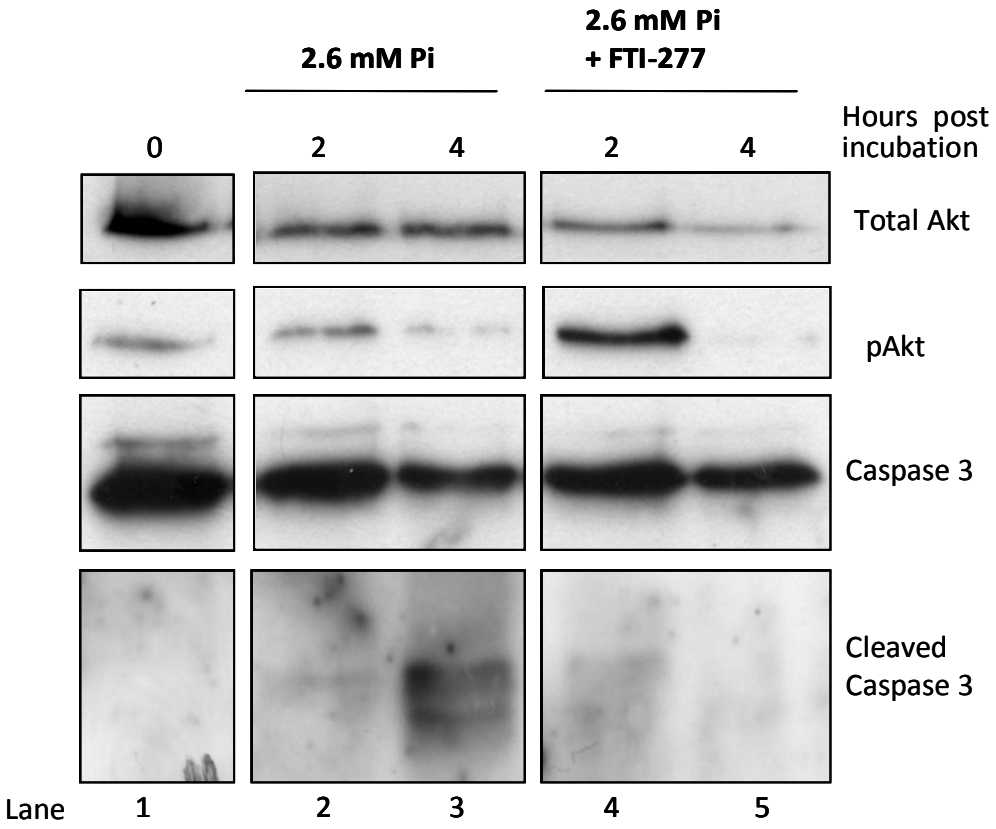

Figure 4.14: FTI-277 increases phosphorylated Akt and reduces cleaved caspase 3 in phosphate-treated HCVSMCs. Samples were prepared as detailed in the legend to Figure 4.7**.** Cell lysates were collected at the start of the experiment (T = 0) and after 2, 4 and 6 hours, and analysedby western blotting for total Akt, phospho-Akt (pAkt), total caspase3 and active caspase 3. Lane 1 contains cell lysates collected at the start of experiment. Lanes 2 and 3 contain cell lysates from cells incubated + 2.6 mM Pi; lanes 4 and 5 from cells incubated + FTI-277 + 2.6 mM Pi) collected after 2 and 4 hours.

(i)

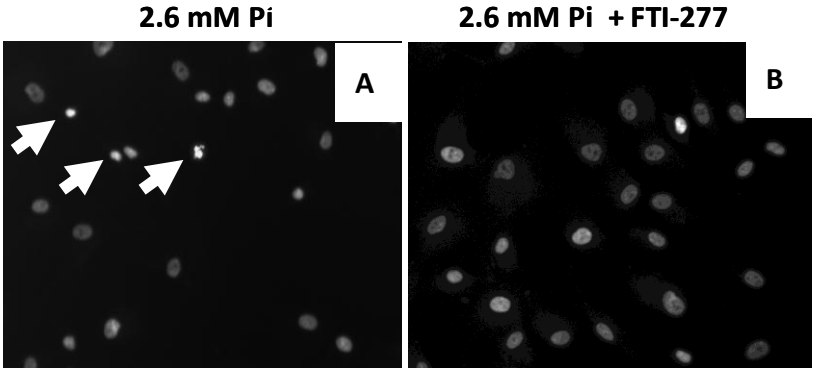

(ii)

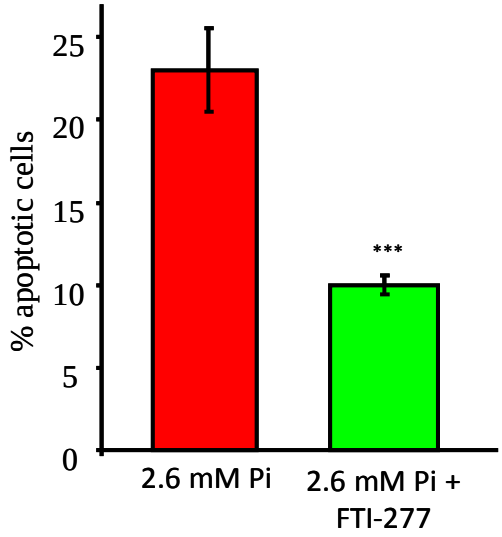

Figure 4.15: FTI-277 inhibits phosphate-induced VSMCs apoptosis (i) Human coronary artery VSMC were plated in chamber slides as detailed in Section 2.6. The next day, HCVSMCs were incubated with either 2.6 mM Pi (A) or 2.6 mM Pi + FTI-277 (10 µM) (B). HCVSMCs stained with DAPI 12 hours later. Apoptotic cells were defined as cells with condensed or fragmented nuclei (arrows). (ii) To quantify apoptosis, at least 300 cells were counted per treatment group per experiment and the results are expressed as percentage of cells with apoptotic nuclei. ***$p<0.05$

4.2.5 FTI-277 inhibits phosphate-induced VSMC apoptosis via Akt signalling

Previous work from this chapter suggests FTI-277 inhibits mineralisation by promoting PI3K/Akt signalling. The PI3K/Akt signalling pathway is important in regulating apoptosis. Therefore, to confirm whether inhibition of apoptosis of FTI-277 is via Akt signalling, HCVSMC were incubated with elevated phosphate (2.6 mM Pi) (Figure 4.16; A), +/- SH6 (B), FTI-277 (C), or FTI-277/SH6 (D). After 12 hours, these cells were stained with DAPI. Apoptotic nuclei were identified and the number of apoptotic cells were counted and expressed as a percentage of the total number of cells present. Figure 4.16 (ii) demonstrates that FTI-277 significantly inhibited phosphate-induced apoptosis of VSMC, SH6 promoted apoptosis (***$p<0.01$) and that the effect of FTI-277 on apoptosis was negated by SH6 (***$p<0.01$).

(i)

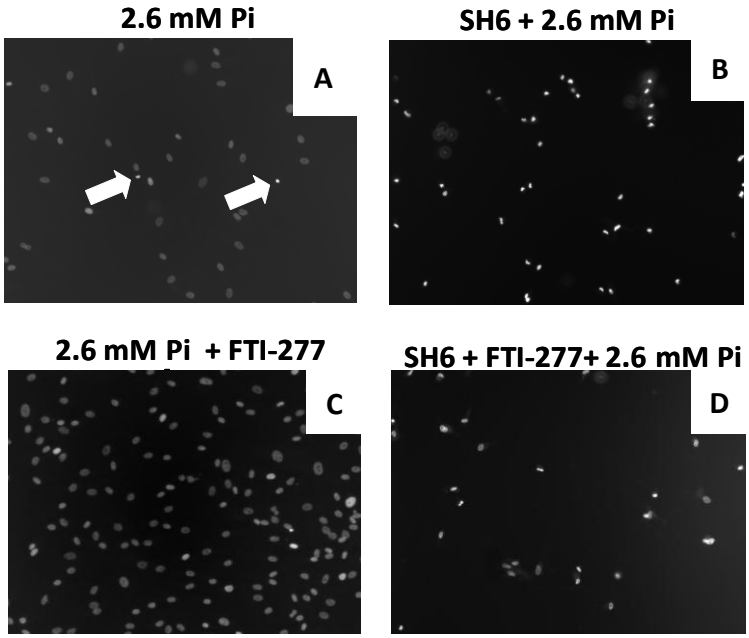

(ii)

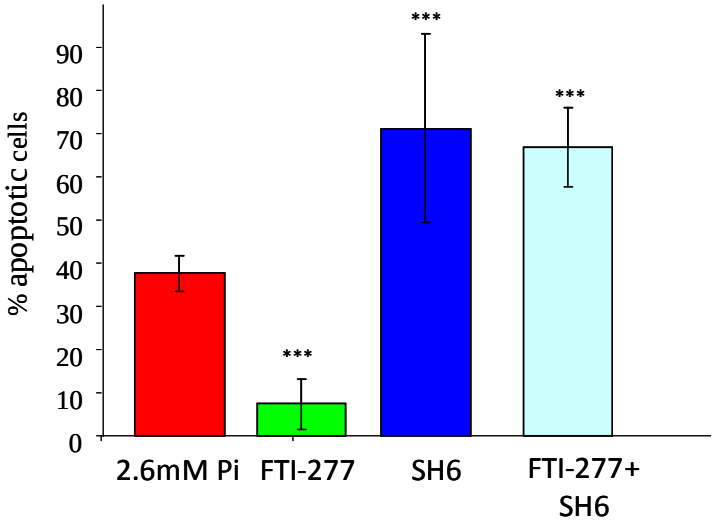

Figure 4.16: FTI-277 inhibits phosphate-induced VSMC apoptosis via Akt signalling. Human coronary artery VSMC were plated in chamber slides as detailed in Section 2.6. The next day, HCVSMCs were incubated with either 2.6 mM Pi (A) or 2.6 mM Pi with SH6 (10 µM) (B) or FTI-277 (10 µM) (C) or SH6 + FTI-277 (D).Arrows point to apoptotic nuclei. (ii) To quantify apoptosis, at least 300 cells were counted per treatment group per experiment and the results are expressed as percentage of cells with apoptotic nuclei. ***p<0.01 FTI-277 vs Pi, SH6 + Pi, FTI-277/SH6.

4.2.6 FTI-277 inhibits VSMCs migration

Increased levels of phosphate have also been demonstrated to promote VSMC migration (Rangrezet al., 2012) and may contribute to the pathogenesis of vascular calcification. FTIs have been shown to inhibit migration of cancer cells (Peng et al., 2012). Therefore, the next aim was to determine the effect of FTI-277 on VSMC migration. In these studies, a scratch/wounding assay was used, in which part of the cell monolayer was removed and the subsequent migration of cells in response to a chemoattractant was monitored. Studies were performed in the absence of serum to exclude the effects of other factors on cell migration.

4.2.6.1 PDGF promotes VSMCs migration in serum-free condition

Previous studies have shown that PDGF-BB is a chemoattractant for VSMC (Grotendorst et al., 1982). Therefore, initial experiments were performed to determine whether PDGF at a concentration of 20 ng/ml would stimulate migration of VSMCs in a wound assay. VSMCs were grown to confluence, incubated in serum-free medium overnight, and migration assays were performed in serum-free conditions +/- PDGF as described in section 2.7. Figure 4.17 shows representative phase contrast images of VSMCs in the two treatment groups at 0, 19, 26 and 41 hours post-wounding. This figure shows that the wounds did not close within the time-frame examined, and that PDGF appeared to stimulate wound closure (Figure 4.17).In order to confirm the differences in wound size between the two treatment groups at each time point, six measurements of the wound width were taken (see Figure 4.17A, solid arrows) and an average measurement of wound width was determined and expressed as a percentage of the original wound. Figure 4.18 confirms that PDGF significantly stimulated VSMC migration at 19 and 26 hours (***$p<0.05$). Based on these results, 20 ng/ml PDGF was used in further migration experiments.

4.2.6.2 FTI-277 inhibits PDGF-inducedVSMC migration in serum-free conditions

To determine the effects of FTI-277 on VSMC migration, migration assays were performed as described above. VSMCs were grown to confluence, and then pre-incubated +/-FTI-277(10 µM) in serum-free DMEM overnight. The next day, cell-free zones were made as detailed above and cells were then incubated with either serum-free DMEM

containing PDGF 20 ng/ml ± FTI-277 (10 μM). Wound closure was monitored after 24, 48 and 72 hours.

Figure 4.19 shows representative phase contrast images of VSMC in the two treatment groups at 0, 24, 48 and 72 hours post-wounding. This figure shows that FTI-277 inhibits PDGF-induced migration of VSMCs at each time point examined, which was confirmed by measuring the wound width (Figure 4.20; *p<0.05, at 24 hours; ***p<0.001 at 48 and 72 hours, compared to PDGF treated cells).

4.2.7 FTI-277 inhibits the osteogenic differentiation of VSMCs

In the next series of experiments, the ability of FTI-277 to modulate the osteogenic differentiation of VSMC was assessed. VSMC were cultured in βGP-containing medium +/- FTI-277 for up to 10 days; additional controls were incubated in regular growth medium in the absence of βGP. Phase contrast images of cells stained with alizarin red are shown in Figure 4.21 (A-C). RNA was extracted from triplicate wells 9 and 10 days after incubation in βGP-containing medium (see section 2.8.). Real time PCR analysis for osteogenic markers was performed and relative gene expression was calculated using comparative C_t method ($2^{-\Delta ct}$) as detailed in section 2.8.4. Data from both time points and from two independent experiments were pooled.

Incubation in the presence of ßGP significantly induces the expression of Runx2 and Msx2 mRNA by VSMC, and FTI-277 significantly inhibited this increase (Figure 4.21 (i), (ii), ***p<0.05). The level of gene expression returned to that of control cells incubated in normal growth medium. FTI-277 also reduced ALP mRNA expression and promoted MGP mRNA expression compared to both control and ßGP-treated cells (Figure 4.21 (iii), (iv), ***p<0.05). Figure 4.22 (i) shows that ASMA mRNA expression is down-regulated during mineralisation in the βGP-treated cells (***p<0.05, control vs βGP). FTI-277 prevented the βGP-induced suppression of ASMA mRNA expression (***p<0.05, FTI-277 vs βGP). BMP-2 mRNA expression was also increased by incubation of VSMC in βGP-containing medium. However, FTI-277 had no effect on the mRNA expression of this growth factor (Figure 4.22 (ii)).

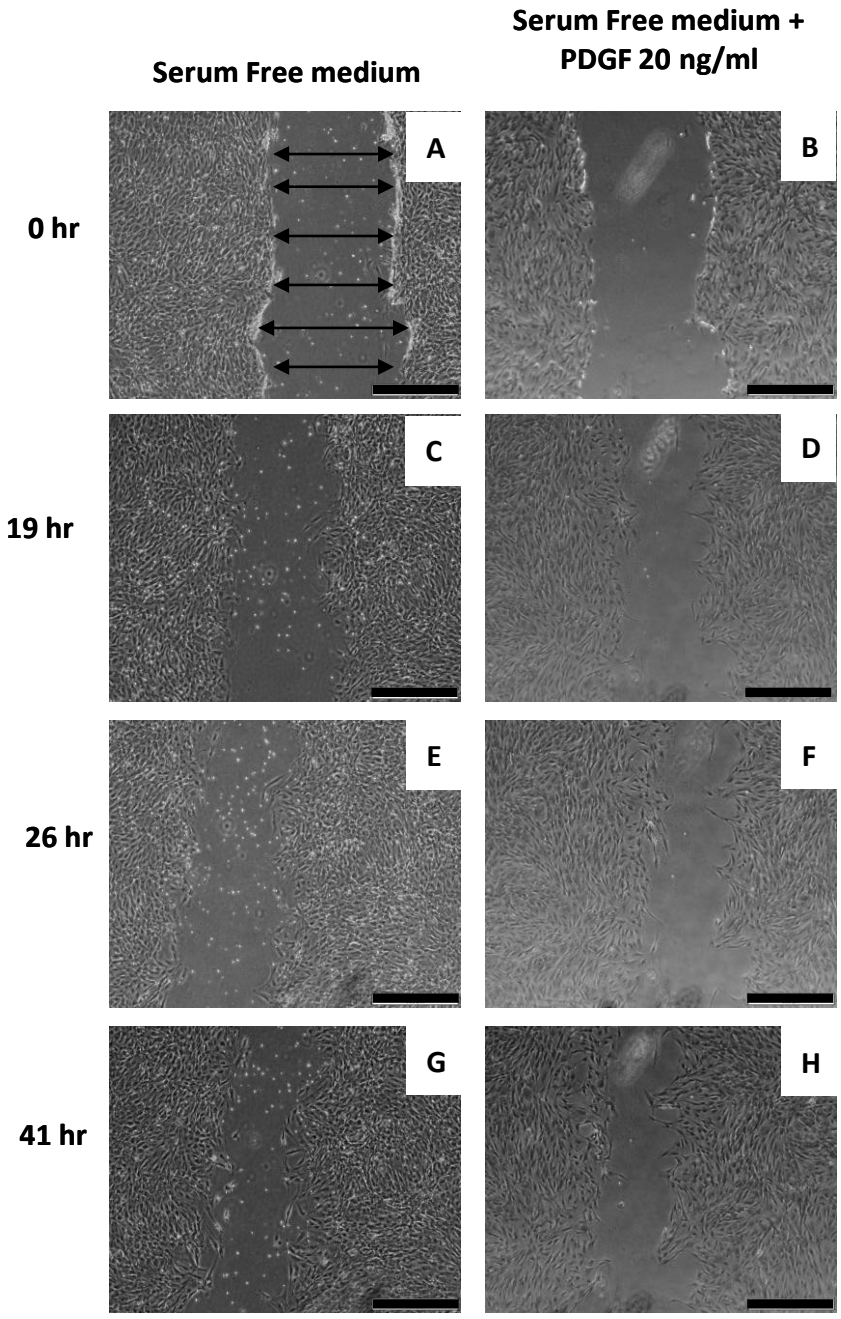

Figure 4.17: PDGF promotes VSMCs migration in serum-free condition. VSMCs were grown to confluence and subsequently incubated in serum-free medium overnight. Cell-free zones were made and VSMCs were then incubated with either serum-free DMEM (SF-DMEM) (A, C, E, G) or SF-DMEM containing PDGF 20 ng/ml (B, D, F, H). Phase contrast images of VSMCs post-wounding at: 0 (A, B), 9 (C, D) 26 (E, F) and 41 (G, H) hours are shown. Scale bar = 500µm.

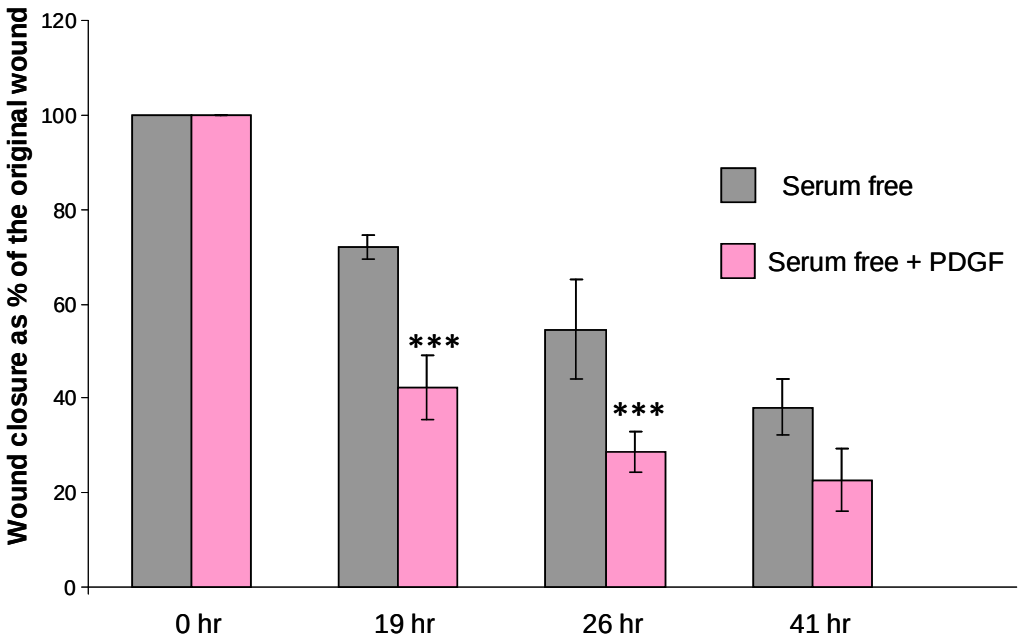

Figure 4.18: PDGF promotes VSMC migrations in serum-free conditions. VSMCs were plated as detailed in the legend to Figure 4.17. Six measurements of the wound width were taken as shown in Figure 4.17 (A, solid arrows) and average measurements of wound width were determined at each time point, and expressed as a percentage of the original wound. ***$p<0.05$ compared to serum-free at that time point.

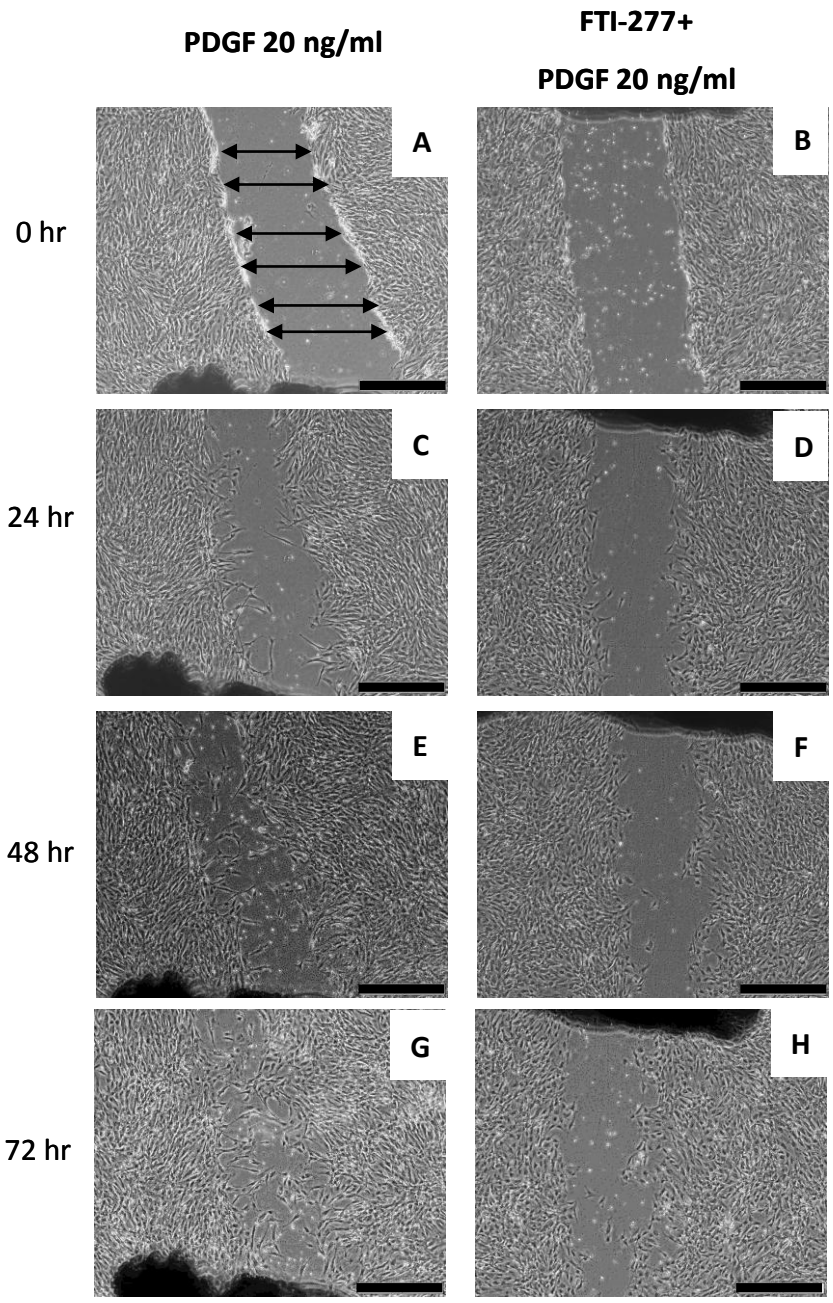

Figure 4.19: FTI-277 inhibits VSMC migration in serum free condition. Confluent VSMCs were incubated in serum-free medium +/- FTI-277 overnight. Cell-free zones were made and VSMCs were then incubated with either (A, C, E, G) serum-free DMEM containing PDGF (20 ng/ml) or (B, D, F, H) serum-free DMEM containing PDGF (20 ng/ml) and FTI-277 (10 µM). These areas were monitored after 24 (C, D), 48 (E, F) and 72 (G, H) hours and phase contrast images were taken.Scale bar = 500µm.

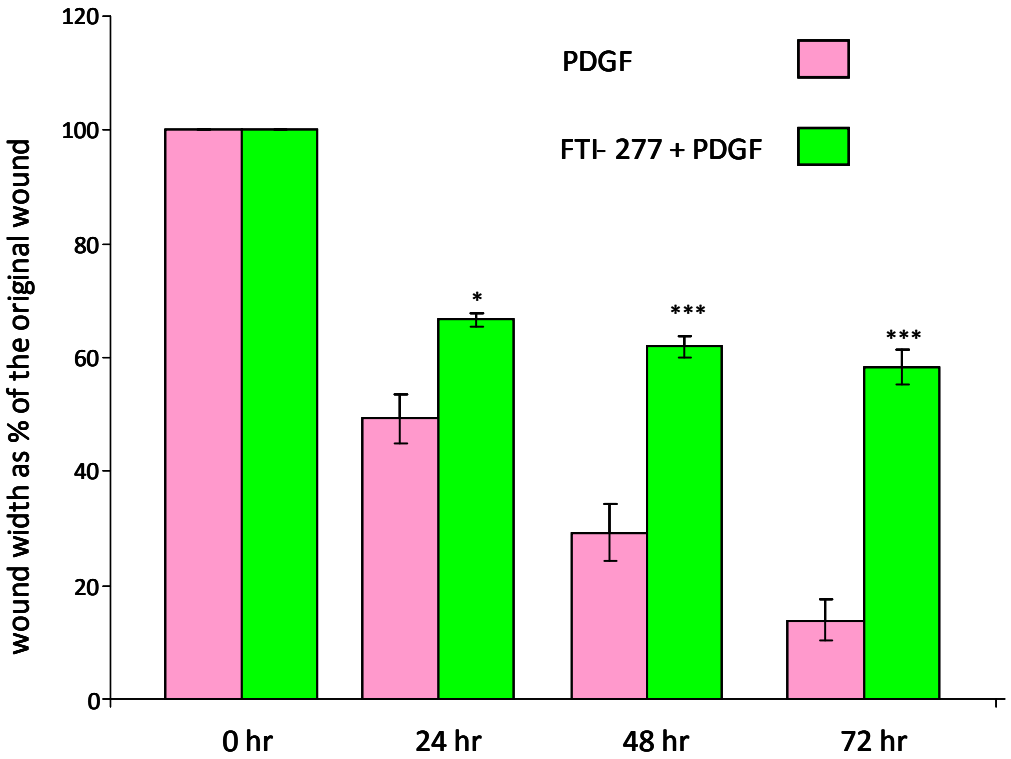

Figure 4.20: FTI-277 inhibits PDGF-induced VSMC migration. VSMCs were plated as detailed in the legend to Figure 4.19. Six measurements of the wound width were taken as shown in Figure 4.19 (A, solid arrows) and average measurements of wound width were determined at each time point, and expressed as a percentage of the original wound. *p<0.05, ***p <0.001, compared to PDGF at that time point.

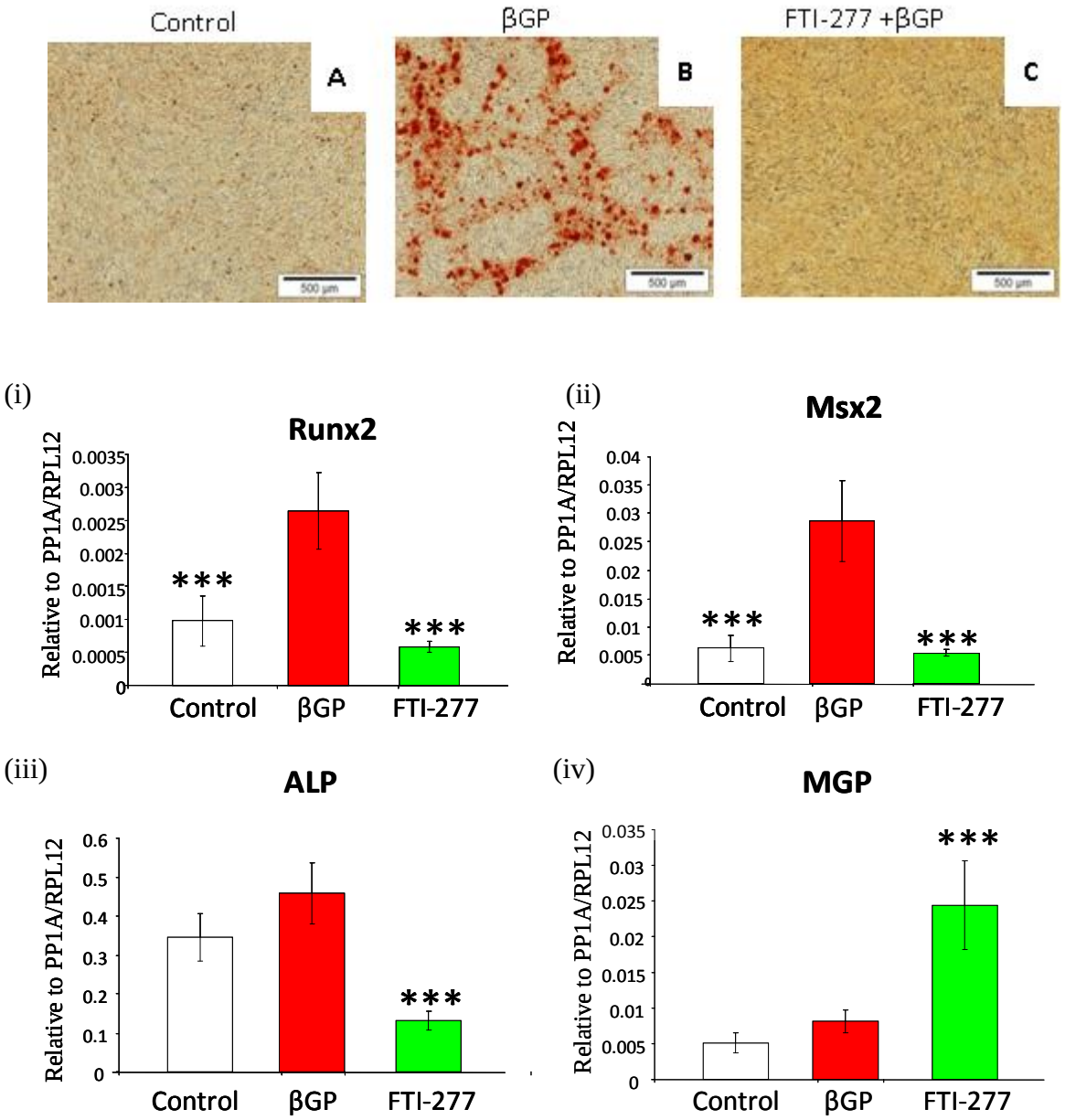

Figure 4.21: **FTI-277 inhibits ßGP-induced Runx2, Msx2, and ALP mRNA expression and promotes MGP mRNA expression.** VSMCwere cultured to approximately 90% confluency and subsequently treated with 10% FCS-DMEM in the presence of DMSO (1:500, control) (A), ßGP-containing medium plus DMSO (B, ßGP), or ßGP-containing medium plus DMSO and FTI-277 (20 µM) (C, FTI-277). RNA was collected from triplicate wells at days 9 and 10. Real Time PCR analysis was performed and results from 2 experiments were pooled and expressed relative to two house-keeping genes (PP1A and RLP12). (i) Runx 2 mRNA expression, n=12; (ii) Msx2 mRNA expression, n=12; (iii) ALP mRNA expression, n=12; (iv) MGP mRNA expression, n=12. ***p<0.05, FTI-277 vs ßGP, control vs ßGP

(i) (ii)

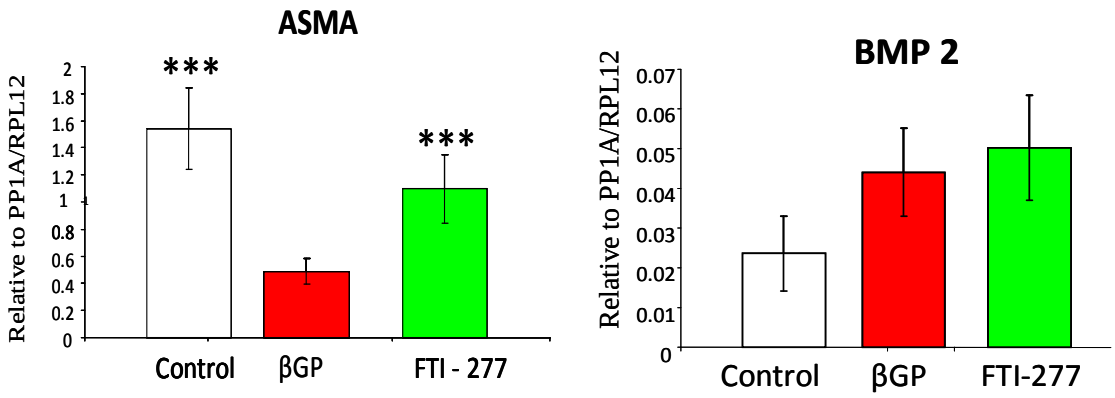

Figure 4.22: FTI-277 prevents βGP-induced suppression of ASMA mRNA expression and has no effect on BMP-2 mRNA expression. VSMC were cultured as detailed in the legend to Figure 4.21 and Real Time PCR analysis was performed. (i) ASMA mRNA expression, n=6;(ii) BMP 2 mRNA expression, n=9, ***p<0.05, FTI-277 vs ßGP, control vs ßGP

4.2.8 The effect of FTI-277 on osteogenic differentiation may be negated by SH6

The results shown in section 4.2.2 suggest that SH6 negates the effect of FTI-277 on Akt phosphorylation and βGP-induced mineralisation. The next aim was to determine whether SH6 abolished the effect of FTI-277 on the osteogenic differentiation of VSMC.

VSMC were cultured in βGP-containing medium +/- FTI-277, +/- SH6 or + SH6+ FTI-277 for up to 8 days; RNA was extracted from triplicate wells on day 8. Real time PCR analysis for osteogenic markers was performed and relative gene expression was calculated as detailed in section 2.10. As shown above, FTI-277 inhibits β-GP-induced Runx2 and Msx2 mRNA expression (Figure 4.23 (i), (ii)). Although the inhibitory effect of FTI-277 on Runx2 and Msx2 expression appears to be negated by SH6, this result was not statistically significant. This experiment was repeated; however a new batch of ßGP was used and mineralisation occurred much earlier in the βGP-treated cells (day 4 compared to day 9 – 10). As before, RNA was collected on day 8, but at this time point Runx2 and Msx3 MRNA expression was the same in all the samples examined (results not shown), suggesting that the induction of expression by ßGP had occurred earlier.

(i)

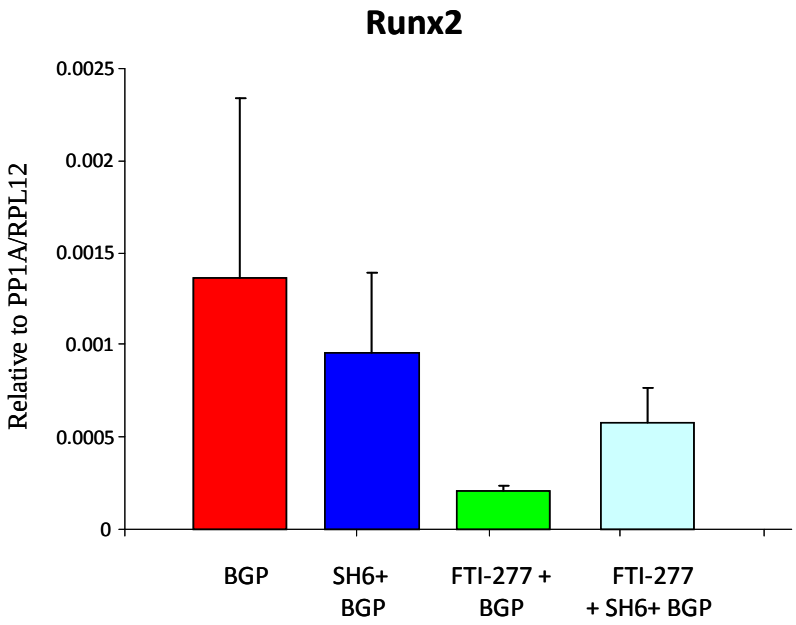

(ii)

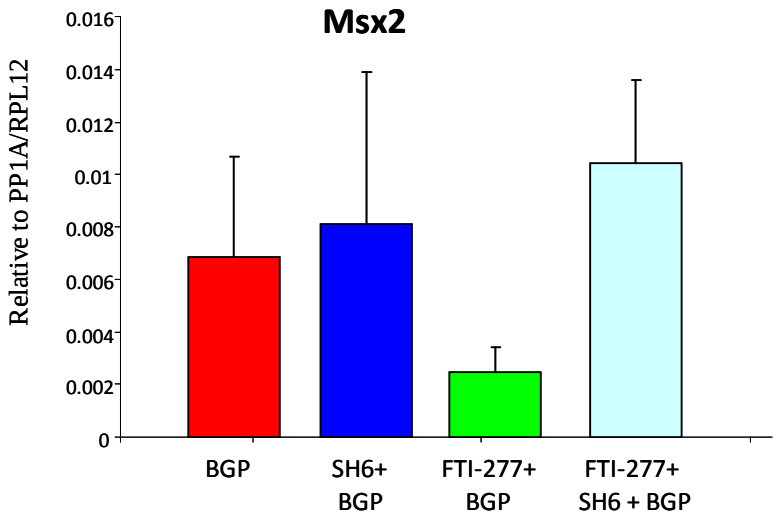

Figure 4.23: The effect of SH6 on the inhibition of βGP-induced Runx2 and Msx2 mRNA expression by FTI-277. VSMCwere cultured to approximately 90% confluency and subsequently treated with ßGP-containing medium in the presence of DMSO with ßGP, FTI-277 (20 µM), SH6 (10 µM), or SH6 + FTI-277. RNA was collected from triplicate wells and Real Time PCR analysis was performed. (i) Runx 2 mRNA expression; (ii) Msx2 mRNA expression.

4.2.9 FTI-277 inhibits phosphate-induced mineralisation of aortic rings from rats with early stage renal disease and sham controls

The results so far have shown that FTI-277 inhibits mineral deposition by VSMC in vitro by promoting PI3K/Akt signalling and preventing the osteogenic differentiation of VSMC. Therefore, the next series of experiments was performed to determine the effect of this drug on *ex vivo* mineralisation of aortic rings obtained from rats undergoing early stage renal disease following 5/6 nephrectomy or sham operated controls (see Section 2.8)

Aorta were obtained from rats 8 weeks following 5/6 nephrectomy or sham surgery. At this time point, these rats were in early stage renal disease as shown by blood urea nitrogen (BUN) levels, creatinine levels and urinary albumin excretion (see Table 7.1, Appendix). Rat aortic rings were incubated in serum-free DMEM containing vehicle (DMSO, 1:1000), or in elevated phosphate (3.3 mM) and alkaline phosphatase (3.75 U/ml) +/- FTI-277(10 μM) for 10 days as detailed in section 2.8. Alizarin red staining and *O*-cresolphthalein complexone assays were performed to determine mineralisation and quantify calcium content. Haematoxylin and eosin staining was performed to assess the ultrastructure of the rings.

4.2.9.1 Early renal disease

Alizarin red staining of the aortic rings incubated with elevated phosphate revealed that mineralisation was present throughout the vessel walls (Figure 4.24). FTI-277 inhibited this Pi-induced mineralisation. No mineralisation was detected in the controls (Figure 4.24). Alizarin red staining was quantified as described in section 2.8.5 and expressed as a percentage of section area. Figure 4.25 (i) shows increased alizarin red staining in the phosphate-treated rings and FTI-277 inhibited this increase. The calcium content of the rings was also quantified using the *O*-cresolphthalein complexone assay (Figure 4.25 (ii)). This assay confirmed that culturing aortic rings in the presence of elevated phosphate increased the calcium content of these rings and this increase was significantly inhibited by co-incubation with FTI-277 (*$p<0.05$).

To evaluate the ultrastructure of the aortic rings, sections were also stained with haematoxylin and eosin (Figure 4.26). This staining demonstrated normal morphology of the aortic rings as seen by nuclear staining and preservation of elastic lamina. The

numbers of nuclei were counted within a fixed 800 μm x 800 μm area, with an average vessel length of ~1000 μm. Interestingly, no difference was detected in nuclei numbers when the different groups were compared (Figure 4.27), although it should be noted that there was large variability in the two phosphate-treated samples that were analysed. The number of nuclei was: 265±8.5 in control, 153±135 in phosphate, and 225± 35 in FTI-277 treated vessels.

4.2.9.2 Sham controls (early time point)

The rings obtained from sham operated rats were analysed as detailed above. Alizarin red staining demonstrated that incubation with elevated phosphate increased calcium deposition in rat aortic rings, and this calcification was present throughout the vessel wall (Figure 4.28, B, E, and H). Low levels of mineralisation were detected in the FTI-277 treated rings. Mineral deposition was mostly localised in the outer layer of the rings, close to the adventitia, although some mineral was noted within the medial layer as well (Figure 4.28, C, F and I). Alizarin red staining was quantified as described in section 2.8.5 and expressed as a percentage of section area. Figure 4.29 (i) shows that FTI-277 significantly inhibited phosphate-induced mineralisation (*$p<0.05$). This result was also confirmed using the *O*-cresolphthalein complexone calcium assay (Figure 4.29 (ii), *$p<0.05$).

Aortic rings were also stained with haematoxylin and eosin to analyse their ultrastructure (Figure 4.30). Similar to early stage renal disease rat aortic rings, this staining demonstrated normal morphology of the aortic rings as seen by nuclear staining and preservation of elastic lamina. Nuclei were counted as detailed above. Interestingly, no difference was detected in nuclei numbers when aortic rings were incubated in control medium, or medium containing elevated phosphate with or without FTI-277 (Figure 4.31). The number of nuclei in control group was 226±25 versus phosphate 199±27 versus FTI-277 205±38.

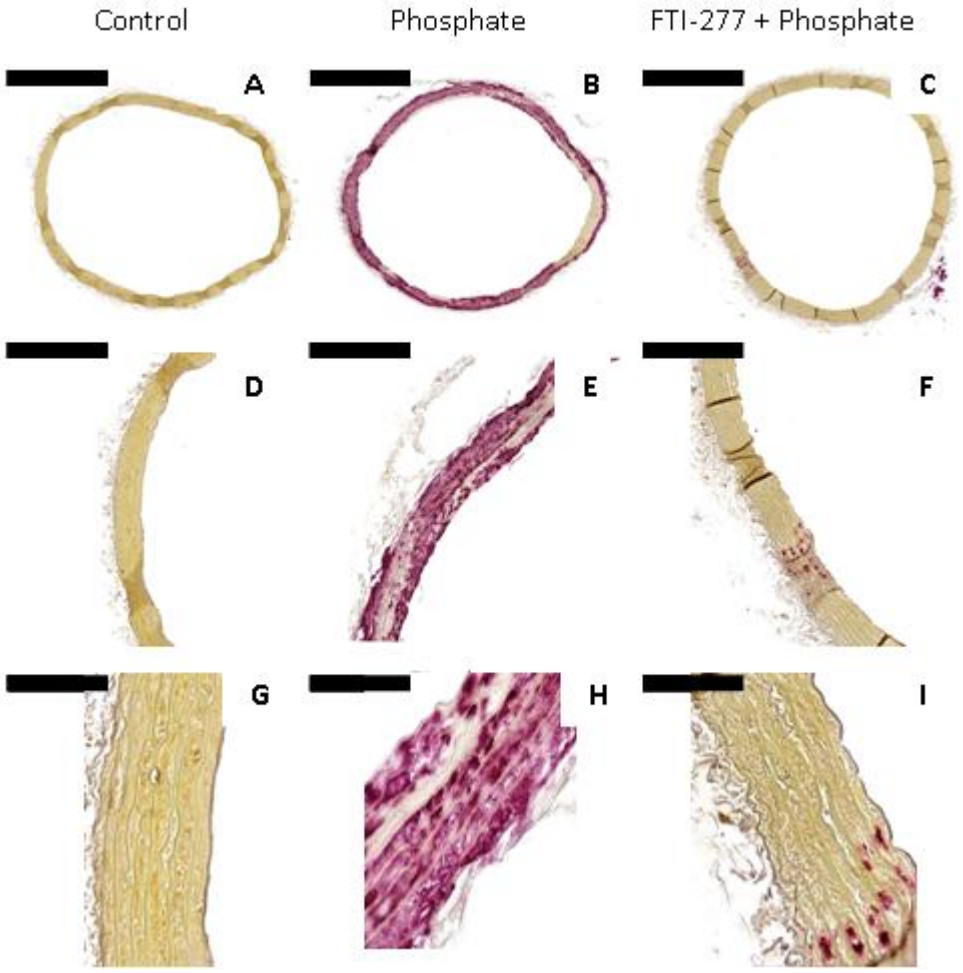

Figure 4.24: FTI-277 inhibits phosphate-induced mineralisation in aortic rings from rats with early stage renal disease. Rat aortic rings were incubated in DMEM with DMSO (1:1000) (A, D, G) or DMEM + DMSO + elevated phosphate and alkaline phosphatase (B, E, H) or DMEM+ elevated phosphate and alkaline phosphatase and FTI-277 (C, F, I) for 10 days. Samples were collected, fixed, sectioned and stained with alizarin red. Representative images are shown (n = 3 rats). Red indicates mineralisation.Scale bars for images A, B, C = 1000 μm; images D, E, F = 200 μm and images G, H, I = 50 μm.

(i)

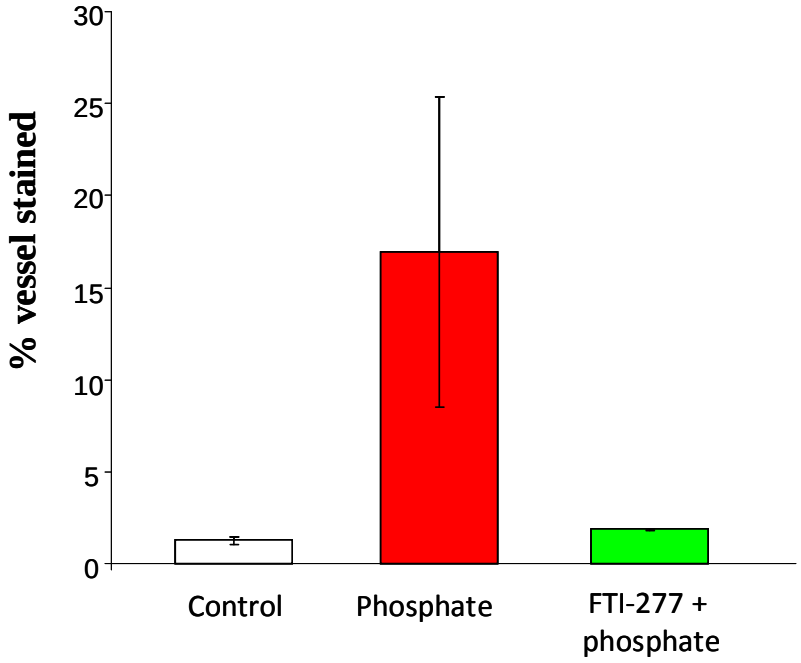

(ii)

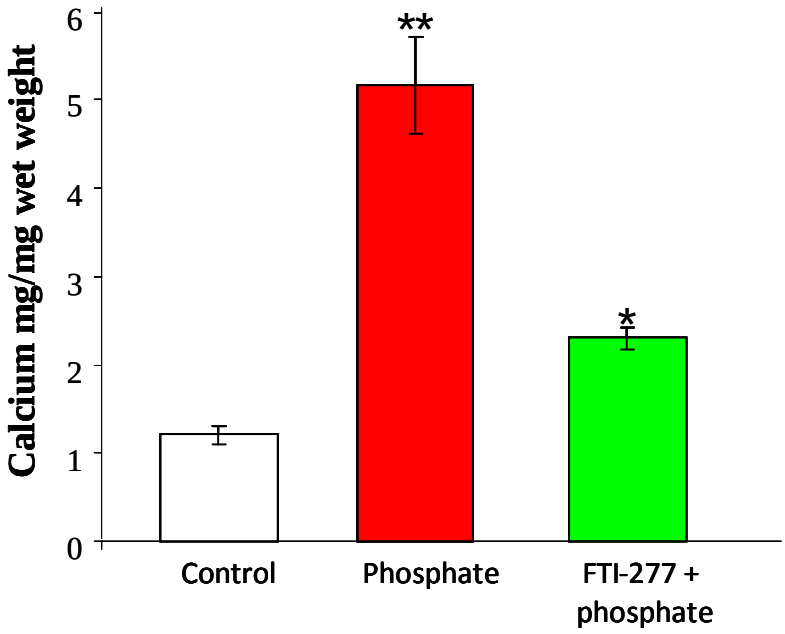

Figure 4.25: FTI-277 inhibits phosphate-induced mineralisation in aortic rings from rats with early stage renal disease (i) Samples were prepared as detailed in the legend to figure 4.24 and alizarin red staining quantified as described in section 2.8.5. Results were pooled from 3 different rats. (ii) *O*-cresolphthalein complexone assay was performed to quantify the amount of calcium in each of the aortic rings. Results were pooled from 3 rats (n=8 aortic rings). *p<0.05, FTI-277 vs phosphate, **p<0.01, phosphate vs control.

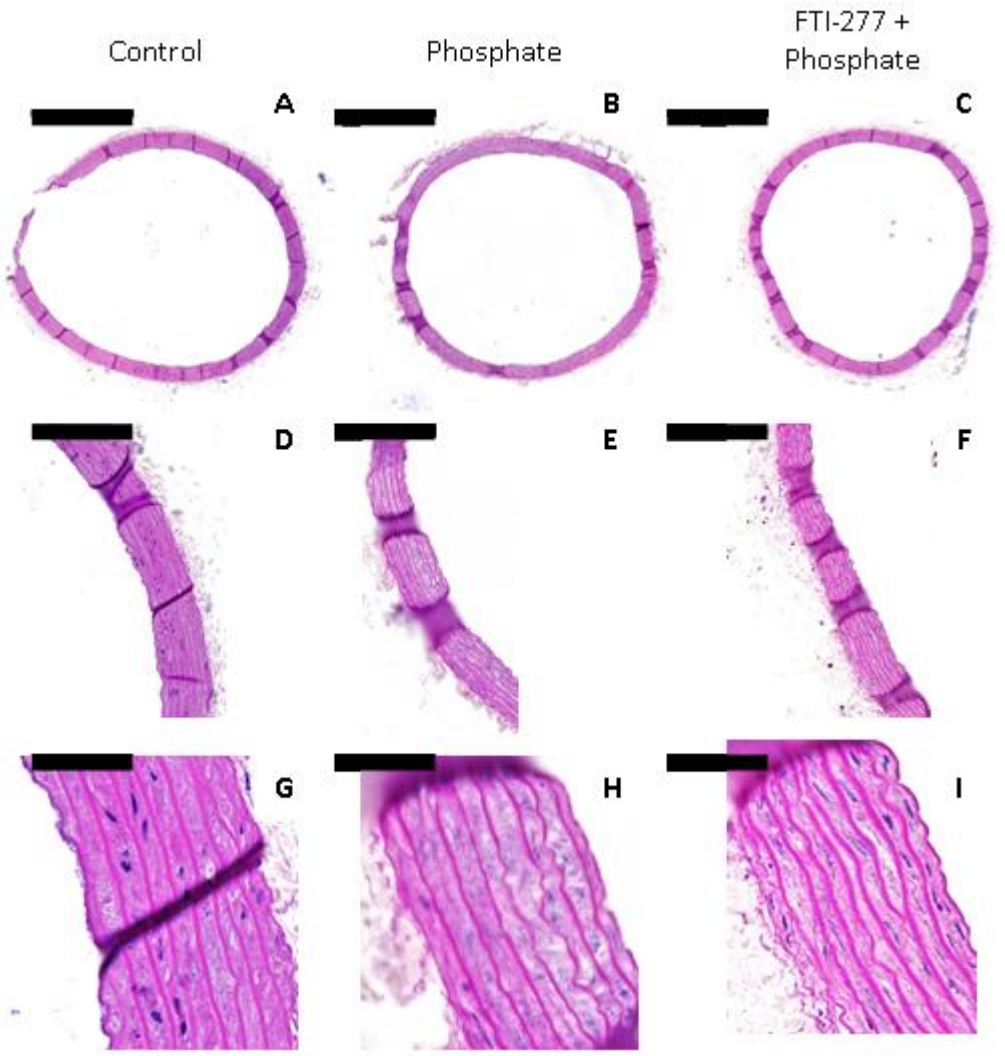

Figure 4.26: H and E staining of aortic rings from rats with early stage renal disease. Rat aortic rings were incubated in DMEM with DMSO (1:1000) (A, D, G) or DMEM + DMSO + elevated phosphate and alkaline phosphatase (B, E, H) or DMEM+ elevated phosphate and alkaline phosphatase and FTI-277 (C, F, I) for 10 days. Samples were collected, fixed, sectioned and stained with haematoxylin and eosin. Representative images are shown (n=2 rats). Scale bars for images A, B, C = 1000 μm; images D, E, F = 200 μm and images G, H, I = 50 μm.

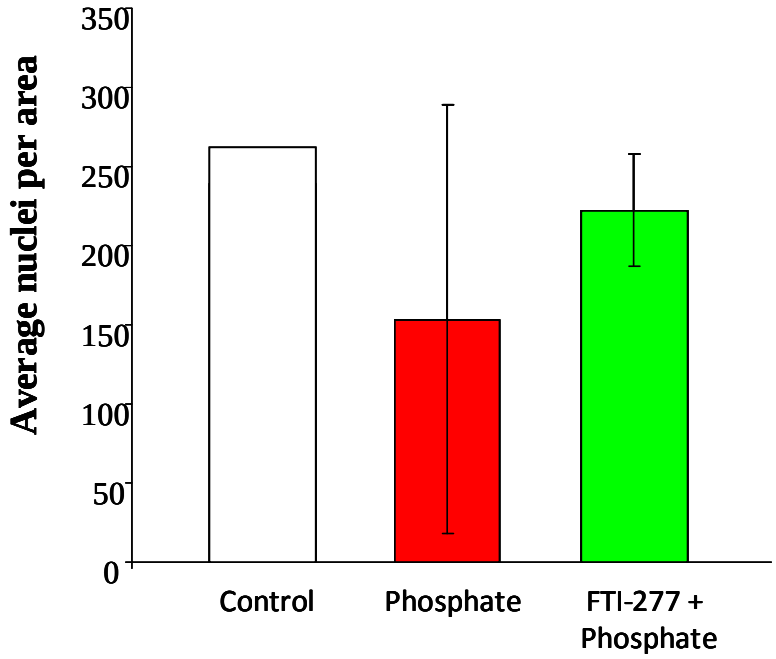

Figure 4.27: No difference was detected in nuclei numbers in the three different groups. Nuclei were counted from haematoxylin and eosin-stained from early stage renal disease rats rings sections (Figure 4.26) within a fixed 800 μm x 800 μm area with an average vessel length of ~1000 μm. Results shown were pooled from 2 different rats and expressed as average nuclei per area.

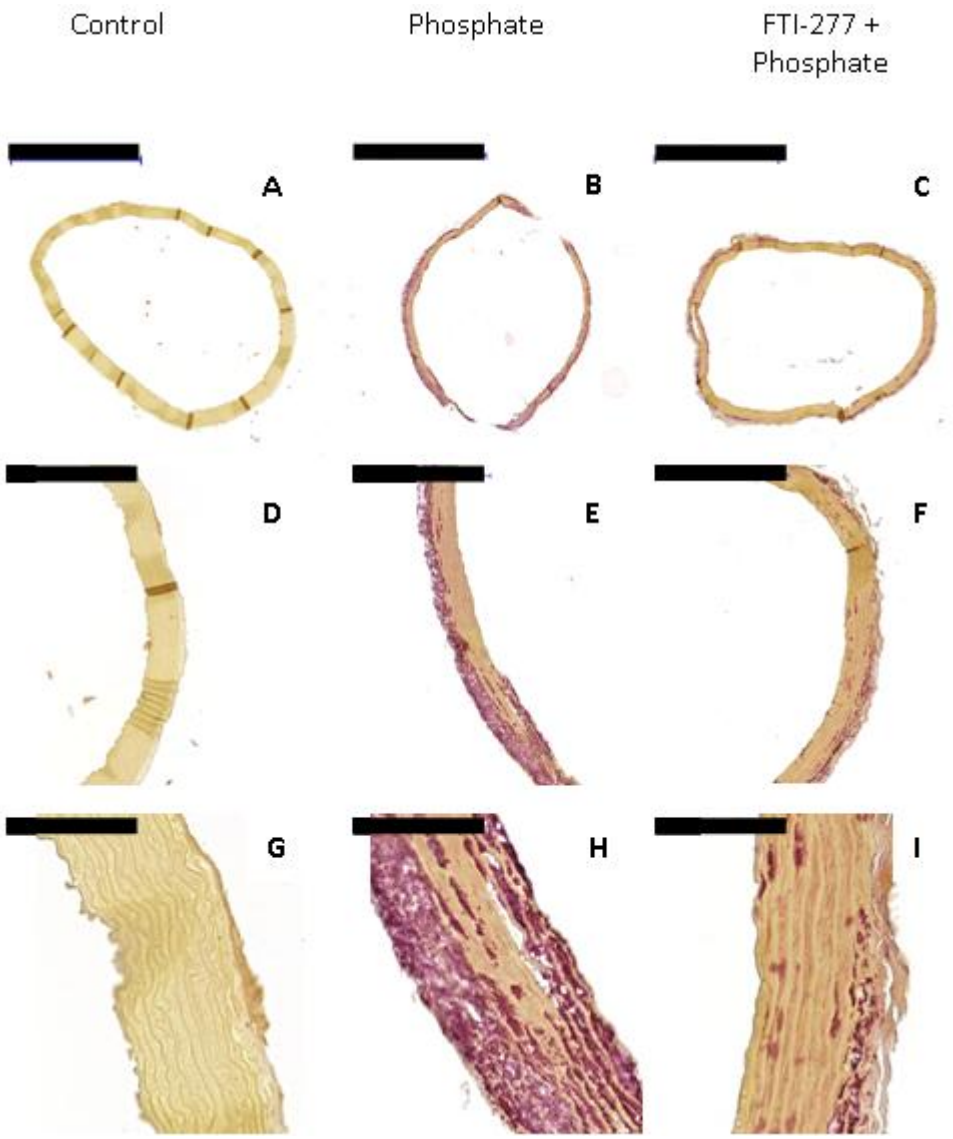

Figure 4.28: FTI-277 inhibits phosphate-induced mineralisation in aortic rings from sham operated rats (early). Rat aortic rings were incubated in DMEM with DMSO (1:1000) (A, D, G) or DMEM + DMSO + elevated phosphate and alkaline phosphatase (B, E, H) or DMEM + elevated phosphate and alkaline phosphatase and FTI-277 (C, F, I) for 10 days. Samples were collected, fixed, sectioned and stained with alizarin red. Representative images are shown (n = 2 rats). Red indicates mineralisation. Scale bars for images A, B, C = 1000 μm; images D, E, F = 200 μm and images G, H, I = 50 μm.

(i)

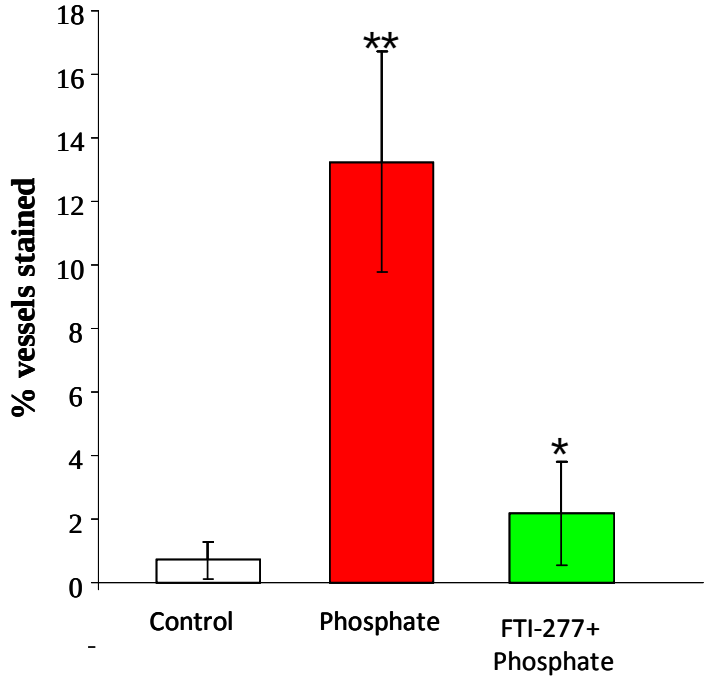

(ii)

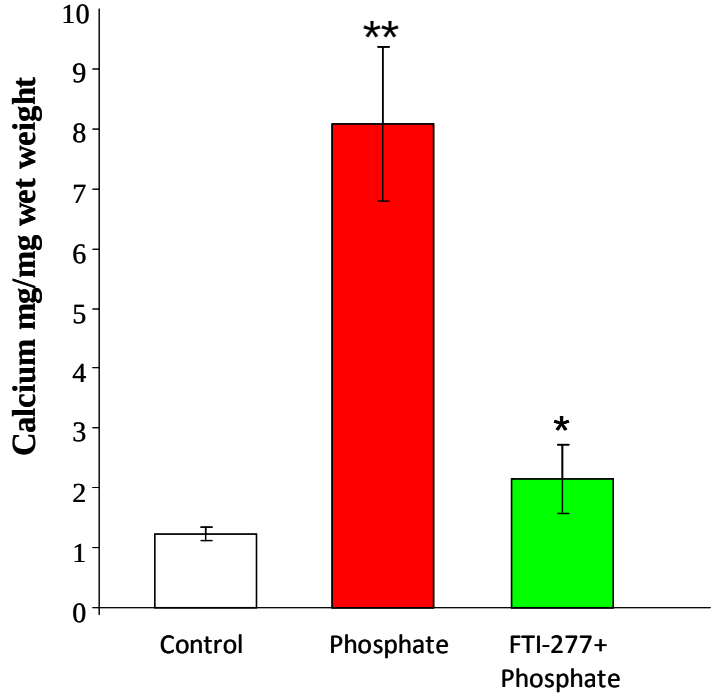

Figure 4.29: FTI-277 inhibits phosphate-induced mineralisation in aortic rings from sham operated rats (early). (i) Samples were prepared as detailed in the legend to figure 4.28 and alizarin red quantified as described in section 2.8.5. Results were pooled from analysis of sections from 2 different rats. (ii) *O*-cresolphthalein complexone assay was performed in order to quantify the amount of calcium in each of the aortic rings. Results were pooled from 3 rats (n=8, aortic rings) (*$p<0.05$, FTI-277 vs phosphate, **$p<0.05$, phosphate vs control)

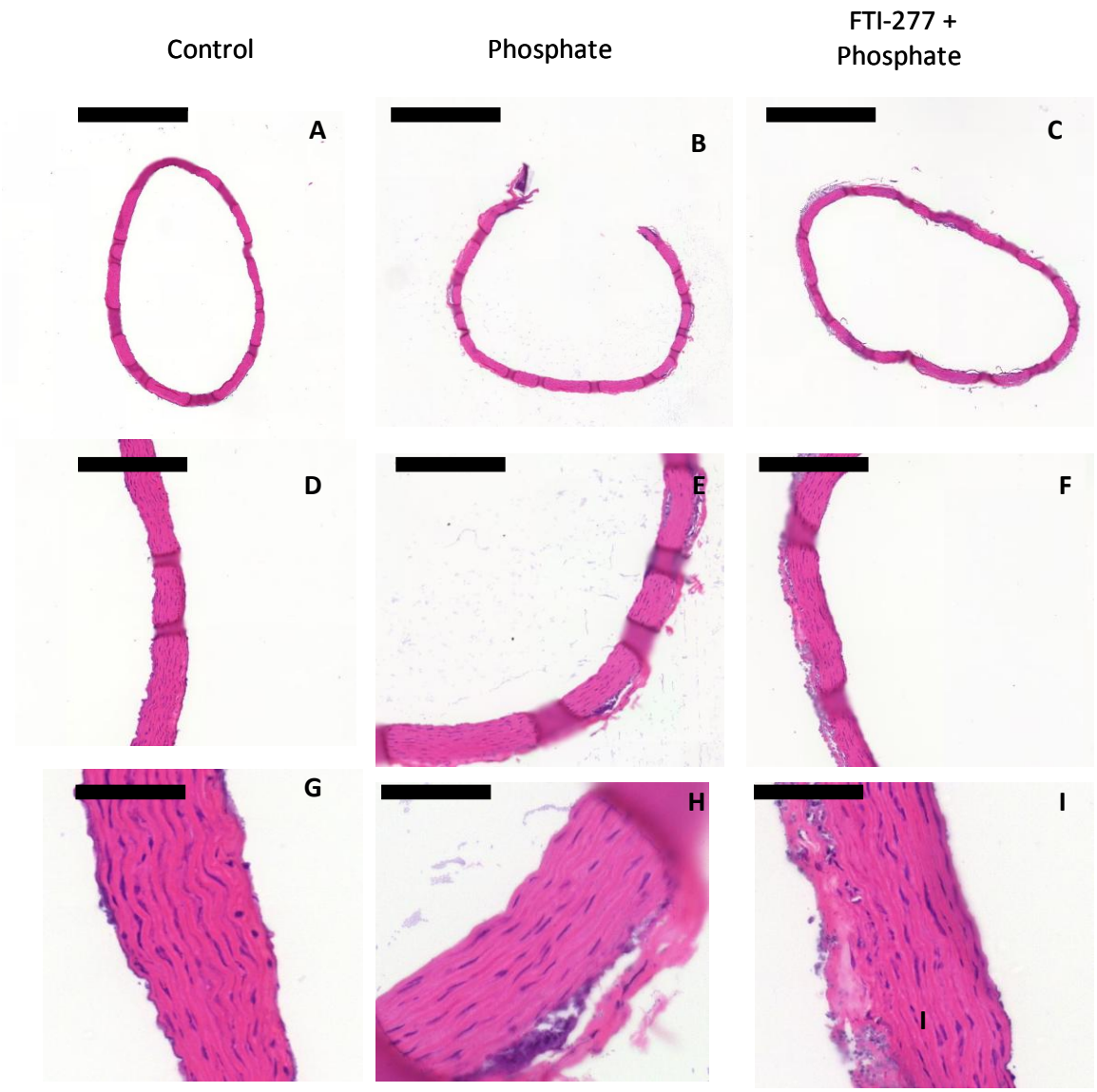

Figure 4.30: H and E staining of aortic rings from sham operated rats (early). Rat aortic rings were incubated in DMEM with DMSO (1:1000) (A, D, G) or DMEM + DMSO + elevated phosphate and alkaline phosphatase (B, E, H) or DMEM+ elevated phosphate and alkaline phosphatase and FTI-277 (C, F, I) for 10 days. Samples were collected, fixed, sectioned and stained with haematoxylin and eosin. Representative images are shown (n = 2). Scale bars for images A, B, C = 1000 μm; images D, E, F = 200 μm and images G, H, I=50 μm.

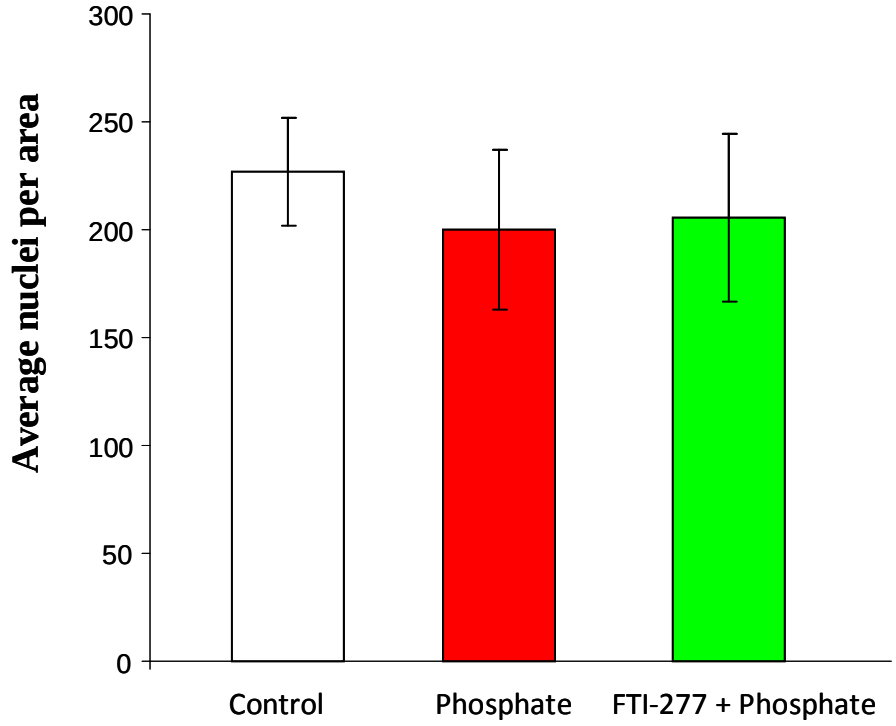

Figure 4.31: No difference was detected in nuclei numbers in the three different groups. Nuclei were counted from haematoxylin and eosin-stained rings from sham operated control rats (early) (Figure 4.30) within a fixed 800 µm x 800 µm area with an average vessel length of ~1000 µm. Results shown were pooled from 2 or 3 different rats, and expressed as average nuclei per area.

4.2.10 FTI-277 inhibits phosphate-induced mineralisation of aortic rings from rats with end stage renal disease and sham controls

The results in the previous section demonstrated that FTI-277 inhibits *ex vivo* mineralisation of aortic rings obtained from rats undergoing early stage renal disease following 5/6 nephrectomy or sham operated controls. Therefore, the next series of experiments was performed to determine whether FTI-277 could also inhibit mineralisation in aortas from rats in end stage renal disease. Aorta were obtained from rats approximately 6 months following 5/6 nephrectomy or sham surgery. At this time point, these rats were in end stage renal disease as shown by BUN, creatinine levels and urinary albumin excretion (see Table 7.2, Appendix). Rat aortic rings were incubated and analysed as detailed in section 4.2.9.

4.2.10.1 End stage renal disease

Alizarin red staining of the aortic rings incubated with elevated phosphate revealed that mineralisation was deposited throughout the vessel walls (Figure 4.32, B, E, and F). In the FTI-277 treated rings there was inhibition of phosphate-induced mineralisation with only spicules of mineralisation detected in the inner layers of some of the rings (Figure 4.32 C, F, I). Quantification of alizarin red staining revealed that FTI-277 significantly inhibited phosphate-induced mineralisation (Figure 4.33 (i)). Calcium content was also quantified using *O*-cresolphthalein complexone assay and this confirms inhibition of mineralisation in FTI-277 treated rings (Figure 4.33 (ii), *$p<0.05$)

Haematoxylin and eosin staining of the three groups showed normal ultrastructure and morphology (Figure 4.34). Nuclei were counted within a fixed 800 μm x 800 μm area with an average vessel length of ~1000 μm. This demonstrated elevated phosphate significantly decreased nuclei numbers in aortic rings compared to controls, and that FTI-277 did not prevent this decrease (Figure 4.35, **$p<0.001$ phosphate or FTI-277 vs control). Nuceli numbers were: control 198$\pm$2, phosphate 96$\pm$23 versus, FTI-277 101$\pm$ 9.6.

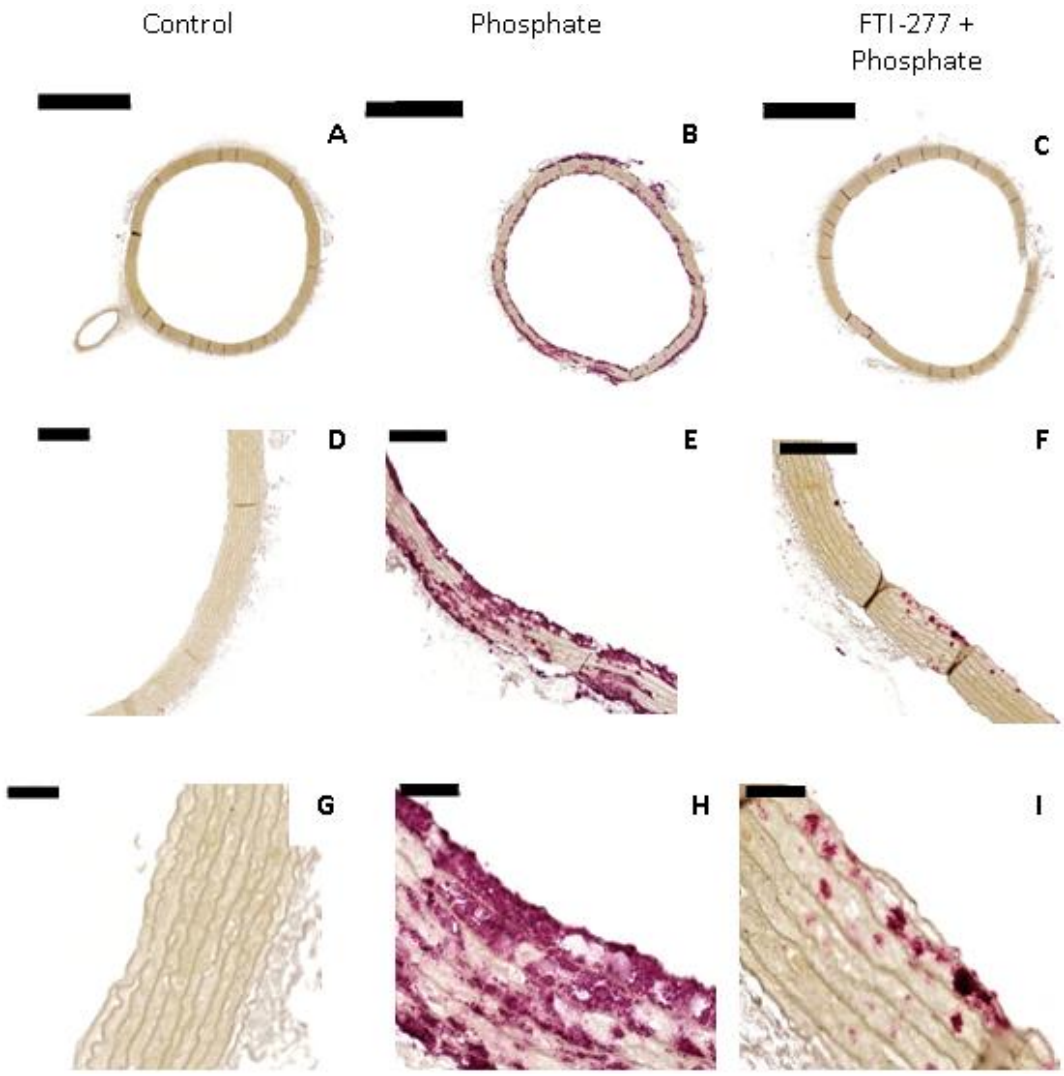

Figure 4.32: FTI-277 inhibits phosphate-induced mineralisation in aortic rings from rats with end stage renal disease. Rat aortic rings were incubated in DMEM with DMSO (1:1000) (A, D, G) or DMEM + DMSO + elevated phosphate and alkaline phosphatase (B, E, H) or DMEM + elevated phosphate and alkaline phosphatase and FTI-277 (C, F, I) for 10 days. Samples were collected, fixed, sectioned and stained with alizarin red. Representative images are shown (n=3 rats). Red indicates mineralisation. Scale bars for images A, B, C = 1000 μm; images D, E, F = 200 μm and images G, H, I = 50 μm.

(i)

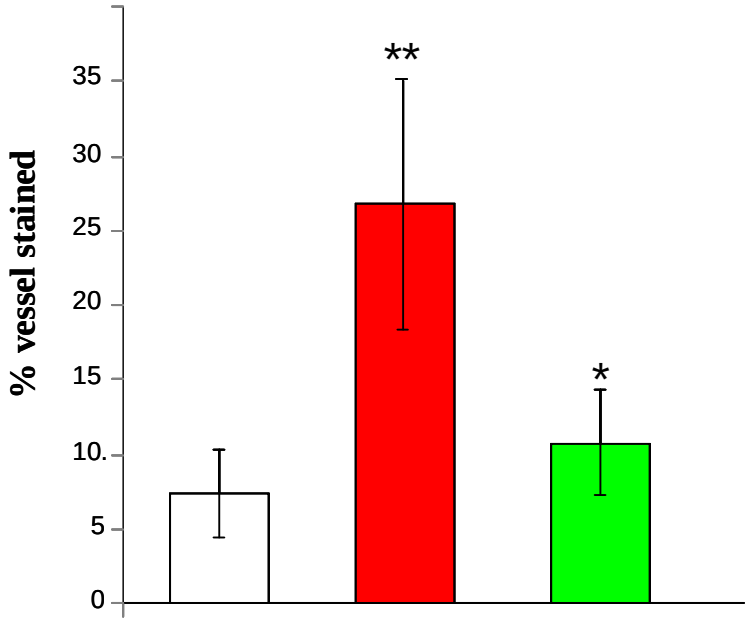

(ii)

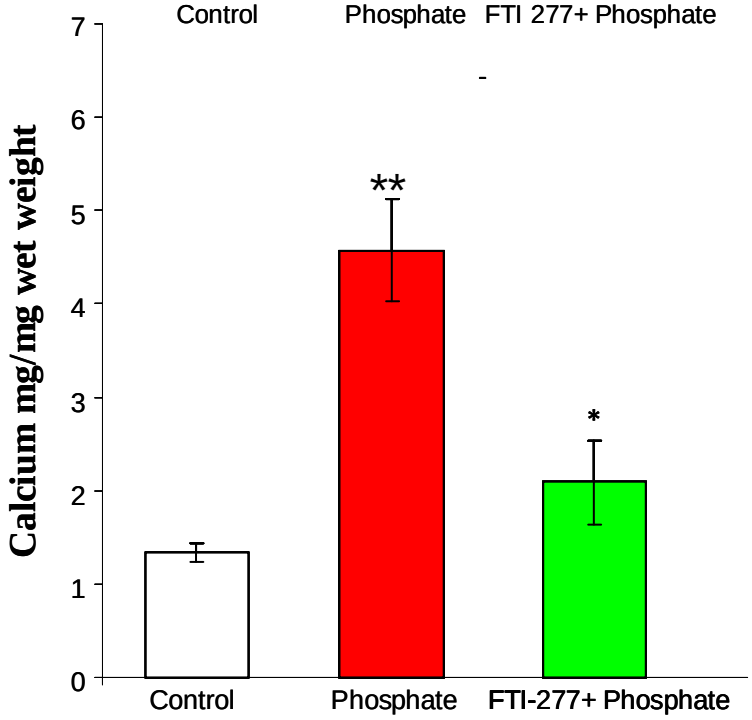

Figure 4.33: FTI-277 inhibits phosphate-induced mineralisation in aortic rings from rats with end stage renal disease. (i) Samples were prepared as detailed in the legend to figure 4.32 and alizarin red quantified as described in section 2.8.5. Results were pooled from analysis of 2 sections from 3 different rats. (ii) *O*-cresolphthalein complexone assay was performed in order to quantify the amount of calcium in each of the aortic rings. Results shown here were pooled from 3 rats (n=8, aortic rings) (*$p<0.05$, FTI-277 vs phosphate, **$p<0.01$, phosphate vs control)

Figure 4.34: H and E staining of aortic rings from rats with end stage renal disease. Rat aortic rings were incubated in DMEM with DMSO (1:1000) (A, D, G) or DMEM + DMSO + elevated phosphate and alkaline phosphatase (B, E, H) or DMEM + elevated phosphate and alkaline phosphatase and FTI-277 (C, F, I) for 10 days. Samples were collected, fixed, sectioned and stained with haematoxylin and eosin. Representative images are shown (n=3 rats). Scale bars for images A, B, C = 1000 μm; images D, E, F = 200 μm and images G, H, I = 50 μm.

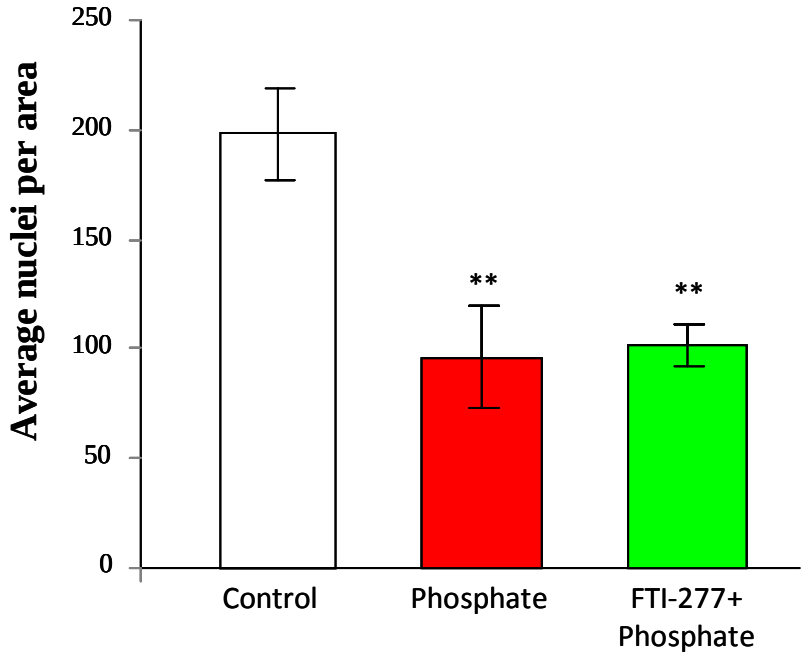

Figure 4.35: FTI-277 did not prevent the reduction in nuclei number induced by elevated phosphate in aortic rings from rats with end stage renal disease. Nuclei were counted from haematoxylin and eosin-stained rings from rats with end stage renal disease (Figure 4.34) within a fixed 800 μm x 800 μm area with an average vessel length of ~1000 μm. Results shown were pooled from 3 different rats, and expressed as average nuclei per area. ** $p<0.001$ phosphate/FTI-277 vs control.

4.2.10.2 Sham controls (late time point)

The rings obtained from sham operated rats were analysed in a similar manner to end stage renal disease. At this time point, the BUN level of sham operated rats was 24.1 mg/dl, which is normal. Incubation with elevated phosphate increased calcium deposition in rat aortic rings which present throughout the vessel wall (Figure 4.36, B, E, and H). Again, only a minimal amount of mineralisation was seen in the FTI-277 treated rings (Figure 4.36, C, F, I). Alizarin red staining was quantified as described in section 2.8.5 and expressed as a percentage of section area. Figure 4.37(i) shows that FTI-277 inhibits phosphate-induced mineralisation. This result was further confirmed using the *O*-cresolphthalein complexone assay (Figure 4.37(ii), *$p<0.05$).

Aortic ring sections were also stained with haematoxylin and eosin (Figure 4.38). This demonstrated normal morphology of the aortic rings as seen by nuclear staining and preservation of elastic lamina. Nuclei were counted as detailed above. Interestingly, no difference was detected in nuclei numbers when the different groups were compared (Figure 4.39). The number of nuclei per group was: control 178$\pm$16, phosphate 163$\pm$17, FTI-277 184$\pm$15.

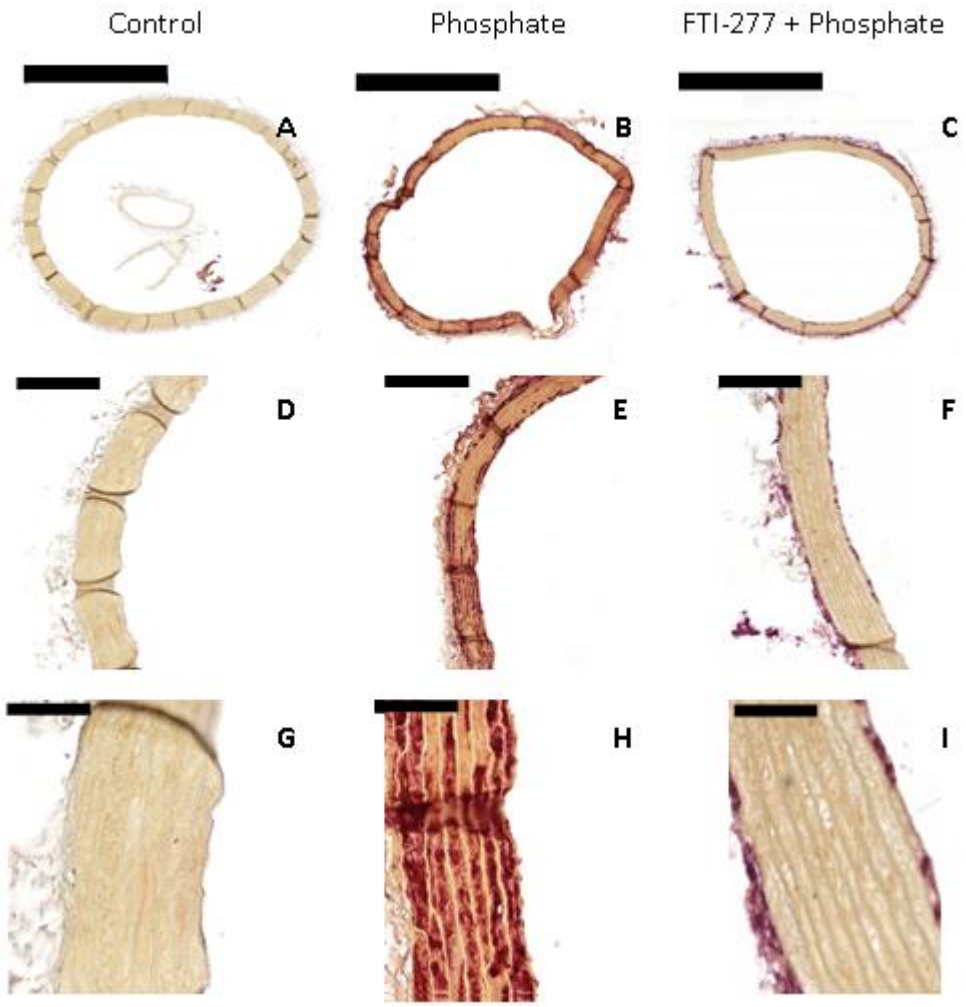

Figure 4.36: FTI-277 inhibits phosphate-induced mineralisation of aortic rings from sham operated rats (late time point). Rat aortic rings were incubated in DMEM with DMSO (1:1000) (A, D, G) or DMEM + DMSO + elevated phosphate and alkaline phosphatase (B, E, H) or DMEM + elevated phosphate and alkaline phosphatase and FTI-277 (C, F, I) for 10 days. Samples were collected, fixed, sectioned and stained with alizarin red. Representative images are shown (n=3). Red indicates mineralisation. Scale bars for images A, B, C = 1000 μm; images D, E, F = 200 μm and images G, H, I = 50 μm.

(i)

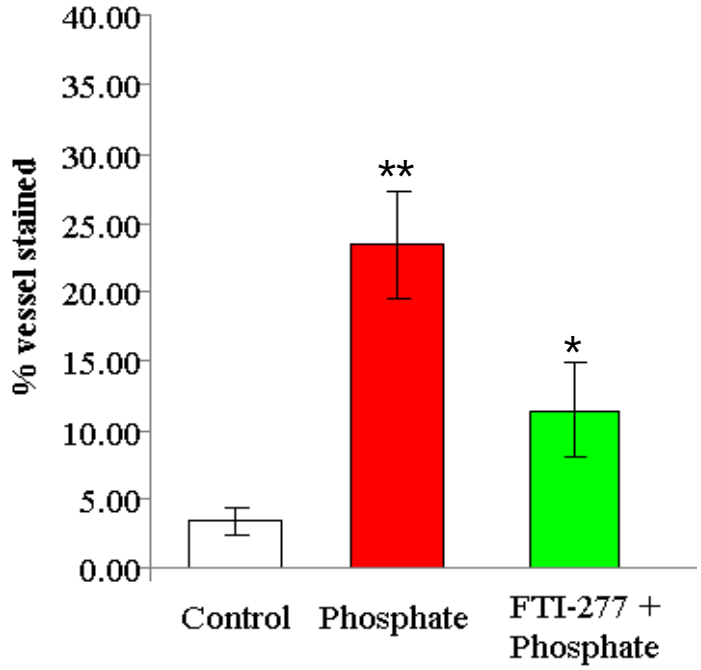

(ii)

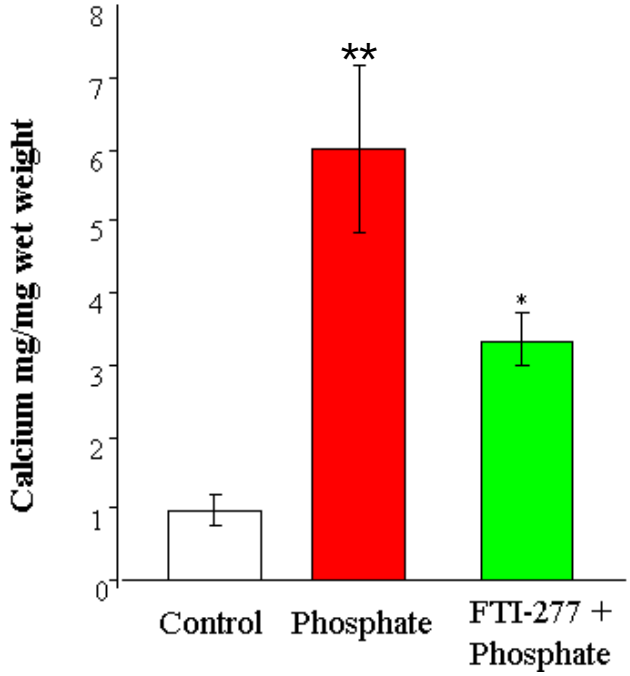

Figure 4.37: FTI-277 inhibits phosphate-induced mineralisation of aortic rings from long term sham operated rats. (i) Samples were prepared as detailed in the legend to figure 4.36 and alizarin red quantified as described in section 2.8.5. Results were pooled from 3 different rats. (ii) *O*-cresolphthalein complexone assay was performed in order to quantify the amount of calcium in each of the aortic rings. Results shown here were pooled from 3 rats (n=8, aortic rings) (*$p<0.05$, FTI-277 vs phosphate, **$p<0.01$, phosphate vs control)

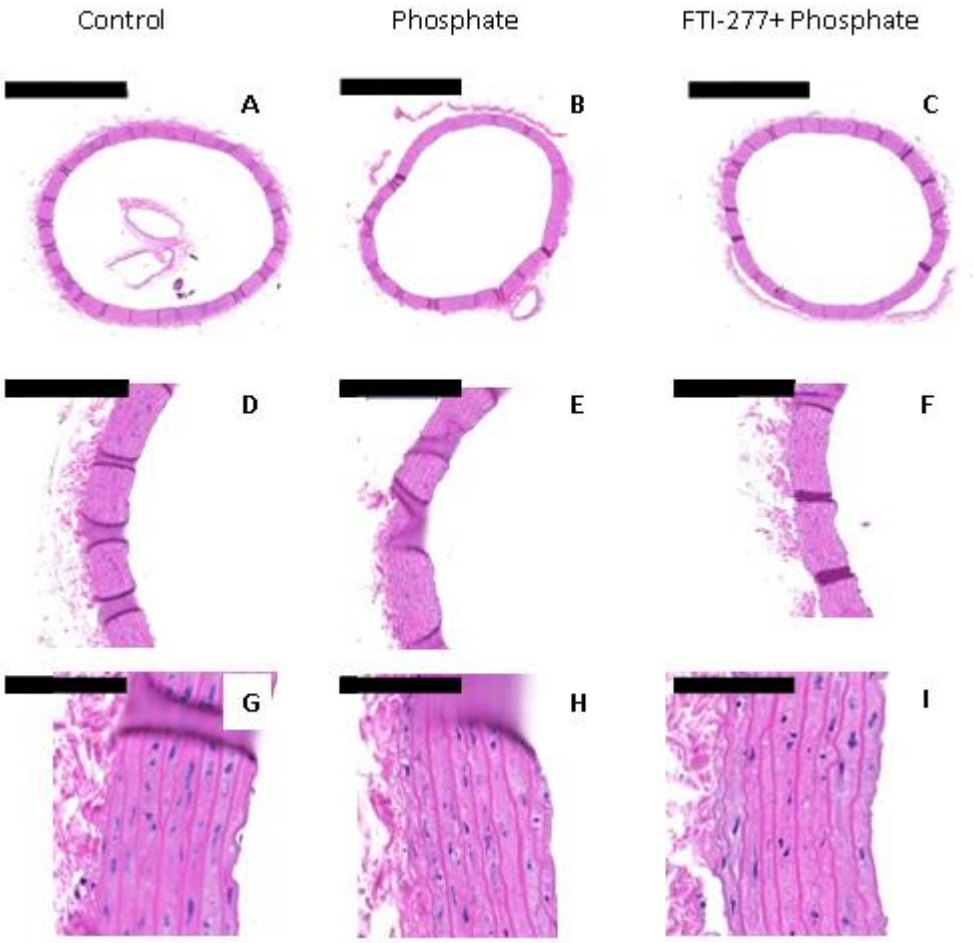

Figure 4.38: H and E stain of sham operated rat aortic rings (late time point). Rat aortic rings were incubated in DMEM with DMSO (1:1000) (A, D, G) or DMEM + DMSO + elevated phosphate and alkaline phosphatase (B, E, H) or DMEM + elevated phosphate and alkaline phosphatase and FTI-277 (C, F, I) for 10 days. Samples were collected, fixed, sectioned and stained with haematoxylin and eosin. Representative images are shown (n=3). Scale bars for images A, B, C = 1000 μm; images D, E, F = 200 μm and images G, H, I = 50 μm.

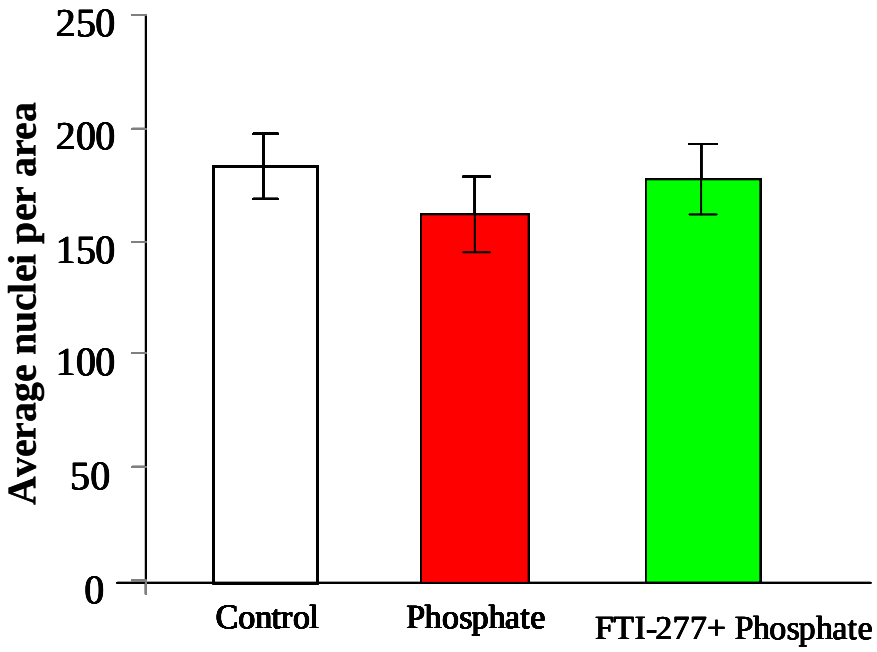

Figure 4.39: No difference was detected in nuclei numbers in the three groups. Nuclei were counted from haematoxylin and eosin-stained rings from sham operated control rats (late) (Figure 4.38) within a fixed 800 μm x 800 μm area with an average vessel length of ~1000 μm. Results shown here were pooled from 3 different rats (n=3) and expressed as average nuclei per area.

4.3 Discussion

The work described in this chapter demonstrates that FTI-277 inhibits mineralisation by promoting PI3K/Akt signalling and inhibiting apoptosis induced by elevated phosphate. FTI-277 also regulates the osteogenic differentiation of VSMC; FTI-277 inhibited Runx2, Msx2 and ALP mRNA expression, promoted MGP mRNA expression, which is an inhibitor of VSMC mineralisation, and maintained the expression of ASMA. Furthermore, it was shown that FTI-277 inhibits mineralisation in an ex vivo assay of vascular calcification using aortic rings from rats with early and end stage renal disease. Interstingly, elevated phosphate significantly decreased the number of cells in aortic rings isolated from end stage, but not early stage, renal disease or sham operated controls. These results suggest that vessels exposed to an ureamic mileu are more susceptible to further insults (e.g. elevated phosphate). These results are discussed below.

4.3.1 FTI-277 inhibits mineralisation by promoting PI3K/Aktsignalling

A number of down-stream signalling pathways are modulated in cells in response to farnesyl transferase inhibitors. As demonstrated in Chapter 3, FTI-277 increases Akt phosphorylation in VSMCs. Therefore, to test whether FTI-277 inhibits mineralisation by activating PI3K/Akt signalling, wortmannin and SH6 were used. Wortmannin is a selective PI3K inhibitor which is upstream of Akt. As predicted, wortmannin promoted, and FTI-277 inhibited, mineralisation (see Figure 4.1). When cells were incubated in the presence of both FTI-277 and wortmannin, some mineralisation was detected, demonstrating that the effects of FTI-277 on mineralisation can be negated, at least in part, by wortmannin.

Pre-incubation of VSMCs with wortmannin reduced serum-induced Akt phosphorylation which was expected based on wortmannin's ability to inhibit PI3K. However, phosphorylated Akt appeared to be increased in the presence of both FTI-277 and wortmannin, compared to the wortmannin only treated group (see Figure 4.3). This result could suggest that in these studies, wortmannin only partially inhibited PI3K signalling, which may explain why some mineralisation was detected in cells treated with both reagents. This finding is in contrast to the study of normal rat islet cells (INS 832/13), where LY294002, a selective PI3 kinase inhibitor, reduced FTI-277-stimulated Akt phosphorylation completely (Kyathanahalli and Kowluru, 2011). However, both these studies suggest that inhibiting farnesylation promotes Akt phosphorylation. In the study

using INS 832/13 and normal rat islet cells, the authors suggested that an unidentified farnesylated protein which they called 'probin' (protein kinase-B inhibitory protein) inhibited Akt phosphorylation and that inactivation of this protein using FTI-277 resulted in phosphorylation of Akt (Kyathanahalli and Kowluru, 2011).

The PI3K/Akt signalling pathway is known to be important for inhibiting mineralisation. Over-expression of a constitutively active form of PI3K inhibited βGP-induced mineral deposition by VSMCs (Hyde and Canfield, unpublished information). Furthermore, inhibition of PI3K signalling with wortmannin prevented the inhibition of mineralisation by over-expressing Axl (Collett et al., 2007)**.** Son *et al* have also shown that wortmannin reduced Akt phosphorylation and increased apoptosis thus increasing calcification of rat VSMCs (Son et al., 2007). Wortmannin is a fungal metabolite and a structural analogue of demethoxyviridin which has been shown to have an inhibitory effect upon PI3K activity at nanomolar concentrations (Cross et al., 1995). However, wortmannin has also been reported to inhibit phospholipase D (Bonser et al., 1991)**,** myosin light chain kinase, and plekstrin phosphorylation (Cross et al., 1995)**,** which casts some doubt on the specificity of this compound.

Thus, to confirm that FTI-277 inhibits mineralisation by promoting Akt signalling, SH6, a commercially available Akt III inhibitor was used. SH6 is a competitive phosphatidylinositol analogue which prevents the translocation of Akt to the membrane. It prevents phosphatidylinositol 3, 4, 5-trisphosphate (PIP3) formation and binding to Akt without affecting activation of the upstream kinase PDK-1. This analogue is metabolically stable because it does not have the hydroxyl group at location 3 of the inositol ring. (Kozikowski et al., 2003). SH6 has been shown to inhibit Akt activation in a number of cell culture studies (Castillo et al., 2004; Wildroudt et al., 2006). SH6 can inhibit Akt phosphorylation either in the presence of serum or after serum starvation (Gills et al., 2006; 2007).

Therefore, to test whether FTI-277 inhibits mineralisation by activating Akt signalling, SH6 was used. First, it was confirmed that pre-incubation of VSMCs with SH6 inhibited Akt phosphorylation following serum stimulation (Figure 4.4). The next aim was to determine whether SH6 negated the effect of FTI-277 on phosphate induced mineralisation of VSMCs. The results showed that SH6-treated VSMCs underwent

mineralisation and FTI-277 inhibited this process (see Figure 4.5). Furthermore, SH6 negated the effect of FTI-277 on mineralisation. Although these results support the suggestion that FTI-277 inhibits mineralisation via Akt signaling, it was important to confirm that SH6 inhibited Akt phosphorylation in the long term mineralisation assays. Western blotting showed a reduction in Akt activation in SH6-treated cells and, as expected, Akt activation was increased in FTI-277 treated cells. Importantly, Akt phosphorylation was reduced to control levels when cells were incubated with SH6 and FTI-277.

SH6 is a competitive inhibitor of phosphatidylinositol. Therefore, its effectiveness relies upon the amounts of PIP2 and PIP3 that are also present. In a serum-containing cell culture environment, there are a number of growth factors that activate signalling pathways culminating in an increase of PIP3 (Krech et al., 2010). This may explain the presence of some Akt phosphorylation in VSMCs following pre-incubation with SH6. Krechet et al., 2010 also demonstrated that although the phosphatidylinositol analogues, SH6 and SH5, did not completely inhibit Akt phosphorylation in the presence of serum, they induced morphological changes in the cells. It is also possible that the effect of SH6 on VSMC mineralisation could be independent of Akt activity, as SH6 can affect other targets besides Akt, including PLC, which also activates a number of downstream survival signalling pathways (Krech et al., 2010).

Therefore, the production of a lentivirus encoding a dominant negative form of Akt (dn-Akt) (see section 4.2.3) was the next aim. The objective was to determine whether over-expressing dn-Akt in VSMCs would prevent the inhibition of mineralisation by FTI-277. The over-expression of dn-Akt in VSMCs was confirmed by immunofluorescence analysis of transduced cells (Figure 4.9) and western blotting (Figure 4.10). Levels of phosphorylated Akt were markedly lower in dn-Akt cells compared to control cells transduced with the Empty vector. However, some basal Akt phosphorylation was still detected in the dn-Akt cells, which may explain their ability to proliferate and survive under serum-containing conditions.

The next step was to determine whether the effect of FTI-277 on mineralisation was negated by dn-Akt. At this stage, the dn-Akt VSMCs were already at passage 13 and were growing more slowly than usual. Empty vector VSMCs mineralised by day 7 in the presence of phosphate, and FTI-277 inhibited this mineralisation (Figure 4.12). In

contrast, dn-Akt VSMCs looked unhealthy and there was a lot of cell debris. The cells did not form multi-layers, and by day 9 most of the monolayer cells had retracted and no mineralisation was detected. It is not known whether this was due to the effects of elevated phosphate on dn-Akt VSMCs or because the cells were at a high passage number.

In summary, the experiments using wortmannin and SH6 suggest that FTI-277 inhibits VSMC mineralisation by promoting PI3K/Akt signaling.

4.3.2 FTI-277 inhibits phosphate- induced VSMC apoptosis

Activation of PI3K/Akt signalling is important for cell survival. The phosphorylation of Akt results in activation of caspase-9 and is a negative regulator of Bad, a pro-apoptotic protein (Datta et al., 1999). It is well established that apoptosis induces vascular calcification (Proudfoot et al., 2000). Thus, the next step in this study was to determine whether FTI-277 inhibited apoptosis of VSMC.

Apoptosis was induced by culturing VSMCs in the presence of serum-free medium and elevated phosphate. When cells were co-incubated with FTI-277, cell loss was less marked compared to controls (Figure 4.13). The effect of FTI-277 on VSMC apoptosis was confirmed by counting the number of apoptotic cells. FTI-277 treated cells were resistant to phosphate-induced apoptosis as shown in Figure 4.15. In addition, western blotting demonstrated that the levels of active caspase 3 were higher in the phosphate-treated cells compared to FTI-277 treated cells (Figure 4.14). Together, these results suggest that elevated phosphate induces cell death due to apoptosis, and that FTI-277 prevents this process.

The inhibition of apoptosis by FTI-277 shown in this study is in contrast to studies using mesenchymal stem cells (MSC), where pre-incubation of these cells with FTI-277 had no effect on caspase 3/7 activity or the number of apoptotic cells (Duque et al., 2011; Bolick et al., 2003). Interestingly, Nikolov et al., (2013) demonstrated that R115777, a non-peptidomimetic farnesyl transferase inhibitor, had no effect on caspase 3 activity or apoptosis in human VSMCs. In breast cancer cells, FTI-277 increased caspase 3 activity, thereby stimulating apoptosis which is in keeping with its anti-tumour property (Ellis et al., 2003). FTI-277 also induced apoptosis of myeloma cells (Bolick et al., 2003). The

differential effects of FTI-277 on caspase activity could be explained by the ability of FTI-277 to increase Akt phosphorylation in some, but not all, cell types (see Figure 4.14; Jiang et al., 2000; Sun et al., 2004).

From these results it is possible to hypothesise that FTI-277 inhibits mineral deposition by activating PI3K/Akt signalling and preventing apoptosis. Therefore, the next aim was to determine whether the effect of FTI-277 on apoptosis was negated by inhibiting Akt phosphorylation using SH6. These studies demonstrated that SH6 increased apoptosis of VSMCs, and negated the inhibitory effect of FTI-277 on apoptosis (Figure 4.16). These results are consistent with previous studies which have shown that SH6 activates caspase 9 and 3 activity in HMEC-E6 cells resulting in death by apoptosis (Dietze et al., 2004). Together, these experiments confirm that the inhibition of apoptosis by FTI-277 is through promotion of Akt signalling.

4.3.3 FTI-277 inhibits the osteogenic differentiation of VSMCs

During the calcification process, the osteogenic conversion of VSMCs is evidenced by the up-regulation of osteogenic transcription factors, such as Cbfa-1/Runx2 and Msx2 (Shanahan et al., 1999). The down-regulation of smooth muscle cell markers, such as ASMA, and up-regulation of inhibitors of calcification for example, MGP has also been shown (reviewed in Giachelli, 2009; Sage et al., 2010). There is also an increase in promoters of calcification, such as ALP and BMP-2 (reviewed in Sage et al., 2010; Toussaint, 2011).

The results presented in this chapter demonstrate that FTI-277 significantly inhibits phosphate-induced Runx2 and Msx2 mRNA expression by VMSCs (Figure 4.21). At the time that this work was being conducted, studies were published showing that FTI-277 also decreased levels of Runx2 expression in MSC which had been induced to undergo osteogenic differentiation (Duque et al., 2011). The change in the expression of this osteogenic transcription factor was detected by western blot analysis in this latter study. Runx2 is known to be essential for osteoblast differentiation, as mice lacking this transcription factor do not develop bone (Ducy et al., 1997). It has also been shown that VSMCs do not undergo osteogenic differentiation when Runx2 is knocked out using

siRNA (Speer et al., 2010). Together, these studies suggest that inhibition of protein farnesylation in VSMCs and MSC attenuates Runx2 expression thereby decreasing osteoblastic differentiation. ALP is another marker of osteogenic differentiation and a promoter of calcification as it cleaves pyrophosphate which is an inhibitor of this process (Toussaint, 2011) and releases phosphate. In this present study, FTI-277 was shown to reduce phosphate-induced ALP mRNA expression. FTI-277 has also been shown to reduce PPARγ expression and activity in MSC incubated in the presence of an adipogenic medium, thus inhibiting differentiation of MSC into adipocytes (Rivas et al., 2007). Therefore protein farnesylation appears to be important for the successful differentiation of cells, although whether this is Ras-mediated or Ras-independent, and/or Akt-dependent is not known.

There have been no published data with regards to the effect of inhibiting farnesylation on MGP expression. In this study, it was demonstrated that FTI-277 treated cells have increased MGP mRNA expression compared to βGP-treated cells. MGP is a known calcification inhibitor in the vasculature (Luo et al., 1997; Moe et al., 2005). MGP also appears to play a role in cell differentiation as shown in the MGP knockout mouse, in which medial smooth muscle cells were replaced by chondrocyte-like cells undergoing endochondral ossification (Luo et al., 1997). The link between inhibiting farnesylation, increased MGP expression and inhibition of mineral deposition by VSMC is not known.

Previous work has shown that MGP is a regulatory protein for BMP-2. In a study using mouse bone marrow stromal cells, it was shown that MGP has dose-dependent effects on BMP-2 induced osteoblastic differentiation of these cells (Zebboudj et al., 2002). Low and high levels of MGP increases BMP-2 activity, but intermediate levels of MGP results in the inhibition of BMP-2 activity. This is further shown in a study of calcifying vascular cells (CVC) whereby MGP appears to either promote or inhibit BMP-2 induced calcification in a dose-dependent manner (Zebboudj et al., 2003). The addition of MGP decreased calcification when the relative BMP-2 levels were high, and increased calcification when the relative levels of BMP-2 were low. Furthermore, another study has shown that the interaction between MGP and BMP-2 prevents the attachment of BMP-2 to its receptor and down-stream activation of Smad1, which is a part of the BMP-2 signalling pathway (Zebboudj et al., 2002). FTI-277 appears to have no effect on phosphate-induced

BMP-2 mRNA expression although there is a trend for an increase in expression. In future studies, it would be interesting to determine whether FTI-277 decreases Smad signalling in VSMC, as this would indicate whether the increased expression of MGP inhibits the autocrine effects of BMPs in these cells.

To further investigate the link between the inhibition of farnesylation, promotion of Akt signalling and downregulation of the osteogenic differentiation factors, Runx2 and Msx2, SH6 was used. In the first experiment, SH6 was found to partially negate the inhibitory effect of FTI-277 on Runx2 and Msx2 mRNA expression (Figure 4.23). However, this effect was not seen when the experiment was repeated, although a downward trend in Msx2 expression was noted. One of the possible reasons for this result is that a fresh batch of βGP was used in the repeat experiment, which resulted in mineralisation occurring much earlier than usual (day 4). As Runx2 expression is associated with early stages of mineralisation, it is therefore possible that this increase was missed in this experiment.

The link between PI3K/Akt signalling and Runx2 expression was also explored in a study using VSMCs by Byon et al., (2008). In this study, the authors suggested that Akt signalling regulated oxidative stress-induced Runx2 expression and VSMC calcification. They showed that inhibition of PI3K/Akt signalling using LY294002 resulted in down-regulation of Runx2 and attenuation of oxidative stress-induced mineralisation. However, they did not investigate the exact link between Runx2 regulation and Akt signalling. This finding is opposite to what is shown in this study, and may reflect differences in model systems used**.**

In summary, FTI-277 appears to inhibit Runx2 and Msx2 expression and at the same time promotes Akt signalling. Both of these mechanisms are important in inhibiting mineralisation. What remains unknown is the relationship between Akt signalling and Runx2 and Msx2 expression.

4.3.4 FTI-277 inhibits VSMCs migration

VSMCs are the principal cells in the medial layer of the blood vessel. There are a number of functions of VSMCs which include regulating vascular tone which plays an important role in blood pressure. VSMCs can transform from a contractile state to a synthetic state (de-differentiated) due to multiple metabolic disturbances such as a high

phosphate level or an increase in the inflammatory state seen in CKD patients (House et al., 2008). These synthetic characteristics result in an increase of VSMC migration and contribute to the pathogenesis of vascular calcification and atherosclerosis (Neven et al., 2011). The induction of VSMC migration by a number of factors including cytokines, growth factors and angiotensin can result in plaque rupture in atherosclerosis (reviewed by Rudjjanto et al., 2007). Increased levels of phosphate have also been demonstrated to promote VSMC migration (Rangrez et al., 2012) and may contribute to the pathogenesis of vascular calcification.

Therefore, the next aim was to determine whether FTI-277 inhibits VSMC migration using a wound assay. Platelet derived growth factor (PDGF) was used as a chemoattractant in these studies, and it was shown that FTI-277 inhibited VSMC migration in response to this growth factor (Figures 4.19, 20). This result is in keeping with other studies that have shown pre-incubation of bovine VSMCs with a farnesyltransferase inhibitor attenuated migration (Willis et al., 2011). Ras GTPase plays an important role in cell migration in response to different stimuli via activation of various downstream effectors (Shirai et al., 2007). One of the possible mechanisms by which Ras GTPase regulates cell migration is by activation of Erk 1/2. However, studies presented in this thesis (Chapter 3) demonstrated that FTI-277 inhibited Ras GTPase activation but had an inconsistent affect on Erk 1/2 phosphorylation in VSMCs. Another possible mechanism by which Ras GTPase mediates cell migration is by activating p38 MAP kinase (Di Luozzo et al., 2005). Although the levels of p38 were not checked in this study, it is possible that increased Akt signalling will in turn increase p38 activation as shown previously (Cabane et al., 2004). It has also been demonstrated that the PI3K/Akt signalling pathway is directly involved in migration of melanoma cells (Ye et al., 2008). Therefore, as the studies presented in this thesis demonstrate that PI3K/Akt signaling is increased by FTI-277, but FTI-277 inhibits VSMC migration, it is possible to hypothesise that FTI-277 inhibits VSMC migration in an Akt independent manner.

VSMC migration plays an important role in the pathogenesis of vascular calcification. Thus, attenuation of VSMC migration by FTI-277 could be one of the mechanisms by which inhibition of calcification is brought about and appear to be unrelated to the PI3K/Akt signalling pathway.

4.3.5 FTI-277 inhibits phosphate-induced mineralisation of aortic rings from rats with renal disease and sham controls

In vitro studies have confirmed that FTI-277 inhibits phosphate-induced VSMC mineralisation. Therefore, the next step was to determine the effect of FTI-277 on mineralisation of aortic tissue using an animal model of CKD. Tissue was used from rats which were in early stage or end stage renal failure or sham-operated controls in an *ex vivo* model of vascular calcification.

Histological examination of sections from early and end stage renal disease aortic rings, and sham controls, showed the induction of mineralisation following incubation with elevated phosphate, although there was no significant difference in calcium content between these groups. These results suggest that aortic rings from rats with end stage renal disease do not appear to have a higher propensity for the development of calcification *ex vivo*, even though they have been exposed to the uraemic milieu for a longer period. This finding contrasts with the results of a study using human epigastic, omental and mesenteric arteries from predialysis (early stage renal disease) and dialysis (end stage renal disease) patients (Shroff et al., 2010). In this latter study, the human vessels were induced to calcify *ex vivo* in the presence of elevated levels of calcium and phosphate, whereas this present study used only elevated phosphate. Blood vessels from dialysis patients showed significantly higher calcium load compared to blood vessels from predialysis patients. The authors suggested that these blood vessels have a diminished ability to prevent calcification. This suggestion was further confirmed by the demonstration of increased alkaline phosphatase activity and up-regulation of Runx2 in blood vessels from dialysis patients compared to the predialysis cohort. Together, these results may suggest that cells from different vascular beds have different propensities to calcify and/or that their ability to respond to different insults is altered.

Importantly, this study demonstrated that FTI-277 inhibited mineralisation in aortic rings derived from rats in early and end stage renal disease and sham controls (Figures 4.24 – 4.36), which is consistent with the *in vitro* studies reported in Chapter 3. During the course of writing this thesis, Nikolov et al., reported that another farnesyl transferase inhibitor, R115777, reduced both plaque lesion area and calcification *in vivo* in female Apoe-/- mice induced to undergo chronic renal failure (CRF) by sub-total nephrectomy (Nikolov et al., 2013). Interestingly, this benefit was not seen when Apo E -/- mice without

CRF were treated with R115777, which contrasts with previous studies showing that manumycin A and FTS reduces atherosclerosis in ApoE-/- mice (Sugita et al., 2007; George et al., 2007). The authors suggested that this difference may be because of different inhibitors, different doses and dosing regimes, and differences in age and gender of the mice used. However, the demonstration that both R115777 and FTI-277 reduce calcification in *in vivo* and *ex vivo* CKD models further strengthens the hypothesis that inhibition of farnesylation may have therapeutic potential in patients with CKD.

To begin to determine the mechanism by which FTI-277 inhibited mineralisation of aortic rings, the effects of elevated phosphate and FTI-277 on cell number was determined. These studies were performed as it had previously been shown that FTI-277 inhibited phosphate-indcued apoptosis of VSMC *in vitro* (see above). These studies demonstrated that treatment with elevated phosphate reduced the number of cells present in aortic rings from rats with end stage renal disease, although FTI-277 did not prevent this decrease (Figure 4.35). Interestingly, no difference was detected in cell numbers when aortic rings from sham-operated and early stage renal disease rats were incubated in any of the conditions studied (Figures 4.27, 4.31 and 4.39), which suggests that cells in vessels exposed to a uraemic milieu for extensive periods have an increased susceptibility to elevated phosphate. Whether there was increased apoptosis in these vessels was not determined in these studies. Interestingly, Shroff et al., 2010 also showed that human vessels from dialysis patients contained less cells when treated with high calcium and phosphate medium compared to pre-dialysis patients. Further analysis also revealed down regulation of ASMA and an increase in apoptotic cells in the vessels from dialysis patients (Shroff et al., 2010).

In summary, these studies demonstrate that elevated phosphate results in mineralisation in aortas from both early and end stage renal disease rats as well as sham controls. Furthermore, cell number was reduced in the aortas from end stage renal disease, but this did not correspond to an increased level of mineralisation. FTI-277 inhibited phosphate-induced mineralisation in all samples, but did not affect cell loss induced by elevated phosphate aortas from rats with end stage renal disease.

Conclusion

FTI-277 inhibits VSMC mineralisation *in vitro* by activating downstream PI3K/Akt signalling and preventing apoptosis, and by inhibiting the osteogenic differentiation of VSMC. FTI-277 also inhibits mineralisation in both aortic rings from rats with early and end stage renal disease, and sham controls, *ex vivo*. However it is not known whether activation of Akt phosphorylation and/or inhibition of mineralisation and differentiation are Ras-dependent or independent. Therefore, a better understanding of the role of RasGTPase in regulating vascular calcification is required. This work is the focus of the studies detailed in the next chapter.

Chapter 5

Determining the effects of inhibiting Ras signalling on vascular calcification using FTS

5.1 Introduction

The studies presented in Chapter 4 show that FTI-277 inhibits phosphate-induced VSMC differentiation, apoptosis and mineralisation by promoting PI3K/Akt signalling. However, it is not known whether the inhibition of Ras GTPase activity by FTI-277 (as shown in Chapter 3) is responsible for mediating these effects. Ras GTPase has been shown to be either anti-apoptotic or pro-apoptotic depending on the cellular context (Cox et al., 2003), and apoptosis is an initiator of calcification. Therefore, the next question was to determine whether inhibiting Ras GTPase activity specifically would inhibit vascular calcification.

To understand the function of Ras in regulating vascular calcification, S-*trans,trans*-farnesyl thiosalicylic acid (FTS) was used. FTS is a synthetic molecule which has a structure similar to the C-terminal farnesyl cysteine motif of Ras that anchors Ras to the membrane (Gana-Weisz et al., 2002); therefore, FTS disrupts membrane localisation of active Ras and is in turn a specific Ras inhibitor which can act on all isoforms of Ras GTPase.

Previous studies have shown that FTS inhibits the growth of human H-Ras-transformed fibroblasts with an IC_{50} value of 7.5 μM (Marciano et al., 1995). FTS has also been shown to modulate the proliferation and migration of mesangial cells and glioblastoma cells *in vitro* (Khawaja et al., 2005, Goldberg et al, .2006). Administration of FTS to ApoE-/- mice fed a high fat diet was also shown to reduce Ras GTPase activation, NF-κB and VCAM-1 expression and atherosclerotic plaque lesion size in these mice (George et al., 2002). This finding further confirms the role of Ras GTPase in vascular disease.

Therefore, the objectives of the studies described in this chapter are to:

(vi) Determine whether inhibition of Ras activity using FTS affects deposition of a mineralised matrix by VSMCs

(vii) Determine whether FTS prevents apoptosis induced by serum deprivation and high phosphate

(viii) Determine the effect of FTS on VSMC migration

(ix) Determine the effect of FTS on *ex vivo* mineralisation of rat aortic rings from early and end stage renal disease

5.2 Results

5.2.1 FTS modulates VSMC mineralisation in a dose-dependent manner

To assess the effects of inhibiting Ras on mineralisation, VSMCs were incubated in βGP-containing medium in the presence or absence of FTS (5 - 40 μM) or DMSO (1:500) + βGP. Although the VSMCs appeared healthy, higher concentrations of FTS (40 μM) appeared to inhibit multilayering of the cells and ridge formation at post-confluence (Figure 5.1). Phase contrast images of cells stained with alizarin red on day 9 and quantification of staining are shown in Figure 5.2. Mineralisation was detected in βGP-treated cells and in cells co-incubated with 5 - 20 μM FTS (Figure 5.2, A–D). Interestingly, as the concentration of FTS increased, the mineralisation appeared to be more diffuse (Figures 5.2, compare A-D). At 40 μM, FTS inhibited βGP-induced VSMC mineralisation (Figure 5.2 E). These results were confirmed when mineralisation was quantified (Figure 5.2 (ii)).

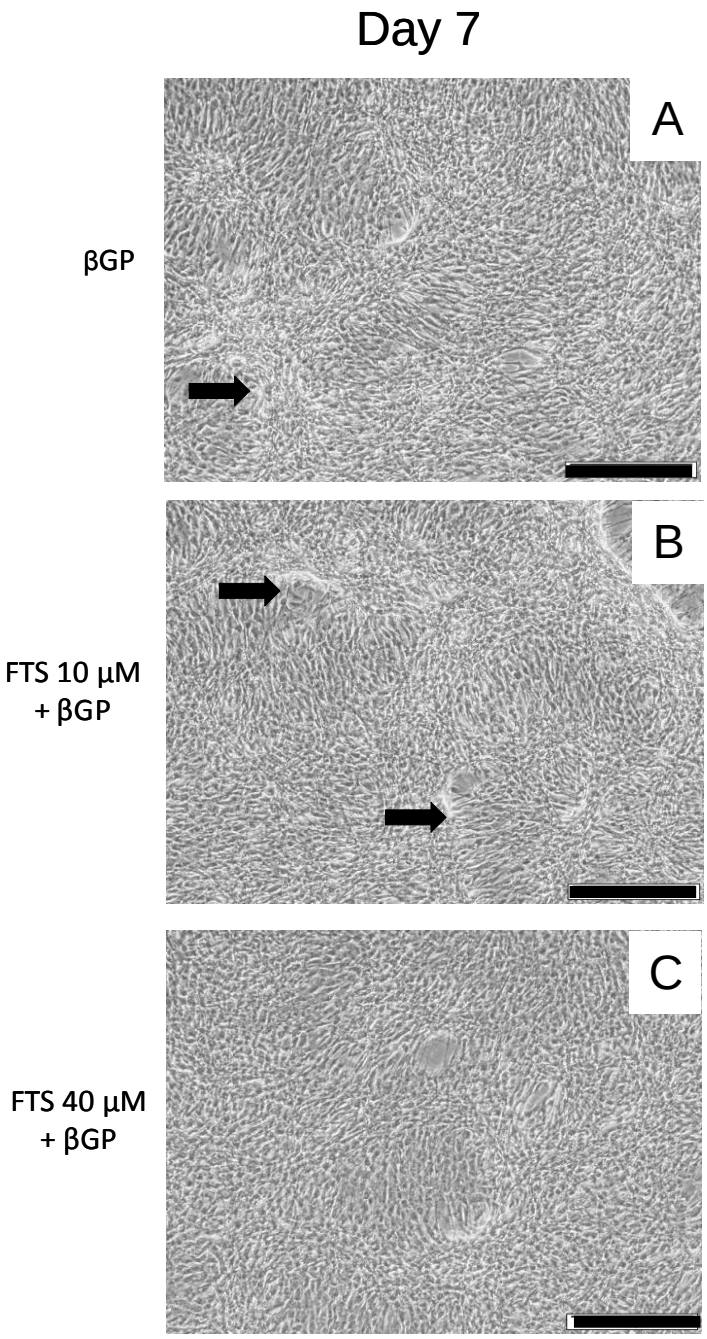

Figure 5.1: FTS prevents VSMCs multilayering and ridge formation in a dose-dependent manner. VSMCs were cultured in six well plates in 10% FCS-DMEM until 90% confluency and were then incubated in 10% FCS-DMEM containing ßGP and DMSO (1:500; control) (A), or with 10% FCS-DMEM + ßGP + FTS (10 µM, B; 40 µM, C). Phase contrast images at day 7 are shown. Scale bar = 500 µm. Arrows point to ridge formation.

(i)

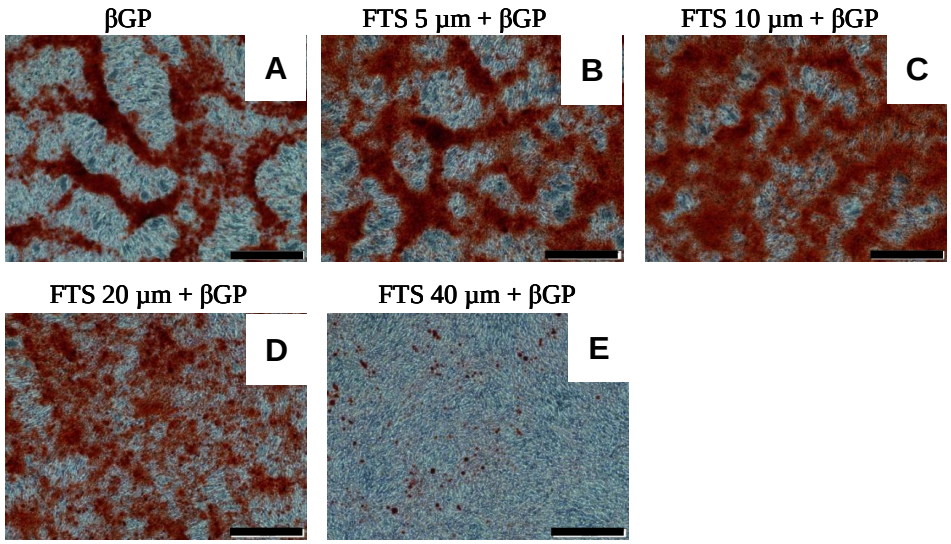

(ii)

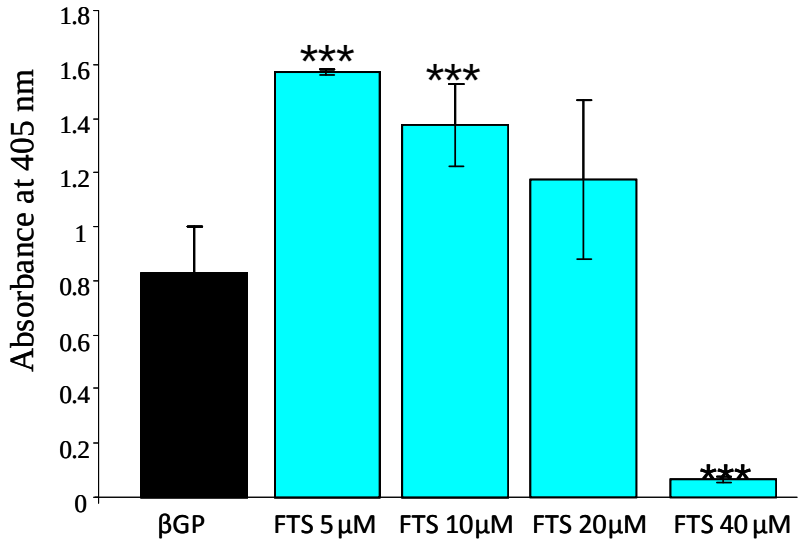

Figure 5.2: FTS regulates βGP-induced VSMC mineralisation. (i) VSMCs were cultured in six well plates in 10% FCS-DMEM until 90% confluency and were then incubated in 10% FCS-DMEM containing ßGP and DMSO (1:500); ßGP) (A), or with 10% FCS-DMEM + ßGP + FTS (5 µM, B) or (10 µM, C) or (20 µM, D) or (40 µM, E). Phase contrast images of alizarin red stained VSMCs on day 9 are shown. Scale bar=500 µm. (ii) Alizarin red dye elution was performed. Results were pooled from two experiments and are presented as mean +/- SEM (n = 9). ***p<0.001, vs ßGP.

5.2.2 The effects of different doses of FTS on Ras activation, Akt phosphorylation and Erk phosphorylation.

FTI-277 has been shown to promote Akt signalling and inhibit Ras GTPase (Chapter 3). However, it is not known whether Ras GTPase inhibition *per se* leads to increase Akt phosphorylation. In order to understand this, the next aim was to determine the effects of different doses of FTS on Ras GTPase activation and Akt phosphorylation; Erk phosphorylation was also examined. VSMCs were pre-incubated with either FTS (10 and 40 µM) or control (DMSO, 1:500) and stimulated with serum-containing medium for 5 and 15 minutes. Ras GTPase pull-down assays were performed on the cell lysates (see section 2.9.2); Akt and Erk phosphorylation was also assessed (see section 2.9.3).

Results show that prior to serum stimulation (T=0) there was no detectable Ras GTPase activity in any of the samples (Figure 5.3 (i), lane 1, 4, 7). FTS (40 µM) was found to delay serum-induced Ras GTPase activation compared to controls; active Ras was detected after 15 minutes serum stimulation in these samples, whereas it was detected after 5 minutes in the controls (Figure 5.3 (i), lanes 2, 3, 8 and 9). In contrast, active Ras was detected in VSMC incubated with 10 µM FTS after 5 and 15 minutes serum stimulation (Figure 5.3 (i), lanes 5 and 6).

Akt and Erk phosphorylation was also assessed in these samples by western blotting. FTS (40 µM) was found to promote serum-induced Akt phosphorylation after 5 minutes compared to controls (Figure 5.3 (ii), compare lanes 2 and 8). This effect was not observed with 10 µM FTS (Figure 5.3 (ii), lane 5). Erk phosphorylation appeared reduced in VSMCs treated with 40 µM FTS after 15 minutes (Figure 5.3 (iii), compare lanes 9 and 3). In contrast, 10 µM FTS had no effect on Erk phosphorylation (Figure 5.3 (iii), compare lanes 5-6 to 2-3).

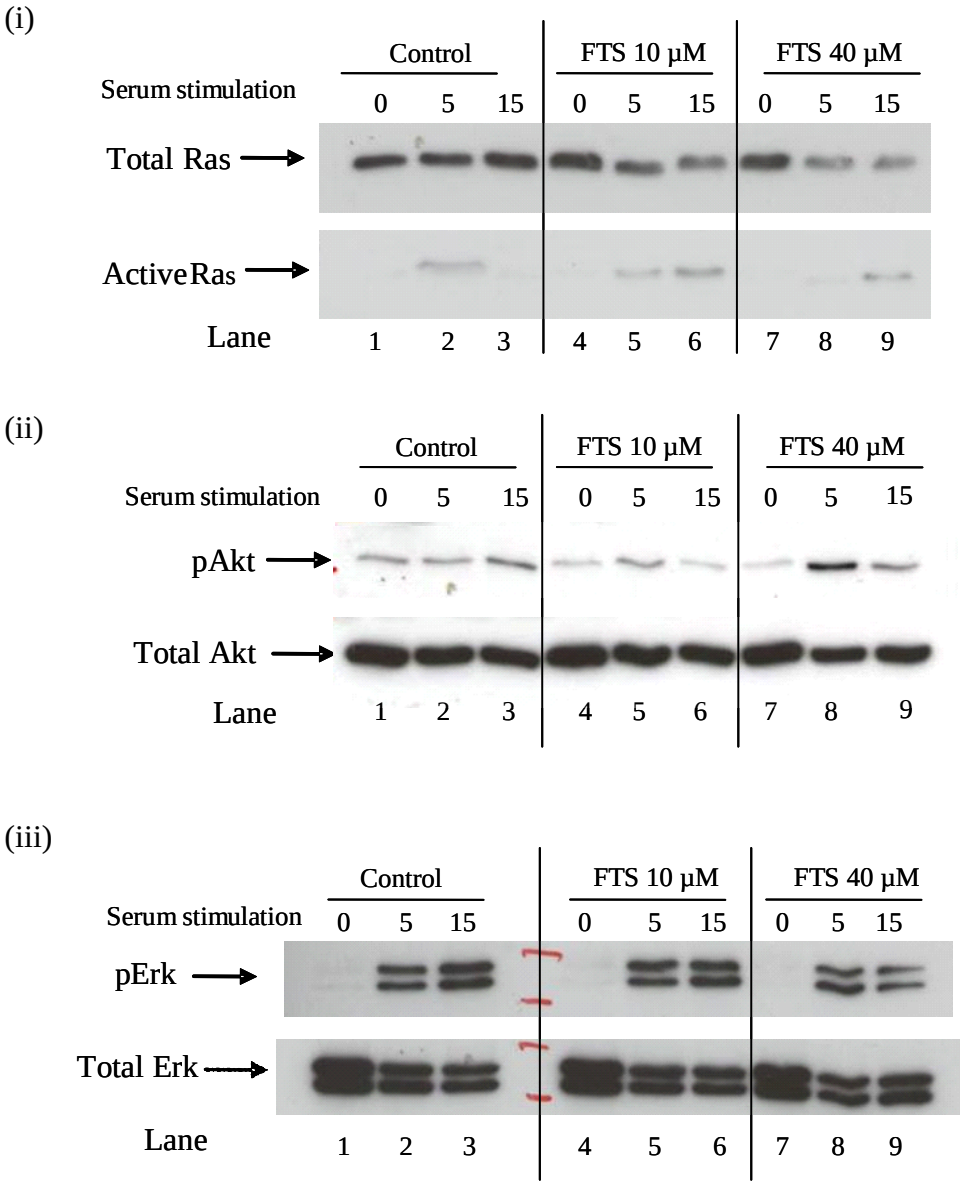

Figure 5.3: The effects of different doses of FTS on Ras activation, and Akt and Erk phosphorylation. Confluent VSMCs were incubated with control medium (10% FCS-DMEM, DMSO 1:500), or with 10% FCS-DMEM + FTS (10 µM) or (40 µM) for 77 hours. Subsequently, VSMCs were incubated with serum-free medium for 2 hours +/- FTS (10 µM or 40 µM), and then stimulated with 10% FCS-DMEM for 5 or 15 minutes. (i) Active Ras pull down assays were performed as detailed in section 2.9.2, and western blotting was conducted using an anti-Ras antibody for active Ras (bottom panel), and for total Ras present in the cell lysates (top panel). (ii, iii) Cell lysates were also analysed for pAkt and total Akt (ii), and pErk and total Erk (iii) expression using western blotting. Lanes 1, 4 and 7 contain samples collected prior to serum stimulation (T=0). Samples in lanes 2, 5 and 8 were collected after 5 minutes stimulation with serum-containing medium; samples in lanes 3, 6, 9 were collected after 15 minutes stimulation.

5.2.3 The effects of FTS on phosphate-induced apoptosis of HCVSMC

The studies presented in chapter 4 showed that FTI-277 inhibited serum-reduced Ras GTPase activity and prevented phosphate-induced apoptosis by promoting Akt signalling. The studies described above showed that FTS (40 μM) also inhibited Ras GTPase activity and promoted Akt signalling. Ras GTPase can be either anti- or pro-apoptotic depending on the cellular context (Cox et al., 2003). Many studies have shown that FTS stimulates apoptosis of cancer cells (Charette et al., 2001); it has also been shown to induce apoptosis of human mesangial cells in the presence of PDGF but not serum (Khwaja et al., 2005). Therefore, the next aim was to determine the effect of FTS on phosphate-induced apoptosis of VSMCs.

HCVSMCs were pre-incubated in the presence of 10 and 40 μM FTS in serum-free medium for 15 minutes. However, it was noted that cells incubated with 40 μM FTS detached from the culture dish almost immediately, suggesting that this concentration of FTS was toxic to the cells when used in serum-free conditions. The majority of cells incubated in serum-free medium containing 10 μM FTS remained attached to the dish, and so elevated phosphate was added to induce apoptosis as described in section 2.6. Control cells were incubated in serum-free medium containing vehicle plus elevated phosphate, and apoptosis was assessed by examining DAPI-stained nuclei. These studies demonstrated that FTS induces rapid apoptosis of HCVSMCs (Figure 5.5), although the loss of some cells due to toxicity cannot be excluded. The majority of cells had apoptotic nuclei 6 hours after addition of FTS (Figure 5.5 B), whereas apoptotic nuclei only started to appear in the controls after 12 hours (Figure 5.5 A).

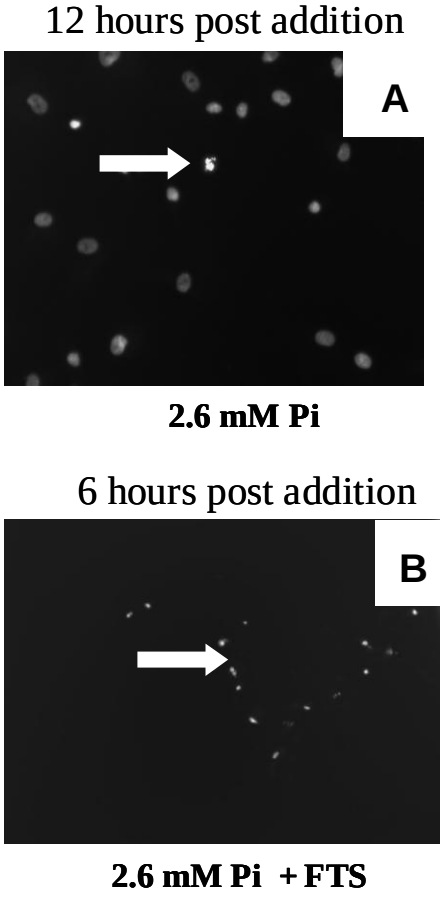

Figure 5.5: FTS appears to increase HCVSMC apoptosis. HCVSMC were plated in chamber slides as detailed in section 2.6. The next day, HCVSMCs were incubated with either 2.6 mM Pi (A) or 2.6 mM Pi + FTS (10 μM) (B) and cells were stained with DAPI after 12 (A) or 6 (B) hours. Apoptotic cells were defined as cells with condensed or fragmented nuclei (arrows).

5.2.4 FTS may delay PDGF-induced VSMC migration

The studies detailed in section 5.2.1 suggested that FTS prevented multilayering and ridge formation of post-confluent VSMCs, and that this effect was dose-dependent. Furthermore, when mineralisation was detected, it appeared more diffuse in these cultures than in the controls. Therefore, the next aim was to determine the effect of FTS on VSMC migration.

Initial experiments were conducted in the same way as for the FTI-277 experiments (section 4.2.6) and VSMCs were pre-incubated with either 10 or 40 µM FTS in serum-free conditions overnight. However, as with the HCVSMCs, the majority of these cells detached from the culture dish. Goldberg et al., (2006) reported that FTS binds to proteins in serum; hence, when it is used in serum-containing medium, the actual concentration of free FTS is lower than when it is used without serum. These authors, therefore, used 12.5 µM FTS in the presence of medium containing 0.5% serum in their migration studies using glioblastoma cells. Under these conditions, FTS was found to inhibit the migration of their cells. Therefore, further migration experiments using VSMCs were conducted in the presence of 0.5% serum.

VSMCs were grown to confluence and incubated overnight in 0.5% FCS-DMEM +/- FTS (10, 20 and 40 µM). However, VSMCs still detached following incubation with 20 µM and 40 µM FTS. In contrast, cells incubated with 10 µM FTS appeared healthy, and so they were used in migration assays as detailed in section 2.7 with wound closure being monitored after 24 and 48 hours. Figure 5.6 shows representative phase contrast images of VSMC at 0, 24 and 48 hours post-wounding. This figure shows that the wounds closed very quickly under these conditions, and that FTS (10 µM) appeared to slightly delay wound closure, particularly at the 24 hour time-point. However, although there was a trend towards delayed closure in the presence of FTS, this result was not significant (Figure 5.7).

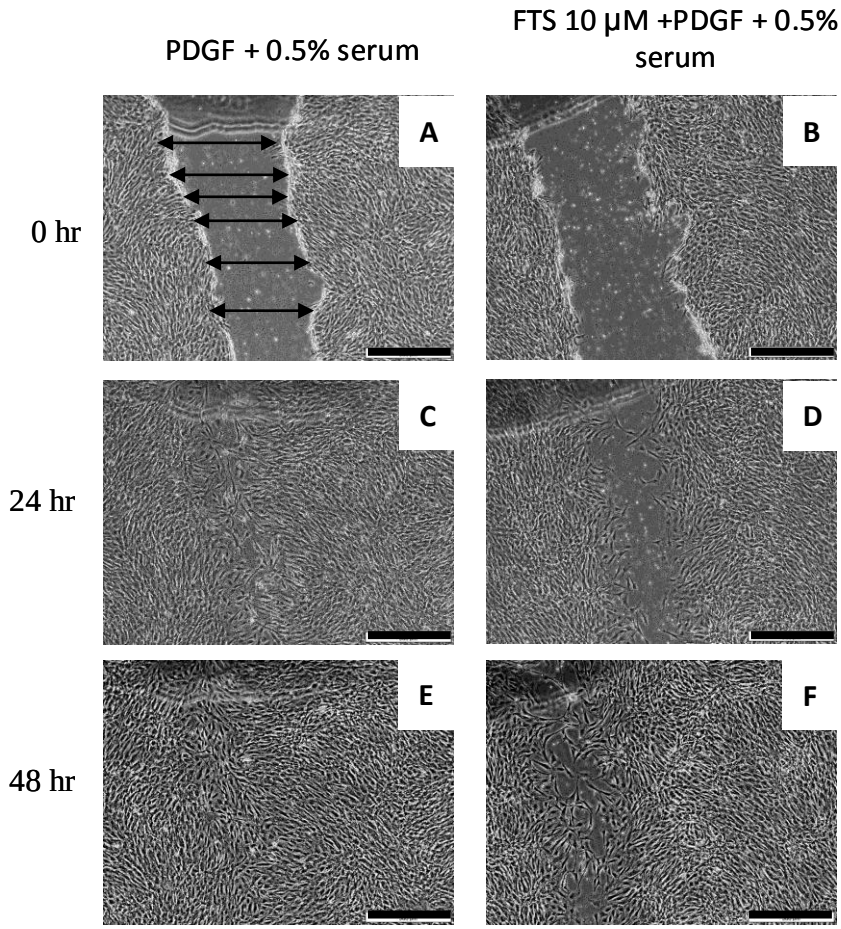

Figure 5.6: The effect of FTS on PDGF-induced VSMC migration. Confluent VSMCs were incubated in 0.5% FCS-DMEM +/- FTS (10 µM) overnight. Cell-free zones were made and VSMCs were then incubated with either (A, C, E) 0.5% FCS-DMEM containing PDGF (20 ng/ml) or (B, D, F, H) 0.5% FCS-DMEM containing PDGF (20 ng/ml) and FTS (10 µM). These areas were monitored after 24 (C, D), 48 (E, F) hours and phase contrast images were taken. Scale bar = 500µm.

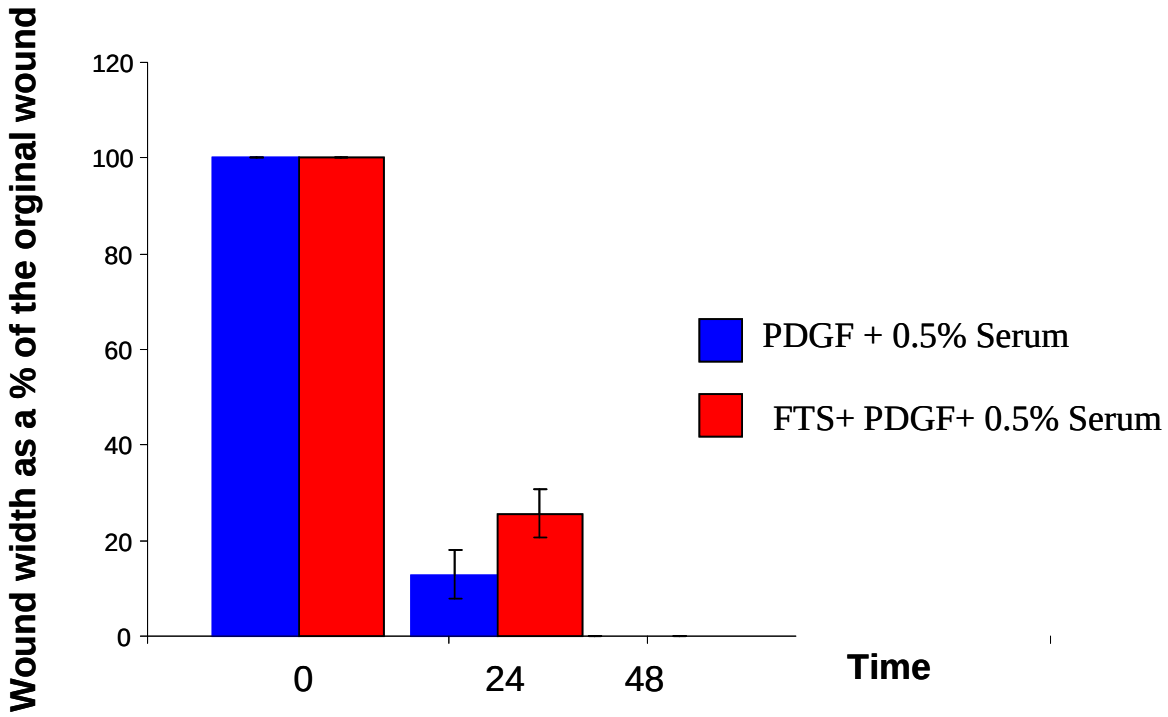

Figure 5.7: The effect of FTS (10 µM) on PDGF-induced wound closure. VSMCs were plated as detailed in the legend to Figure 5.6. Six measurements of the wound width were taken as shown in Figure 5.6 (A, solid arrows) and average measurements of wound width were determined at each time point, and expressed as a percentage of the original wound. The wounds were closed by 48 hours. The results shown are from six wounds from two separate experiments and are the mean +/- SEM.

5.2.5 FTS inhibits phosphate-induced mineralisation of aortic rings from rats with end stage renal disease and sham controls

Initial work demonstrated that FTS modulated βGP-induced mineralisation in a dose-dependent manner (Figure 5.2); lower doses of FTS increased mineralisation, whereas higher doses inhibited it. It was also noted that higher concentrations of FTS (40 μM) decreased Ras GTPase activity and increased Akt phosphorylation, but these effects were not detected at lower concentrations of FTS (Figure 5.3). Higher concentrations of FTS were toxic to both bovine and human VSMCs in serum-free medium. FTS (10 μM) stimulated phosphate-induced apoptosis of human VSMCs in serum-free medium (Figure 5.5), and delayed but did not inhibit PDGF-induced migration of VSMC in the presence of 0.5% serum (Figure 5.6). These results are consistent with previous studies demonstrating that the effect of FTS on cell behaviour is both dose-dependent and dependent upon the presence of other factors, including serum (Khwaja et al., 2005; Goldberg et al., 2006).

The studies presented in chapter 4 showed that FTI-277 inhibited phosphate-induced mineralisation of aortic rings from rats with both early and end stage renal disease, and sham-operated controls. These experiments were conducted in the absence of serum. Furthermore, although elevated phosphate also reduced the cell number in aortas from rats with end stage renal disease, this did not translate into increased mineralisation. In addition, it was shown that aortas from rats with end stage renal disease did not have a higher propensity to develop calcification *ex vivo* even though they had previously been exposed to a highly uraemic environment (BUN = 167-209 mg/dl) in end stage renal disease compared to (BUN = 53-89 mg/dl) in early stage renal disease - see table 7.1, 7.2, Appendix).

Therefore, this set of experiments aimed to determine the effects of FTS on *ex vivo* mineralisation using aortas from rats with end stage renal disease and sham-operated controls. These experiments were also conducted in the absence and presence of 10% FCS, and the rings were analysed as described in section 4.2.9.

5.2.5.1 End stage renal disease

The BUN level of the rats used for the experiments conducted in serum-free medium was 167-209 mg/dl (n=3 rats) and for the 10% serum experiments was 111-148 mg/dl (n=3 rats), indicating they all had end stage renal disease. Alizarin red staining of the aortic rings incubated with elevated phosphate in serum-free conditions (Figure 5.8) and in the presence of 10% serum (Figure 5.9) revealed that mineralisation was deposited throughout the vessel walls. FTS inhibited this phosphate-induced mineralisation both in the absence (Figure 5.8) and presence (Figure 5.9) of serum. Only spicules of mineralisation were detected in some of the rings. Quantification of alizarin red staining demonstrated that FTS significantly inhibited phosphate-induced mineralisation under both conditions (Figure 5.10, *$p<0.05$). The calcium content was also quantified using the *O*-cresolphthalein complexone assay. This assay revealed that elevated phosphate increased the calcium content of aortic rings but, surprisingly, FTS did not appear to inhibit this effect (Figure 5.11), which suggests that FTS may interfere with this assay as previously suggested for other compounds (Young et al., 1975).

Haematoxylin and eosin staining showed normal ultrastructure and morphology of aortic rings cultured under all the conditions tested (Figure 5.12, 5.13). Nuclei were counted as described in section 2.8.5. This analysis revealed that there was no significant difference in cell numbers when aortic rings were cultured +/- elevated phosphate and +/- FTS in serum-free conditions, although there was a trend towards reduced cell numbers with elevated phosphate (Figure 5.14 (i)). The number of cells in control medium was 153$\pm$35 versus phosphate 122$\pm$4 versus FTS 137$\pm$20. However, in the presence of 10% serum, there was a small but significant reduction in the number of nuclei in phosphate-treated rings (161$\pm$4 + phosphate compared to 177$\pm$4 control; *$p<0.05$). The number of cells in rings that were incubated with FTS was not significantly different from either control rings or rings incubated with elevated phosphate, although this finding may reflect the variability in cell numbers noted in these rings (169$\pm$10).

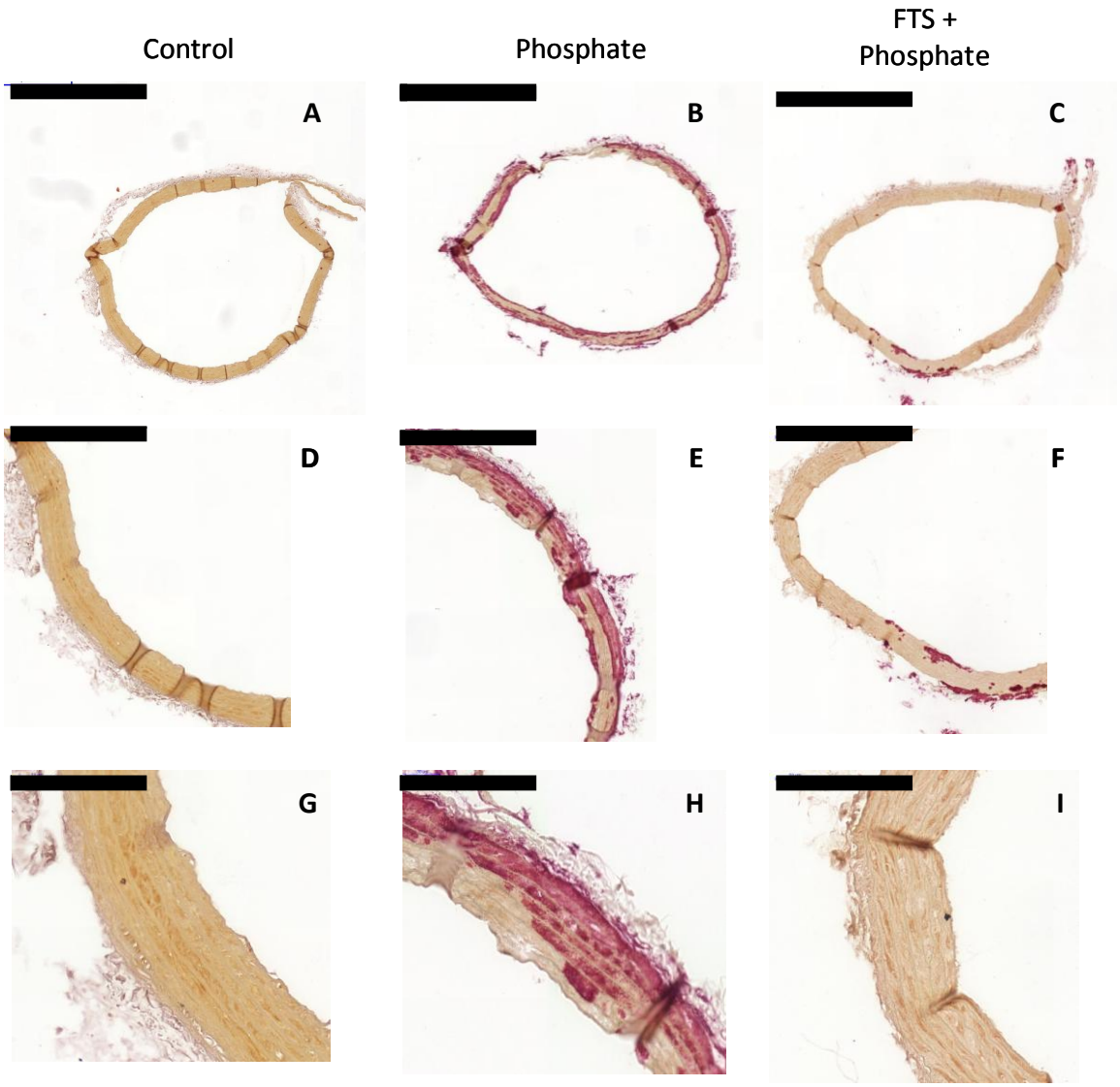

Figure 5.8: FTS inhibits phosphate-induced mineralisation in aortic rings from rats with end stage renal disease in the absence of serum. Rat aortic rings were incubated in DMEM with DMSO (1:500) (A, D, G) or DMEM + DMSO + elevated phosphate and alkaline phosphatase (B, E, H) or DMEM + elevated phosphate and alkaline phosphatase and FTS (40 µM, C, F, I) for 10 days. Samples were collected, fixed, sectioned and stained with alizarin red. Representative images are shown (n=2 rats). Red indicates mineralisation. Scale bars for images A, B, C = 1000 µm; images D, E, F = 200 µm and images G, H, I = 50 µm

Figure 5.9: FTS inhibits phosphate-induced mineralisation in aortic rings from rats with end stage renal disease in the presence of 10% serum. Rat aortic rings were incubated in 10% FCS-DMEM with DMSO (1:500) (A, D, G) or 10% FCS-DMEM + DMSO + elevated phosphate and alkaline phosphatase (B, E, H) or 10% FCS-DMEM + elevated phosphate and alkaline phosphatase and FTS (40 µM, C, F, I) for 10 days. Samples were collected, fixed, sectioned and stained with alizarin red. Representative images are shown (n=2 rats). Red indicates mineralisation. Scale bars for images A, B, C = 1000 µm; images D, E, F = 200 µm and images G, H, I = 50 µm.

(i)

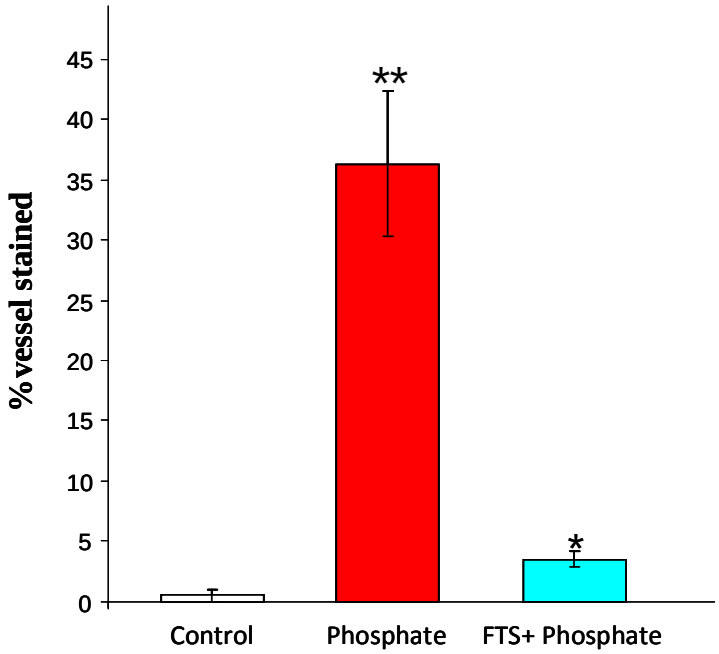

(ii)

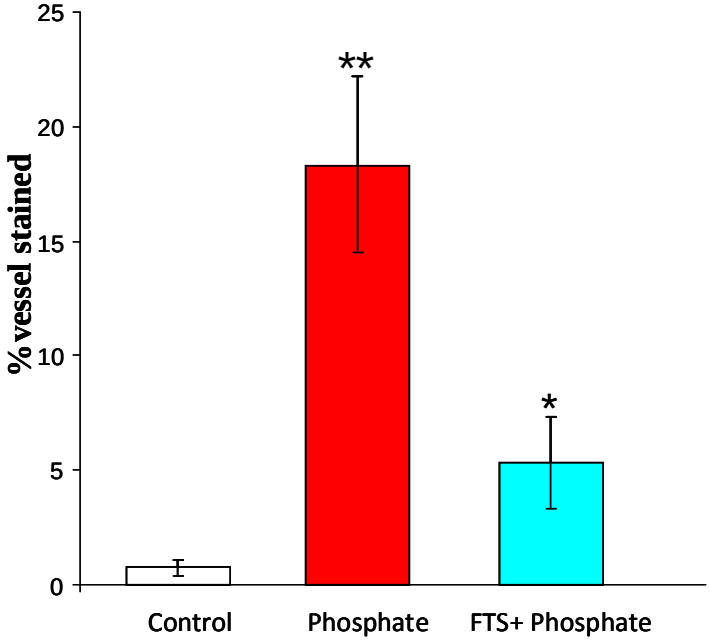

Figure 5.10: FTS inhibits phosphate-induced mineralisation in aortic rings from rats with end stage renal disease in both conditions. Samples were prepared as detailed in the legend to Figures 5.8 and 5.9. Quantification of alizarin red staining in aortic rings from 2 rats was performed as described in section 2.8.5. (i) no serum, (ii) 10% serum. *p<0.05, FTS vs phosphate, **p<0.01, phosphate vs control.

(i)

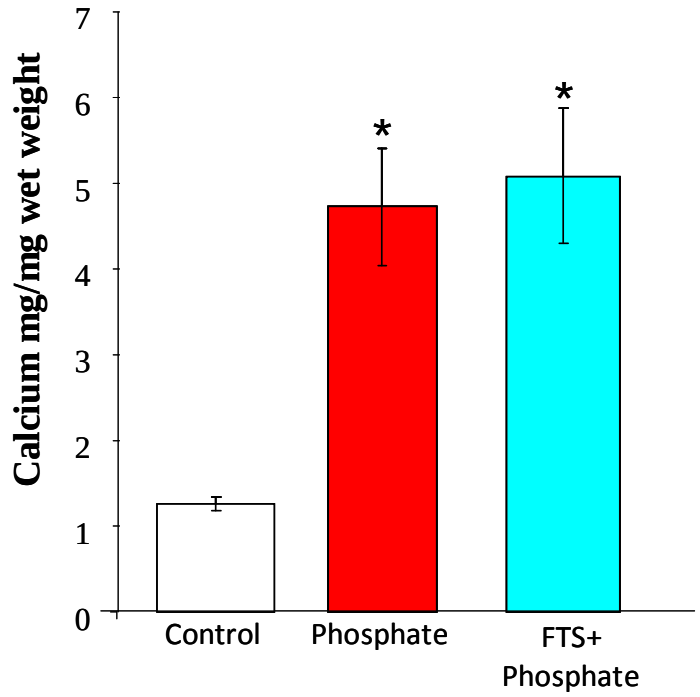

(ii)

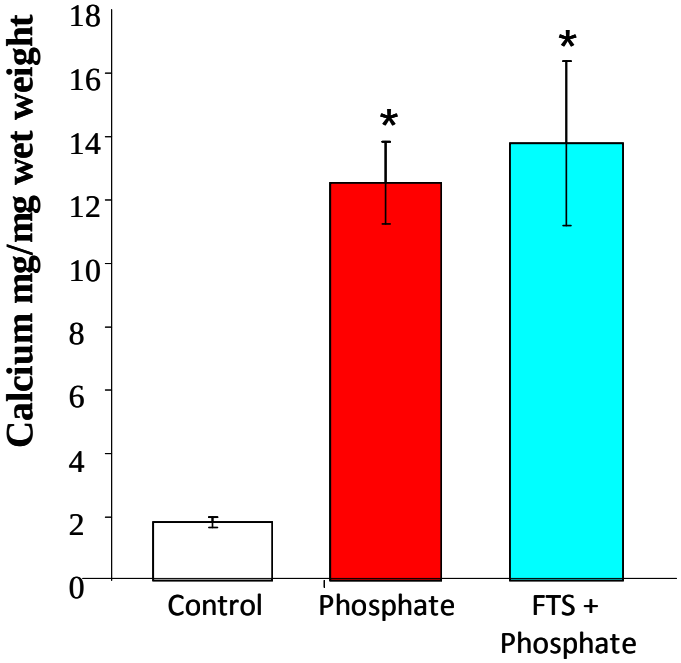

Figure 5.11: Calcium assay on aortic rings from rats with end stage renal disease. Aortic rings were incubated as detailed in the legends to Figures 5.8 and 5.9 and the calcium content determined using the *O*-cresolphthalein complexone assay. (i) no serum, (ii) 10% serum. Data are from 2 experiments, n=6 aortic rings. *p<0.05 phosphate or FTS vs control.

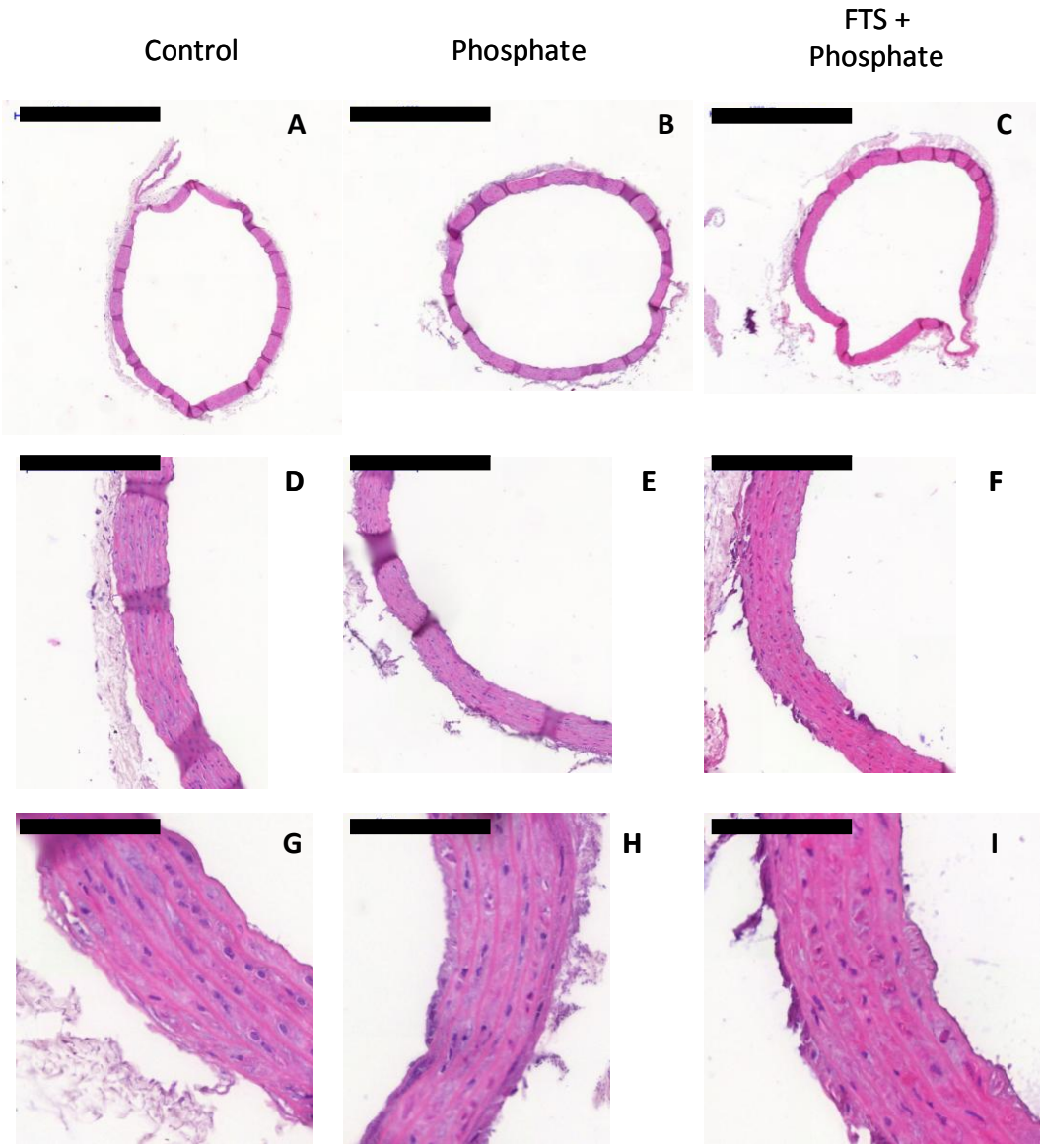

Figure 5.12: H and E staining of aortic rings from rats with end stage renal disease in no serum conditions. Rat aortic rings were incubated in DMEM with DMSO (1:500) (A, D, G) or DMEM + DMSO + elevated phosphate and alkaline phosphatase (B, E, H) or DMEM + elevated phosphate and alkaline phosphatase and FTS (40 µM, C, F, I) for 10 days. Samples were collected, fixed, sectioned and stained with haematoxylin and eosin. Representative images are shown (n=2 rats). Scale bars for images A, B, C = 1000 µm; images D, E, F = 200 µm and images G, H, I = 50 µm.

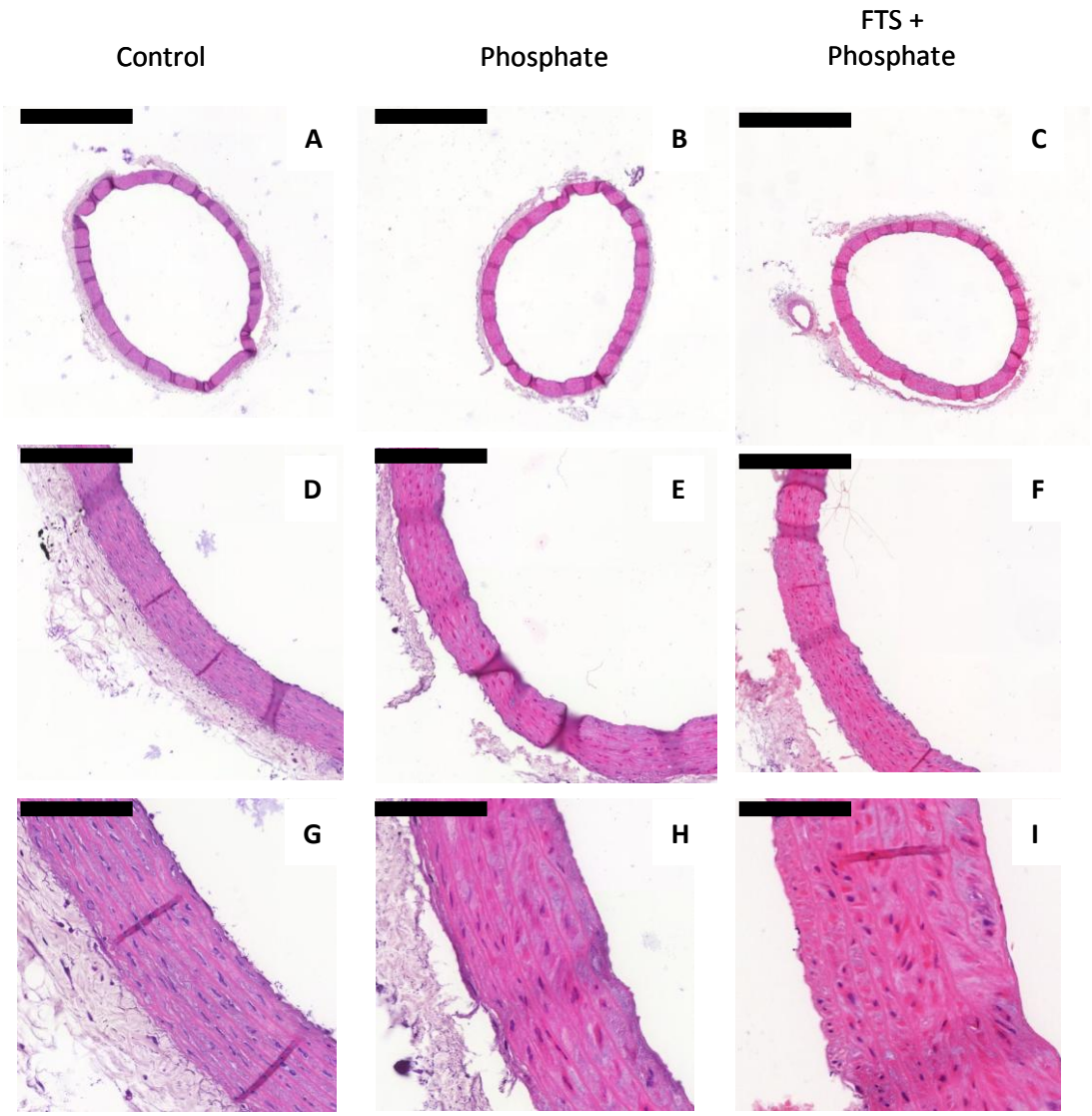

Figure 5.13: H and E staining of aortic rings from rats with end stage renal disease in 10% serum. Rat aortic rings were incubated in 10% FCS -DMEM with DMSO (1:500) (A, D, G) or 10% FCS-DMEM + DMSO + elevated phosphate and alkaline phosphatase (B, E, H) or 10% FCS-DMEM + elevated phosphate and alkaline phosphatase and FTS (40 µM, C, F, I) for 10 days. Samples were collected, fixed, sectioned and stained with haematoxylin and eosin. Representative images are shown (n=3 rats). Scale bars for images A, B, C = 1000 µm; images D, E, F = 200 µm and images G, H, I = 50 µm.

(i)

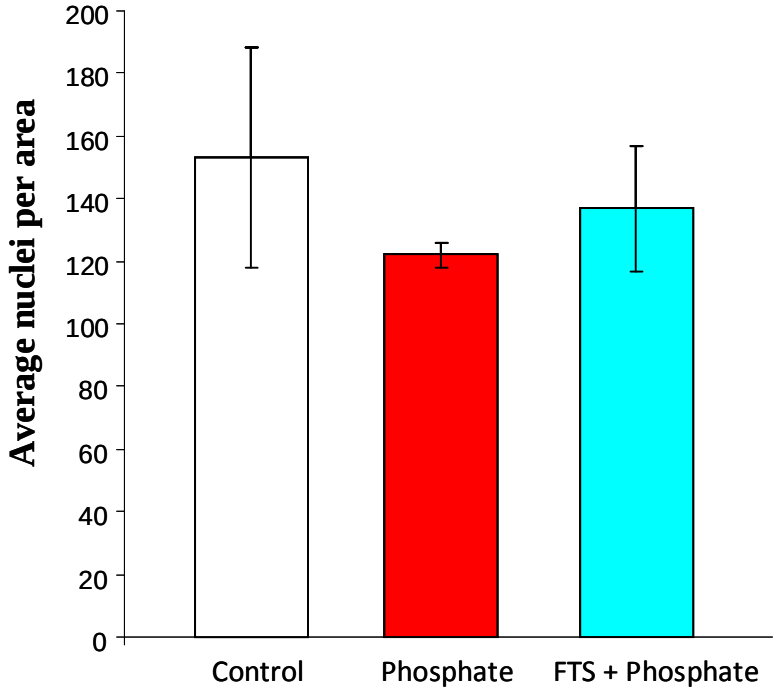

(ii)

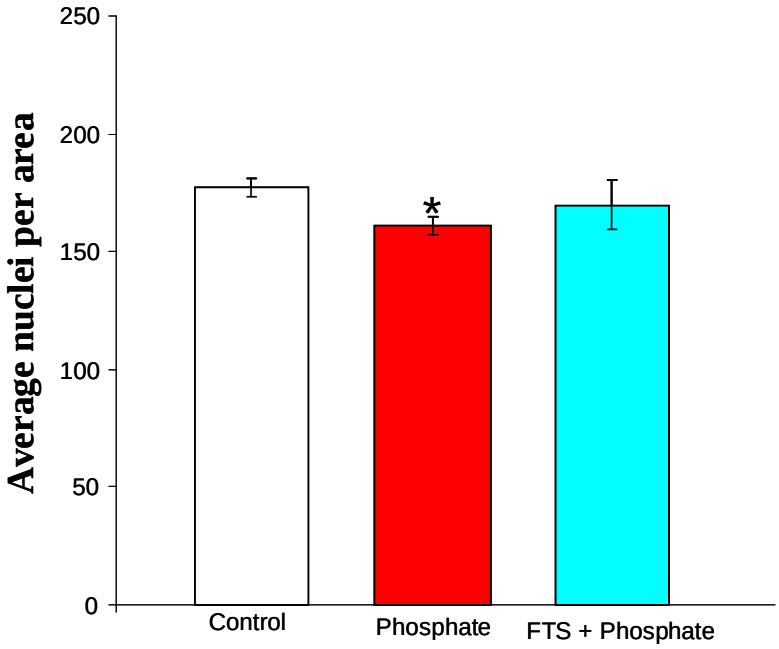

Figure 5.14: Nuclei number in aortic rings from rats with end stage renal disease. The number of nuclei present within a fixed 800 μm x 800 μm area of H and E stained sections, with an average vessel length of ~1000 μm, was determined. The results shown are from aortic rings cultured in (i) the absence of serum (n=2 rats) and (ii) 10% FCS-DMEM (n=3 rats), and are expressed as average nuclei number per area +/- SEM.*$p<0.05$, phosphate vs control

5.2.5.2 Sham-operated (late time point)

The rings obtained from sham-operated rats were also cultured in the presence or absence of FTS, as described above. At this time point, the BUN levels of the rats used for the experiments conducted in serum-free medium were 17.3-34.1 mg/dl (n=3 rats) and for the 10% serum experiments were 26-50.3 mg/dl (n=3 rats), which is normal. Incubation with elevated phosphate in the absence or presence of serum increased mineralisation in rat aortic rings, as evidenced by the presence of alizarin red staining (Figures 5.15 and 5.16, B, E, H). Little or no mineralisation was detected in the FTS-treated rings (Figures 5.15 and 5.16, C, F, I). Alizarin red staining was quantified as described in section 2.8.5 and expressed as a percentage of section area. Figure 5.17 (i) shows that FTS significantly inhibited phosphate-induced mineralisation in the absence of serum (*$p<0.05$). In the presence of serum, the extent of mineralisation varied markedly in the different rings analysed. However, a trend towards a reduction of phosphate-induced mineralisation by FTS was still apparent when the alizarin red staining was quantified (Figure 5.17 (ii)). The calcium content of the rings was also quantified using the *O*-cresolphthalein complexone assay. This assay confirmed that incubating aortic rings in the presence of elevated phosphate increased the calcium content of these rings (Figure 5.18). However, again, using this assay FTS did not appear to significantly inhibit this increase.

Aortic ring sections were also stained with haematoxylin and eosin (Figures 5.19 and 5.20). This demonstrated normal morphology of the aortic rings as seen by nuclear staining and preservation of elastic lamina. Nuclei were counted as detailed above. No significant difference was detected in nuclei numbers when the different groups were compared (Figure 5.21).

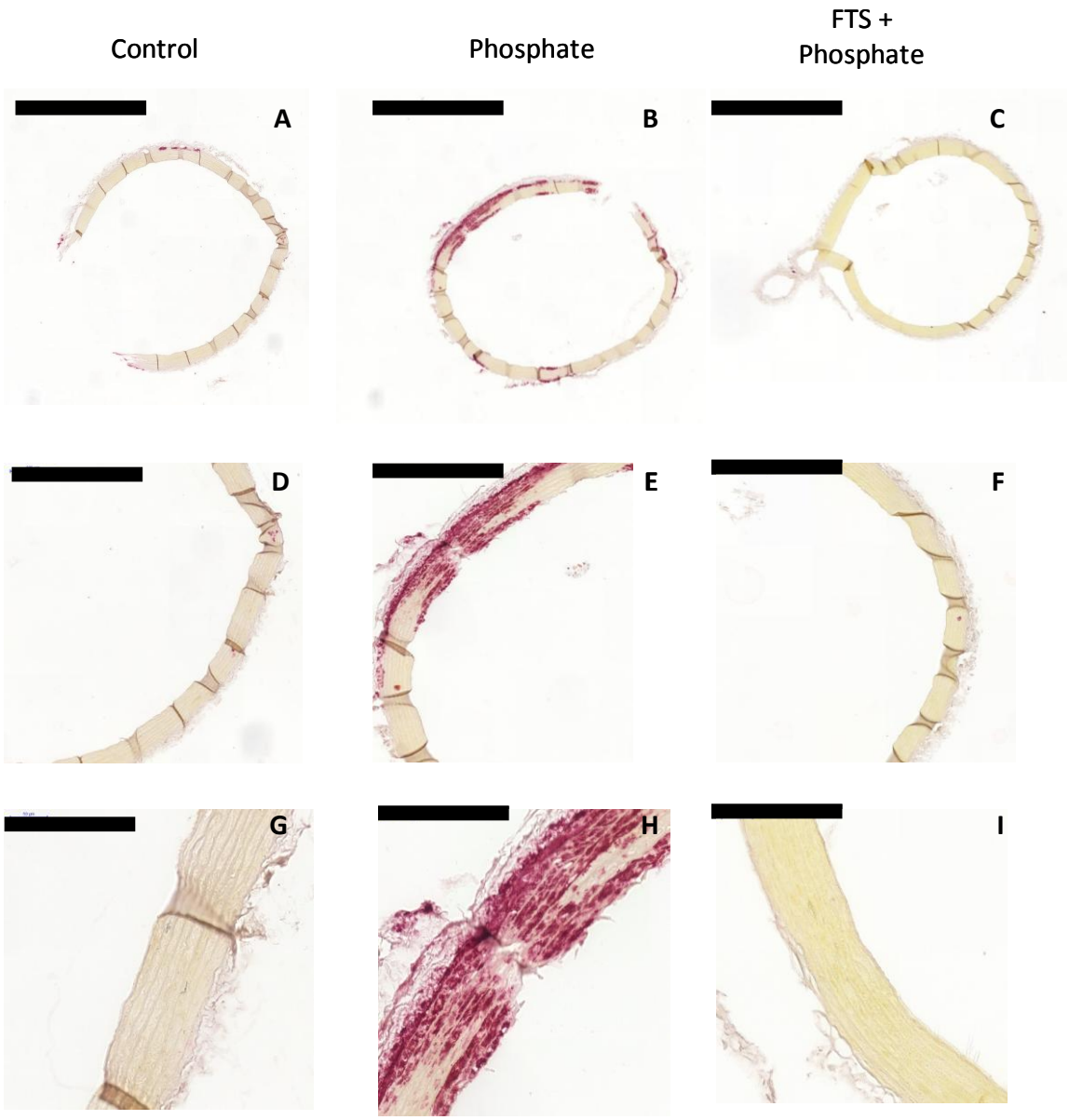

Figure 5.15: FTS inhibits phosphate-induced mineralisation in rat aortic rings from sham operated (late time point) cultured in the absence of serum. Rat aortic rings were incubated in DMEM with DMSO (1:500) (A, D, G) or DMEM + DMSO + elevated phosphate and alkaline phosphatase (B, E, H) or DMEM + elevated phosphate and alkaline phosphatase and FTS (40 μM, C, F, I) for 10 days. Samples were collected, fixed, sectioned and stained with alizarin red. Representative images are shown (n=2 rats). Red indicates mineralisation. Scale bars for images A, B, C = 1000 μm; images D, E, F = 200 μm and images G, H, I = 50 μm.

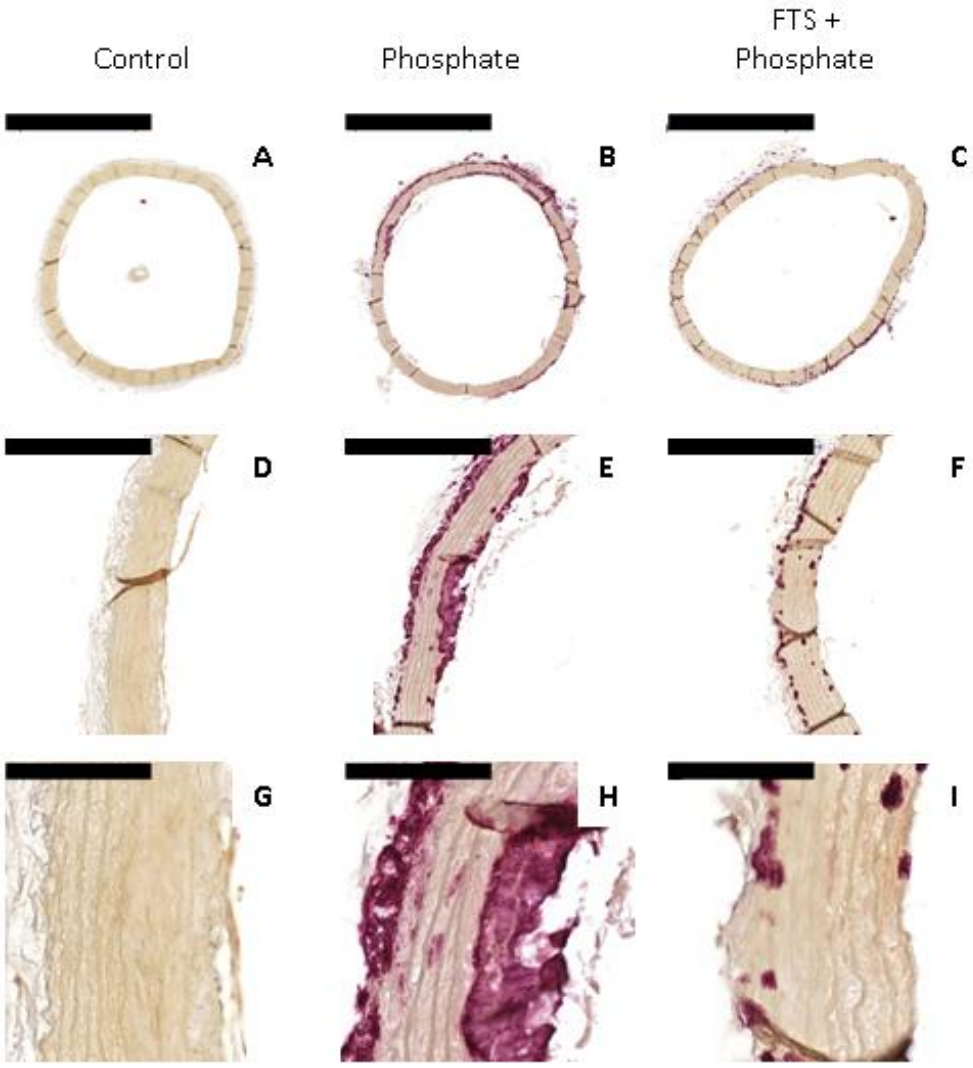

Figure 5.16: FTS inhibits phosphate-induced mineralisation in rat aortic rings from sham operated (late time-point) in 10% serum. Rat aortic rings were incubated in 10% FCS DMEM with DMSO (1:500) (A, D, G) or 10% FCS-DMEM + DMSO + elevated phosphate and alkaline phosphatase (B, E, H) or 10% FCS-DMEM + elevated phosphate and alkaline phosphatase and FTS (40 μM, C, F, I) for 10 days. Samples were collected, fixed, sectioned and stained with alizarin red. Representative images are shown (n=2 rats). Red indicates mineralisation. Scale bars for images A, B, C = 1000 μm; images D, E, F = 200 μm and images G, H, I = 50 μm.

(i)

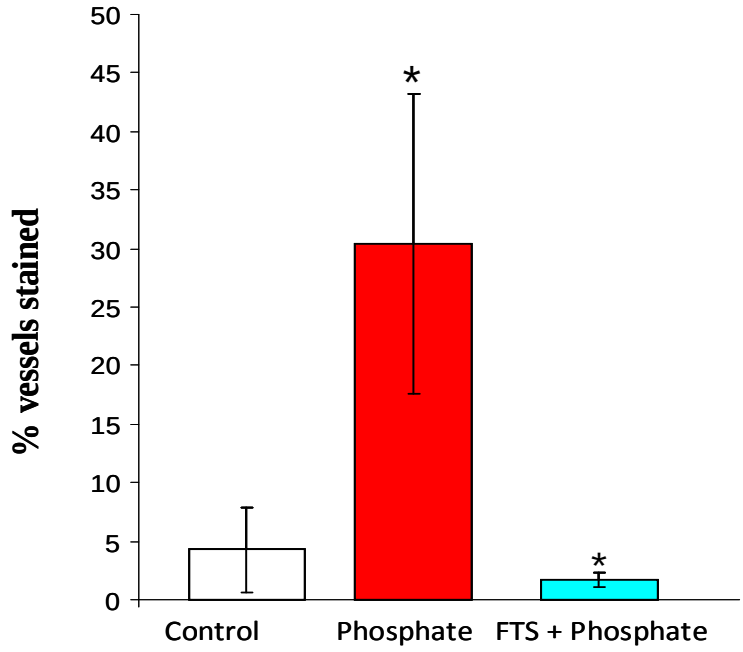

(ii)

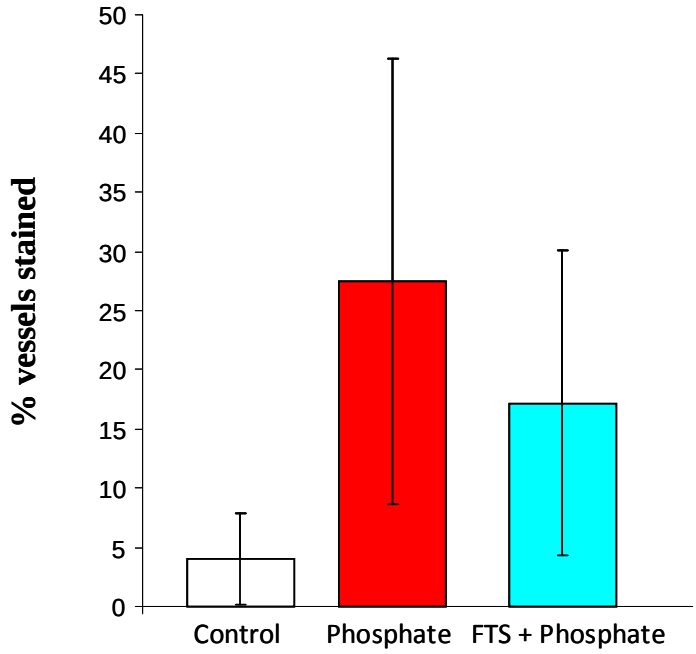

Figure 5.17: FTS appears to inhibit phosphate-induced mineralisation of aortic rings from long term sham operated rats. Samples were prepared as detailed in the legends to Figure 5.15 (i), and Figure 5.16 (ii). Alizarin red staining was quantified as described in section 2.8.5. Results were pooled from 2 different rats and are shown as mean +/- SEM. (*$p<0.05$, FTS-277 vs phosphate, phosphate vs control).

(i)

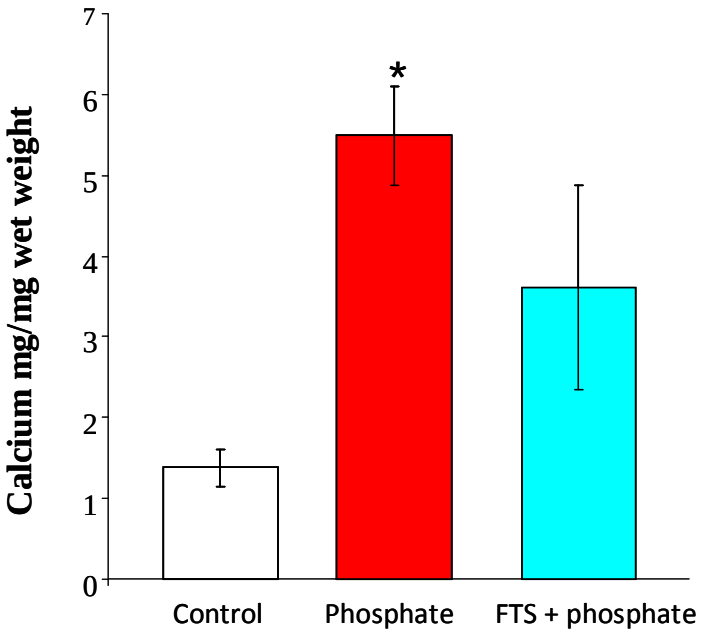

(ii)

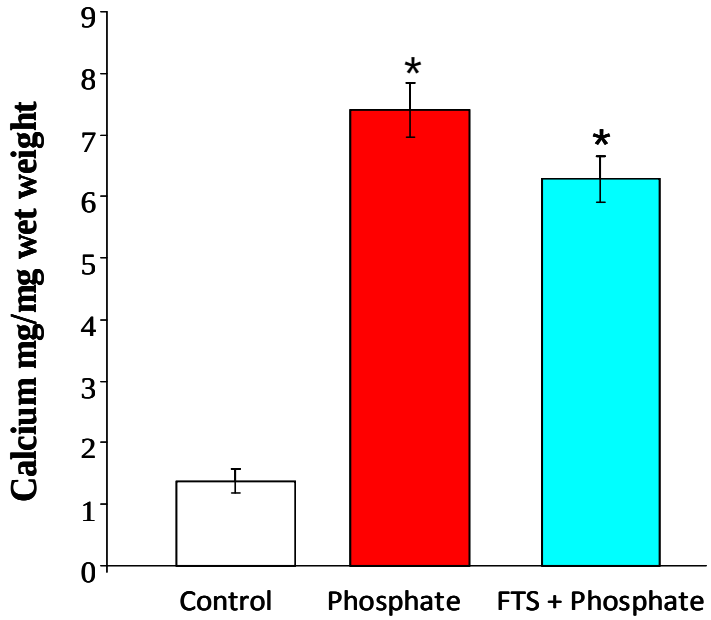

Figure 5.18: Calcium assay on aortic rings from sham-operated control rats. Aortic rings were incubated as detailed in the legends to Figures 5.15 and 5.16 and the calcium content determined using the *O*-cresolphthalein complexone assay. (i) no serum, (ii) 10% serum. Data are from of 2 experiments, n=5 different aortic rings. (*$p<0.05$ FTS or phosphate vs control).

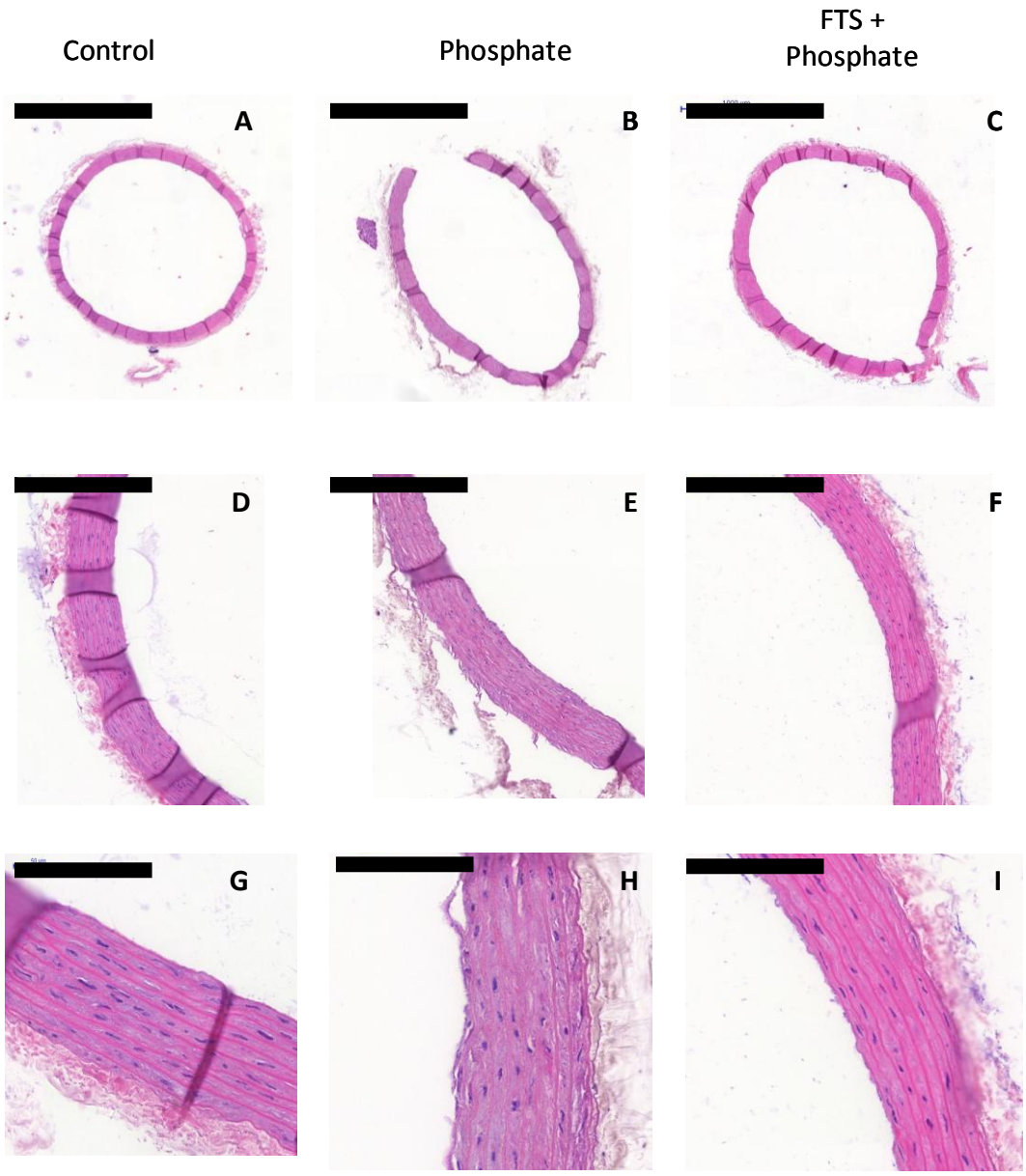

Figure 5.19: H and E stain of sham-operated rat aortic rings (late time point) incubated in the absence of serum. Rat aortic rings were incubated in DMEM with DMSO (1:500) (A, D, G) or DMEM + DMSO + elevated phosphate and alkaline phosphatase (B, E, H) or DMEM + elevated phosphate and alkaline phosphatase and FTS (40 µM, C, F, I) for 10 days. Samples were collected, fixed, sectioned and stained with haematoxylin and eosin. Representative images are shown (n=2). Scale bars for images A, B, C = 1000 µm; images D, E, F = 200 µm and images G, H, I = 50 µm.

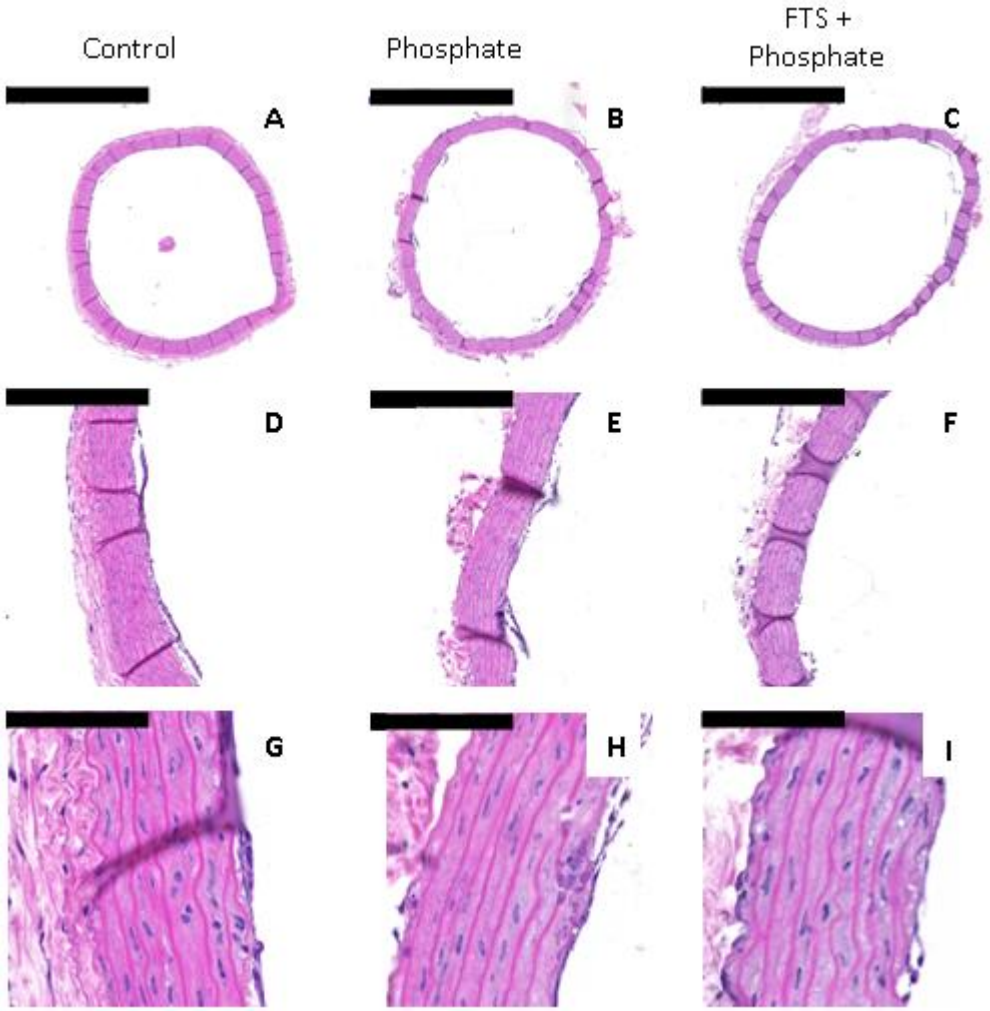

Figure 5.20: H and E stain of sham-operated rat aortic rings (late time point) incubated in the presence of 10% serum. Rat aortic rings were incubated in 10% FCS-DMEM with DMSO (1:500) (A, D, G) or 10% FCS-DMEM + DMSO + elevated phosphate and alkaline phosphatase (B, E, H) or 10% FCS-DMEM + elevated phosphate and alkaline phosphatase and FTS (40 µM, C, F, I) for 10 days. Samples were collected, fixed, sectioned and stained with haematoxylin and eosin. Representative images are shown (n=2). Scale bars for images A, B, C = 1000 µm; images D, E, F = 200 µm and images G, H, I = 50 µm.

(i)

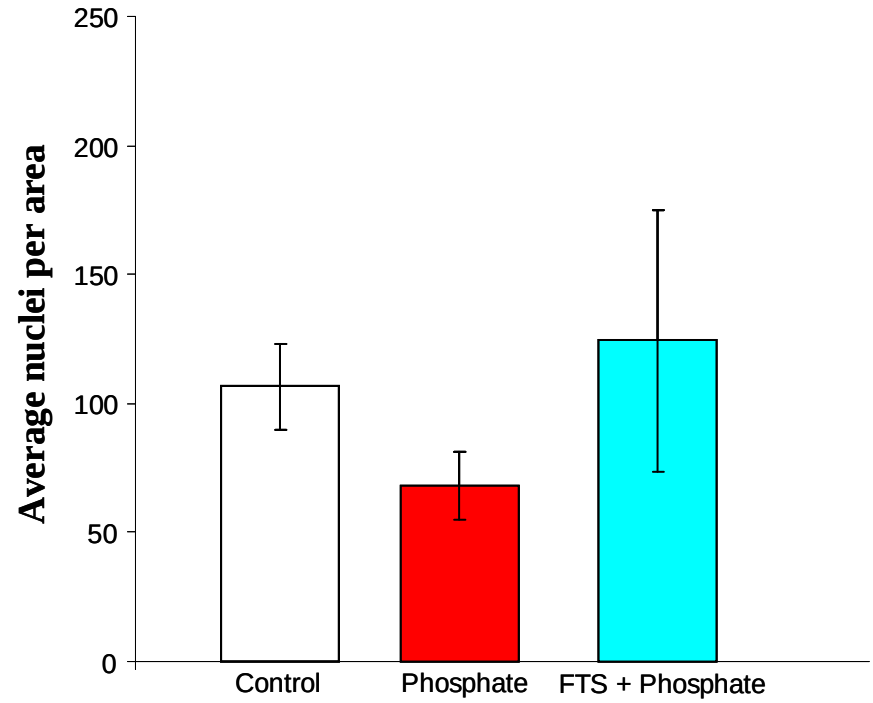

(ii)

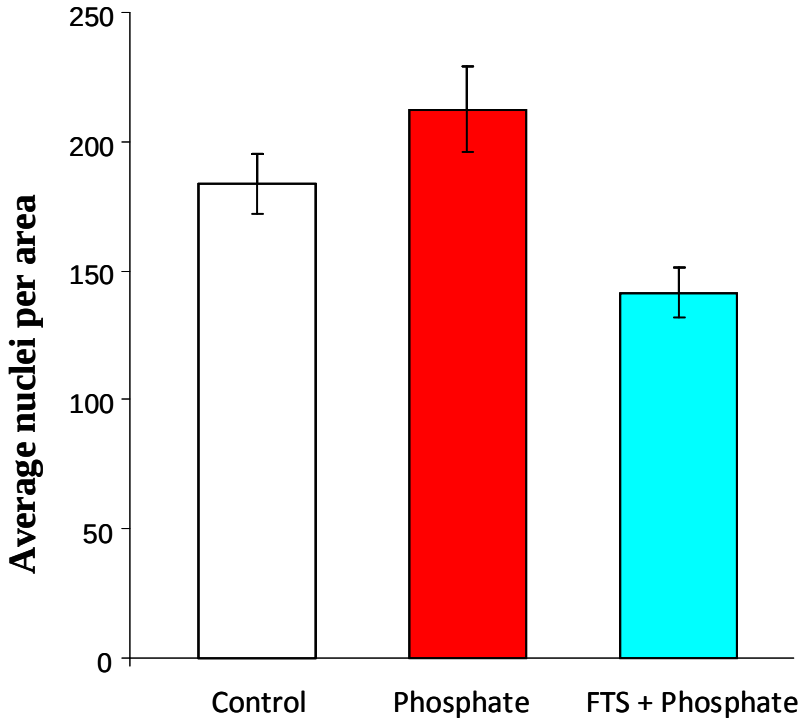

Figure 5.21: No difference was detected in nuclei numbers in the three groups. Nuclei were counted from haematoxylin and eosin-stained rings from sham-operated control rats (see Figures 5.19 and 5.20) within a fixed 800 µm x 800 µm area with an average vessel length of ~1000 µm. Results shown were pooled from 2 different rats, and are expressed as average nuclei per area +/- SEM.

5.3 Discussion

Results in this chapter demonstrated for the first time that FTS at 40 µM inhibited mineral deposition in VSMCs *in vitro*, but at lower concentrations, it appeared to increase mineralisation. Further analysis of Ras activity and downstream signalling pathways showed that 40 µM, but not 10 µM FTS, decreased Ras GTPase activation, increased Akt phosphorylation and inhibited Erk phosphorylation. These studies also indicated that 10 µM FTS induced apoptosis of VSMCs in serum-free conditions, and delayed, but did not inhibit, PDGF-induced VSMC migration in the presence of 0.5% serum. Subsequently, 40 µM FTS was shown to inhibit phosphate-induced mineralisation in aortic rings from rats with end stage renal disease and sham-operated controls. Together these results suggest that FTS can inhibit mineralisation *in vitro* and *ex vivo*, although the mechanism by which this occurs is not clear. Furthermore, the effects of FTS on cell behavior *in vitro* are complex, and appear context-dependent. These results are discussed below.

5.3.1 FTS modulates VSMC mineralisation in a dose-dependent manner

Experimental results showed that 5-10 µM FTS increased phosphate-induced mineralisation. In the presence of 20 µM FTS, mineralisation was more diffuse than in the control cells and at 40 µM, FTS inhibited mineralisation. Together these results demonstrate that FTS modulates VSMC mineralisation in a dose dependent-manner.

Mineralisation is normally detected in high density regions of VSMC cultures, where cells have migrated and proliferated to form multilayered ridges. In the presence of 40 µM FTS, this multilayering was reduced (figure 5.1). Furthermore, at 20 µM FTS, mineralisation was diffuse, suggesting that the ridges were not as tightly formed as in the controls. In these experiments, FTS was added to confluent cultures to minimise any potential effects on proliferation. However, we cannot exclude the possibility that FTS may have inhibited proliferation and/or migration of post-confluent VSMCs at these concentrations. George et al. (2004) have previously shown that FTS inhibited serum-induced proliferation (IC_{50} = 10 µM) and Erk phosphorylation of sub-confluent rat carotid artery VSMCs in a dose-dependent manner *in vitro*. FTS also inhibited Ras activity, Erk phosphorylation and neointima formation in balloon-injured rat carotid arteries *in vivo* (George et al., 2004).

In summary, although 40 µM FTS inhibited mineral deposition by VSMCs, lower doses exhibited an opposite effect and promoted mineralisation. The potential reasons for the effects of different concentrations of FTS on mineralisation were explored further in the next set of experiments.

5.3.2 FTS inhibits Ras activation, promotes Akt phosphorylation, and inhibits Erk phosphorylation in a dose-dependent manner.

FTS is a synthetic molecule with a structure similar to the C-terminal-farnesyl-cysteine motif of Ras that anchors Ras to the membrane (Gana-Weisz et al., 2002)**.** FTS thereby disrupts membrane localisation of active Ras and does not interfere with maturation of Ras GTPase or affect other farnesylated proteins (Marom et al., 1995). Previous studies have shown that the IC_{50} of FTS varies between 7.5 and 85 µM in different cell types cultured under different conditions (as reviewed in Marciano et al., 1995; George et al., 2004; Charette et al., 2010); therefore, the effects of two different concentrations (10 and 40 µM) of FTS on Ras GTPase activity in VSMCs was investigated. These concentrations were chosen as 10 µM FTS increased mineralisation, whereas 40 µM inhibited it.

These experiments showed that 40 µM FTS decreased Ras GTPase activation, whereas 10 µM FTS had no effect. Analysis of the downstream effectors of Ras GTPase, Akt and Erk, demonstrated that Akt phosphorylation was increased with 40 µM FTS, but not 10 µM FTS. Furthermore, 40 µM FTS, but not 10 µM FTS, reduced Erk phosphorylation. These results are consistent with the study by George et al. (2004) who also showed that FTS also reduced Erk phosphorylation in rat VSMCs. The mechanism(s) by which 10 µM FTS promoted mineral deposition by VSMCs in the absence of any effects on Ras activity, Akt or Erk phosphorylation remains to be determined.

The finding that 40 µM FTS decreased Ras activity, promoted Akt phosphorylation and inhibited mineralisation is similar to the results obtained when VSMCs were incubated with FTI-277 (see Chapter 4), and suggests that the inhibition of mineralisation at this concentration of FTS may be linked to increased Akt signalling. In a study using human mesangial cells, it was shown that 10-20 µM FTS inhibited PDGF-induced Akt phosphorylation, but when the cells were stimulated with 10% serum, there was an upward trend in Akt phosphorylation in the presence of FTS, although this result was not

significant (Khwaja et al., 2005). These authors suggested the PI3K/Akt pathway was activated in these cells by other mitogens present in the serum, such as Lysophosphatidic acid (LPA), and that this activation occurred in a Ras-independent manner (Khwaja et al., 2005). In contrast, FTS has been shown to reduce Akt phosphorylation in tumor cells, resulting in caspase activation and apoptosis (Amos et al., 2006). Taken together, these studies show that the effect of FTS of Akt phosphorylation is dependent on the cell line and culture conditions, but they re-enforce the potential involvement of Ras GTPase and Akt in mineralisation.

Speer et al. (2009) previously highlighted the role of increased Erk phosphorylation in the development of calcification. This group showed that inhibition of Erk phosphorylation in VSMCs using the MEK inhibitor U0126 prevented phosphate-induced up-regulation of Runx2 expression and down-regulation of VSMC lineage markers (Speer et al., 2009). Erk phosphorylation has also been implicated in the osteogenic differentiation of C2C12 cells (Gallea et al., 2001). In this study, 40 µM FTS reduced serum-induced Erk phosphorylation suggesting another potential mechanism by which it may inhibit mineralisation. It is also possible that the inhibition of Erk phosphorylation may play a role in the delay in multilayering, proliferation and/or migration of post-confluent VSMCs induced by FTS (see section 5.3.4).

In summary, the studies described in this section suggest two potential mechanisms by which FTS inhibits mineralisation. One is via the increase in Akt phosphorylation and the other is via the reduction in Erk phosphorylation. The increase in Akt signalling and inhibition of Ras GTPase activity demonstrated with FTS is similar to the results obtained using FTI-277, further supporting a role for Ras GTPase in modulating calcification.

5.3.3 Effects of FTS on phosphate-induced apoptosis of HCVSMCs

Activation of PI3K/Akt signalling is important for cell survival, and induction of apoptosis induces vascular calcification (Proudfoot et al., 2000). Thus, the next step in this study was to determine whether FTS inhibited or promoted apoptosis of VSMCs. The studies presented in Figure 5.5 demonstrated that at a concentration of 40 µM, FTS was toxic to HCVSMCs and that 10 µM FTS induced rapid apoptosis of HCVSMCs. As for the studies with FTI-277, these experiments were performed in serum-free conditions. FTS has previously been shown to either induce apoptosis or to have no effect on apoptosis in other studies. For example, FTS (50 – 150 µM) induced dose-dependent apoptosis of

hepatocellular carcinoma cell lines (HepG2 and Hep3B) in the presence of serum as evidenced by an increase in caspase 3/7 activity (Charette et al., 2010). This is in contrast to another study using human mesangial cells where it was shown that FTS did not induce apoptosis of these cells in the presence of serum (Khwaja et al., 2005). Furthermore, in another study using rat VSMCs, pre-incubation of these cells with FTS in the presence of 10% serum for 48 hours, did not increase cell death compared to control cells (Rodriguez-vita et al., 2008). Whether FTS had any effect on VSMC apoptosis in the presence of serum was not determined specifically in this study, although cell loss in the presence of FTS was not noted. Taken together, these studies suggest that the effect of FTS on apoptosis is dependent on cell type and culture conditions. Whether there is any link between FTS, apoptosis and mineralisation is not known.

5.3.4 FTS may delay PDGF-induced VSMC migration

Studies herein showed that 10 µM FTS does not inhibit PDGF-induced VSMC migration in the presence of 0.5% serum. It was noted, however, that wound closure appeared delayed in FTS-treated cells (Figures 5.6 and 5.7), although this finding was not statistically significant, and wounds were closed by 48 hours in the presence and absence of FTS. These results may appear contrary to previous studies which have shown that FTS inhibited the migration of glioblastoma cells and TSC2-null ELT3 cells in the presence of 0.5% serum (Goldberg et al., 2006; Makovski et al., 2012). However, it is possible that examination of VSMCs at an earlier time point may have revealed that FTS did, in fact, significantly delay migration. Furthermore, in the presence of serum, 40 µM (but not 10 µM) FTS was also shown to decrease the multilayering of VSMCs as well as reducing Erk phosphorylation, suggesting that migration of cells was also reduced. The concentration-dependent effects of FTS on VSMCs seen in this study may be due to the reduced availability of 'free' FTS in the presence of 10% serum (Goldberg et al., 2006). As Erk phosphorylation is known to be involved in inducing cell migration (as reviewed by Huang et al 2004), together these results suggest that FTS may delay, but not inhibit, VSMC migration.

5.3.5 FTS inhibits phosphate-induced mineralisation in aortic rings from rats with end stage renal disease and sham-operated controls

Elevated phosphate increased mineralisation of aortic rings from rats with end stage renal disease both in the presence and absence of 10% serum (Figures 5.8 – 5.11). Cell numbers were also reduced in the presence of elevated phosphate (Figure 5.14). These results are consistent with the results presented in chapter 4, and suggest that these cells are susceptible to elevated phosphate. Interestingly, higher levels of calcium were detected in the presence of elevated phosphate in 10% serum than in serum-free conditions (Figure 5.11). Although phosphate also increased mineralisation of aortic rings from sham-operated rats, no difference was detected in the presence and absence of serum (Figure 5.15 - 5.18). The reason for the induction in mineralisation by 10% serum in aortic rings from rats with end stage renal failure is not clear. A possible explanation is that factors (for example TGFβ) present in serum may promote mineralisation, and that cells in these aortas are more susceptible to these factors than in the sham-operated aortas. Another possibility is that the rats used for these experiments were more prone to calcification than the rats used in the serum-free studies, although it is noteworthy that these rats had slightly lower BUN levels (111-148 mg/dl) than the 'serum-free' group (167-209 mg/dl). Patients with CKD also have varying propensity to develop calcification, as evidence with only 50% patients on dialysis having calcification (as reviewed by Eddington et al., 2009)

These studies also show for the first time that FTS inhibits phosphate-induced mineralisation when aortic rings from rats with end stage renal disease were cultured in both serum-free conditions and in the presence of 10% serum, as evidenced using alizarin red staining (Figures 5.8 – 5.11). Similar results were obtained with sham-operated rats (Figures 5.15 – 5.18). These results are consistent with the studies presented in chapter 4 which demonstrated that FTI-277 inhibits Ras activity and prevents mineralisation. Surprisingly, when calcium was quantified using the calcium assay, FTS appeared to have no effect. These results suggest that FTS may interfere with the calcium assay, as has been reported for other compounds (Young et al., 1975). It is important to note that FTS appeared to have no effect on cell number under any of the conditions tested. These results contrast with the *in vitro* studies which demonstrated that in serum-free conditions, this

concentration of FTS was toxic to VSMCs, although this may not be surprising in view of the different model systems used (i.e. cells vs aortic rings).

Interestingly, previous studies have shown that have shown that FTS prevents the progression of atherosclerosis in ApoE -/- mice (George et al., 2002). These authors suggested the reduction in atherosclerosis was brought about by inhibition of Ras resulting in a reduction in *NF*-κB and VCAM-1. Inflammation is also associated with vascular calcification (as reviewed by (New and Aikawa, 2011). The effect of FTS on vascular calcification *in vivo* has not been investigated. However, together these studies suggest that FTS may inhibit vascular calcification associated with elevated phosphate and/or inflammation.

Conclusion

The studies described in this chapter have shown for the first time that FTS can inhibit phosphate-induced mineralisation both *in vivo* and *ex vivo* model systems. FTS also decreased Ras activation, stimulated Akt phosphorylation and inhibited Erk phosphorylation by VSMCs *in vitro*. However, whether the inhibition of mineralisation by Ras is due to activation of Akt phosphorylation and/or inhibition of Erk phosphorylation remains to be determined.

Chapter 6

General Discussion

Vascular calcification, which involves mineral deposition, cartilage and bone formation within the atherosclerotic plaque, vessel medial layer and cardiac valve, is strongly associated with both diabetes and CKD, and has been established as an independent risk factor for the development of CVD (Johnson et al., 2006). Considerable advances have been made in understanding the pathophysiology of vascular calcification, and many different signalling pathways have been identified. It is well known that increased levels of phosphate are associated with an increased incidence of calcification. However, the use of various phosphate binders in patients is not associated with better cardiovascular outcome. The use of non-calcium based phosphate binders results in lower calcium loads but this was not translated into improved mortality and morbidity in patients with CKD as reviewed by Assimon et al., (2010). Thus treatment options remain limited.

The aim of this study was to identify a pathway that regulates multiple processes of vascular calcification in order to develop future therapeutic targets. The mevalonate pathway regulates a number of vascular pathologies via its role in dyslipidaemia and inflammation. This pathway is involved in multiple processes including synthesis of both cholesterol and non-sterol isoprenoids (Buhaescu and Izzedine, 2007). Statins have been shown to reduce cardiovascular death (from major atherosclerotic events) in CKD patients by inhibiting HMG CoA reductase in this mevalonate pathway (Baigent et al., 2011). Non-sterol isoprenoids are vital for the post translational modification of small GTPases, including Ras, through a process called 'prenylation' (Coxon et al., 2004)

The hypothesis of this study was that vascular calcification is regulated by a type of prenylation known as farnesylation. This process is mediated by an enzyme called farnesyl transferase. Therefore, this study investigated the effects of farnesyl transferase inhibitors (FTI-277 and manymycin A), as well as a specific Ras inhibitor (FTS), on vascular calcification *in vitro* using VSMCs, and *ex vivo* using aortic rings from rats with early or end stage renal disease or sham-operated controls. The mechanisms by which FTI-277 and FTS exert their effects on VSMCs were also investigated.

This study demonstrated that farnesylation inhibitor, FTI-277, inhibited mineral deposition by VSMC *in vitro*. Interestingly, the inhibitory effect was still seen even when FTI-277 was added up to 6 days post-induction of mineralisation in the cell culture model. This is an important finding for the future development of novel therapeutics against vascular calcification, as it shows that FTI-277 can still inhibit this process even after it has

been initiated. Furthermore, FTI-277 was shown to promote Akt signalling thus preventing apoptosis of VSMCs. In contrast, manumycin A, another FTI, had no effect on mineral deposition by VSMCs and did not increase Akt signalling. Apoptosis play an important role in the pathogenesis of vascular calcification and inhibition of apoptosis reduces calcification (Proudfoot et al., 2000; Collett et al., 2007). These results suggest that one of the mechanisms that FTI-277 inhibits mineralisation is by promoting of Akt signalling by FTI-277, and this suggestion was confirmed in this study using inhibitors of both PI3K and Akt. In addition, FTI-277 was shown to prevent the phosphate-induced osteogenic differentiation of VSMC and increased MGP expression which is an inhibitor of calcification. As a prelude to pre-clinical trials, FTI-277 was also used in an *ex vivo* model of vascular calcification. These studies demonstrated that FTI-277 inhibited phosphate-induced mineralisation of aortic rings from rats with early and with end stage renal disease, and sham-operated controls. These results are summarised in Figure 6.1.

Therefore, the important findings of chapter 3 and 4 in this study include:

- FTI-277 inhibits Ras GTPase activation and VSMCs mineralisation *in vitro*
- Manumycin A inhibits Ras GTPase activation, but has no effect on mineral deposition by VSMCs and does not induce Akt signalling
- FTI-277 inhibits mineralisation by promoting PI3K/Akt signalling
- FTI-277 inhibits phosphate-induced apoptosis of VSMCs
- FTI-277 inhibits VSMCs migration
- FTI-277 inhibits the expression of osteogenic transcription factors (Runx2, Msx2) by VSMCs and maintains the expression of smooth muscle cell markers by these cells
- FTI-277 promotes the expression of inhibitors (MGP) and suppresses promoters (ALP) of calcification
- FTI-277 inhibits phosphate-induced mineralisation of aortic rings from rats with early and end stage renal disease and sham-operated controls

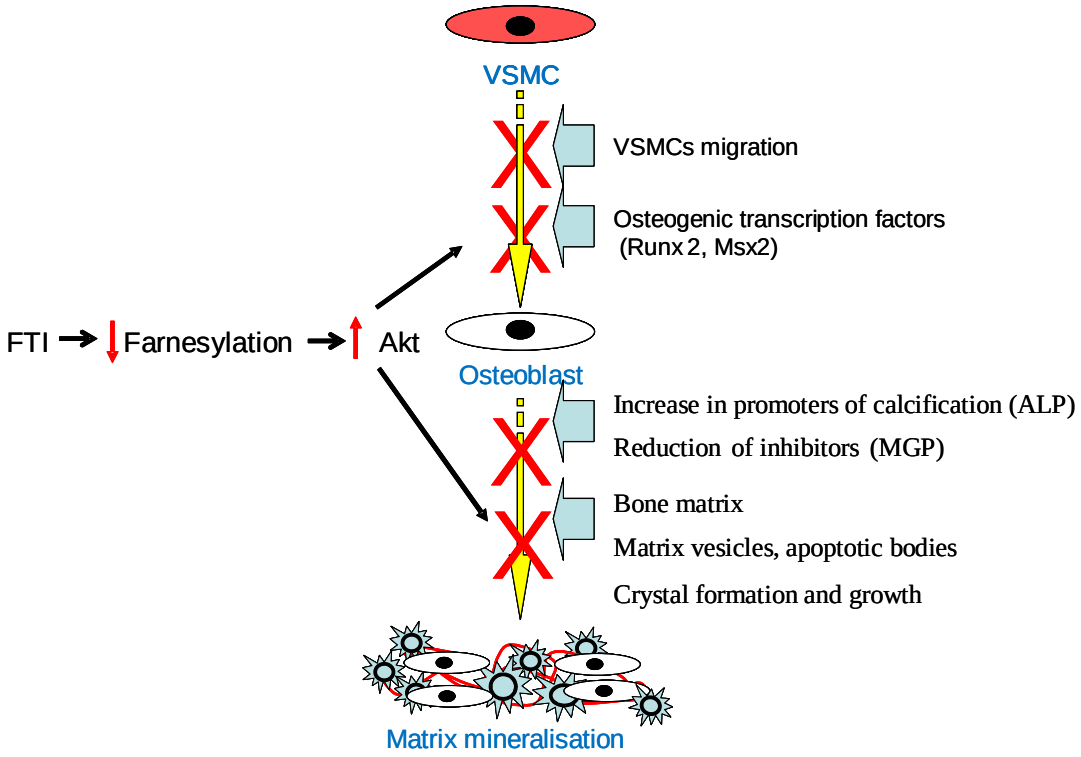

Figure 6.1: FTI-277 inhibits mineralisation by a number of mechanisms. Treatment of VSMCs with FTI-277 leads to inhibition of farnesylation of Ras, or other as yet unidentified proteins, which results in activation of the PI3K/Akt signalling pathway. Increased Akt signalling reduces VSMC apoptosis leading to inhibition of mineralisation. Akt signalling also prevents differentiation of VSMC and increases the expression of MGP. FTI-277 also inhibits VSMC migration.

At the time of the writing of this thesis, a study by Nikolov et al., (2013) was published which demonstrated that treating uraemic ApoE-/- mice with R115777, another type of farnesyl transferase inhibitor, resulted in a reduction of atherosclerotic lesion formation and calcification in these mice. This effect was seen in both the intimal and medial layers of the blood vessels with an inhibitory effect on protein farnesylation. These authors also showed that R115777 decreased collagen I synthesis by VSMCs and suggested that the Ras-Raf pathway was involved in the inhibition of mineralisation (Nikolov et al., 2013), although they did not identify the mechanism by which R115777 regulated calcification. However, their results do support the studies presented in this thesis, and strengthen the suggestion that targeting this pathway may have therapeutic potential against this devastating pathology.

There are a number of key questions that remain unanswered: First, what is the prenylated protein that is being targeted by FTI-277? Is it Ras? If so, how does the inhibition of Ras bring about promotion of Akt signalling? In order to begin to determine whether Ras *per se* is involved in regulating calcification, the effects of FTS, a Ras inhibitor, were investigated.

The key findings of chapter 5 in this study are:

- FTS inhibits mineralisation *in vitro* in a dose-dependent manner
- FTS reduces Ras GTPase activation and promotes Akt phosphorylation; it also inhibits Erk phosphorylation
- FTS inhibits phosphate-induced mineralisation of aortic rings from rats with end stage renal disease and sham-operated controls

In addition to Ras, there are a number of other farnesylated proteins that could be affected by FTIs, including RhoB and prelamin A (see Table 1.4). Interestingly, Hutchinson-Gilford progeria syndrome results from a point mutation in the gene encoding lamin A, which gives rise to a truncated, permanently farnesylated form of prelamin A, called progerin (reviewed by Pollex and Hegele, 2004). Progerin disrupts nuclear structure, leading to premature aging and death in the early teens, usually due to a heart attack or stroke. Inhibiting farnesylation of progerin using the farnesyl transferase inhibitor R115777 reduces the progression of cardiovascular disease in an animal model of

Hutchinson-Gilford progeria syndrome (Capell et al., 2008). Furthermore, the results of the recent clinical trial on children with Hutchinson-Gilford progeria syndrome demonstrated that the farnesyl transferase inhibitor, lonafarnib, decreased arterial pulse wave velocity in these patients suggesting that it improved vascular stiffness (Gordon et al., 2012), which is associated with vascular calcification. It is, therefore, an exciting possibility that another mechanism by FTI-277 may also prevent calcification is by inhibiting the farnesylation of prelamin A in VSMCs.

In conclusion, these studies have demonstrated for the first time that both FTI-277 and FTS inhibit mineral deposition by VSMCs *in vitro* and in rat aortic rings *ex vivo.* Interestingly, both FTI-277 and FTS also inhibited Ras GTPase activation and promoted Akt signalling. These results, therefore, suggest that Ras GTPase plays a role in regulating mineralisation, although it is still unclear how (or whether) inhibition of Ras GTPase leads to an increase in Akt signalling, or whether inhibition of another farnesylated protein is involved. Farnesyl transferase inhibitors and Ras inhibitors have also been shown to reduce atherosclerosis *in vivo* (George et al., 2002, Sugita et al., 2007). Therefore, together these studies suggest a role for prenylation in modulating vascular calcification and regulating atherosclerosis. Farnesyl transferase inhibitors are being investigated in various cancer trials with reasonable success and good safety profile (as reviewed by Sebti and Hamilton, 2000). Therefore, the potential use of farnesyl transferase inhibitors in the treatment of vascular calcification in CKD patients in the future is an exciting possibility.

Future work

- **Confirm that FTI-277 inhibits calcification by regulating Akt phosphorylation**

The studies detailed in this report suggest that one of the mechanisms by which FTI-277 inhibits calcification is by promoting PI3K/Akt signalling and inhibiting apoptosis. This was confirmed by using wortmannin and SH6 and by assessing in the presence of FTI-277. Over-expressing dominant negative-Akt, (dn-Akt) resulted in VSMC death. Further studies should be directed towards knocking-down Akt using siRNA which could then confirm whether FTI-277 and FTS inhibit mineralisation by activating Akt

signalling. It would also be important to determine the effect of FTI-277 and FTS on Akt phosphorylation and apoptosis in the rat aortic rings with early and end stage renal disease.

- **Elucidate the role of Ras GTPase and/or prenylation in regulating vascular calcification**

FTS inhibited mineralisation both *in vitro* and *ex* vivo, suggesting that Ras GTPase may play a role in regulating calcification. However, these effects were very dose-dependent; lower concentrations of FTS had no effect on Ras GTPase activity, but increased mineralisation. Therefore, to confirm the role of Ras in vascular calcification, this GTPase should be knocked-down in VSMCs using siRNA. Alternatively a dominant negative Ras could be over-expressed in VSMCs using lentiviruses. To confirm that farnesylation is important, farnesyl transferase could also be knocked-down using siRNA. The effects of knocking-down Ras or farnesyl transferase on the ostegenic differentiation of VSMCs and mineral deposition by these cells could then be determined.

- **Determine whether FTI-277 and / or FTS inhibits calcification *in vivo***

This study has demonstrated that both FTI-277 and FTS inhibited mineralisation *in vitro* and *ex vivo*. The next step would be to determine the effect of FTI-277 and FTS in an animal model of vascular calcification in uraemic rats (Lopez et al., 2008).

Chapter 7

Appendix

7.1 Rat model of Chronic Kidney Disease

Experiments were performed in accordance with UK Animals (Scientific Procedures) Act 1986 and received local ethical approval.

Male Sprague-Dawley rats (200-250 g Charles River UK Ltd, Kent, UK) were subject to a two-stage subtotal nephrectomy (SNx). In the first phase, under isoflurane anaesthesia (4% in O_2 at 2 litres/min), partial nephrectomy of the left kidney was performed via incision of the left flank. The capsule was removed carefully, to prevent damage to the adrenal gland, and the renal vessels were occluded before the poles of the kidney were removed. The cut faces were sealed with tissue glue (Histoacryl®, Braun) to prevent blood loss. Blood flow was allowed to return to the remnant kidney, which was returned to the abdominal cavity and the wound closed (3-0 Coated VICRYL, Ethicon). Buprenorphine (50 µg/Kg, subcutaneous injection) analgesia and saline fluid replacement (1 ml 0.154 mM NaCl, subcutaneous injection) were administered prior to recovery from anaesthesia. One week later the right kidney was removed completely via a right flank incision, under isoflurane anaesthesia. The right renal vessels were tied off and care was taken to ensure that the right adrenal gland remained intact; analgesia and fluid replacement were administered as before. Sham-operated controls underwent similar procedures, one week apart, in which the kidneys were exteriorised and returned to the abdominal cavity, followed by wound closure with analgesia and fluid replacement administered as above.

Body weight was recorded weekly; systolic blood pressure was measured in conscious rats using a non-invasive tail cuff method (NIBP system model LE5002, Panlab Harvard Apparatus Ltd, Kent, UK) every 2-3 weeks; spot urine samples were collected by housing animals in metabolism cages (typically 2-3 hours) once every two weeks in order to determine the urinary albumin:creatinine ratio. SNx rats were killed, by exsanguination under isoflurane anaesthesia, when they reached either 8-weeks after initial surgery (early stage renal disease) or when they reached end-stage renal disease (CKD stage 5) as judged by progressive increases in systolic blood pressure to >150 mmHg, a urinary albumin:creatinine ratio > 1.0 mg/µmol and finally rapid weight loss (>20% body weight) over 24-48 hours; age matched sham animals were killed at the same time as each SNx rat. A terminal urine sample was collected from the bladder for the determination of urinary

albumin:creatinine ratio; the terminal blood sample was used to determine plasma creatinine and blood urea nitrogen (BUN).

Urinary albumin concentration was determined using an ELISA (Rat Albumin ELISA Quantitation Set E110-125, Bethyl Laboratories, USA); urine and plasma creatinine concentrations were determined using a standard colorimetric assay (Creatinine Urinary Detection Kit K002, Arbor Assays, USA); blood urea nitrogen was determined using a standard colorimetric assay (Urea Nitrogen Test (Enzymatic-Endpoint) cat. no. 2050-450, Stanbio Laboratory, USA), each according to the manufacturer's instructions.

Data are shown as the median and (interquartile range); statistical comparisons were not made as the n numbers are too small.

	Systolic blood pressure (mmHg)	Urine albumin:creatinine ratio (mg/µmol)	Serum creatinine (mg/dl)	Blood urea nitrogen (BUN) (mg/dl)
SNx	160 (145 -169)	0.7 (0.19-1.3)	1.12 (1.14-1.25)	62.5 (53-89)
Sham	142 (139 -150)	0.04 (0.01-0.05)	0.34 (0.26-0.48)	15.2 (12.9-16.9)

Table 7.1: Laboratory findings of early stage renal disease rat and sham operated rat (early).

	Systolic blood pressure (mmHg)	Urine albumin:creatinine ratio (mg/µmol)	Serum creatinine (mg/dl)	Blood urea nitrogen (BUN) (mg/dl)
SNx	163.8 (158.9-164.3)	2.96 (1.55-3.55)	2.98 (1.99-5.20)	174.4 (167.1-209.5)
Sham	130.3 (124.6-136.2)	0.31 (0.06-0.54)	0.86 (0.62-1.00)	24.1 (17.3-34.1)

Table 7.2: Laboratory findings of end stage renal disease rat and sham operated rat (late) used no serum experiments.

	Systolic blood pressure (mmHg)	Urine albumin:creatinine ratio (mg/µmol)	Serum creatinine (mg/dl)	Blood urea nitrogen (BUN) (mg/dl)
SNx	186.4 (184.9-196.8)	8.3 (1.4-17.4)	3.45 (2.4-4.9)	144 (111-148)
Sham	146 (144-148)	0.14 (0.09-0.19)	0.52 (0.4-0.6)	38 (26.8-50.3)

Table 7.2: Laboratory findings of end stage renal disease rat and sham operated rat (late) used 10% serum experiments.

7.2 Materials

Acetic acid glacial (Fisher, UK)
Acetone (Fisher, UK)
Agar (Melford, UK)
Agarose (Lonza, USA)
Amersham HyperfilmTM ECL (GE Healthcare, UK)
AmershamTM ECL Plus Western Blotting Detection System (GE Healthcare, UK)
ammonium acetate (BDH Laboratories, UK)
bovine serum albumine - BSA (Sigma, UK)
bromophenol blue (Sigma, UK)
EDTA-free Protease Inhibitor Cocktail Tablets (Roche, Germany)
D19 film developer (Kodak)
dextran sulphate (Sigma, UK)
Diethylpyrocarbonate DEPC (Sigma, UK)
disodium carbonate (BDH Laboratories, UK)
disodium hydrogen orthophosphate (BDH Laboratories, UK)
dithiothreitol - DTT (ApliChem, Germany)
DMSO (Sigma,UK)
dNTP set (Bioline, UK)
Dulbecco's Modified Eagle's Medium (Sigma, UK)
EDTA (Fisher, UK)
Ethanol (Fisher, UK)
Expand High Fidelity PCR system (Roche, Germany)
ficoll 400 (Sigma, UK)
foetal bovine serum - FBS origin: EU Approved (South American) (Invitrogen, UK)
FuGENE® HD Transfection Reagent (Promega, UK)
glycine (Fisher, UK)
Guanidinium-HCl (Fluka, UK)
Ham's F12 medium (Sigma, UK)

HCl (Fisher, UK)
hematoxyline
HEPES (Fisher, UK)
HyperLadderTM I (Bioline, UK)
HyperLadderTM IV (Bioline, UK)
imidazole (Sigma, UK)
iodoacetamide (Sigma, UK)
K5 nuclear emulsion (Ilford, UK)
L-ascorbic acid 2-phosphate (Wako, Japan)
L-glutamine (Sigma, UK)
Methanol (Fisher, UK)
MOPS (BDH Laboratories, UK)
N-etylmaleimide (Sigma, UK)
NuPAGE® MOPS SDS Running Buffer (Invitrogen, UK)
NuPAGE® Novex 10% Bis-Tris Gel (Invitrogen, UK)
paraformaldehyde - PFA (Sigma, UK)
PBS (Sigma-Aldrich, UK)
penicillin/streptomycin (100x) (Sigma, UK)
PerfectPro Ni-NTA Agarose (5Prime, Germany)
Phenol-Chloroform-Isoamyl alcohol (Sigma, UK)
Polyvinylpyrrolidone - PVP (Sigma, UK)
potassium chloride (BDH Laboratories, UK)
potassium dihydrogen ortophosphate (BDH Laboratories, UK)
proteinase K (Roche, Germany)
Puromycin (InvivoGen, USA)
PVDF transfer membrane Amersham HybondTM - P (GE Healthcare, UK)
QIAGEN Plasmid Maxi Kit (Qiagen, Germany)
QIAprep Spin Miniprep Kit (Qiagen, Germany)
QIAquick Gel Extraction Kit (Qiagen, Germany)
Riboprobe® System (Promega, UK)
Rnase (Roche, Germany)
RNeasy Mini Kit (Qiagen Ltd., UK)
sodium acetate (BDH Laboratories, UK)
sodium chloride (Fluka, UK)
sodium citrate (Sigma, UK)
Sodium deoxycholate -DOC (Sigma, UK)
sodium dihydrogen ortophosphate (BDH Laboratories, UK)
sodium dodecyl sulphate - SDS (Fisher, UK)
sodium hydrogen carbonate (BDH Laboratories, UK)
Strep-Tactin Sepharose (IBA, Germany)
SYBR® green PCR mastermix (Applied Biosystems, UK)
Taq polymerase (Bioline, UK)
Trichloroacetic acid - TCA (BDH Laboratories, UK)
Tris Base (Fisher, UK)

Trypsine-EDTA (Sigma-Aldrich, UK)
Tween 20 (Sigma, UK)
xylene (Genta Enviremental, UK)
β-glycerophosphate (Sigma, UK)
β-mercaptoethanol (Sigma, UK)

7.3 Buffers

Phosphate Buffered Saline (PBS) (Fisher Bioreagents) 1X
11.9 mM Phosphates (Sodium phosphate dibasic and Potassium phosphate monobasic)
137 mM Sodium chloride
27 mM Potassium chloride

Phosphate Buffered Saline Tween (PBST)
PBS 1X
0.05% (v/v) Tween

Lamelli's Sample Buffer 5X
250 mM Tris, pH 6.8
10% (w/v) SDS
50% (v/v) Glycerol
0.05% (w/v) Bromophenol blue
5% (v/v) β–Mercaptoethanol added to 1X sample buffer solution

2X SDS Sample Buffer (Pierce, Pull down assay)
125 mM Tris, pH 6.8
2% (v/v) Glycerol
4% (w/v) SDS
0.05% (w/v) Bromophenol blue

Saturated Butanol Solution
40.8 mM Tris, pH 8.8
83% (v/v) Butanol

Resolving Buffer
1.4 M Tris, pH 8.8
0.1% (w/v) SDS

Stacking Buffer
0.9 M Tris, pH 6.8
0.1% (w/v) SDS

Tris/Glycine/SDS Buffer 1X (BioRad)
25 mM Tris, pH 8.3
192 mM Glycine
0.1% (w/v) SDS

Tris Buffered Saline
25 mM Tris, pH 7.5
150 mM Sodium chloride

Semi Dry Transfer (SDT) Buffer
39 mM Glycine
48 mM Tris, pH 8.3
20% (v/v) Methanol
0.037% (w/v) SDS

Blocking Buffers
5% (w/v) Marvel in PBST (for Akt, phospho Akt)
1% (w/v) BSA in 0.2% Tween in PBS (for Erk, phospho Erk)
3% (w/v) BSA in TBST (for Ras)
2% (v/v) Fish Gelatin in TBST (for Caspase/Active Caspase 3)

Lysis Buffer
20 mM Tris, pH 7.6
150 mM Sodium chloride
1 mM EDTA
1% (v/v) Igepal
50 mM Sodium flouride
Calbiochem protease inhibitor cocktail (1x)
1 mM Sodium orthovanadate
1 mM Sodium pyrophosphate

Lysis Buffer (Pierce, Pull down assay)
25 mM Tris, pH 7.5
150 mM Sodium chloride
5 mM Magnesium chloride
1% (w/v) NP-40
5% (v/v) Glycerol

Alizarin Red Dye
40 mM Alizarin red, pH 4.1

GST-Raf1-RBD
50 mM Tris, pH 7.2
150 mM Sodium chloride

0.5% (v/v) Triton® X-100
5 mM Magnesium chloride
1 mM DTT
10% (v/v) Glycerol

Stock FTI 277
10 mM FTI-277 in DMSO

Stock Manumcyin A
50 mM Manumycin A in DMSO

Stock wortmannin
10 mM wortmannin in DMSO

Stock Farnesyl Thiosalicylic Acid (FTS)
10 mM FTS in DMSO

Tris-acetate EDTA (TAE) buffer
40 mM Tris
20 mM acetic acid
1 mM EDTA

Luria Bertani (LB) broth
10 gm/l sodium chloride
10 gm/l Tryptone
5 gm yeast extract

LB agar
LB broth
1.5% (w/v) agar

Soc buffer
5 gm (w/v) Bacto Tryptone
2 gm (w/v) Bacto Yeast Extract
0.1 M NaCl
0.1 M KCl.
10 mM $MgCl_2$
10 mM $MgSO_4$
20 mM glucose

AMP buffer (ph 10.7)

2, amino, 2 methyl, 1 propanolol (AMP) (Sigma)

Chapter 8

References

Al-Aly, Z., Shao, J.S., Lai, C.F., Huang, E., Cai, J., Behrmann, A., Cheng, S.L., and Towler, D.A. (2007). Aortic Msx2-Wnt calcification cascade is regulated by TNF-alpha-dependent signals in diabetic Ldlr-/- mice. Arteriosclerosis, thrombosis, and vascular biology *27*, 2589-2596.

Alam MU, Kirton JP, Wilkinson FL, Towers E, Sinha S, Rouhi M, Vizard TN, Sage AP, Martin D, Ward DT, Alexander MY, Riccardi D, Canfield AE. (2009) Calcification is associated with loss of functional calcium-sensing receptor in vascular smooth muscle cells. Cardiovasc Res;81(2):260-8

Alvarado, Y., and Giles, F.J. (2007). Ras as a therapeutic target in hematologic malignancies. Expert Opin Emerg Drugs *12*, 271-284.

Assimon MM, Mousa S, Shaker O, Pai AB. (2010) The effect of sevelamer hydrochloride and calcium-based phosphate binders on mortality in hemodialysis patients: a need for more research.Consult Pharm.;25(1):41-54.

Amos S, Redpath GT, Polar G, McPheson R, Schiff D, Hussaini IM (2006) Farnesylthiosalicylic acid induces caspase activation and apoptosis in glioblastoma cells. Cell Death Differ13(4):642-51.

Baigent C, Landray MJ, Reith C, Emberson J, Wheeler DC, Tomson C, Wanner C, Krane V, Cass A, Craig J, Neal B, Jiang L, Hooi LS, Levin A, Agodoa L, Gaziano M, Kasiske B, Walker R, Massy ZA, Feldt-Rasmussen B, Krairittichai U, Ophascharoensuk V, Fellström B, Holdaas H, Tesar V, Wiecek A, Grobbee D, de Zeeuw D, Grönhagen-Riska C, Dasgupta T, Lewis D, Herrington W, Mafham M, Majoni W, Wallendszus K, Grimm R, Pedersen T, Tobert J, Armitage J, Baxter A, Bray C, Chen Y, Chen Z, Hill M, Knott C, Parish S, Simpson D, Sleight P, Young A, Collins R; SHARP Investigators. (2011) The effects of lowering LDL cholesterol with simvastatin plus ezetimibe in patients with chronic kidney disease (Study of Heart and Renal Protection): a randomised placebo-controlled trial. Lancet. 377(9784):2181-92.

Barreto, D.V., Barreto, F.C., Liabeuf, S., Temmar, M., Boitte, F., Choukroun, G., Fournier, A., and Massy, Z.A. (2009). Vitamin D affects survival independently of vascular calcification in chronic kidney disease. Clin J Am Soc Nephrol *4*, 1128-1135.

Basalyga, D.M., Simionescu, D.T., Xiong, W., Baxter, B.T., Starcher, B.C., and Vyavahare, N.R. (2004). Elastin degradation and calcification in an abdominal aorta injury model: role of matrix metalloproteinases. Circulation *110*, 3480-3487.

Basso, A.D., Kirschmeier, P., and Bishop, W.R. (2006). Lipid posttranslational modifications. Farnesyl transferase inhibitors. J Lipid Res *47*, 15-31.

Bolick, S.C., Landowski, T.H., Boulware, D., Oshiro, M.M., Ohkanda, J., Hamilton, A.D., Sebti, S.M., and Dalton, W.S. (2003). The farnesyl transferase inhibitor, FTI-277, inhibits growth and induces apoptosis in drug-resistant myeloma tumor cells. Leukemia *17*, 451-457.

Bonser, R.W., Thompson, N.T., Randall, R.W., Tateson, J.E., Spacey, G.D., Hodson, H.F., and Garland, L.G. (1991). Demethoxyviridin and wortmannin block phospholipase C and D activation in the human neutrophil. Br J Pharmacol *103*, 1237-1241.

Boota, A., Johnson, B., Lee, K.L., Blaskovich, M.A., Liu, S.X., Kagan, V.E., Hamilton, A., Pitt, B., Sebti, S.M., and Davies, P. (2000). Prenyltransferase inhibitors block superoxide production by pulmonary vascular smooth muscle. Am J Physiol Lung Cell Mol Physiol *278*, L329-334.

Boriack-Sjodin, P.A., Margarit, S.M., Bar-Sagi, D., and Kuriyan, J. (1998). The structural basis of the activation of Ras by Sos. Nature *394*, 337-343.

Bostrom, K., Watson, K.E., Horn, S., Wortham, C., Herman, I.M., and Demer, L.L. (1993). Bone morphogenetic protein expression in human atherosclerotic lesions. The Journal of clinical investigation *91*, 1800-1809.

Brunet, A., Bonni, A., Zigmond, M.J., Lin, M.Z., Juo, P., Hu, L.S., Anderson, M.J., Arden, K.C., Blenis, J., and Greenberg, M.E. (1999). Akt promotes cell survival by phosphorylating and inhibiting a Forkhead transcription factor. Cell *96*, 857-868.

Bucay, N., Sarosi, I., Dunstan, C.R., Morony, S., Tarpley, J., Capparelli, C., Scully, S., Tan, H.L., Xu, W., Lacey, D.L., *et al.* (1998). osteoprotegerin-deficient mice develop early onset osteoporosis and arterial calcification. Genes & development *12*, 1260-1268.

Buhaescu, I., and Izzedine, H. (2007). Mevalonate pathway: a review of clinical and therapeutical implications. Clin Biochem *40*, 575-584.

Byon CH, Javed A, Dai Q, Kappes JC, Clemens TL, Darley-Usmar VM, McDonald JM, Chen Y (2008).Oxidative stress induces vascular calcification through modulation of the osteogenic transcription factor Runx2 by AKT signaling. J Biol Chem. 283(22):15319-27

Cabane C, Coldefy AS, Yeow K, Dérijard B. Cell Signal. (2004) The p38 pathway regulates Akt both at the protein and transcriptional activation levels during myogenesis;16(12):1405-15.

Canfield, A.E., Doherty, M.J., Wood, A.C., Farrington, C., Ashton, B., Begum, N., Harvey, B., Poole, A., Grant, M.E., and Boot-Handford, R.P. (2000). Role of pericytes in vascular calcification: a review. Zeitschrift fur Kardiologie 89 Suppl 2, 20-27.

Capell, B.C., Olive, M., Erdos, M.R., Cao, K., Faddah, D.A., Tavarez, U.L., Conneely, K.N., Qu, X., San, H., Ganesh, S.K., et al. (2008). A farnesyltransferase inhibitor prevents both the onset and late progression of cardiovascular disease in a progeria mouse model. Proc Natl Acad Sci U S A 105, 15902-15907.

Casey, P.J., Thissen, J.A., and Moomaw, J.F. (1991). Enzymatic modification of proteins with a geranylgeranyl isoprenoid. Proc Natl Acad Sci U S A 88, 8631-8635.

Castillo SS, Brognard J, Petukhov PA, Zhang C, Tsurutani J, Granville CA, Li M, Jung M, West KA, Gills JG, Kozikowski AP, Dennis PA: (2004) Preferential inhibition of Akt and killing of Akt-dependent cancer cells by rationallydesigned phosphatidylinositol ether lipid analogues. Cancer Res,64:2782-2792.

Charette N, De Saeger C, Lannoy V, Horsmans Y, Leclercq I, Stärkel P.(2010) Salirasib inhibits the growth of hepatocarcinoma cell lines in vitro and tumor growth in vivo through ras and mTOR inhibition. Mol Cancer.;9:256. doi: 10.1186/1476-4598-9-256.

Ciceri P, Volpi E, Brenna I, Arnaboldi L, Neri L, Brancaccio D, Cozzolino M.(2012). Combined effects of ascorbic acid and phosphate on rat VSMC osteoblastic differentiation. Nephrol Dial Transplant.;27(1):122-7.

Clarke, H.C., Kocher, H.M., Khwaja, A., Kloog, Y., Cook, H.T., and Hendry, B.M. (2003). Ras antagonist farnesylthiosalicylic acid (FTS) reduces glomerular cellular proliferation and macrophage number in rat thy-1 nephritis. J Am Soc Nephrol *14*, 848-854.

Clarke, M.C., Littlewood, T.D., Figg, N., Maguire, J.J., Davenport, A.P., Goddard, M., and Bennett, M.R. (2008). Chronic apoptosis of vascular smooth muscle cells accelerates atherosclerosis and promotes calcification and medial degeneration. Circ Res *102*, 1529-1538.

Clarke, S. (1992). Protein isoprenylation and methylation at carboxyl-terminal cysteine residues. Annu Rev Biochem *61*, 355-386.

Collett, G.D., Sage, A.P., Kirton, J.P., Alexander, M.Y., Gilmore, A.P., and Canfield, A.E. (2007). Axl/phosphatidylinositol 3-kinase signaling inhibits mineral deposition by vascular smooth muscle cells. Circ Res *100*, 502-509.

Collett GD, Canfield AE. (2005). Angiogenesis and pericytes in the initiation of ectopic calcification.Circ Res.; 96(9):930-8

Covic, A., Kanbay, M., Voroneanu, L., Turgut, F., Serban, D.N., Serban, I.L., and Goldsmith, D.J. (2010) Vascular calcification in chronic kidney disease. Clin Sci (Lond) *119*, 111-121.

Cox, A.D., and Der, C.J. (1997). Farnesyltransferase inhibitors and cancer treatment: targeting simply Ras? Biochim Biophys Acta *1333*, F51-71.

Cox, A.D., and Der, C.J. (2003). The dark side of Ras: regulation of apoptosis. Oncogene *22*, 8999-9006.

Coxon, J.P., Oades, G.M., Kirby, R.S., and Colston, K.W. (2004). Zoledronic acid induces apoptosis and inhibits adhesion to mineralized matrix in prostate cancer cells via inhibition of protein prenylation. BJU Int *94*, 164-170.

Cross, D.A., Alessi, D.R., Cohen, P., Andjelkovich, M., and Hemmings, B.A. (1995a). Inhibition of glycogen synthase kinase-3 by insulin mediated by protein kinase B. Nature *378*, 785-789.

Cross, M.J., Stewart, A., Hodgkin, M.N., Kerr, D.J., and Wakelam, M.J. (1995b). Wortmannin and its structural analogue demethoxyviridin inhibit stimulated phospholipase A2 activity in Swiss 3T3 cells. Wortmannin is not a specific inhibitor of phosphatidylinositol 3-kinase. J Biol Chem *270*, 25352-25355.

Crul, M., de Klerk, G.J., Beijnen, J.H., and Schellens, J.H. (2001). Ras biochemistry and farnesyl transferase inhibitors: a literature survey. Anticancer Drugs *12*, 163-184.

Datta, S.R., Brunet, A., and Greenberg, M.E. (1999). Cellular survival: a play in three Akts. Genes Dev *13*, 2905-2927.

Davies, M.R., Lund, R.J., and Hruska, K.A. (2003). BMP-7 is an efficacious treatment of vascular calcification in a murine model of atherosclerosis and chronic renal failure. J Am Soc Nephrol *14*, 1559-1567.

Demer, L.L., and Tintut, Y. (2008). Vascular calcification: pathobiology of a multifaceted disease. Circulation *117*, 2938-2948.

Di Paolo, A., Danesi, R., Nardini, D., Bocci, G., Innocenti, F., Fogli, S., Barachini, S., Marchetti, A., Bevilacqua, G., and Del Tacca, M. (2000). Manumycin inhibits ras signal transduction pathway and induces apoptosis in COLO320-DM human colon tumour cells. British journal of cancer *82*, 905-912.

Diehl, J.A., Cheng, M., Roussel, M.F., and Sherr, C.J. (1998). Glycogen synthase kinase-3beta regulates cyclin D1 proteolysis and subcellular localization. Genes Dev *12*, 3499-3511.

Dietze EC, Troch MM, Bean GR, Heffner JB, Bowie ML, Rosenberg P, Ratliff B, Seewaldt VL. (2004) Tamoxifen and tamoxifen ethyl bromide induce apoptosis in acutely damaged mammary epithelial cells through modulation of AKT activity Oncogene.6;23(21):3851-62

Di Luozzo G, Pradhan S, Dhadwal AK, Chen A, Ueno H, Sumpio BE. (2005) Nicotine induces mitogen-activated protein kinase dependent vascular smooth muscle cell migration. Atherosclerosis.;178(2):271-277.

Doisneau-Sixou, S.F., Cestac, P., Faye, J.C., Favre, G., and Sutherland, R.L. (2003). Additive effects of tamoxifen and the farnesyl transferase inhibitor FTI-277 on inhibition of MCF-7 breast cancer cell-cycle progression. International journal of cancer *106*, 789-798.

Ducy P, Zhang R, Geoffroy V, Ridall AL, Karsenty G (1997) Osf2/Cbfa1: a transcriptional activator of osteoblast differentiation. Cell;89 (5):747-54.

Duan XY, Xie PL, Ma YL, Tang SY. (2011). Omentin inhibits osteoblastic differentiation of calcifying vascular smooth muscle cells through the PI3K/Akt pathway.Amino Acids.;41(5):1223-31

Duque, G., Vidal, C., and Rivas, D. (2011). Protein isoprenylation regulates osteogenic differentiation of mesenchymal stem cells: effect of alendronate, and farnesyl and geranylgeranyl transferase inhibitors. Br J Pharmacol *162*, 1109-1118.

Eddington H., Sinha S, Kalra P.A. (2009). Vascular calcification in chronic kidney disease: A clinical review. Journal of RenalCare35(s1), 45–50

El-Abbadi, M.M., Pai, A.S., Leaf, E.M., Yang, H.Y., Bartley, B.A., Quan, K.K., Ingalls, C.M., Liao, H.W., and Giachelli, C.M. (2009). Phosphate feeding induces arterial medial calcification in uremic mice: role of serum phosphorus, fibroblast growth factor-23, and osteopontin. Kidney Int *75*, 1297-1307.

Ellis, C.A., Vos, M.D., Wickline, M., Riley, C., Vallecorsa, T., Telford, W.G., Zujewskil, J., and Clark, G.J. (2003). Tamoxifen and the farnesyl transferase inhibitor FTI-277 synergize to inhibit growth in estrogen receptor-positive breast tumor cell lines. Breast Cancer Res Treat *78*, 59-67.

End, D.W., Smets, G., Todd, A.V., Applegate, T.L., Fuery, C.J., Angibaud, P., Venet, M., Sanz, G., Poignet, H., Skrzat, S., *et al.* (2001). Characterization of the antitumor effects of the selective farnesyl protein transferase inhibitor R115777 in vivo and in vitro. Cancer Res *61*, 131-137.

Eriksson, M., Brown, W.T., Gordon, L.B., Glynn, M.W., Singer, J., Scott, L., Erdos, M.R., Robbins, C.M., Moses, T.Y., Berglund, P., *et al.* (2003). Recurrent de novo point mutations in lamin A cause Hutchinson-Gilford progeria syndrome. Nature *423*, 293-298.

Erlich, S., Tal-Or, P., Liebling, R., Blum, R., Karunagaran, D., Kloog, Y., and Pinkas-Kramarski, R. (2006). Ras inhibition results in growth arrest and death of androgen-dependent and androgen-independent prostate cancer cells. Biochemical pharmacology *72*, 427-436.

Everhart, J.E., Pettitt, D.J., Knowler, W.C., Rose, F.A., and Bennett, P.H. (1988). Medial arterial calcification and its association with mortality and complications of diabetes. Diabetologia *31*, 16-23.

Krech T, Thiede M, Hilgenberg E, Schäfer R, Jürchott K (2010) Characterization of AKT independent effects of the synthetic AKT inhibitors SH-5 and SH-6 using an integrated approach combining transcriptomic profiling and signaling pathway perturbations,BMC Cancer;10:287

Fang Y, Ginsberg C, Sugatani T, Monier-Faugere MC, Malluche H, Hruska KA.(2013). Early chronic kidney disease-mineral bone disorder stimulates vascular calcification Kidney Int. [Epub]

Feig, L.A., and Buchsbaum, R.J. (2002). Cell signaling: life or death decisions of ras proteins. Curr Biol *12*, R259-261.

Foley, R.N., Parfrey, P.S., and Sarnak, M.J. (1998). Clinical epidemiology of cardiovascular disease in chronic renal disease. Am J Kidney Dis *32*, S112-119.

Franceschi, R.T., and Xiao, G. (2003). Regulation of the osteoblast-specific transcription factor, Runx2: responsiveness to multiple signal transduction pathways. Journal of cellular biochemistry *88*, 446-454.

Fruman, D.A., Meyers, R.E., and Cantley, L.C. (1998). Phosphoinositide kinases. Annu Rev Biochem *67*, 481-507.

Fry, M.J. (1994). Structure, regulation and function of phosphoinositide 3-kinases. Biochim Biophys Acta *1226*, 237-268.

Fry, M.J. (2001). Phosphoinositide 3-kinase signalling in breast cancer: how big a role might it play Breast Cancer Res *3*, 304-312.

Galaria, II, Nicholl, S.M., Roztocil, E., and Davies, M.G. (2005). Urokinase-induced smooth muscle cell migration requires PI3-K and Akt activation. The Journal of surgical research *127*, 46-52.

Galvin, K.M., Donovan, M.J., Lynch, C.A., Meyer, R.I., Paul, R.J., Lorenz, J.N., Fairchild-Huntress, V., Dixon, K.L., Dunmore, J.H., Gimbrone, M.A., Jr., *et al.* (2000). A role for smad6 in development and homeostasis of the cardiovascular system. Nature genetics *24*, 171-174

Gallea S, Lallemand F, Atfi A, Rawadi G, Ramez V, Spinella-Jaegle S, Kawai S, Faucheu C, Huet L, Baron R, Roman-Roman S. (2001) Activation of mitogen-activated protein kinase cascades is involved in regulation of bone morphogenetic protein-2-induced osteoblast differentiation in pluripotent C2C12 cells 28(5):491-8

Gana-Weisz, M., Halaschek-Wiener, J., Jansen, B., Elad, G., Haklai, R., and Kloog, Y. (2002). The Ras inhibitor S-trans,trans-farnesylthiosalicylic acid chemosensitizes human tumor cells without causing resistance. Clin Cancer Res *8*, 555-565.

George, J., Afek, A., Keren, P., Herz, I., Goldberg, I., Haklai, R., Kloog, Y., and Keren, G. (2002). Functional inhibition of Ras by S-trans,trans-farnesyl thiosalicylic acid attenuates atherosclerosis in apolipoprotein E knockout mice. Circulation *105*, 2416-2422

George J, Sack J, Barshack I, Keren P, Goldberg I, Haklai R, Elad-Sfadia G, Kloog Y, Keren G. (2004) Inhibition of intimal thickening in the rat carotid artery injury model by a nontoxic Ras inhibitor. Arterioscler Thromb Vasc Biol.24(2):363-8.

Giachelli, C.M. (2009). The emerging role of phosphate in vascular calcification. Kidney international *75*, 890-897.

Gills JJ, Castillo SS, Zhang C, Petukhov PA, Memmott RM, Hollingshead M, Warfel N, Han J, Kozikowski AP, Dennis PA: (2007) Phosphatidylinositol ether lipid analogues that inhibit AKT also independently activate the stress kinase, p38alpha, through MKK3/6-independent and –dependent mechanisms. *J Biol Chem* , 282:27020-27029.

Gills JJ, Holbeck S, Hollingshead M, Hewitt SM, Kozikowski AP, Dennis PA(2006) Spectrum of activity and molecular correlates of response to phosphatidylinositol ether lipid analogues, novel lipid-based inhibitors of Akt. Mol Cancer Ther, 5:713-722.

Glomset, J.A., and Farnsworth, C.C. (1994). Role of protein modification reactions in programming interactions between ras-related GTPases and cell membranes. Annu Rev Cell Biol *10*, 181-205.

Goldberg L, Kloog Y. (2006). A Ras inhibitor tilts the balance between Rac and Rho and blocks phosphatidylinositol 3-kinase-dependent glioblastoma cell migration. Cancer Research; 66:11709-11717.

Grotendorst GR, Chang T, Seppä HE, Kleinman HK, Martin GR.(1982) Platelet-derived growth factor is a chemoattractant for vascular smooth muscle cells. J Cell Physiol. 1982 Nov;113(2):261-6.

Gu, X., and Masters, K.S. (2009). Role of the MAPK/ERK pathway in valvular interstitial cell calcification. Am J Physiol Heart Circ Physiol *296*, H1748-1757.

Guijarro, C., Blanco-Colio, L.M., Ortego, M., Alonso, C., Ortiz, A., Plaza, J.J., Diaz, C., Hernandez, G., and Egido, J. (1998). 3-Hydroxy-3-methylglutaryl coenzyme a reductase and isoprenylation inhibitors induce apoptosis of vascular smooth muscle cells in culture. Circulation research *83*, 490-500.

Hancock, J.F., Magee, A.I., Childs, J.E., and Marshall, C.J. (1989). All ras proteins are polyisoprenylated but only some are palmitoylated. Cell *57*, 1167-1177.

Harmey, D., Hessle, L., Narisawa, S., Johnson, K.A., Terkeltaub, R., and Millan, J.L. (2004). Concerted regulation of inorganic pyrophosphate and osteopontin by akp2, enpp1, and ank: an integrated model of the pathogenesis of mineralization disorders. The American journal of pathology *164*, 1199-1209.

Hayashi M. (2013). Calciphylaxis: diagnosis and clinical features. Clin Exp Nephro l17(4):498-503

Henley, C., Colloton, M., Cattley, R.C., Shatzen, E., Towler, D.A., Lacey, D., and Martin, D. (2005). 1,25-Dihydroxyvitamin D3 but not cinacalcet HCl (Sensipar/Mimpara) treatment mediates aortic calcification in a rat model of secondary hyperparathyroidism. Nephrol Dial Transplant *20*, 1370-1377.

Hosaka, N., Mizobuchi, M., Ogata, H., Kumata, C., Kondo, F., Koiwa, F., Kinugasa, E., and Akizawa, T. (2009). Elastin degradation accelerates phosphate-induced mineralization of vascular smooth muscle cells. Calcif Tissue Int *85*, 523-529.

House SJ, Potier M, Bisaillon J, Singer HA, Trebak M (2008) The non-excitable smooth muscle: calcium signaling and phenotypic switching during vascular disease. Pflugers Arch 456: 769–785.

Hu, M.C., Shi, M., Zhang, J., Quinones, H., Griffith, C., Kuro-o, M., and Moe, O.W. (2011). Klotho deficiency causes vascular calcification in chronic kidney disease. J Am Soc Nephrol *22*, 124-136.

Huang C,Jacobson K, Schaller (2004) MAP kinases and cell migration. J Cell Sci. 20; 117(Pt 20):4619-28.

Hunt, J.L., Fairman, R., Mitchell, M.E., Carpenter, J.P., Golden, M., Khalapyan, T., Wolfe, M., Neschis, D., Milner, R., Scoll, B., *et al.* (2002). Bone formation in carotid plaques: a clinicopathological study. Stroke; a journal of cerebral circulation *33*, 1214-1219.

Hur, D.J., Raymond, G.V., Kahler, S.G., Riegert-Johnson, D.L., Cohen, B.A., and Boyadjiev, S.A. (2005). A novel MGP mutation in a consanguineous family: review of the clinical and molecular characteristics of Keutel syndrome. American journal of medical genetics *135*, 36-40.

Indolfi, C., Avvedimento, E.V., Rapacciuolo, A., Di Lorenzo, E., Esposito, G., Stabile, E., Feliciello, A., Mele, E., Giuliano, P., Condorelli, G., *et al.* (1995). Inhibition of cellular ras prevents smooth muscle cell proliferation after vascular injury in vivo. Nat Med *1*, 541-545.

Janzen, J., and Vuong, P.N. (2001). Arterial calcifications: morphological aspects and their pathological implications. Zeitschrift fur Kardiologie *90 Suppl 3*, 6-11.

Jiang, K., Coppola, D., Crespo, N.C., Nicosia, S.V., Hamilton, A.D., Sebti, S.M., and Cheng, J.Q. (2000). The phosphoinositide 3-OH kinase/AKT2 pathway as a critical target for farnesyltransferase inhibitor-induced apoptosis. Molecular and cellular biology 20, 139-148.

Johnson, R.C., Leopold, J.A., and Loscalzo, J. (2006). Vascular calcification: pathobiological mechanisms and clinical implications. Circ Res 99, 1044-1059.

Kapustin, A., and Shanahan, C.M. (2009). Targeting vascular calcification: softening-up a hard target. Curr Opin Pharmacol 9, 84-89.

Kauffmann-Zeh, A., Rodriguez-Viciana, P., Ulrich, E., Gilbert, C., Coffer, P., Downward, J., and Evan, G. (1997). Suppression of c-Myc-induced apoptosis by Ras signalling through PI(3)K and PKB. Nature 385, 544-548.

Keelan, P.C., Bielak, L.F., Ashai, K., Jamjoum, L.S., Denktas, A.E., Rumberger, J.A., Sheedy, I.P., Peyser, P.A., and Schwartz, R.S. (2001). Long-term prognostic value of coronary calcification detected by electron-beam computed tomography in patients undergoing coronary angiography. Circulation 104, 412-417.

Khokhlatchev, A., Rabizadeh, S., Xavier, R., Nedwidek, M., Chen, T., Zhang, X.F., Seed, B., and Avruch, J. (2002). Identification of a novel Ras-regulated proapoptotic pathway. Curr Biol 12, 253-265.

Khwaja, A., Dockrell, M.E., Hendry, B.M., and Sharpe, C.C. (2006). Prenylation is not necessary for endogenous Ras activation in non-malignant cells. Journal of cellular biochemistry 97, 412-422.

Khwaja, A., Sharpe, C.C., Noor, M., Kloog, Y., and Hendry, B.M. (2005). The inhibition of human mesangial cell proliferation by S-trans, trans-farnesylthiosalicylic acid. Kidney international 68, 474-486.

Kouchi, H., Nakamura, K., Fushimi, K., Sakaguchi, M., Miyazaki, M., Ohe, T., and Namba, M. (1999). Manumycin A, inhibitor of ras farnesyltransferase, inhibits proliferation and migration of rat vascular smooth muscle cells. Biochem Biophys Res Commun 264, 915-920.

Kozikowski AP, Sun H, Brognard J, Dennis PA: (2003) Novel PI analogues selectively block activation of the pro-survival serine/threonine kinaseAkt. J Am Chem Soc, 125:1144-1145.

Krech T, Thiede M, Hilgenberg E, Schäfer R, Jürchott K.(2010) Characterization of AKT independent effects of the synthetic AKT inhibitors SH-5 and SH-6 using an integrated approach combining transcriptomic profiling and signaling pathway perturbations. BMC Cancer. ;10:287

Kyathanahalli, C.N., and Kowluru, A. (2011). A farnesylated G-protein suppresses Akt phosphorylation in INS 832/13 cells and normal rat islets: regulation by pertussis toxin and PGE. Biochem Pharmacol 81, 1237-1247.

Lerner, E.C., Qian, Y., Blaskovich, M.A., Fossum, R.D., Vogt, A., Sun, J., Cox, A.D., Der, C.J., Hamilton, A.D., and Sebti, S.M. (1995). Ras CAAX peptidomimetic FTI-277 selectively blocks oncogenic Ras signaling by inducing cytoplasmic accumulation of inactive Ras-Raf complexes. The Journal of biological chemistry 270, 26802-26806.

Liberman M, Johnson RC, Handy DE, Loscalzo J, Leopold JA.(2011) Bone morphogenetic protein-2 activates NADPH oxidase to increase endoplasmic reticulum stress and human coronary artery smooth muscle cell calcification.
Biochem Biophys Res Commun ;413:436–441.

Lewis, T.S., Shapiro, P.S., and Ahn, N.G. (1998). Signal transduction through MAP kinase cascades. Adv Cancer Res 74, 49-139.

Liu, M., Bryant, M.S., Chen, J., Lee, S., Yaremko, B., Lipari, P., Malkowski, M., Ferrari, E., Nielsen, L., Prioli, N., et al. (1998). Antitumor activity of SCH 66336, an orally bioavailable tricyclic inhibitor of farnesyl protein transferase, in human tumor xenograft models and wap-ras transgenic mice. Cancer Res 58, 4947-4956.

Lomashvili, K.A., Monier-Faugere, M.C., Wang, X., Malluche, H.H., and O'Neill, W.C. (2009). Effect of bisphosphonates on vascular calcification and bone metabolism in experimental renal failure. Kidney Int *75*, 617-625.

Lowy, D.R., and Willumsen, B.M. (1993). Function and regulation of ras. Annu Rev Biochem *62*, 851-891.

Lopez I, Mendoza FJ, Aguilera-Tejero E, Perez J, Guerrero F, Martin D, Rodriguez M. (2008). The effect of calcitriol, paricalcitol, and a calcimimetic on extraosseous calcifications in uremic rats. Kidney Int;73(3):300-7

Luo, G., Ducy, P., McKee, M.D., Pinero, G.J., Loyer, E., Behringer, R.R., and Karsenty, G. (1997). Spontaneous calcification of arteries and cartilage in mice lacking matrix GLA protein. Nature *386*, 78-81.

Malumbres, M., and Barbacid, M. (2003). RAS oncogenes: the first 30 years. Nat Rev Cancer *3*, 459-465.

Marciano, D., Ben-Baruch, G., Marom, M., Egozi, Y., Haklai, R., and Kloog, Y. (1995). Farnesyl derivatives of rigid carboxylic acids-inhibitors of ras-dependent cell growth. J Med Chem *38*, 1267-1272.

Makovski V, Haklai R, Kloog Y.(2012) Farnesylthiosalicylic acid (salirasib) inhibits Rheb in TSC2-null ELT3 cells: a potential treatment for lymphangioleiomyomatosis,130(6):1420-9

Marom, M., Haklai, R., Ben-Baruch, G., Marciano, D., Egozi, Y., and Kloog, Y. (1995). Selective inhibition of Ras-dependent cell growth by farnesylthiosalisylic acid. J Biol Chem *270*, 22263-22270.

Mazzocca, A., Giusti, S., Hamilton, A.D., Sebti, S.M., Pantaleo, P., and Carloni, V. (2003). Growth inhibition by the farnesyltransferase inhibitor FTI-277 involves Bcl-2 expression and defective association with Raf-1 in liver cancer cell lines. Molecular pharmacology *63*, 159-166.

McTaggart SJ. (2006) Isoprenylated proteins. Cell Mol Life Sci.;63(3):255-67.

Mehta, I.S., Bridger, J.M., and Kill, I.R. Progeria, the nucleolus and farnesyltransferase inhibitors. Biochem Soc Trans *38*, 287-291.

Mizobuchi, M., Towler, D., and Slatopolsky, E. (2009). Vascular calcification: the killer of patients with chronic kidney disease. J Am Soc Nephrol *20*, 1453-1464.

Moe, S.M., Duan, D., Doehle, B.P., O'Neill, K.D., and Chen, N.X. (2003). Uremia induces the osteoblast differentiation factor Cbfa1 in human blood vessels. Kidney Int *63*, 1003-1011.

Moe, S.M., Reslerova, M., Ketteler, M., O'Neill, K., Duan, D., Koczman, J., Westenfeld, R., Jahnen-Dechent, W., and Chen, N.X. (2005). Role of calcification inhibitors in the pathogenesis of vascular calcification in chronic kidney disease (CKD). Kidney Int *67*, 2295-2304.

Montes de Oca, A., Madueno, J.A., Martinez-Moreno, J.M., Guerrero, F., Munoz-Castaneda, J., Rodriguez-Ortiz, M.E., Mendoza, F.J., Almaden, Y., Lopez, I., Rodriguez, M., *et al.* (2010). High-phosphate-induced calcification is related to SM22alpha promoter methylation in vascular smooth muscle cells. J Bone Miner Res *25*, 1996-2005.

Moolenaar wh, (1999) Bioactive lysophospholipids and their G protein-coupled receptors.Exp Cell Res 253:230–238, 199

Nadra, I., Mason, J.C., Philippidis, P., Florey, O., Smythe, C.D., McCarthy, G.M., Landis, R.C., and Haskard, D.O. (2005). Proinflammatory activation of macrophages by basic calcium phosphate crystals via protein kinase C and MAP kinase pathways: a vicious cycle of inflammation and arterial calcification Circulation research *96*, 1248-1256.

Nahar, N.N., Missana, L.R., Garimella, R., Tague, S.E., and Anderson, H.C. (2008). Matrix vesicles are carriers of bone morphogenetic proteins (BMPs), vascular endothelial growth factor (VEGF), and noncollagenous matrix proteins. J Bone Miner Metab *26*, 514-519.

Neven E, D'Haese PC (2011) Vascular calcification in chronic renal failure: what have we learned from animal studies Circ Res 108: 249–264.

New SE, Aikawa E.(2011) Molecular imaging insights into early inflammatory stages of arterial and aortic valve calcification Circ Res. 108(11):1381-91

Nikolov IG, Joki N, Galmiche A, Nguyen-Khoa T, Guerrera IC, Guillonneau F, Ivanovski O, Phan O, Maizel J, Marçon F, Benchitrit J, Lucas A, Edelman A, Lacour B, Drüeke TB, Massy ZA.(2013) Farnesyltransferase inhibitor R115777 protects against vascular disease in uremic mice. Atherosclerosis.;229(1):42-51.

Olson, M.F., Paterson, H.F., and Marshall, C.J. (1998). Signals from Ras and Rho GTPases interact to regulate expression of p21Waf1/Cip1. Nature *394*, 295-299.

Ortiz-Vega, S., Khokhlatchev, A., Nedwidek, M., Zhang, X.F., Dammann, R., Pfeifer, G.P., and Avruch, J. (2002). The putative tumor suppressor RASSF1A homodimerizes and heterodimerizes with the Ras-GTP binding protein Nore1. Oncogene *21*, 1381-1390.

Ozes, O.N., Mayo, L.D., Gustin, J.A., Pfeffer, S.R., Pfeffer, L.M., and Donner, D.B. (1999). NF-kappaB activation by tumour necrosis factor requires the Akt serine-threonine kinase. Nature *401*, 82-85.

Persy, V., and D'Haese, P. (2009). Vascular calcification and bone disease: the calcification paradox. Trends in molecular medicine *15*, 405-416.

Prendergast, G.C., and Oliff, A. (2000). Farnesyltransferase inhibitors: antineoplastic properties, mechanisms of action, and clinical prospects. Seminars in cancer biology *10*, 443-452.

Pollex, Hegele (2004). Hutchinson-Gilford progeria syndrome.Clin Genet 2004, 66: 375-81.

Proudfoot, D., Skepper, J.N., Hegyi, L., Bennett, M.R., Shanahan, C.M., and Weissberg, P.L. (2000). Apoptosis regulates human vascular calcification in vitro: evidence for initiation of vascular calcification by apoptotic bodies. Circulation research *87*, 1055-1062.

Pumiglia, K., Chow, Y.H., Fabian, J., Morrison, D., Decker, S., and Jove, R. (1995). Raf-1 N-terminal sequences necessary for Ras-Raf interaction and signal transduction. Mol Cell Biol *15*, 398-406.

Radziwill, G., Erdmann, R.A., Margelisch, U., and Moelling, K. (2003). The Bcr kinase downregulates Ras signaling by phosphorylating AF-6 and binding to its PDZ domain. Mol Cell Biol *23*, 4663-4672.

Rangrez AY, M'Baya-Moutoula E, Metzinger-Le Meuth V, Hénaut L, Djelouat MS, Benchitrit J, Massy ZA, Metzinger L.(2012) Inorganic phosphate accelerates the migration of vascular smooth muscle cells: evidence for the involvement of miR-223. PLoS One.;7(10):e47807. doi: 10.1371/journal.pone.0047807. Epub 2012 Oct 18.

Ragnauth, C.D., Warren, D.T., Liu, Y., McNair, R., Tajsic, T., Figg, N., Shroff, R., Skepper, J., and Shanahan, C.M. (2010) Prelamin A acts to accelerate smooth muscle cell senescence and is a novel biomarker of human vascular aging. Circulation *121,* 2200-2210.

Penido MG, Alon US. 2012 Phosphate homeostasis and its role in bone health.Pediatr Nephrol. Nov;27(11):2039-48. doi: 10.1007/s00467-012-2175-z. Epub 2012 May 3.

Rao, D.S., Goldin, J.G., and Fishbein, M.C. (2005). Determinants of plaque instability in atherosclerotic vascular disease. Cardiovasc Pathol *14*, 285-293.

Reif, S., Weis, B., Aeed, H., Gana-Weis, M., Zaidel, L., Avni, Y., Romanelli, R.G., Pinzani, M., Kloog, Y., and Bruck, R. (1999). The Ras antagonist, farnesylthiosalicylic acid (FTS), inhibits experimentally-induced liver cirrhosis in rats. J Hepatol *31*, 1053-1061.

Reynolds JL, Joannides AJ, Skepper JN, McNair R, Schurgers LJ, Proudfoot D, Jahnen-Dechent W, Weissberg PL, Shanahan CM.(2004). Human vascular smooth muscle cells undergo vesicle-mediated calcification in response to changes in extracellular calcium and phosphate concentrations: a potential mechanism for accelerated vascular calcification in ESRD; 15(11):2857-67

Rivas, D., Akter, R., and Duque, G. (2007). Inhibition of Protein Farnesylation Arrests Adipogenesis and Affects PPARgamma Expression and Activation in Differentiating Mesenchymal Stem Cells. PPAR Res *2007*, 81654.

Romashkova, J.A., and Makarov, S.S. (1999). NF-kappaB is a target of AKT in anti-apoptotic PDGF signalling. Nature *401*, 86-90.

Rodríguez-Vita J, Sánchez-Galán E, Santamaría B, Sánchez-López E, Rodrigues-Díez R, Blanco-Colio LM, Egido J, Ortiz A, Ruiz-Ortega M. (2008). Essential role of TGF-beta/Smad pathway on statin dependent vascular smooth muscle cell regulation. PLoS One.;3(12):e3959

Rubin, M.R., and Silverberg, S.J. (2004). Vascular calcification and osteoporosis--the nature of the nexus. J Clin Endocrinol Metab *89*, 4243-4245.

Russell, R.G., Smith, R., Bishop, M.C., and Price, D.A. (1972). Treatment of myositis ossificans progressiva with a diphosphonate. Lancet *1*, 10-11.

Rudijanto A.(2007) The role of vascular smooth muscle cells on the pathogenesis of atherosclerosis Acta Med Indones

Sage, A.P., Tintut, Y., and Demer, L.L. (2010). Regulatory mechanisms in vascular calcification. Nat Rev Cardiol *7*, 528-536.

Saxena, N., Lahiri, S.S., Hambarde, S., and Tripathi, R.P. (2008). RAS: target for cancer therapy. Cancer Invest *26*, 948-955.

Sebti SM, Hamilton AD. (2000). Farnesyltransferase and geranylgeranyltransferase I inhibitors and cancer therapy: lessons from mechanism and bench-to-bedside translational studies.Oncogene.;19(56):6584-93

Schafer, C., Heiss, A., Schwarz, A., Westenfeld, R., Ketteler, M., Floege, J., Muller-Esterl, W., Schinke, T., and Jahnen-Dechent, W. (2003). The serum protein alpha 2-Heremans-Schmid glycoprotein/fetuin-A is a systemically acting inhibitor of ectopic calcification. The Journal of clinical investigation *112*, 357-366.

Schlessinger, J. (1993). How receptor tyrosine kinases activate Ras. Trends Biochem Sci *18*, 273-275.

Schlieper, G., Aretz, A., Verberckmoes, S.C., Kruger, T., Behets, G.J., Ghadimi, R., Weirich, T.E., Rohrmann, D., Langer, S., Tordoir, J.H., *et al.* (2010). Ultrastructural analysis of vascular calcifications in uremia. J Am Soc Nephrol *21*, 689-696.

Sears, K.T., Daino, H., and Carey, G.B. (2008). Reactive oxygen species-dependent destruction of MEK and Akt in Manumycin stimulated death of lymphoid tumor and myeloma cell lines. Int J Cancer *122*, 1496-1505.

Sedding, D.G., Trobs, M., Reich, F., Walker, G., Fink, L., Haberbosch, W., Rau, W., Tillmanns, H., Preissner, K.T., Bohle, R.M., *et al.* (2009). 3-Deazaadenosine prevents smooth muscle cell proliferation and neointima formation by interfering with Ras signaling. Circulation research *104*, 1192-1200.

Shanahan, C.M. (2006). Vascular calcification--a matter of damage limitation? Nephrol Dial Transplant *21*, 1166-1169.

Shanahan, C.M., Cary, N.R., Salisbury, J.R., Proudfoot, D., Weissberg, P.L., and Edmonds, M.E. (1999). Medial localization of mineralization-regulating proteins in association with Monckeberg's sclerosis: evidence for smooth muscle cell-mediated vascular calcification. Circulation *100*, 2168-2176.

Shantsila, E., and Lip, G.Y. (2009). Systemic inflammation as a driver of vascular calcification: a proof of concept. Journal of internal medicine *266*, 453-456.

She, M., Pan, I., Sun, L., and Yeung, S.C. (2005). Enhancement of manumycin A-induced apoptosis by methoxyamine in myeloid leukemia cells. Leukemia *19*, 595-602.

Shi, Y., Wu, J., Mick, R., Cerniglia, G.J., Cohen-Jonathan, E., Rhim, J.S., Koch, C.J., and Bernhard, E.J. (2005). Farnesyltransferase inhibitor effects on prostate tumor micro-environment and radiation survival. The Prostate *62*, 69-82.

Shroff, R.C., McNair, R., Figg, N., Skepper, J.N., Schurgers, L., Gupta, A., Hiorns, M., Donald, A.E., Deanfield, J., Rees, L., *et al.* (2008). Dialysis accelerates medial vascular calcification in part by triggering smooth muscle cell apoptosis. Circulation *118*, 1748-1757.

Shroff RC, McNair R, Skepper JN, Figg N, Schurgers LJ, Deanfield J, Rees L, Shanahan CM. (2010) Chronic mineral dysregulation promotes vascular smooth muscle cell adaptation and extracellular matrix calcification J Am Soc Nephrol.;21(1):103-12.

Sinha S, PhD Thesis. (2010). The Effects of Bisphosphonates and Modulation of Protein Prenylation on Vascular Calcification

Solomon, C.S., and Goalstone, M.L. (2001). Dominant negative farnesyltransferase alpha-subunit inhibits insulin mitogenic effects. Biochem Biophys Res Commun *285*, 161-166.

Son, B.K., Akishita, M., Iijima, K., Kozaki, K., Maemura, K., Eto, M., and Ouchi, Y. (2008). Adiponectin antagonizes stimulatory effect of tumor necrosis factor-alpha on vascular smooth muscle cell calcification: regulation of growth arrest-specific gene 6-mediated survival pathway by adenosine 5'-monophosphate-activated protein kinase. Endocrinology *149*, 1646-1653.

Son, B.K., Kozaki, K., Iijima, K., Eto, M., Kojima, T., Ota, H., Senda, Y., Maemura, K., Nakano, T., Akishita, M., *et al.* (2006). Statins protect human aortic smooth muscle cells from inorganic phosphate-induced calcification by restoring Gas6-Axl survival pathway. Circulation research *98*, 1024-1031.

Son BK, Kozaki K, Iijima K, Eto M, Nakano T, Akishita M, Ouchi Y.(2007). Gas6/Axl-PI3K/Akt pathway plays a central role in the effect of statins on inorganic. Eur J Pharmacol.; 556(1-3):1-8.

Shirai H, Autieri M, Eguchi S.(2007)Small GTP-binding proteins andmitogen-activated protein kinases as promising therapeutic targets of vascular remodeling. Curr Opin Nephrol Hypertension;16(2):111-115

Speer, M.Y., McKee, M.D., Guldberg, R.E., Liaw, L., Yang, H.Y., Tung, E., Karsenty, G., and Giachelli, C.M. (2002). Inactivation of the osteopontin gene enhances vascular calcification of matrix Gla protein-deficient mice: evidence for osteopontin as an inducible inhibitor of vascular calcification in vivo. The Journal of experimental medicine *196*, 1047-1055.

Speer, M.Y., Yang, H.Y., Brabb, T., Leaf, E., Look, A., Lin, W.L., Frutkin, A., Dichek, D., and Giachelli, C.M. (2009). Smooth muscle cells give rise to osteochondrogenic precursors and chondrocytes in calcifying arteries. Circulation research *104*, 733-741.

Steitz SA, Speer MY, Curinga G, Yang HY, Haynes P, Aebersold R, Schinke T, Karsenty G, Giachelli CM.(2001) Smooth muscle cell phenotypic transition associated with calcification: upregulation of Cbfa1 and downregulation of smooth muscle lineage markers. Circulation research 7;89(12):1147-54

Sugita, M., Sugita, H., and Kaneki, M. (2007). Farnesyltransferase inhibitor, manumycin a, prevents atherosclerosis development and reduces oxidative stress in apolipoprotein E-deficient mice. Arteriosclerosis, thrombosis, and vascular biology *27*, 1390-1395.

Sun, S.Y., Zhou, Z., Wang, R., Fu, H., and Khuri, F.R. (2004). The farnesyltransferase inhibitor Lonafarnib induces growth arrest or apoptosis of human lung cancer cells without downregulation of Akt. Cancer Biol Ther *3*, 1092-1098; discussion 1099-1101.

Swanson, K.M., and Hohl, R.J. (2006). Anti-cancer therapy: targeting the mevalonate pathway. Curr Cancer Drug Targets *6*, 15-37.

Takai, Y., Kikuchi, A., Kawata, M., Yamamoto, K., and Hoshijima, M. (1990). Purification, characterization, and possible functions of small molecular weight GTP-binding proteins. Am J Hypertens *3*, 220S-223S.

Takai, Y., Sasaki, T., and Matozaki, T. (2001). Small GTP-binding proteins. Physiol Rev *81*, 153-208.

Tomiyama, C., Carvalho, A.B., Higa, A., Jorgetti, V., Draibe, S.A., and Canziani, M.E. (2010). Coronary calcification is associated with lower bone formation rate in CKD patients not yet in dialysis treatment. J Bone Miner Res *25*, 499-504.

Toussaint, N.D. (2011). Extracellular matrix calcification in chronic kidney disease. Curr Opin Nephrol Hypertens *20*, 360-368.

Tsuneoka, M., and Mekada, E. (2000). Ras/MEK signaling suppresses Myc-dependent apoptosis in cells transformed by c-myc and activated ras. Oncogene *19*, 115-123.

Tyson, K.L., Reynolds, J.L., McNair, R., Zhang, Q., Weissberg, P.L., and Shanahan, C.M. (2003). Osteo/chondrocytic transcription factors and their target genes exhibit distinct patterns of expression in human arterial calcification. Arteriosclerosis, thrombosis, and vascular biology *23*, 489-494.

Ueno, H., Yamamoto, H., Ito, S., Li, J.J., and Takeshita, A. (1997). Adenovirus-mediated transfer of a dominant-negative H-ras suppresses neointimal formation in balloon-injured arteries in vivo. Arterioscler Thromb Vasc Biol *17*, 898-904.

van Weeren, P.C., de Bruyn, K.M., de Vries-Smits, A.M., van Lint, J., and Burgering, B.M. (1998). Essential role for protein kinase B (PKB) in insulin-induced glycogen synthase kinase 3 inactivation. Characterization of dominant-negative mutant of PKB. J Biol Chem *273*, 13150-13156.

Varga, R., Eriksson, M., Erdos, M.R., Olive, M., Harten, I., Kolodgie, F., Capell, B.C., Cheng, J., Faddah, D., Perkins, S., *et al.* (2006). Progressive vascular smooth muscle cell defects in a mouse model of Hutchinson-Gilford progeria syndrome. Proceedings of the National Academy of Sciences of the United States of America *103*, 3250-3255.

Virtanen, S.S., Sandholm, J., Yegutkin, G., Kalervo Vaananen, H., and Harkonen, P.L. Inhibition of GGTase-I and FTase disrupts cytoskeletal organization of human PC-3 prostate cancer cells. Cell biology international *34*, 815-826.

Vos, M.D., Ellis, C.A., Bell, A., Birrer, M.J., and Clark, G.J. (2000). Ras uses the novel tumor suppressor RASSF1 as an effector to mediate apoptosis. J Biol Chem *275*, 35669-35672.

Weiner DE, Tabatabai S, Tighiouart H, Elsayed E, Bansal N, Griffith J, Salem DN, Levey AS, Sarnak MJ. (2006) Cardiovascular outcomes and all-cause mortality: exploring the interaction between CKD and cardiovascular disease. Am J Kidney Dis. :392-401.

Willis AI, Sadowitz B, Fuse S, Maier KG, Lee TS, Wang XJ, Tuszynski GP, Sumpio BE, Gahtan V. (2011) Thrombospondin 1, fibronectin, and vitronectin are differentially dependent upon RAS, ERK1/2, and p38 for induction of vascular smooth muscle cell chemotaxis. Vasc Endovascular Surg.;45(1):55-62

Wildroudt ML, Freeman EJ.(2006) Regulation of Akt by arachidonic acid and phosphoinositide 3-kinase in angiotensin II-stimulated vascular smooth muscle cells. Biochim Biophys Acta.;1761(1):11-6.

Wolthuis, R.M., and Bos, J.L. (1999). Ras caught in another affair: the exchange factors for Ral. Curr Opin Genet Dev *9*, 112-117.

Work, L.M., McPhaden, A.R., Pyne, N.J., Pyne, S., Wadsworth, R.M., and Wainwright, C.L. (2001). Short-term local delivery of an inhibitor of Ras farnesyltransferase prevents neointima formation in vivo after porcine coronary balloon angioplasty. Circulation *104*, 1538-1543.

Yaari, S., Jacob-Hirsch, J., Amariglio, N., Haklai, R., Rechavi, G., and Kloog, Y. (2005). Disruption of cooperation between Ras and MycN in human neuroblastoma cells promotes growth arrest. Clin Cancer Res *11*, 4321-4330.

Yang, H., Curinga, G., and Giachelli, C.M. (2004). Elevated extracellular calcium levels induce smooth muscle cell matrix mineralization in vitro. Kidney Int *66*, 2293-2299.

Yeung, S.C., Xu, G., Pan, J., Christgen, M., and Bamiagis, A. (2000). Manumycin enhances the cytotoxic effect of paclitaxel on anaplastic thyroid carcinoma cells. Cancer research *60*, 650-656.

Ye M, Hu D, Tu L, Zhou X, Lu F, Wen B, Wu W, Lin Y, Zhou Z, Qu J.(2008) Involvement of PI3K/Akt signaling pathway in hepatocyte growth factor-induced migration of uveal melanoma cells.Invest Ophthalmol Vis Sci.;49(2):497-504.

Young, D.S, et al., (1975): Effects of drugs on clinical laboratory tests. Clin. Chem. 21:1D

Zaka, R., Stokes, D., Dion, A.S., Kusnierz, A., Han, F., and Williams, C.J. (2006). P5L mutation in Ank results in an increase in extracellular inorganic pyrophosphate during proliferation and nonmineralizing hypertrophy in stably transduced ATDC5 cells. Arthritis research & therapy *8*, R164.

Zebboudj, A.F., Imura, M., and Bostrom, K. (2002). Matrix GLA protein, a regulatory protein for bone morphogenetic protein-2. J Biol Chem *277*, 4388-4394.

Zebboudj, A.F., Shin, V., and Bostrom, K. (2003). Matrix GLA protein and BMP-2 regulate osteoinduction in calcifying vascular cells. J Cell Biochem *90*, 756-765.

Zhang, F.L., and Casey, P.J. (1996). Protein prenylation: molecular mechanisms and functional consequences. Annu Rev Biochem *65*, 241-269.

Zhou, J.M., Zhu, X.F., Pan, Q.C., Liao, D.F., Li, Z.M., and Liu, Z.C. (2003). Manumycin inhibits cell proliferation and the Ras signal transduction pathway in human hepatocellular carcinoma cells. International journal of molecular medicine *11*, 767-771.

Zhou, Q., and Liao, J.K. (2009). Rho kinase: an important mediator of atherosclerosis and vascular disease. Curr Pharm Des *15*, 3108-3115.